Optical Design and Characterization of Solar Concentrators for Photovoltaics

Johan Nilsson

Division of Energy and Building Design
Department of Architecture and Built Environment
Lund University
Faculty of Engineering LTH, 2005
Report EBD-T--05/6

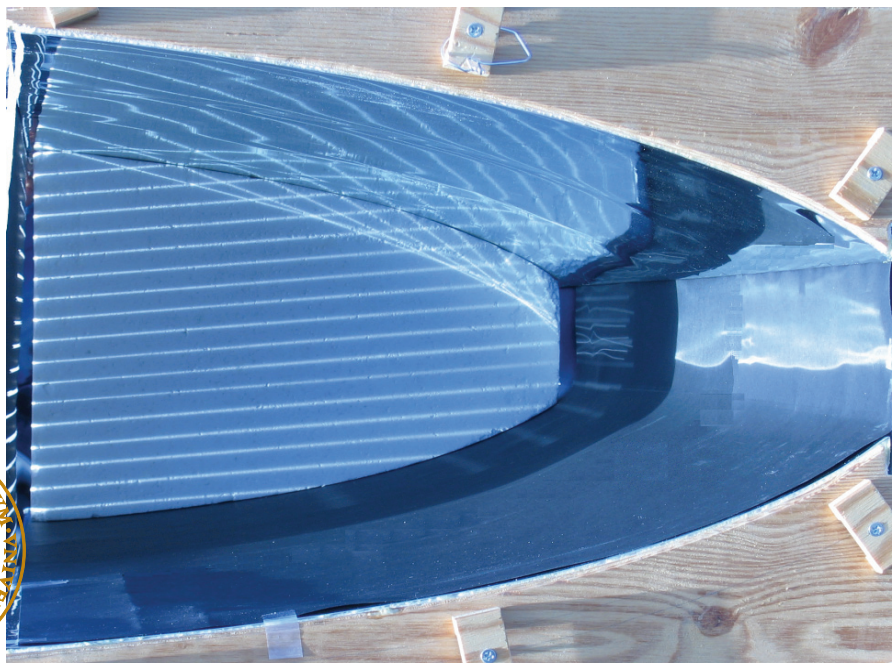

Lund University

Lund University, with eight faculties and a number of research centres and specialized institutes, is the largest establishment for research and higher education in Scandinavia. The main part of the University is situated in the small city of Lund which has about 101 000 inhabitants. A number of departments for research and education are, however, located in Malmö. Lund University was founded in 1666 and has today a total staff of 6 006 employees and 41 000 students attending 90 degree programmes and 1 000 subject courses offered by 88 departments.

Division of Energy and Building Design

Reducing environmental effects of construction and facility management is a central aim of society. Minimising the energy use is an important aspect of this aim. The recently established division of Energy and Building Design belongs to the department of Construction and Architecture at the Lund Institute of Technology in Sweden. The division has a focus on research in the fields of energy use, passive and active solar design, daylight utilisation and shading of buildings. Effects and requirements of occupants on thermal and visual comfort are an essential part of this work. Energy and Building Design also develops guidelines and methods for the planning process.

Optical Design and Characterization of Solar Concentrators for Photovoltaics

Johan Nilsson

Licentiate Thesis

Key words

Solar concentrators, parabolic reflectors, photovoltaic cells, photovoltaic-thermal systems, optical efficiency, non-imaging optics, optical properties, building integrated photovoltaics

The English language corrected by L. J. Gruber BSc(Eng) MICE MIStructE.
Layout: Hans Follin, LTH, Lund.
Cover photo: Solar rays seen in CPC cross section, Håkan Håkansson.

Printed by KFS AB, Lund 2005

Report No EBD-T--05/6
Optical Design and Characterization of Solar Concentrators for Photovoltaics.
Department of Architecture and Built Environment, Division of Energy and Building Design,
Lund University, Lund

ISSN 1651-8136
ISBN 91-85147-15-X

Lund University, Lund Institute of Technology
Department of Architecture and Built Environment
Division of Energy and Building Design
P.O. Box 118
SE-221 00 LUND
Sweden

Telephone: +46 46 - 222 73 52
Telefax: +46 46 - 222 47 19
E-mail: ebd@ebd.lth.se
Home page: www.ebd.lth.se

Abstract

Stationary solar energy concentrators are a promising option for decreasing the price of photovoltaic electricity. This thesis studies stationary concentrators in PV/Thermal applications. The studied systems are parabolic troughs intended for building integration.

The first chapters briefly explain the optics of solar energy concentrators. The theoretical maximum concentration ratios of two and three dimensional systems were derived using the concept of étendue conservation and a review of current concentrators was presented.

An asymmetrically truncated compound parabolic concentrator, CPC, for flat roof integration was characterized as an example of a stationary concentrator. The current-voltage characteristics were measured, the optical efficiency was calculated, and the annual thermal and electrical output were simulated. This was done for two systems, one with aluminium reflectors, and one with aluminium laminated steel reflectors. The output estimates show no difference in annual output between the two materials. It was estimated that the bifacial system would produce 37% more electricity than a reference mounted in the plane of the concentrator aperture. The estimated annual output of thermal energy was 145 kWh/m^2 of hot water at 50°C. It was concluded that the system should have cells facing both the front and back reflectors to maximize the system performance.

The actual output of stationary concentrators with standard photovoltaic cells is often lower than what could be expected. This is due to the highly non-uniform irradiation distribution on the cells created by the parabolic reflectors. Three microstructured reflectors in asymmetric CPC troughs were evaluated using ray tracing in an attempt to homogenize the irradiation on the cells. The simulations show that all three proposed structures reduce the peak irradiance with only small reductions in the optical efficiency. The microstructured reflectors were shown to increase the concentration ratio of the troughs which gives higher flexibility in designing new concentrators. The structured reflector troughs had a high optical efficiency when the sun was in the meridian plane, but the structures lowered the efficiency outside this plane. This was due to the dis-

ruption of the translational symmetry when the microstructured reflectors were introduced. It was concluded that structured reflectors are used at their largest benefit if they are applied in new concentrators designed for structures. For the existing designs, only a small input increase can be expected when structured reflectors are used. A new biaxial model for the incidence angle dependent optical efficiency of concentrators was presented. It is valid for translationally symmetric concentrators, flat plate collectors, and planar photovoltaic modules. It models the reflector and the cover glazing separately, and these model functions are multiplied at each angle of incidence to form the system model. The optical efficiency of the reflector was modelled as a function of the transverse angle of incidence. Existing models tend to overestimate the optical losses of the cover glazing, and the proposed model addressed this problem by modelling the optical efficiency of the glazing as a function of the true angle of incidence. The biaxial model was used to estimate the annual output of electricity from a concentrator and the estimates were compared with measurements during two summer months. The comparison showed that the proposed model is a good tool for estimating the output of photovoltaic concentrators.

Contents

Nomenclature

Latin

A,a	aperture area	[m^2]
b_o	incidence angle modifier	[-]
C	concentration ratio	[-]
C_g	geometrical concentration ratio	[-]
C_{max}	maximum concentration ratio	[-]
f	focal point	[-]
FF	fill factor	[-]
f_L	optical efficiency of glazing as a function of angle of incidence	[-]
f_l	focal length	[m]
G	incident irradiation	[W/m^2]
I	current	[A]
I_0	dark current	[A]
I_{1000}	short-circuit current at an incident irradiation of $1000W/m^2$	[A]
I_L	light generated current	[A]
I_{SC}	short-circuit current	[A]
I_{SC}^{conc}	short-circuit current of concentrator module	[A]
$I_{SC}^{reference}$	short-circuit current of reference module	[A]
K	optical efficiency according to McIntire	[-]
K_L	longitudinal optical efficiency according to McIntire	[-]
K_T	transversal optical efficiency according to McIntire	[-]
k_x	x direction cosine	[-]
k_y	y direction cosine	[-]
n	index of refraction	[-]
P_{max}	maximum power delivered by the cell	[W]
R	resistance	[Ω]
R_L	load resistance	[Ω]
R_P	shunt resistance	[Ω]

R_S	series resistance	[Ω]
R_T	transverse optical efficiency of concentrator	[-]
V	voltage	[V]
V_{OC}	open-circuit voltage	[V]

Greek

α	opening angle of V-trough	[°]
β	aperture tilt	[°]
η_{cell}	cell efficiency	[-]
η_n	optical efficiency at normal incidence	[-]
η_{opt}	optical efficiency	[-]
θ	angle of incidence	[°]
θ_i	angle of incidence	[°]
θ_L	longitudinal angle of incidence	[°]
θ_{max}	maximum angle of incidence accepted by the system	[°]
θ_r	reflected angle	[°]
θ_T	transverse projected angle of incidence	[°]
θ_t	transmitted angle	[°]
φ	rotation angle around the z-axis	[°]

List of articles

I. Nilsson, J., Håkansson, H., & Karlsson, B. (2005). *Electrical and thermal characterization of a PV-CPC hybrid*. Submitted to Solar Energy July 2005

II. Nilsson, J., Brogren, M., Helgesson, A., Karlsson, B., & Roos, A. (2005). *Biaxial model for the incidence angle dependence of the optical efficiency of photovoltaic systems with asymmetric reflectors*. Accepted for publication in Solar Energy.

III. Nilsson, J., Leutz, R., & Karlsson, B. (2005). *Micro-structured reflector surfaces for a stationary asymmetric parabolic solar concentrator.* Submitted to Applied Optics September 2005.

IV. Brogren, M., Helgesson, A., Karlsson, B., Nilsson, J., & Roos, A. (2004). *Optical properties, durability, and system aspects of a new aluminium-polymer-laminated steel reflector for solar concentrators.* Solar Energy Materials & Solar Cells Vol. 82, pp 387-412

V. Fieber, A., Gajbert, H., Håkansson, H., Nilsson, J., Rosencrantz, T., & Karlsson, B. (2003). *Design, Building Integration and Performance of a Hybrid Solar Wall Element.* Proceedings of ISES Solar World Congress 2003, Gothenburg, Sweden

VI. Fieber, A., Nilsson, J., & Karlsson, B. (2004). *PV performance of a multifunctional PV/T hybrid solar window.* Proceedings of 19th European Photovoltaic Solar Energy Conference and Exhibition, Paris, France

VII. Helgesson, A., Nilsson, J., & Karlsson, B. (2004). *A new model and method for determination of the incidence angle dependence of the optical efficiency of solar concentrators*. Accepted for publication after revision in Solar Energy Materials & Solar Cells.

VIII. Rosencrantz, T., Nilsson, J., & Karlsson, B. (2005). *A new model and method for determination of the incidence angle dependent g-value of windows and sunshades*. Proceedings of North Sun 2005, Vilnius, Lithuania

Acknowledgements

This work was financed by FORMAS, The Swedish Research Council for Environment, Agricultural Sciences and Spatial Planning.

I wish to thank my supervisors Prof. Björn Karlsson and Dr. Håkan Håkansson for their support. Björn for always being positive and having valuable comments on my work. Håkan for helping me with measurements and for being an inventor who always has new ideas on how to solve the problem.

Dr. Ralf Leutz and Prof. Harald Ries of Philipps University of Marburg, Germany are acknowledged for teaching me the fundamentals of optics and ray tracing, and for welcoming me to Marburg.

I would also like to acknowledge my colleague Bengt Hellström for valuable discussions which have helped me many times.

I have appreciated the cooperation with Helena Gajbert, Tobias Rosencrantz, Andreas Fieber, Maria Brogren and Anna Helgesson in co-authoring the articles.

Everyone at the division of Energy and Building Design is acknowledged for being part of a warm and friendly working environment.

Finally, I wish to thank my ever-supporting family, especially Anna. I love you!

1 Introduction

1.1 Background

The energy sector is currently in a state of change. Conventional energy sources are questioned and discussions about the greenhouse effect are on the agenda in many countries. In Sweden, the decision to start closing the nuclear power plants has highlighted the need for new energy sources even more. There is now a global consensus that the new sources of energy have to be renewable to satisfy the global energy demand in the long term. In view of these facts, the time for large scale implementation of solar generated heat and electricity is now. The government subsidies or regulations for solar energy in countries like Japan, Germany and Spain are a clear sign of this.

The main obstacle preventing a large scale implementation of photovoltaic electricity production is the high price of the photovoltaic modules. This is due both to the high material cost of the photovoltaic cell and to the highly manual production of the modules. If photovoltaic solar energy conversion is to be widely used in a market without subsidies such as feed-in tariffs or investment grants, the price per generated kWh has to be reduced significantly. In general, this problem can be addressed either by increasing the system efficiency or by reducing the total system price.

If the modules are integrated into the built environment, this has a large potential to reduce the price of the mounting, both in terms of space and components. Wall or roof integration are examples of such integration that will decrease the system price. Another benefit from building integration is that the energy production will be located at the point of use. There is in most cases a large difference between the cost of electricity generation and the price of the electricity at the consumer side which is largely due to taxes and fees that are outside the control of the utilities. To be able to compete with conventional electricity production, the price of photovoltaic electricity probably has to be around € 0.2/kWh,year if it is to be an interesting option for the utilities. On the other

hand, if the consumer can produce the PV-electricity as a means of reducing the amount of bought electricity, the price is allowed to be at least 5 times higher while still being a good investment.

If the system efficiency can be increased, the size of the system can be reduced. This is of great importance when the technology is applied where space is limited such as for example on buildings in high density urban areas. However, limited space is not the problem in most applications. In these cases, systems with lower efficiency per surface area might be an interesting option as long as the cost per kWh of electricity is lower.

One approach to get a lower system price is to use light concentrators to increase the output of the photovoltaic cells. As the current from the photovoltaic cells is proportional to the irradiation on the cells, more light on the cells will increase the electrical output. Since the photovoltaic module is the expensive component of the system, the use of concentrators to increase the irradiation of the cells has the potential of using the cells more efficiently as long as the price of the concentrator is lower than the price of the substituted photovoltaic cells.

The research on solar concentrators is mainly divided into three categories: low, medium, and high concentration systems.

High concentration systems is the term commonly used for systems with concentration ratios from 100-1000. It is necessary for the systems to have two-axis tracking of the sun to achieve such high concentrations. The high flux that is generated by the concentrators can be used to generate very high temperatures. At these temperatures, it is possible to generate electricity in a number of ways, e.g. using steam turbines or sterling cycles. It can also be used as heat for industrial processes that require high grade thermal energy. If the concentrator is used to concentrate the irradiation onto a photovoltaic cell, the cell can be extremely small due to the small spot size. If the cell is small, the price of the materials used will be low due to the low material consumption and it is possible to use advanced cell concepts that otherwise would be too expensive. Parabolic dishes or lenses are used to obtain high levels of concentration for photovoltaics. Concentrating lens systems for high concentration photovoltaics are discussed in (Miñano, González, and Benítez 1995) and (Leutz et. al. 1999). Parabolic dishes are discussed in (Feuermann and Gordon 2001). Central receivers with heliostat fields reflecting the light towards the receiver are used to obtain high temperatures by concentrating the solar radiation(Vant-Hull and Hildebrandt 1976) (Schramek and Mills 2003).

The second area of research is in systems concentrating the light 10-100 times. This is refered to as medium concentration. Such systems require one-axis tracking. The concentrators are translationally symmet-

ric, i.e. trough shaped. It can be shown that the concentration of translationally symmetric concentrators is independent of the light incident parallel to the axis of symmetry, and this removes the constraint of two-axis tracking. The existing systems are based on parabolic reflectors (Coventry 2005) and (Sala et. al. 1996) or Fresnel lenses (Piszczor et. al. 1993). The PV cells have to be designed for concentrator applications due to the high intensities and thus high currents, and the systems require cooling of the cells. The heat is collected in some systems by heat exchangers, or dissipated in others.

The last category is for systems with a concentration ratio from 1 to 10. Low concentrating systems can be stationary due to the low concentration ratio. This makes it possible to integrate the systems rationally into buildings without moving parts or complex mounting. Another benefit of the low concentration ratio is that, in principle it should be possible to use standard PV cells made for non-concentrating applications. This will reduce the price significantly. Cooling still has to be applied to maintain cell efficiency, but as for the other concentrator categories, the heat generated by the cooling can be utilized if the systems are well designed. Most systems are based on two dimensional CPCs (Compound Parabolic Concentrators) in some form (Karlsson and Wilson 1999) and (Mallick et. al. 2004), but other geometries are also considered (Fraidenraich 1998).

Building integration of PV is attractive as a means of lowering the cost of PV installations. The investment cost will be reduced if other materials are replaced by the PV system (IEA-PVPS Task 7 2005).

If the system is designed to utilize the cooling of the cells for generating heat, the system is referred to as a PV/Thermal hybrid. The cooling media are in most cases water or air. The hot water can be used for space heating or domestic hot water, and the air can be used for pre-heating of ventilation. The heat can also be used in absorption chillers to cool the building.

1.2 Objectives

The aim of this thesis has been to investigate the use of building integrated low concentration PV/Thermal hybrids. This has previously been shown to decrease the price of the electricity production (Perers and Karlsson 1993). The investigated concentrators were parabolic reflector troughs with low cost reflector materials such as aluminium or steel. One important part of the work was to characterize the state of the art low

concentration systems that are available today and to quantify the outputs and losses to gain a better understanding of the loss mechanisms. One of the major sources of losses in the system is the high local irradiance created by the parabolic reflectors. High local irradiance creates local hot spots which considerably reduce the electrical output. The losses are due partly to the elevated local temperatures and partly to the high local currents in the cells at the hot spots. The problems of high temperatures can be reduced considerably by using water cooled hybrid absorbers. The high local irradiance was one of the main problems addressed in this thesis due to the large resistive losses in the cells at high currents.

Another objective was to formulate accurate models for the optical efficiency of the concentrators to facilitate future feasibility studies on new concentrator types. This was addressed by measurements on full size prototypes, and by ray tracing simulations.

1.3 Outline

Chapter 2 gives an introduction to the theory of light concentration and the limits of concentration. Important concepts used in the literature such as étendue, conservation of phase space and skew rays are explained. The theoretical limits of two and three dimensional concentrators are derived using these concepts.

Design principles for concentrators are discussed in Chapter 3. The edge-ray principle is explained and used to derive ideal two-dimensional concentrators. The chapter describes existing two- and three-dimensional symmetrical concentrators such as the V-trough and the CPC. It also describes asymmetrical concentrators as well as truncated parabolic concentrators.

The equivalent circuit and one diode model are briefly discussed in Chapter 4. The effects of increasing temperature and non-uniform irradiation are discussed. These effects are an important part of the thesis as they are the two main sources of electrical losses in low concentrating systems.

Chapter 5 describes ray tracing, the optical simulation method used throughout the thesis to characterize the concentrators. A commercial ray tracing package was used to perform the simulations, and the benefits of using a commercial package instead of a problem specific program written by the author are discussed.

The different measurements that were conducted during the work on this thesis are described in Chapter 6. The method used to measure current-voltage characteristics, including short-circuit current, is explained. Another important measurement, the irradiation distribution over the cells in the concentrator, is also described.

Chapter 7 summarizes the findings of article I, characterization of the MaReCo hybrid with two different reflector materials. The two prototypes are compared from the aspects of short-circuit current, fill factor, current-voltage characteristics and irradiation distribution. The absorber angle and placement of PV cells are discussed. The chapter also presents annual output simulations of heat and electricity for the two prototypes.

A model for estimating the output of heat and electricity using measurements of the optical efficiency is presented in Chapter 8. The model is used to estimate the output of a wall integrated MaReCo and the estimates are compared with actual measurements of the electrical output. The reason that stationary concentrators are suitable for northern latitudes such as Sweden is discussed at the end of the chapter.

Article III is summarized in Chapter 9. It presents simulations on microstructured reflectors in a MaReCo concentrator. The structured reflectors have a homogenizing effect on the irradiation distribution on the absorber, as well as increasing the concentration ratio. The chapter discusses the expected changes to the annual output using the new reflectors and presents ideas on how to improve current concentrator designs.

Chapter 10 describes the author's contribution to articles IV-VIII, as well as other related work.

2 The optics of concentrating systems

2.1 Concentration ratio

The geometric concentration ratio of a concentrator system is defined as the ratio between the entry aperture and the exit aperture, or

$$C = \frac{A_1}{A_2} \qquad \text{Equation 2.1}$$

where A_1 is the area of the entry aperture and A_2 is the area of the exit aperture.

Concentrators can be divided into two groups, two dimensional concentrators (2D) and three dimensional concentrators (3D). Three dimensional concentrators such as the 3D Compound Parabolic Collector change all three direction vectors, direction cosines, of the incoming rays, and will typically concentrate the incoming irradiation to a spot. Two dimensional concentrators are symmetric around one axis, only two of the direction cosines are affected by the concentrator. The illumination profile from an axisymmetric concentrator is a line.

According to the laws of thermodynamics it is not possible to concentrate light infinitely, there is a theoretical upper limit for the concentration ratio. These limits are derived in the following sections.

I will use the concept of étendue, and the conservation of this quantity, to derive the maximum concentration ratio. The étendue of an optical system is a measure of the power transmitted along the beam, or the flux transfer. It is defined according to Equation 2.2, where a is the aperture area, n is the index of refraction of the media that the beam is passing through, and θ_{max} is the maximum extent of a beam that will still strike the exit aperture. Figure 2.1 shows the parameters of Equation 2.2.

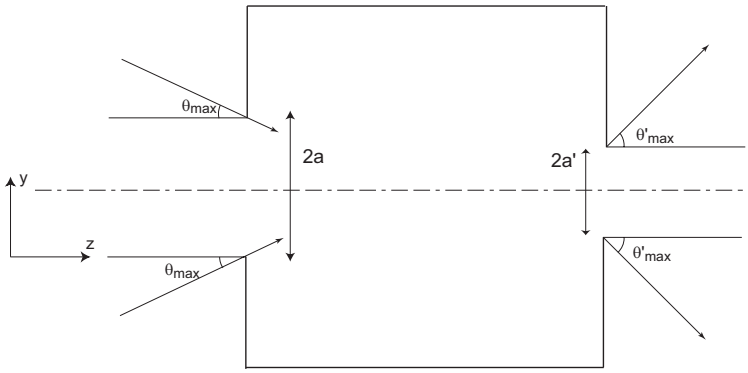

Figure 2.1 *Two dimensional concentrator modelled as a black box. The maximum angle of acceptance is θ_{max}.*

$$étendue = n^2 a^2 \theta_{max}^2 \qquad \text{Equation 2.2}$$

The étendue of an ideal, lossless, optical system is conserved at any point throughout the system (Winston et. al. 2005), i.e. the étendue of the entry aperture is equal to the étendue of the exit aperture, and this will be used in the derivation. Conservation of étendue means that the flux transmitted through the system is constant; if the entry beam is e.g. larger, the system will accept a smaller angular interval of the beam.

A ray of light in optics is defined by three position coordinates along the ray and by three direction coordinates (direction cosines) at this point. The phase space of an optical system consists of all possible rays that can exist in the system, i.e. all combinations of the six coordinates that describe possible rays in the system. The volume in phase space filled up by a light source is the extent of the source in three dimensions and the angular extent of the source. The magnitude of this six dimensional volume can never be increased in any optical system, but the shape of the volume can be arbitrary. This statement is equivalent to Equation 2.2, if e.g. the width of the beam of light is decreased, the angular extent, the three direction coordinates, will increase.

Changes in the phase space volume of the beam entering the system have to be compensated for by equal changes at the exit aperture, which results in Equation 2.3, where k_x and k_y are the direction cosines of the incident rays.

$$n^2 dxdydk_x dk_y = n'^2 dx' dy' dk_x' dk_y' \qquad \text{Equation 2.3}$$

The coordinate system at the exit aperture can be chosen arbitrarily without affecting the conservation (Winston et. al. 2005).

The concentration ratio will now be derived for the two dimensional case where the incident ray is unchanged in the x direction. Figure 2.1 models a two dimensional concentrator as a black box. It has an entry aperture of $2a$ and an exit aperture of $2a'$.

The system is axisymmetric in the x direction, and accepts light in the interval $-\theta_{max}$ to θ_{max}. The light exits the system with exit angles in the interval $-\theta'_{max}$ to θ'_{max}.
k_y will then be equal to

$$k_y = \sin(\theta)$$

and dk_y is equal to

$$dk_y = \cos(\theta)d\theta$$

The conserved quantity is then defined as

$$n\cos(\theta)dyd\theta = n'\cos(\theta')dy'\,d\theta'$$

integrating this expression results in

$$\int_0^{2a}\int_{-\theta_{\max}}^{\theta_{\max}} n\cos(\theta)dyd\theta = \int_0^{2a'}\int_{-\theta'_{\max}}^{\theta'_{\max}} n'\cos(\theta')dy'\,d\theta'$$

or, after integration

$$4an\sin(\theta_{\max}) = 4a'n'\sin(\theta'_{\max})$$

The concentration ratio is defined as the ratio between the entry aperture and the exit aperture, and we obtain

$$C = \frac{a}{a'} = \frac{n'\sin(\theta'_{\max})}{n\sin(\theta_{\max})}$$

This expression has its maximum when the exit angle is equal to 90°, and the maximum concentration ratio for a two dimensional concentrator is

$$C_{\max} = \frac{n'}{n\sin(\theta_{\max})} \qquad \text{Equation 2.4}$$

Consider the same black box model for a three dimensional system, with an entry aperture of A_1 and an exit aperture of A_2. The maximum angle of incidence is a cone with an angle of θ_{max}.

The direction cosines in this case are

$$k_x = \sin(\theta)\sin(\varphi)$$
$$k_y = \sin(\theta)\cos(\varphi)$$

where φ is the rotation angle around the z axis in the xy plane, and

$$dk_y dk_x = \cos(\theta)\sin(\theta)d\theta d\varphi$$

The conserved quantity for the three dimensional case is

$$n^2 \cos(\theta)\sin(\theta)dxdyd\theta d\varphi = n'^2 \cos(\theta')\sin(\theta')dx'\,dy'\,d\theta'\,d\varphi'$$

Integrating this expression, we get

$$n^2 A_1 \int_0^{2\pi}\int_0^{\theta_{\max}} \cos(\theta)\sin(\theta)d\theta d\varphi = 2\pi n^2 A_1 \frac{\sin^2(\theta_{\max})}{2} = \pi n'^2 A_2 \sin^2(\theta'_{\max})$$

The concentration ratio, as stated by Equation 2.1, will be

$$C = \frac{A_1}{A_2} = \frac{n'^2 \sin^2(\theta'_{\max})}{n^2 \sin^2(\theta_{\max})}$$

Again, maximum concentration ratio is obtained when the exit angle is 90°, and the maximum concentration ratio of a three dimensional system is

$$C_{\max} = \left(\frac{n'}{n\sin(\theta_{\max})}\right)^2 \qquad \text{Equation 2.5}$$

To obtain this maximum concentration is of course difficult in practice, it assumes no losses anywhere in the system, due either to manufacturing imperfections or losses due to non-ideal materials used in the system. But the derivation of the theoretical maximum concentration ratio shows two important points in designing concentrator systems. First of all, the smaller the angular interval of acceptance, the higher the concentration ratio, and secondly, it is important to have rays exiting at all angles up to 90° to get a high concentration ratio.

Another way to increase the concentration ratio is to use a dielectric medium with an index of refraction > 1 inside the concentrator. Due to the laws of refraction, the beam will be refracted to a smaller angle of incidence when the medium has a higher index of refraction than the surroundings. This makes it possible to accept light at a larger angular interval, an effect that can be utilized to decrease the acceptance angle of the system while still accepting the original angular interval. Figure 2.2 shows a concentrator filled with a dielectric material with index of refraction n', which could e.g. be low iron glass with n'=1.523 which in that case would increase the concentration ratio by 52% (Zacharopoulos et. al. 2000).

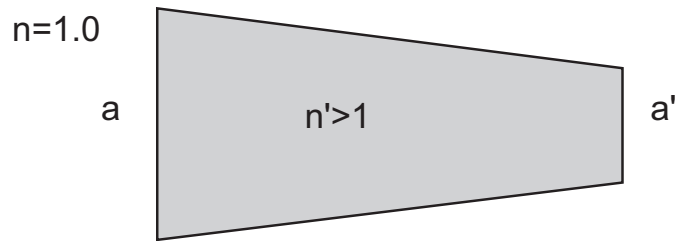

Figure 2.2 *Concentrator filled with low-iron glass for increasing the concentration ratio. Low iron glass has an index of refraction n′ of 1.523.*

There are several definitions of concentration ratio. The theoretical maximum concentration ratio is the ideal concentration ratio of a system. The geometrical concentration ratio is the ratio between the entry aperture size and the exit aperture size. If rays are traced through the system, the ratio between the number of rays at the entry aperture and the collected number of rays at the exit aperture is called the optical concentration ratio. Unless stated to the contrary, the geometrical concentration ratio will be the concentration ratio discussed throughout this thesis.

2.2 Skew rays

A skew ray is a ray that is not within any of the meridian planes of the system. The meridian planes are the three planes containing two axes in Figure 2.3.

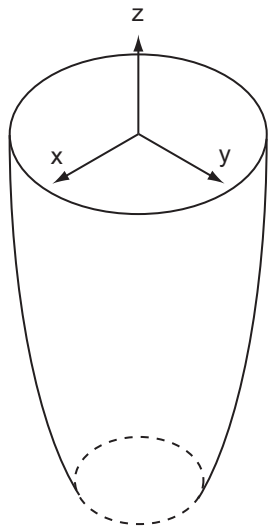

Figure 2.3 *The three meridian planes of a three dimensional concentrator are the planes containing two of the coordinate axes i.e. the xy-plane, the xz-plane, and the yz-plane.*

For a two dimensional system, e.g. one defined by the plane of the x and the z axis and axisymmetric in the y direction, a skew ray would be any ray with a non-zero y directional cosine, k_y. The k_y component will not influence where the ray will strike the exit aperture in the x direction. The optical performance of an axisymmetric two dimensional system is thus not affected by skew rays. For three dimensional concentrators there will always be rays out of the meridian planes as long as the incident light has a non-zero x or y component. This means that parallel rays that will strike the reflector at the same z coordinate in Figure 2.3 will be reflected in different directions due to the fact that the surface normals will be different. For the two dimensional case, parallel rays that strike one of the reflectors at the same z coordinate will have identical directional cosines after the reflection. As the analysis of the three dimensional concentrator is more complex, it is important that an analysis of skew rays is included in the study.

3 Design of concentrators for Solar Energy applications

3.1 Design - The edge-ray principle and the string method

I will first describe an important principle used in the design of ideal concentrators, the edge-ray principle. It can be shown that if a ray at the edge of the aperture, incident at the extreme angle of acceptance, is transported to the rim of the exit aperture, it is sufficient for transferring all the incident rays within the interval of acceptance to the exit aperture (Winston et. al. 2005). This is equivalent to saying that the phase space boundary of the beam is transported to the exit aperture. If this is achieved, we have produced an ideal concentrator.

The first problem discussed will be the two dimensional problem illustrated in Figure 3.1. Transporting the boundary of the phase space volume from *a* to *a'* is in this case identical to transporting all the light within an angle of $\pm\theta_{max}$ from aperture *a* to aperture *a'* since θ_{max} represents the boundary in directional space and the extent of the aperture represents the boundary in position space.

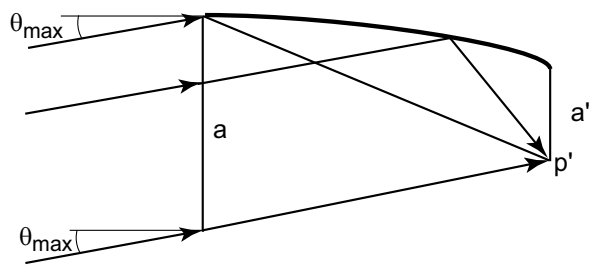

Figure 3.1 *Concentrator with flat absorber. All rays at the extreme angle θ_{max} emerge through the rim point p' of the exit aperture.*

The basis of the method is Fermat's principle which states that the optical path length between the object and the image in an image forming system is the same for all rays. If strings are used instead of rays, we get the edge-ray principle. The method will be explained by one example with a flat absorber and one example with a cylindrical absorber. The problem is to design an ideal 2-dimensional concentrator for a flat and a cylindrical absorber. First, the example with a flat absorber, the problem of Figure 3.1.

Figure 3.2 shows the solution to the problem using the string method for a flat absorber. A rod is placed at the aperture, and it is tilted θ_{max} from the horizontal, where θ_{max} is the maximum angle at which the system will accept rays. A string is tied to a ring that is put around the rod at one end, and fastened at the absorber at point *d*.

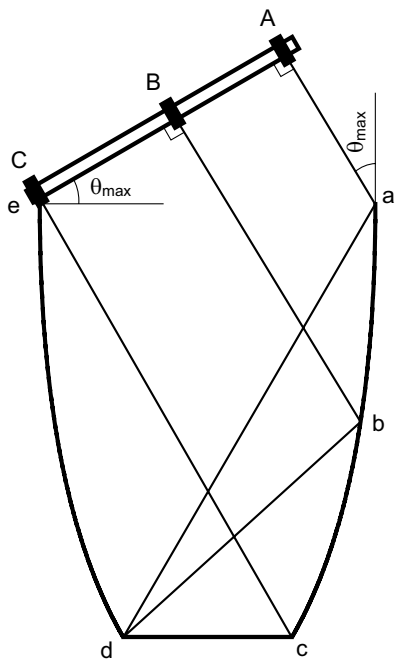

Figure 3.2 *String method for creating an ideal concentrator for a flat absorber. The ring at the end of the string is free to move along the rod from A to C.*

When the ring is placed at the end of the string at point *A*, the length of the string should be such that the string *Aad* is taut. The length of the string is now fixed and will keep this length through the whole design

process. A pen is now placed at *a*, which will be the first point of the reflector. The ring is now moved from *A* to *B* and the pencil is simultaneously moved from *a* to *c* in the figure while keeping the string taunt and the angle between the rod and the string at 90°. The pencil will then generate the shape of the reflector.

When the ring reaches point *C*, the pen will be at point *c*. When this method is applied to the flat absorber as shown here, the generated concentrator shape is a parabola with its focal point at *d*, and the optical axis parallel to *cC*. The optical term for this concentrator is CPC, Compound Parabolic Concentrator. It is discussed in more detail in Section 3.3.

Applying Fermat's principle of equal optical path lengths of the edge rays yields:

$$Cc + cd = ad + ea\sin(\theta_{\max})$$

Looking at the figure, we see that $Cc=ad$ and we get:

$$cd = ea\sin(\theta_{\max})$$

The concentration ratio is defined as the entry aperture divided by the exit aperture:

$$C = \frac{ea}{cd} = \frac{ea}{ea\sin(\theta_{\max})} = \frac{1}{\sin(\theta_{\max})}$$

This proves that the new concentrator is indeed ideal.

Figure 3.3 shows an example with a cylindrical absorber such as e.g. a vacuum tube for heat collection. The edge ray principle generalized for non plane absorbers states that all rays incident at θ_{max} should be reflected once and strike the circular pipe tangentially to its surface. All rays with a smaller angle of incidence will then reach the cylinder at an angle of less than 90° with the surface normal.

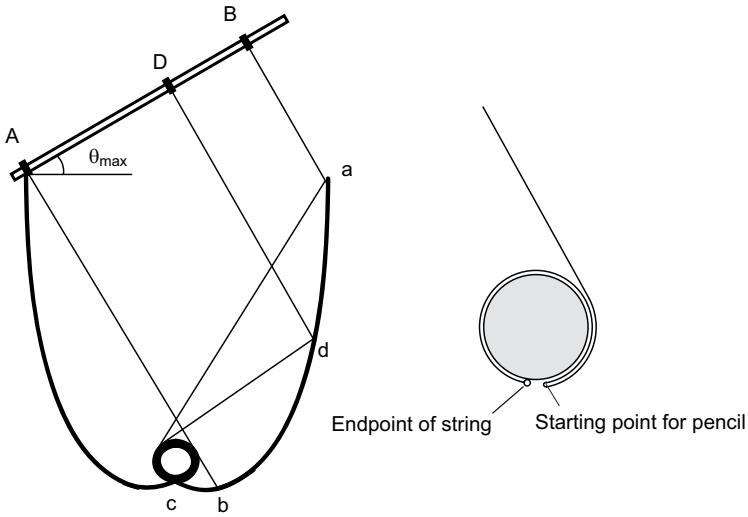

Figure 3.3 *String method for construction of an ideal concentrator for a cylindrical absorber. The reflector is plotted when the ring is moved from A to B.*

The rod is placed in the same way as in the example of the flat absorber, but the string is in this case fastened at point *c*. The loop of the string is placed at point *A*, and it is wound around the absorber as shown to the right in the figure. The length is adjusted as in the previous example. The pen is placed at point *c*, and the string is kept stretched as the pen is moved from *c* to *b*. When the pen reaches *b*, the loop of the string is moved slowly from *A* to *B*, keeping the pen in a position to keep the string stretched and at right angles to the rod. The resulting geometry is an involute from *c* to *b*, and the rest of the mirror from *b* to *a* is at each point sloped to reflect the ray incident at θ_{max} onto the tangent of the absorber.

The constructed geometries for both the flat and for the circular absorber are ideal and fulfil the theoretical maximum concentration ratio $1/\sin\theta_{max}$, since all the light incident at angles less than θ_{max} will be absorbed in a system without optical losses or imperfections.

3.2 The light cone concentrator and the V-trough

One of the first three dimensional concentrator systems used for the collection of light was the light cone (Williamson 1952). Figure 3.4 shows a cross section of a cone concentrator.

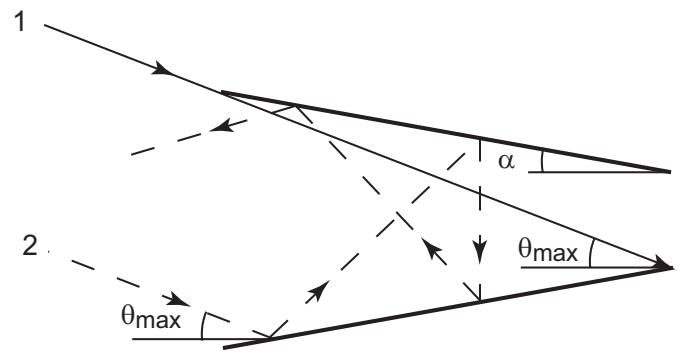

Figure 3.4 *Cross section of a light cone concentrator. Some of the rays incident at angle θ_{max} are turned back instead of striking the exit aperture.*

The design is straightforward, it is formed by mirrors mounted at an angle α and rotated around the axis of symmetry. This makes the manufacture of the concentrator simple. The length of the concentrator should be such as to make ray 1 in Figure 3.4 incident at the desired extreme angle θ_{max} strike the edge of the exit aperture. Given a certain exit aperture, this results in an expression for the length of the concentrator. As can be seen in the figure, some of the rays incident at the same angle, such as ray 2, are reflected out of the system. For skew rays, rays out of the symmetry planes, the fraction of rays reflected out is even larger.

The two dimensional version of the cone concentrator is the V-trough. It consist of plane mirrors mounted as in the cross section shown in Figure 3.4. Due to the symmetry of the V-trough, the skew rays are not a problem, but the problem shown in Figure 3.4 still exists.

The cone concentrator and V-trough are clearly not ideal as some light is discarded, but if the shape of the reflectors could be changed for the system to accept ray 2 and skew rays, they would approach ideal concentration. This leads to the development of the compound parabolic concentrator that will be discussed in the next section.

3.3 Two dimensional compound parabolic concentrators

When the edge-ray principle is applied to the flat absorber case as was done in Section 3.1, the result is the two dimensional CPC shown in Figure 3.2. This concentrator achieves the maximum theoretical concentration ratio.

A parabolic mirror will reflect all the light incident along the optical axis to its focal point. Light which falls in at a positive angle of incidence will be reflected below the focus and light from negative angles will be reflected above the focus. This is illustrated in Figure 3.5.

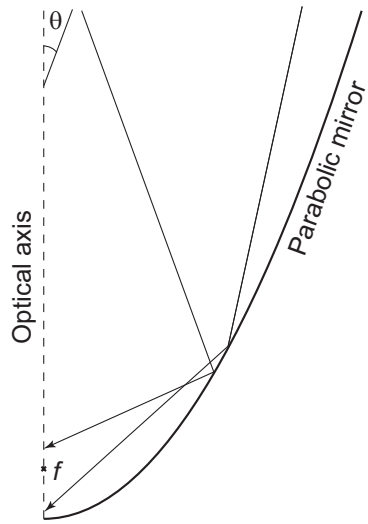

Figure 3.5 *Parabolic mirror with its optical axis drawn as a dashed line. The focal point is indicated by f. The angle of incidence θ is positive clockwise.*

The concentrator is constructed by tilting the parabola in order to make the optical axis parallel to the angle of the extreme rays. If, for example, the CPC is supposed to accept rays at 20°, the parabola is tilted 20°. This is shown in Figure 3.6.

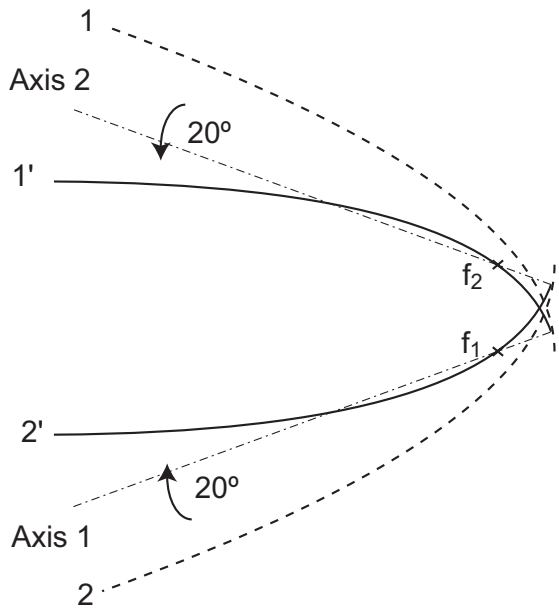

Figure 3.6 *Construction of a CPC with an acceptance angle of 20°. The original parabolas are rotated 20° from 1 to 1' and from 2 to 2'.*

The CPC in Figure 3.6 has an acceptance angle of 20°. Parabolas 1 and 1' have their focus at f_1 and parabola 2 and 2' have their focus at f_2. The absorber will cover the area between f_1 and f_2. The original parabolas are drawn with dashed lines. The parabolas are identical, but mirrored and displaced a distance of 2*a*' from each other. 2*a*' is the absorber area. The optical axis of both original parabolas is horizontal in the figure. To construct the CPC, the parabolas are rotated to the angle of acceptance, in this case 20°, around their respective focal point. This is how parabolas 1' and 2' are obtained. The resulting optical axes are drawn in the figure. The parabolas are cut off at the focal point of the parabola. Light at angles larger than the angle of acceptance will be reflected from one of the mirrors to the other mirror and out of the system. Light incident at smaller angles will strike the absorber at a point between the focal point and the mirror.

A mathematical description of the CPC in polar coordinates is defined according to Equation 3.1 (Winston et. al. 2005). The parameters in the equations are shown in Figure 3.7.

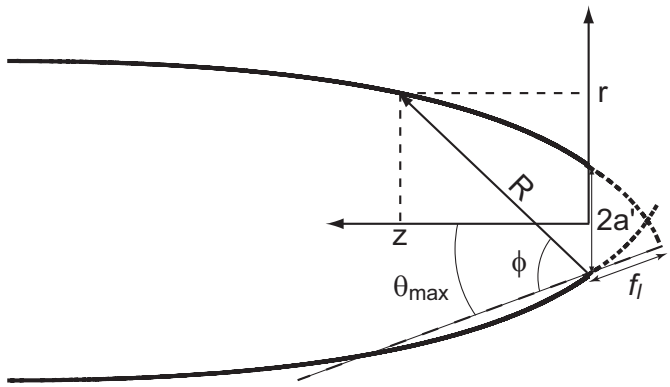

Figure 3.7 *Construction of a two dimensional CPC. The focal length of the upper parabola is indicated by f_l. The dashed parts of the parabolas are cut off to form the CPC.*

$$
\begin{aligned}
R &= \frac{2f_l}{1-\cos(\phi)} \\
r &= R\sin(\phi-\theta_{\max})-a' = \frac{2f_l\sin(\phi-\theta_{\max})}{1-\cos\phi}-a' \\
z &= R\cos(\phi-\theta_{\max}) = \frac{2f_l\cos(\phi-\theta_{\max})}{1-\cos\phi} \\
f_l &= a'\left(1-\cos(90+\theta_{\max})\right) = a'\left(1+\sin\theta_{\max}\right) \\
2a' &= \frac{2f_l}{1-\cos(90+\theta_{\max})}
\end{aligned}
$$

Equation 3.1

f_l is the focal length of the parabolas.

The two dimensional CPC is an ideal concentrator with a concentration ratio of $1/\sin\theta_{max}$. It is ideal since all the light incident at angles less than the angle of acceptance will arrive at the absorber, and it satisfies Equation 2.4.

Due to the translational symmetry of the trough system, the direction component of the rays parallel to the translational axis of symmetry does not influence where the ray will strike the absorber in the r-direction. This is determined by the two components in the plane of the paper in Figure 3.6. As can be seen in Figure 3.6 and Figure 3.7, the CPC is deep in comparison with the width of the absorber, something that is both

impractical and costly when the concentrator is manufactured. Increasing the concentration ratio is equal to reducing the angle of acceptance, and this will result in a considerably deeper trough.

Truncating the trough will not have a large impact on the entry aperture, if e.g. the leftmost third of the length of the trough of Figure 3.6 were truncated it would only reduce the aperture area by 3%. Studies on truncation have been made by e.g. (Winston and Hinterberger 1975) and (Rabl 1976).

As the maximum concentration ratio is $n/\sin\theta_{max}$ it is possible to increase the concentration ratio by filling the trough with a dielectric, preferably with an index of refraction greater than $\sqrt{2}$ (Winston et. al. 2005). In principle, the concentration ratio is increased when the index of refraction is greater than unity, but the benefit of having an index of refraction greater than $\sqrt{2}$ is that total internal reflection will occur in each reflection. This means a concentrator without reflectors can be constructed, something that will significantly increase the flux throughput of the system as there will be no reflection losses.

3.4 Wedge type CPCs

Figure 3.8 shows a CPC of wedge type. The parabolic mirrors have identical parameters and share the same focal point.

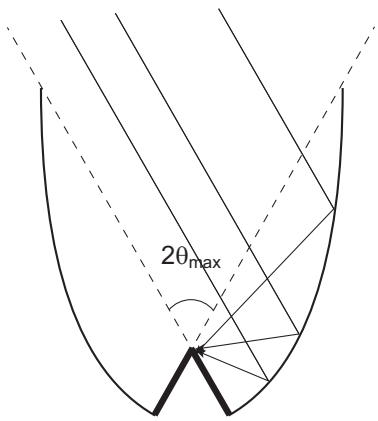

Figure 3.8 *CPC of wedge type. Both mirrors have the same focal point on the top of the absorbers.*

The absorber is mounted from the focal point to the reflector along the optical axis of the parabola. When the light is incident along the optical axis, at an angle of incidence of θ_{max} with the normal of the aperture as shown in the figure, all the light is concentrated to the focal point. When the angle of incidence is less than θ_{max}, the light is focused at the absorber below the focal point. This two dimensional concentrator is ideal, the concentration ratio is $1/\sin(\theta_{max})$.

3.5 Three dimensional compound parabolic concentrators

The three dimensional CPC is constructed by rotating the two dimensional CPC around the z axis of Figure 3.7. All the rays incident in the meridian plane will be collected at the exit aperture, just as was the case for the two dimensional CPC. But the three dimensional CPC is not an ideal concentrator since some of the skew rays outside the meridian plane, but inside the angle of acceptance, are reflected back out of the concentrator instead of being collected at the aperture.

The three dimensional CPC can be described mathematically in polar coordinates with z as described by Equation 3.1 but with r replaced by x and y according to Equation 3.2.

$$x = \frac{2 f_l \sin\psi \sin(\phi - \theta_{\max})}{1 - \cos\phi} - a' \sin\psi$$
$$y = \frac{2 f_l \cos\psi \sin(\phi - \theta_{\max})}{1 - \cos\phi} - a' \cos\psi \qquad \text{Equation 3.2}$$

ψ in Equation 3.2 is the azimuth angle introduced to account for the rotation of the two dimensional system.

Since the three dimensional CPC is not ideal, it is interesting to find ways to improve the performance of the concentrator. One option is to fill it with a dielectric material with an index of refraction greater than 1 as was discussed in the previous section about two dimensional CPCs. However, the volume of a three dimensional CPC is large, and the cost of manufacturing the concentrator increases significantly when it is filled with a dielectric material.

One solution to this problem is to make a small CPC and introduce it at the exit aperture of a concentrator filled with air and use the CPC as a secondary concentrator. This will increase the concentration ratio of all non-ideal concentrators, or increase the interval of acceptance of any

concentrator. The small size of the secondary CPC, due to the fact that the size of the entry aperture of this CPC is the same as the exit aperture of the first concentrator, solves the problem of high manufacturing cost for the full size CPC. In theory, this two stage system makes it possible to approach the theoretical limit of $n^2/\sin^2(\theta_{max})$. The three dimensional CPC is mostly used in solar tracking applications where a very high irradiation level at the exit aperture is desired e.g. in parabolic dish systems.

3.6 Asymmetrical CPCs

The yearly irradiation at different angles outside the atmosphere is symmetrical over the year with peaks at the summer and winter solstices. The incidence angles of the peaks differ depending on the latitude, and at northern latitudes the solar altitude of the winter peak is close to the horizon. This, in combination with a large cloud cover, reduces the winter peak considerably which makes the yearly irradiation asymmetrical with just one peak in the summer (Rönnelid and Karlsson 1997). This can be seen from Figure 3.9 that shows the annual direct irradiance projected onto the meridian plane for two sites, Lund, lat. 55.72° and Sydney, lat. -33.92°.

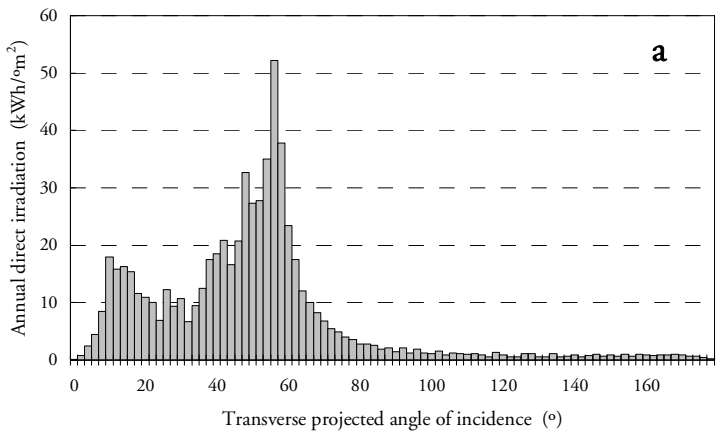

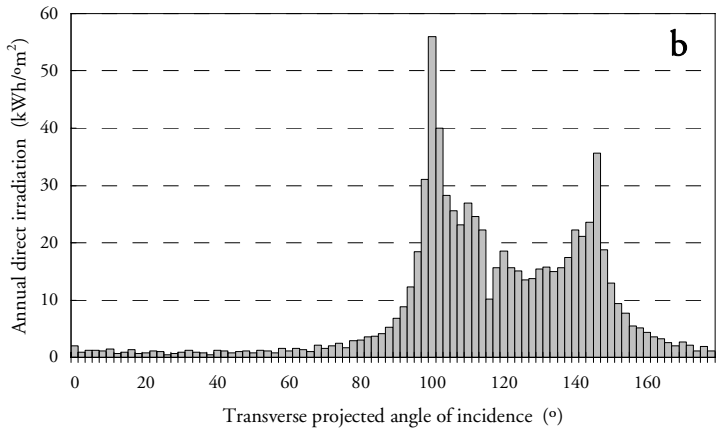

Figure 3.9 *Annual direct irradiation distribution in Lund (a) and in Sydney (b) on a surface facing south. The winter peak in Lund is suppressed. Both peaks are visible in Sydney.*

The fact that there is only one main peak at northern latitudes such as Lund makes it possible to use stationary concentrators that will collect most of the light without tracking the sun.

Figure 3.10 shows an example of an asymmetrical CPC that accepts all light incident between 10° and 60° from the horizontal.

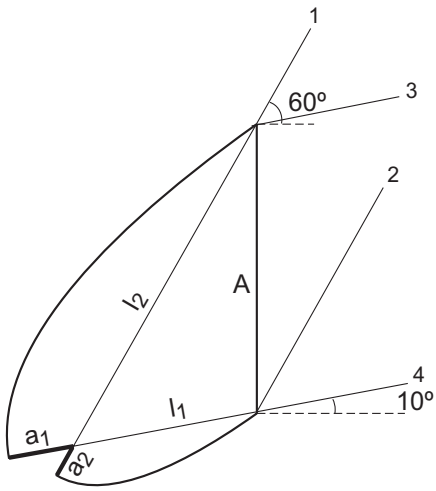

Figure 3.10 *Asymmetrical CPC with acceptance angles 10° and 60°.*

The concentration ratio of an asymmetrical CPC is different from the symmetrical CPC as the interval of acceptance is asymmetrical around the normal to the aperture. The concentration ratio of an ideal asymmetrical CPC is defined by Equation 3.3. Note that the angle is positive for both the upper and lower limit in Figure 3.10.

$$C_{\max} = \frac{2}{\sin(\theta_1) - \sin(\theta_2)} \qquad \text{Equation 3.3}$$

It can be derived using Fermat's principle which states that the path length of ray 1 and ray 2 has to be equal, and the same applies to the path length of ray 3 and ray 4. For ray 1 and ray 2 this leads to:

$$l_1 + a_2 = l_2 - a_1 + A\sin 60$$

For ray 3 and ray 4 the equation is:

$$l_1 - a_2 = l_2 + a_1 + A\sin 10$$

Subtracting the two equations yields

$$2a_2 = A\sin 60 - A\sin 10 - 2a_1$$

$$2(a_1 + a_2) = A(\sin 60 - \sin 10)$$

$$C = \frac{A}{a_1 + a_2} \Rightarrow C = \frac{2}{\sin 60 - \sin 10} = 2.89$$

The maximum flux concentration of an asymmetrical CPC is $2/\tan(\theta_{max}/2)$ (Mills and Giutronich 1978) where θ_{max} is the interval of acceptance. The interval of acceptance is in the example of Figure 3.10 equal to 60°-10°=50° and the maximum flux concentration is thus 2/(tan(50/2))=4.29. This occurs at the extreme angles of incidence 10° and 60°. The maximum limit can only be obtained if the absorber is placed along the optical axis of the parabola, it will be lower in all other cases.

3.7 Asymmetrically truncated CPCs

Figure 3.11 shows an example of a stationary, asymmetrically truncated wedge CPC, the MaReCo (MaximumReflectorCollector) which is designed to be placed on a horizontal surface. It is symmetrical in the sense that both parabolic mirrors have the same focal length and focal point, indicated by *f* in the figure. However, it is truncated asymmetrically to collect as much irradiation as possible per reflector area at Swedish latitudes (Rönnelid and Karlsson 2003). Another change from the classic wedge CPC is that one of the absorbers has been removed and the remaining one has been designed to accept irradiation on both sides. The irradiation will reach the absorber on both sides due to the circular section inserted between the endpoints of the two parabolas, indicated by *B* and *C* in the figure. The circular section will always reflect all incoming irradiation onto the absorber.

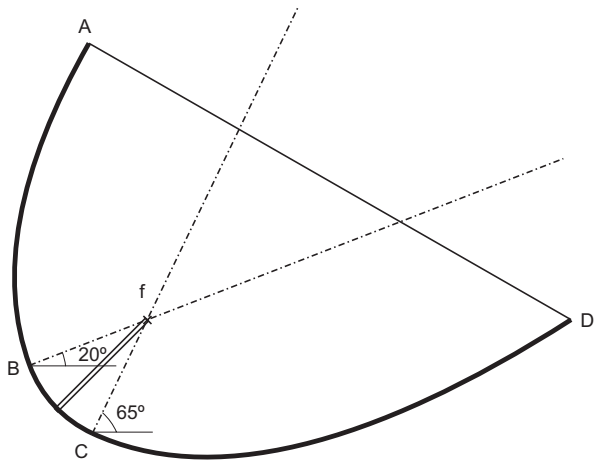

Figure 3.11 *Stand-alone MaReCo, a stationary asymmetrically truncated wedge CPC. Both parabolas have a common focal point in f. The acceptance interval is between 20° and 65°.*

As the yearly irradiation is incident in an asymmetric angular interval, where most of the light arrives in the summer at high solar altitudes, the front reflector is larger than the back reflector to collect as much annual irradiation as possible. A system such as this collects all the light incident between a solar altitude of 20° and 65° i.e. the tilt of the back and front reflector. Depending on the angles at which the irradiance maxima oc-

cur, and the way the irradiation is distributed during the year at different latitudes, the length and the tilt of the reflectors will change and create other asymmetrical forms.

As the concentrator is ideal before truncation, the concentration ratio should be $1/\sin(\theta_{max})=1/\sin((65-20)/2)=2.61$ but due to the truncation, the geometrical concentration ratio is 2.20.

One interesting option is to remove one of the reflectors. If the back reflector is removed it is possible to make a concentrator that works well for high solar altitudes. If the front reflector is removed, it is possible to integrate the concentrator into a façade without using too much space. As less irradiation is incident on a vertical surface than on a horizontal surface, the back reflector collects less light but this could in many cases be compensated for by the fact that it is easy to integrate into a building. Figure 3.12 shows an asymmetric concentrator where the front reflector has been removed and the absorber has been turned slightly.

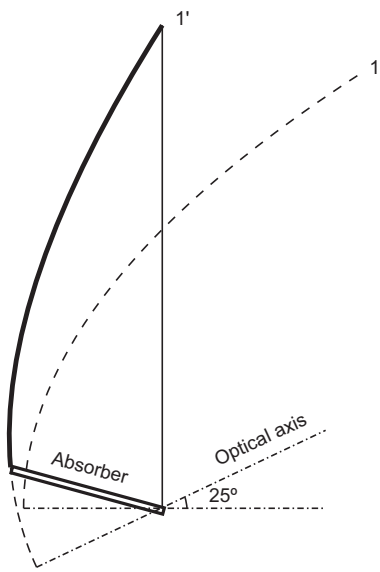

Figure 3.12 *Back reflector concentrator for wall integration. The parabola is tilted 25°, which is the lower acceptance limit of the concentrator.*

As can be seen in the figure, the parabola has been rotated 25° which means that the system accepts irradiation at solar altitudes above 25°. This example is easy to fit into a wall element due to its small width compared with its height.

4 Solar cells

4.1 Basic principles

A solar cell is often represented by an equivalent circuit, which is shown in Figure 4.1.

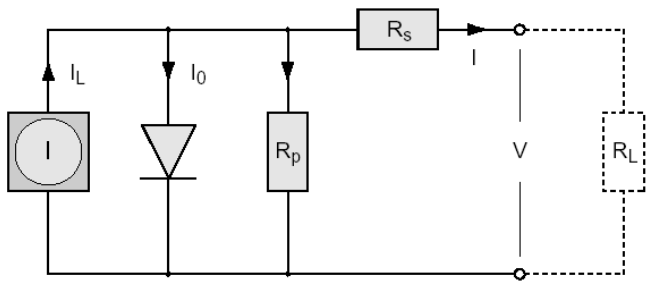

Figure 4.1 *Equivalent circuit representing a solar cell. The incident light generates a current I_L.*

The current, *I,* is then

$$I = I_L - I_0\left(e^{\frac{q(V+IR_s)}{nkT}} - 1\right) - \frac{V + IR_s}{R_P} \qquad \text{Equation 4.1}$$

where I_L is the light generated current of the cell, R_P the shunt resistance, and R_S the series resistance.

The series resistance R_S represents the bulk resistance of the semiconductor material, the resistance of the metallic contacts and interconnections and the resistance between the semiconductor and the contacts. The shunt resistance R_P represents the impurities and defects around the PN-junction of the cell.

4.2 Effects of increasing temperature

The band gap of the semiconductor material will decrease when the temperature increases. When the band gap is decreased, more photons will have enough energy to excite an electron to the conduction band, and a larger part of the light spectrum can be utilized. This will lead to an increasing short-circuit current. A commonly used value for silicon is an increase of 0.06%/K.

When the temperature is increased, more and more electrons and holes move freely in the material since the increased energy makes it easier to move between the conduction band and the valence band. This increases the recombination rate, and as the open-circuit voltage V_{OC} is limited by the recombination rate, V_{OC} decreases (Wenham, Green, and Watt). The decrease is approximately -0.3%/K for silicon cells.

The fill factor *FF* is to the first order only a function of the open-circuit voltage and it decreases as V_{OC} decreases with increasing temperature. FF decreases by -0.15%/K for a standard silicon cell.

The efficiency η_{cell} is proportional to $I_{SC} \cdot V_{OC} \cdot FF$ and this results in a decrease in the efficiency by -0.4%/K. It is therefore of great importance to keep the cells as cold as possible, especially in concentrator systems where the temperatures can be high if cooling is not taken into account when designing the system.

4.3 Effects of non-uniform illumination

A parabolic mirror will focus all the incident light to its focal point if the light is incident along the optical axis of the parabola. This is the reason for the non-uniform irradiation distribution on the cells of concentrators based on parabolic mirrors. Figure 4.2 shows an example of the irradiation distribution measured in a MaReCo concentrator.

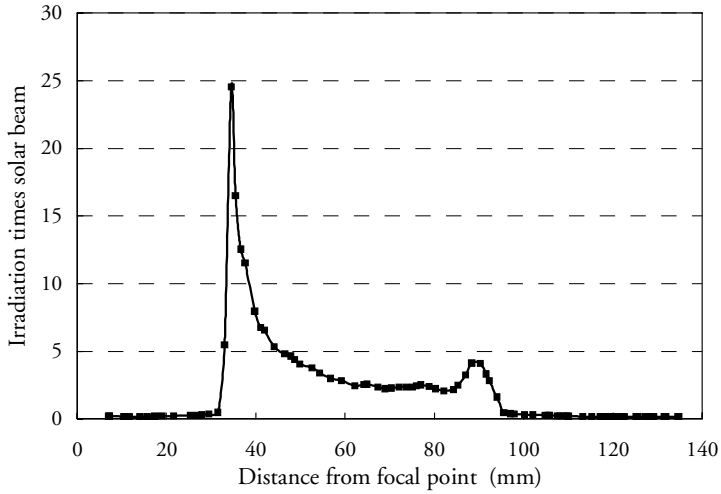

Figure 4.2 *Light distribution on a cell in the MaReCo concentrator. The absorber has a width of 143 mm. The distance on the x-axis is measured from the focal point at the top of the absorber.*

As can be seen in the figure, the intensity peaks at 25 times the solar beam.

The short-circuit current increases linearly and the open-circuit voltage increases logarithmically with increasing intensity. I_{SC} is a linear function of the light generated current I_L which is proportional to the photon flux incident on the cell. V_{OC} is proportional to $\ln(I_L)$. In principle, this shows that increased irradiance increases the efficiency of solar cells. However, the high local currents in part of the cell created by the peak intensity generate resistive losses in the cell. The internal losses in the cell are proportional to the square of the current, RI^2, and the output power of the cell is proportional to VI, i.e. Iln(I)- RI^2. Figure 4.3 shows a typical example of the relationship between cell efficiency and light intensity of a solar cell.

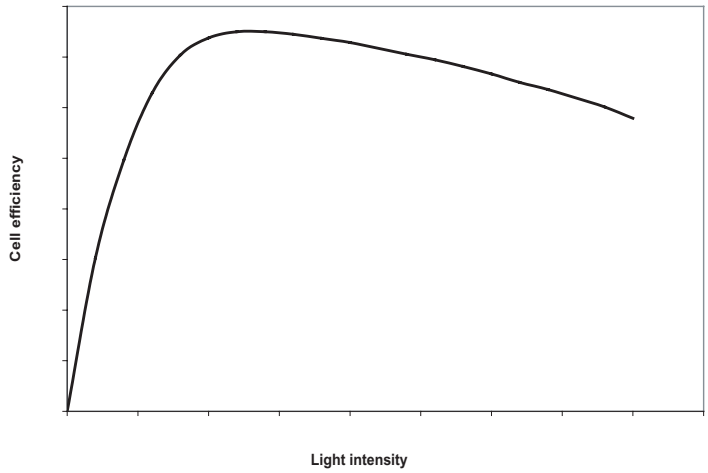

Figure 4.3 *Sketch showing the cell efficiency as a function of the incident irradiation.*

The efficiency increases at low intensities as the resistive losses are small. At some point, the increase in resistive losses is equal to the efficiency increase due to the light generated current. That is the optimum intensity for this particular solar cell. As the intensity continues to increase, the resistive losses increase more than the delivered power and the efficiency drops. Standard photovoltaic cells have a relatively high series resistance and the efficiency will start to decrease at low intensities, the optimum intensity is less than two suns. Calculations based on Equation 4.1 suggest that the efficiency of a standard cell will drop 14% when the irradiation is 4 suns

The optimum will move to higher light intensities if R_S is reduced. This is obtained in concentrator cells by decreasing the spacing between the conducting fingers, using a low resistance substrate for the cell and introducing a back surface field (highly doped back substrate). This will lower the bulk and contact resistance. Using techniques like these makes it possible to manufacture cells optimized for several hundred suns.

5 Monte Carlo ray tracing

The concept used when analysing and designing optical systems is called geometrical optics. It studies the path of a ray of light as it traverses the optical system.

A ray of light travels through the system and the path of the ray is defined by the origin of the ray and the reflections and refractions along the path to the exit aperture. Irradiation incident on the system follows the path of the ray which makes the concept useful for understanding the characteristics of the optical system.

When it strikes a surface, the ray can be reflected, absorbed, or transmitted. The law of reflection states that the angle between the surface normal and the entering ray is equal to the angle between the surface normal and the exiting ray. For refraction, the expression is different since it involves the relative speed of light in the new material. Figure 5.1 shows the relation between the ray incident on the surface and the ray leaving the surface for both reflection and refraction.

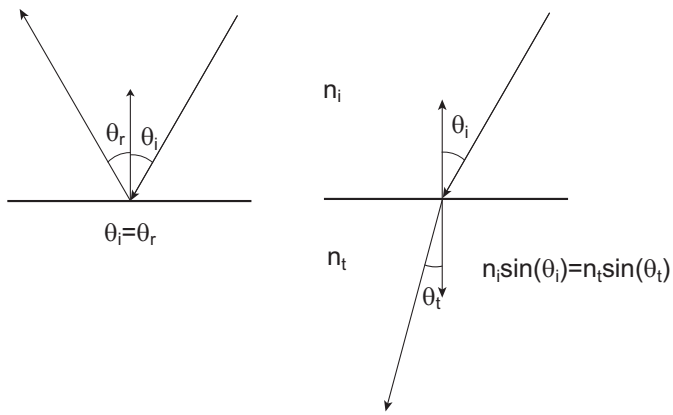

Figure 5.1 *The laws of reflection and refraction. The rays are refracted towards the normal if $n_t > n_i$.*

Monte Carlo ray tracing is the process of using the principles of geometrical optics as a statistical method to get a complete and statistically viable analysis of an optical system. The method will be briefly described in the following section.

In three dimensional ray tracing it is necessary to formulate the equations of geometrical optics in vector form, which has been done in Equation 5.1. The geometrical proof can be seen in Figure 5.2.

$$\mathbf{r_r} = \mathbf{r_i} - 2(\mathbf{n} \cdot \mathbf{r_i})\mathbf{n} \qquad \text{Equation 5.1}$$

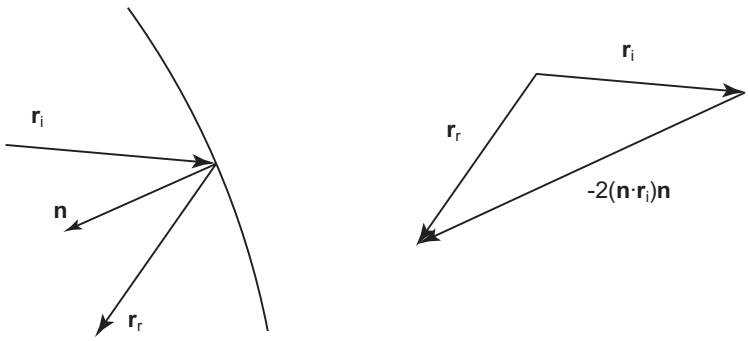

Figure 5.2 *Vector formulation of the law of reflection.*

In the process of tracing one ray, the starting point is randomized within a certain start area or volume, the *source* of the rays. Depending on the properties of the source, the direction of the ray can be either the same for all rays or randomized in a pattern defined by the source. It could for example be a Gaussian source or a completely diffuse source. The next step is to find the first intersection between the ray and the optical system. It is calculated knowing the origin and the direction of the ray, as well as the geometry of the traced object. At the point of intersection, the surface normal is determined in order to calculate the direction of the ray after interaction with the system. The ray could be reflected, refracted and/or absorbed. When the new direction of the ray/rays has been calculated, the next intersection is calculated. This process continues until either the ray is lost from the system, completely absorbed, or intersects with the *target* that detects the ray.

The resolution of the detector is an important parameter in the simulation as it is closely connected to the number of rays that has to be traced to obtain a certain statistical accuracy.

The number of rays that needs to hit the detector is calculated according to Equation 5.2:

$$NumberOfRays = \frac{NumberOfPixels}{Accuracy^2}$$ Equation 5.2

If e.g. the detector has 10 pixels and the desired accuracy at the detector is 1% then the number of rays hitting the detector has to be $10/0.01^2$=100 000 rays.

The ray tracing simulations presented in this thesis have been performed using ZEMAX (ZEMAX 2005), a commercial ray tracing package. The two main benefits in using a commercial software compared with a problem specific Matlab program are that it is easier to simulate different kinds of systems with different characteristics and that the commercial package is well tested and documented. A well tested software can be trusted to give good results as long as the inputs are verified. To go through this process of verification for a new Matlab program is very time consuming. A commercial ray tracing package is generic in the sense that most of the parameters can be changed easily. As it is not made for a specific system or geometry, most geometries can be evaluated. It also has numerous libraries of sources, ways to display output data etc.

6 Measurements

6.1 IV characteristics and fill factor

The performance of a photovoltaic cell can be characterised by its current-voltage (IV) characteristic.It describes the relationship between the current extracted from a photovoltaic cell and the voltage over the cell as the resistive load connected to the cell changes. The IV characteristics of PV cells in a concentrator are highly dependent on the concentrator. It is influenced both by the total irradiation on the cells and on how the light is distributed over the cells. If the concentrator is to be used for photovoltaic applications it is important to measure these characteristics in the concentrator to be able to estimate the efficiency of the complete system.

An electronic load controlled by a data logger was constructed for the measurements. The electronic load is described in more in detail in Appendix A. The data logger sent control signals to the electronic load that was connected to the cells. The load was able to vary the voltage over the cells from 0 to V_{OC} in approximately 100 ms. The current and voltage over the cells were measured simultaneously with a CR-10 data logger from Campbell Scientific. 9 current and voltage pairs were measured in each measurement. The points were not evenly distributed between 0 and V_{OC}, the majority of the points were taken around the maximum power point. The maximum power point was calculated through a parabolic fit to the three points closest to the maximum power point. Figure 6.1 shows an example of a measured IV-characteristic.

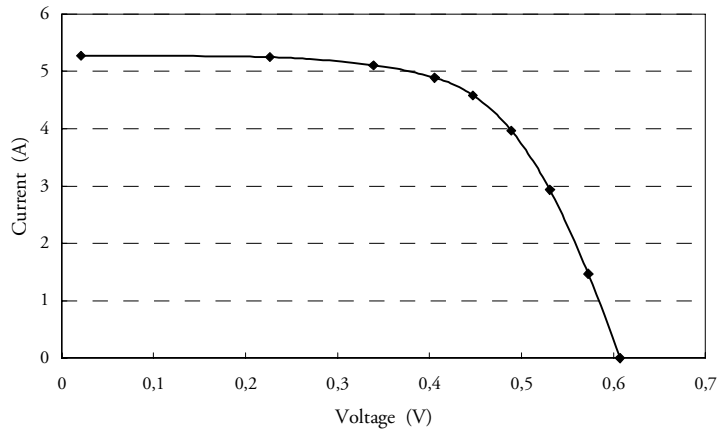

Figure 6.1 Measured IV-characteristic for one cell.

Since the short circuit current is proportional to the irradiation, it is important to measure the incident irradiation during the measurements. The irradiation was measured using a pyranometer from Kipp & Zonen. The surface of the pyranometer was mounted normal to the sun.

The efficiency of the cells is proportional to the fill factor, which is calculated at the maximum power point. A high fill factor translates to a high efficiency. The fill factor was calculated according to Equation 6.1 where I_{SC} is the short-circuit current, V_{OC} is the open circuit voltage and P_{max} is the power at the maximum power point.

$$FF = \frac{P_{max}}{I_{SC} \cdot V_{OC}} \qquad \text{Equation 6.1}$$

Figure 6.2 shows typical current voltage characteristics of one cell with a high fill factor and one cell with a low fill factor.

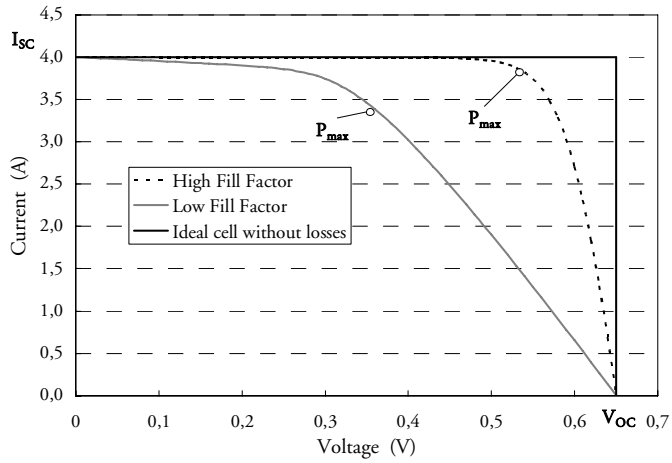

Figure 6.2 *Current-voltage characteristics for two photovoltaic cells. The full line shows an ideal cell without losses. The short-circuit current, open circuit voltage, and the maximum power point are indicated.*

The fill factor for the dashed curve is 0.79 and the fill factor for the curve labelled Low Fill Factor is 0.47. The fill factor of the cells in a concentrator is highly dependent on how the light is distributed on the cells, high irradiation levels on small parts of the cell reduce the fill factor considerably. Since the efficiency of the system is proportional to the fill factor, it is important to monitor the fill factor of the PV cells in a parabolic concentrator.

The fill factor was calculated using the current voltage characteristics and the parabolic fit for the maximum power point.

6.2 Optical efficiency

The photovoltaic cells used in the measurements were CIGS thin film cells, polycrystalline silicon cells, or monocrystalline silicon cells.

The short-circuit current of the used photovoltaic cells is independent of the illumination distribution on the cell as long as the strip of light is not very narrow (< 1 mm) (McMahon and von Roedern 1997). Because of the divergence of 0.28° for the solar beam, and the manufacturing precision of the troughs, the concentrated strip of light has a width of 1 cm at maximum concentration. This is sufficient for the short-circuit current to be independent of the irradiation distribution.

The short-circuit current increases with the temperature by approximately 0.06%/K (Wenham, Green and Watt). In view of other errors in the measurements, this increase can be neglected for the small temperature increases of the low concentration systems measured.

Since the short-circuit current of a photovoltaic module in a concentrating system, at a constant temperature, depends only on the irradiance on the module, which is determined solely by the optical efficiency of the concentrator, measurements of the short-circuit current as a function of the angle of incidence can be used to determine the optical efficiency of the concentrator system if it is compared with the short-circuit current of a reference module. The reference cells should be identical to the cells used in the concentrator.

The optical efficiency was measured using two different techniques, one that can be used at all times of the year, and one that is used around the spring or fall equinox. Both methods will be described in the following sections.

In the first method, the concentrator was placed with the sun in the meridian plane. The transverse projected angle of incidence was varied by rotating the concentrator trough. The concentrator remained in the meridian plane during the entire measurement since the whole measurement was finished in approximately 5 minutes. The setup is described by Figure 6.3.

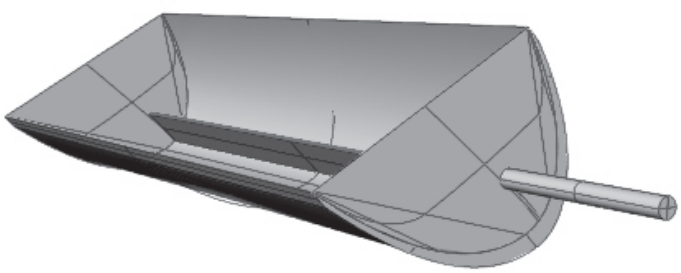

Figure 6.3 *Concentrator trough for measurement of the optical efficiency. The axis attached to the side of the trough is used to measure the rotation of the concentrator.*

As can be seen in the figure, an axis was mounted on the gable of the trough at the focal point of the two parabolic mirrors. Between the trough and the axis there was a potentiometer that recorded the rotation of the

trough as the axis was fixed at the right end in the figure. The trough was rotated around the axis with the sun in a fixed position in the meridian plane, which made it possible to measure at all transverse angles of incidence. The short circuit current was measured by a data logger that simultaneously recorded the insolation using a pyranometer mounted normal to the sun. The data logger and the pyranometer were the same as those used in the current-voltage measurements.

A graduated arc was mounted on the side of the trough for manual measurement of the transverse angle of incidence . The maximum and minimum angles of incidence were measured with both the graduated arc and the potentiometer at the beginning of each measurement. These values were used to convert the voltage over the potentiometer into the true angle of incidence in the meridian plane.

Using the measurements of the short-circuit current, the optical efficiency of the system was calculated according to Equation 6.2.

$$\eta_{opt}(\theta_T) = \frac{I_{sc} \cdot 1000}{I_{1000} \cdot C_g \cdot G \cdot \cos(\theta_T - \beta)} \qquad \text{Equation 6.2}$$

I_{1000} is the short circuit current at an irradiance of 1000 W/m^2 on the reference module, which in this case was 4.55 A. C_g is the geometrical concentration of the concentrator system defined as the glazed aperture area divided by the cell area. θ_T is the transverse projected angle of incidence, and G is the total intensity normal to the sun. To get the efficiency relative to the incoming irradiation, the expression was divided by C_g. $G(\cos(\theta_T - \beta))$ is the irradiance on the glazing, where β is the tilt of the aperture normal relative to a horizontal surface. The measurements were performed on very clear days with a low fraction of diffuse irradiation, and the total irradiation was treated as a beam irradiation incident at the incidence angle of the beam. This method can easily be used any time of the year as long as the trough is small and flexible enough to be rotated.

The second method requires the measurements to be conducted around the equinox.

Figure 6.4 shows measurements of the angles of incidence on a south facing surface. The measurements were performed at Älvkarleby, Sweden (60.5°N, 17.4°E) on September 23, at the autumn equinox. As can be seen from the figure, the transverse projected angle of incidence θ_T was constant at 90-latitude = 30° all day. The fact that the transverse projected angle of incidence is constant around the equinox is the basis of this method.

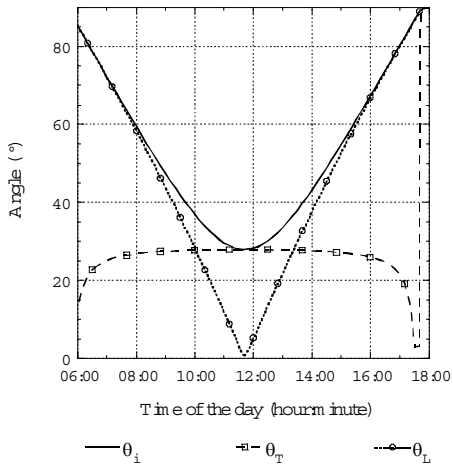

Figure 6.4 *Angles of incidence on a south facing surface during the day on September 23 in Älvkarleby, Sweden.*

At the equinox, the concentrator was rotated 90° around the North-South axis. It was then tilted to the latitude angle around the East-West axis. In this setup, the sun will move in the meridian plane of the concentrator all day, and noon will be equal to a transverse angle of 0°. A reference was mounted parallel to the aperture and the short-circuit current of the reference and concentrator were measured with a data logger. The optical efficiency was calculated according to Equation 6.3.

$$\eta(\theta_T) = \frac{1}{C_g} \frac{I_{SC}^{conc}(\theta_T)}{I_{SC}^{reference}(\theta_T)} \qquad \text{Equation 6.3}$$

To get an optical efficiency between 0 and 1, the measured short-circuit current was divided by the concentration ratio.

This technique requires less labour as it is completely automated, all that is required is that the system is mounted as described above.

6.3 Light distribution on the absorber

The light distribution over the cell is an important parameter for a concentrator since the output of the PV cell or thermal collector is largely affected by this distribution. High local intensities increase the electrical and thermal losses. The electrical losses can be explained by the fact that the internal resistive losses increase with the square of the current.

The light distribution over the cells is translationally symmetric in translationally symmetric concentrators, i.e. it is concentrated to a line along the length of the trough. The cells are placed series connected on this line. It is thus enough to measure the distribution in the transverse direction over the cells to make a full measurement of the light distribution as long as there are no large deviations from the translational symmetry. A device, which is shown in Figure 6.5, was constructed for measuring the light distribution.

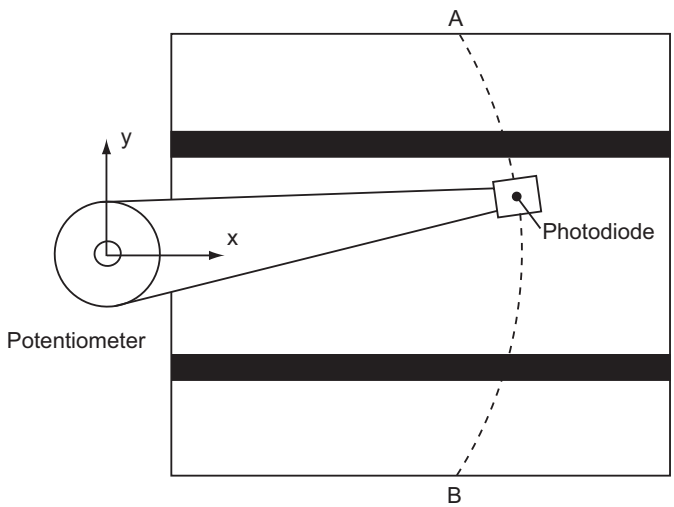

Figure 6.5 *Device for measuring the irradiation distribution over the cells. The lever has a photodiode for measuring the light intensity at one end and is mounted to a potentiometer on the other.*

The device consisted of a lever with a photodiode mounted on the tip. It was placed on the cells in the trough, in the plane of the cells. The lever was rotated along the cell surface from *A* to *B* during one distribution measurement. A plate with a small hole was glued over the photodiode to

increase the resolution of the detector as the resolution gets higher when the measuring aperture decreases. The centre of rotation for the lever was a potentiometer that measured the rotation angle of the lever.

A measurement started by measuring the voltage of the potentiometer for point *A* and point *B* to get a conversion factor from potentiometer voltage to angle. The lever was then slowly swept over the surface of the cell while a data logger measured the voltage over the potentiometer and the current from the photodiode. The y position for each intensity point was then calculated knowing the length and the angle of the lever. Figure 6.6 shows a typical measured irradiation distribution over the cell.

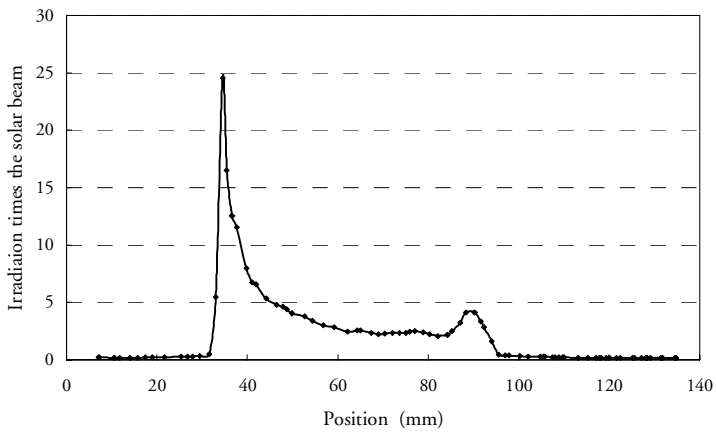

Figure 6.6 *Irradiation distribution over the cell in a MaReCo concentrator. The position on the x-axis is measured from the focal point at the top of the absorber.*

The importance of having a high spatial resolution in the irradiance measurement can clearly be seen in the figure as the irradiation peak is very narrow.

7 Electrical and thermal characterization of a concentrating PV/T hybrid

A characterization of the stand-alone MaReCo was performed in order to understand and quantify the characteristics of a concentrating photovoltaic/thermal hybrid (Helgesson, Krohn and Karlsson 2004).

The system is shown in Figure 7.1.

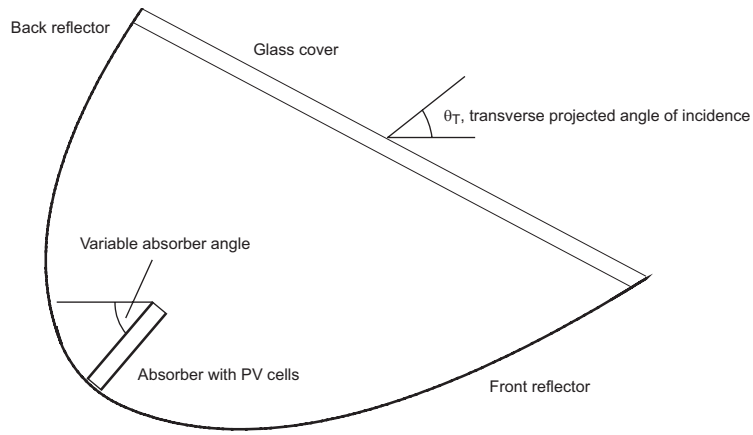

Figure 7.1 *The MaReCo PV/thermal hybrid. Both parabolic reflectors have the same focal point, at the top of the absorber. The photovoltaic cells are laminated on the absorber. The glass cover tilted at 30° is for weather protection. The absorber angle is the angle between the absorber and the horizontal. Also shown is the transverse projected angle of incidence.*

The asymmetrical concentrator system is intended to be placed on a horizontal surface. It is designed to collect all direct irradiance between transverse angles of incidence of 20° and 65°. The system is thoroughly de-

scribed in (Adsten, Helgesson, and Karlsson 2005). Two prototypes were evaluated, one with aluminium reflectors and one with aluminium laminated steel reflectors. The aluminium concentrator was constructed with a variable absorber angle to make it possible to investigate the influence of the absorber angle on the electrical and thermal output. The aluminium trough had cells facing both the front and back reflector, and the steel trough had cells facing the back reflector. Table 7.1 describes the different properties of the two prototypes.

Table 7.1 Properties of the two prototypes. The absorber angle and the description of the reflectors are shown in Figure 7.1.

	Aluminium trough	Steel trough
Cells facing upper reflector	2	12
Cells facing lower reflector	3	0
Absorber angle	45	20
Trough material	Anodized aluminium	Steel with aluminium coating
Length (m)	1	2

7.1 Reflector materials

MaReCo in its current design is equipped with reflectors made of anodized aluminium but this has some disadvantages. When large troughs are made, the aluminium construction tends to deviate from the profile given by the supporting gables. These deviations which are seen mostly as dents in the reflector create undesired reflections. This results in optical losses. It is difficult to produce the aluminium concentrators without these imperfections, and this creates an interest in investigating other materials for the reflector construction. Another problem is the thermal expansion of the aluminium reflectors. When the construction heats up during operation, more dents appear in the reflector.

A newly developed aluminium-polymer-laminated steel reflector was used in one of the troughs to investigate if this could solve the problems of the aluminium reflector. The optical properties and durability of the new material have been investigated by Brogren, (Brogren et. al. 2004). The steel base of the reflector makes this material more rigid. The problems due to dents and thermal movement of the reflector were therefore to be solved by using this material. A visual inspection of the two prototypes

shows a clear difference in the number of dents between the two troughs. The optical properties of the steel based reflector are different from the aluminium reflector, Figure 7.2 shows the reflectance of the aluminium reflector and the steel based reflector as a function of the wavelength of the incident light. The responsitivity of a PV cell as a function of wavelength is also shown in the figure. The responsivity was calculated as the ratio between the current from the illuminated diode and the incident light power.

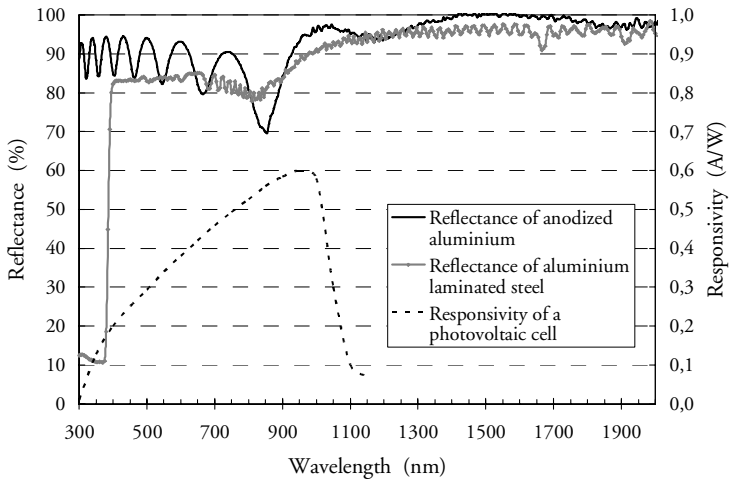

Figure 7.2 *Reflectance as a function of the incident wavelength for the two materials. The responsivity of the silicon cell as a function of the wavelength is also shown to illustrate the relevant wavelength interval.*

The reflectance of the steel based reflector is low below 350 nm due to a plastic coating that absorbs light below this wavelength. This coating is necessary as the thin aluminium film is vacuum coated on this plastic film. It also protects the aluminium surface from oxidation. The total reflectance of the aluminium reflector is higher at most wavelengths, and this will influence the total amount of light collected by the concentrators. An optical property that is not visible in Figure 7.2 is that the steel based reflector diffuses the light slightly, whereas the aluminium has an almost specular reflectance.

7.2 Current-Voltage characteristics

The current-voltage (IV) characteristics of the two prototypes were measured according to Section 6.1. It is important to note that the steel based prototype only had cells facing the back reflector, and a comparison between the two materials can only be made for the back reflector.

Figure 7.3 shows the IV characteristics for the reflectors at 35° transverse projected angle. The transverse projected angle of incidence is defined in Figure 7.1. This angle of incidence was chosen to be in the optimum range for the back reflector. The voltage was normalized to show voltage/cell to enable a comparison between the two systems.

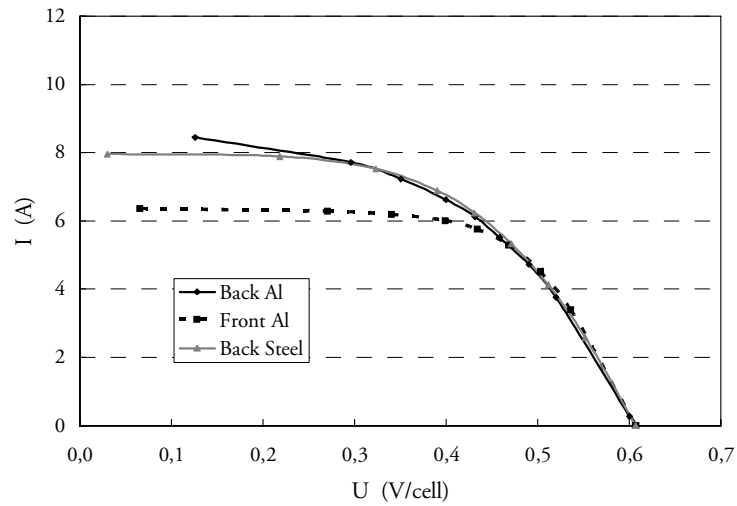

Figure 7.3 IV characteristics at 35° transverse projected angle of incidence.

As can be seen from the figure, the short circuit current of the cells facing the back aluminium reflector is higher than that of the cells in the steel based reflector trough. This is due to the lower total reflectance of the steel based reflector. Due to the partly diffusing reflections of the steel-based reflector, the cells were more uniformly illuminated which leads to a higher fill factor for this prototype.

Figure 7.4 shows the IV characteristics at 57° transverse projected angle of incidence. This angle of incidence is within the optimal range for the front reflector.

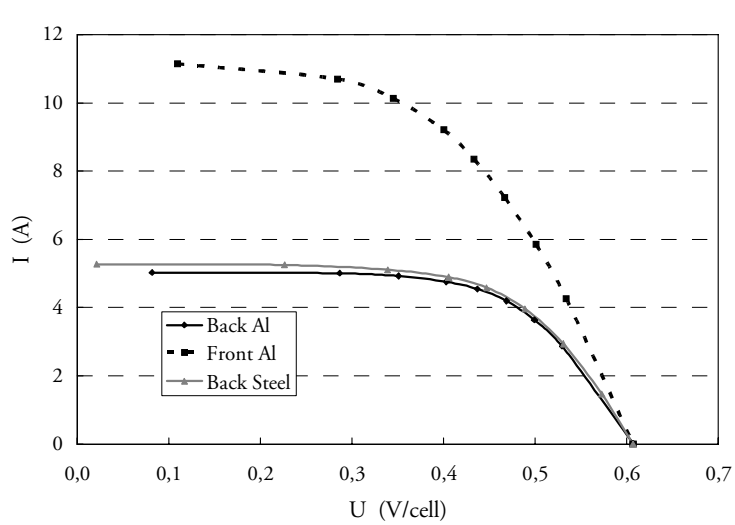

Figure 7.4 IV characteristics at 57° transverse projected angle of incidence.

As expected, the cells facing the front reflector delivered a significantly higher current than the cells facing the back reflectors in this measurement. This is due to the angle of incidence which is beneficial for the front reflector, and to the larger surface area of the front reflector compared with the back reflector.

The maximum power was calculated using a parabolic fit to the IV-curves and the results can be seen in Table 7.2.

Table 7.2 Maximum power calculated from Figure 7.3 and Figure 7.4

Angle of incidence	Back steel reflector	Back Al reflector	Front Al reflector
35°	2.7 W/cell	2.6 W/cell	2.4 W/cell
57°	2.0 W/cell	1.9 W/cell	3.8 W/cell

7.3 Short circuit current

The short circuit current was measured as a function of the transverse angle of incidence according to Section 6.2. Figure 7.5 and Figure 7.6 show the measured short circuit current and fill factor for the cells facing the back reflector.

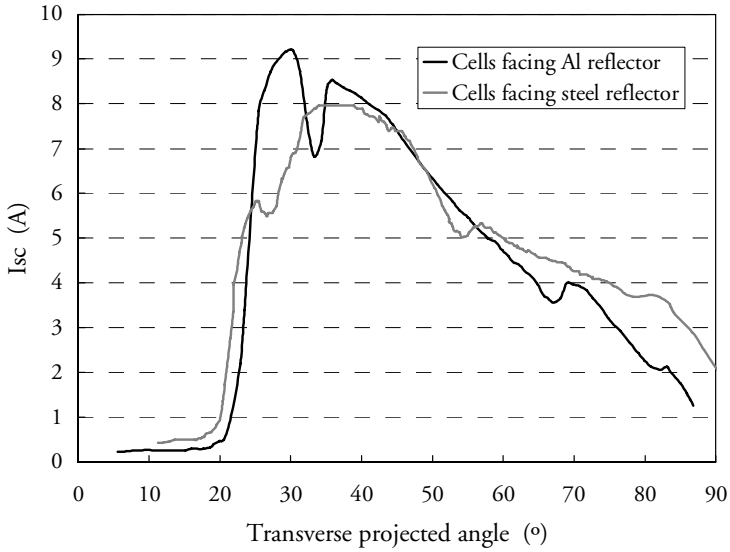

Figure 7.5 *Measured short circuit current for the cells facing the back reflectors.*

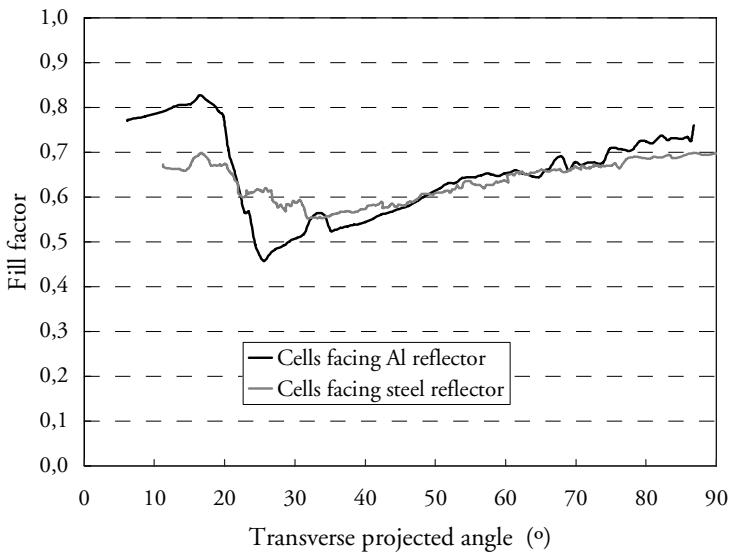

Figure 7.6 *Fill factor for the cells facing the back reflectors.*

The back reflector is designed to collect light in the winter, spring, and fall and this is validated as the highest currents are measured at low angles of incidence.

As expected, the short circuit current of the cells in the aluminium trough is higher for most angles due to the higher total reflectance. The fact that the short circuit current of the cells facing the steel reflector is higher at large angles of incidence is due to the different absorber angles. This angle affects the distribution of light on the cells and the average number of reflections.

The fill factor is in general higher for the steel reflector system in the range where the short circuit current is high. The strip of light on the cells is slightly wider for the steel reflector trough due to the diffuse reflectance and this increases the fill factor.

The internal losses in the cell are proportional to the square of the current, RI^2, and the output power of the cell is proportional to the current, VI, where V's dependence on the irradiance can be neglected. As the current increases when the irradiation on the cell increases, the relative losses increase more than the delivered power, and the fill factor decreases. This is discussed in more detail in Section 4.3.

Figure 7.7 shows the short circuit current and fill factor of the cells facing the front reflector in the aluminium trough.

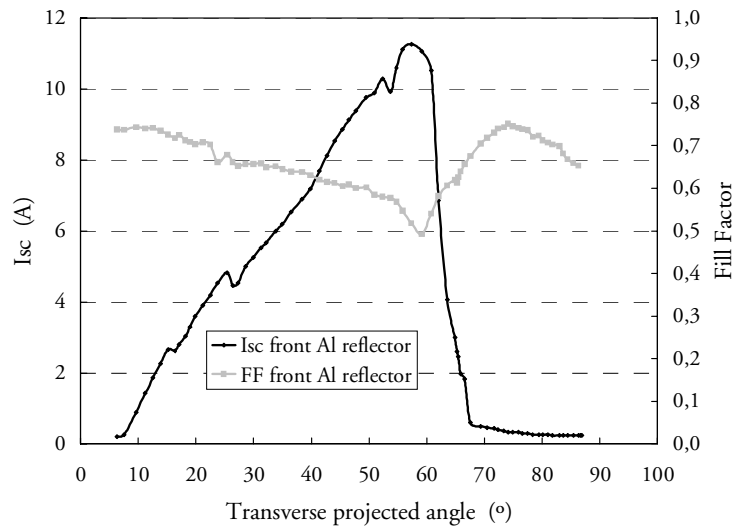

Figure 7.7 *Short circuit current and fill factor of the cells facing the front reflector.*

As in the case of the back reflectors, the fill factor is higher when the short circuit current is lower. The front reflector collects most of the light at larger transverse angles. It is suitable for collecting the irradiation in the summer.

7.4 Irradiation distribution

As was discussed in the previous section, the output of the cells is affected by the distribution of irradiation on the cells. Figure 7.8 shows the irradiation distribution on the cells facing the back reflector at 33° transverse angle of incidence.

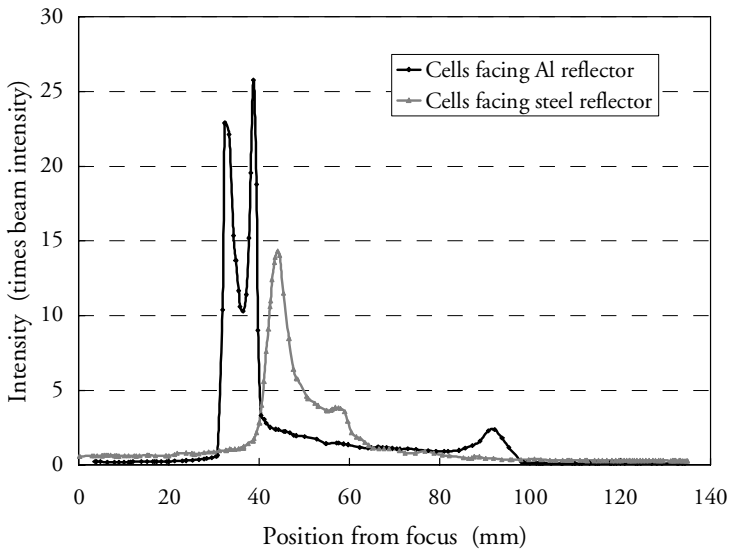

Figure 7.8 *Irradiation on the cells facing the back reflector as a function of the position from focus. The position is measured from the focal point at the top of the absorber.*

The peak irradiation is higher for the cells in the aluminium trough, 25 times the beam compared with 14 times the beam for the steel trough. The width of the strip of light is approximately 10 mm for the aluminium reflector and 20 mm for the steel reflector. The wider strip of the steel

reflector is due to the more diffuse reflections of this reflector. All the light reaches the cells for both troughs, which is shown by the fact that the irradiance is zero at both ends of the absorber.

7.5 The influence of the absorber angle on the electrical output

The distribution of light on the cells depends on the absorber angle. The number of reflections at a specific angle of incidence changes as the absorber angle changes. When the absorber is turned towards the horizontal, the back reflector will have a lower average number of reflections, but the front reflector will have more. Simulations show that the annual output will be independent of the absorber angle if the absorber is kept in the same position all year. However, if the absorber can be placed at different angles during the year, turning the absorber towards the back reflector would be favourable for winter, spring and fall, and turning the absorber towards the front reflector would be favourable during the summer.

7.6 Estimation of the electrical output

The measured short circuit current as a function of the transverse angle of incidence was used to calculate the optical efficiency. It was calculated according to Equation 6.2.

Figure 7.9 shows the calculated optical efficiencies.

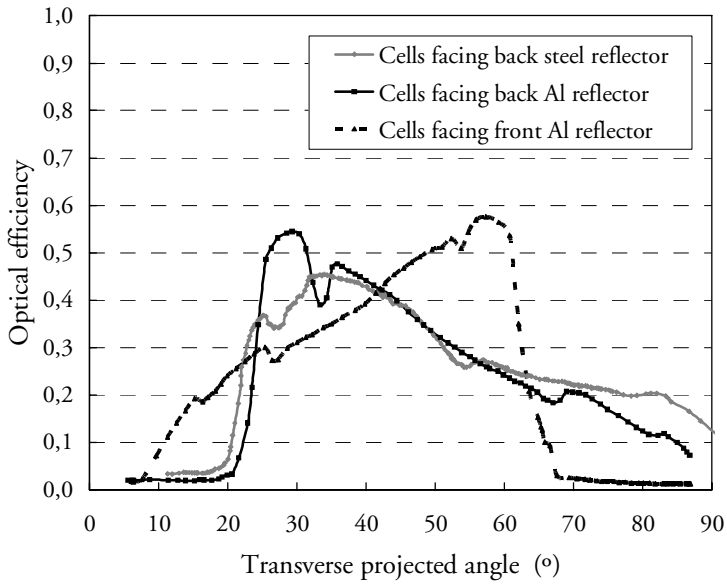

Figure 7.9 *Optical efficiency as a function of the transverse angle of incidence. The back reflectors have a high efficiency at low angles of incidence and the front reflector has a high efficiency at high angles of incidence.*

The optical efficiency was used as input to MINSUN (Chant and Håkansson 1985) for estimating the annual output. MINSUN uses climatic data for a specific site to calculate the annual output for a system with known optical efficiency in the longitudinal and transverse directions. The transmittance of the cover glazing as a function of the angle of incidence was used to model the optical efficiency in the longitudinal direction. A comparison was made with a standard PV panel that was mounted on the aperture, at 30° tilt from the horizontal.

Table 7.3 shows the result of the simulations

Table 7.3 Annual electrical output as simulated by MINSUN.

Case	Annual output per m² cell area	Improvement
Cells facing back Al reflector	168 kWh	22.6%
Cells facing front Al reflector	205 kWh	49.1%
Cells facing back steel reflector	168 kWh	22.6%
Reference at 30° tilt	136 kWh	0%

The simulations show that the annual output from the cells facing the back reflectors is the same for both reflector types. An increase of approximately 23% can be expected compared with the reference. The cells facing the front reflector are expected to deliver 49% more electricity. This shows that if cells are to be placed on one side of the absorber only, they should be facing the front reflector in order to maximize the electrical output.

7.7 Estimation of the thermal output

MINSUN was used to calculate the thermal output of the hybrid using the optical efficiency and the thermal losses of the system. The estimated annual thermal output was 145 kWh/(m^2 glassed area) for a water temperature of 50°C. The low estimated output is probably due to the prototype construction of the absorber, which is shown if Figure 7.10.

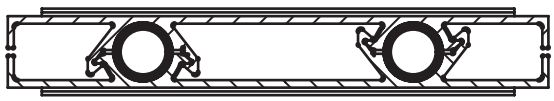

Figure 7.10 *Hybrid PV/thermal absorber (Fieber 2005). The copper pipes inside the absorber transport the heat collecting fluid.*

The absorber is designed for in-situ assembly when the system is erected, but the manufacturing precision is too low. The air gap between the absorber and the pipes creates a large thermal resistance. The low heat conduction to the copper pipes containing the heat collecting fluid increases the absorber temperature, and the increased temperature results in higher thermal losses. The manufacturing precision has to be higher in future prototypes, or a less flexible absorber has to be used to increase the thermal output and reduce the overheating of the photovoltaic cells.

7.8 Placement of the PV cells

MaReCo is designed to maximize the annual collection of irradiation. The front reflector collects most of the irradiation during the summer months, and the back reflector collects more during the rest of the year. If

the cells are placed on one side of the absorber, and the other side is used for heat collection only, the electricity generation will be asymmetric over the year. This is an important aspect since the system is intended to be integrated mostly into residential buildings where the use of electricity for household appliances etc. is fairly constant over the year. If the absorber has cells on both sides, it will increase the total annual output considerably, which will be an important factor for the investor that might have limited space for mounting the system.

If space is unlimited, and the most important parameter is to minimize the cost of electricity production, it is probably best to remove the cells from the back side of the absorber since the cells facing the front absorber have the highest annual output. In this case, it would be better to mount two systems with cells facing the front absorber instead of having one system with cells on both sides. However, this will probably not be the case for most applications and the best choice for most situations is to have cells on both sides of the absorber to maximize the annual system performance.

8 Models for calculating the output of electricity and heat

The use of solar concentrators for increasing the output from solar collectors and photovoltaic modules is often cost effective (Perers and Karlsson 1993). However, before investment in a concentrating solar energy system is made, it is appropriate to estimate the annual thermal or electrical energy output. To be able to predict the output of a system at a specific location requires knowledge of the yearly irradiation at the site and knowledge of the angular dependence of the optical efficiency of the concentrator. Measurement of the optical efficiency at all angles is time consuming and expensive, and models are therefore used to estimate the optical efficiency. These models are based on measurements at certain specific angles, and the model is used to extrapolate these measurements to the full spectrum of incidence angles.

8.1 Planar solar energy systems

The optical efficiency of planar solar collectors, glazings, or photovoltaic modules is often estimated using Equation 8.1 (Souka and Safwat 1966) (Duffie and Beckman 1980).

$$\eta_{opt}(\theta_i) = \eta_n \left(1 - b_0 \left(\frac{1}{\cos\theta_i} - 1 \right) \right) \qquad \text{Equation 8.1}$$

The optical efficiency is a product of the optical efficiency at normal incidence, η_n, and a factor that describes the reduced efficiency as the angle of incidence θ_i increases. b_0 is the incidence angle modifier

coefficient and it is calculated by fitting measurement data to the model. A commonly used value for glazings and flat plate solar thermal collectors is 0.1-0.2. It is slightly lower for photovoltaic panels.

Figure 8.1 shows a typical optical efficiency curve for a planar system calculated by Equation 8.1.

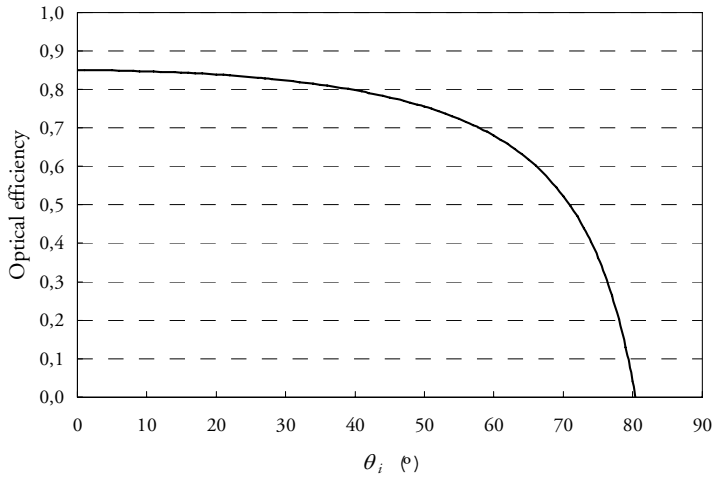

Figure 8.1 *Transmittance of a glass sheet modelled according to Equation 8.1 (η_n=0.85, b_0=0.2).*

The model can be widely used to model the system at low and medium angles of incidence. However, at large angles of incidence, the modelled values decrease faster than the physical quantity. This is clear in the figure; the transmittance of a glass sheet is not 0 at 80° angle of incidence.

8.2 Biaxial models

Non symmetric systems have to be modelled by a biaxial model that accounts for the difference in optical efficiency at different planes of incidence. A commonly used model is shown in Equation 8.2.

$$K(\theta_L,\theta_T) = K_L(\theta_L,0)K_T(0,\theta_T) \qquad \text{Equation 8.2}$$

where θ_L is the longitudinal angle and θ_T is the transverse projected angle of incidence. The angles are defined in Figure 8.2 (McIntire 1982).

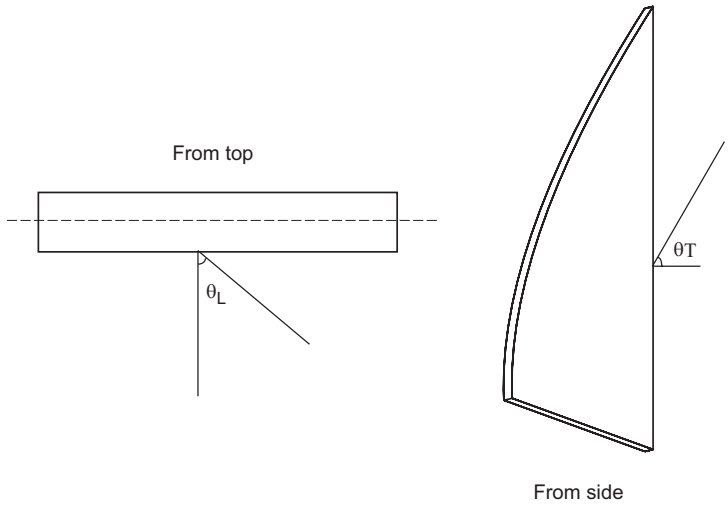

Figure 8.2 *Definition of the longitudinal angle θ_L and the transverse projected angle θ_T.*

This model estimates the optical efficiency K by measurements of the optical efficiency in the perpendicular longitudinal and transverse directions.

Measuring at θ_T =0 can be a problem for many asymmetrical concentrator systems that do not accept light at this angle of incidence; the minimum angle of acceptance is often 15-20°.

Another problem, that is more serious, is that this model tends to overestimate the influence of the cover glazing. As the model is a product of two measurements, the influence of the glazing is accounted for twice. The largest error occurs when both the longitudinal and the transverse angles are large.

To solve this problem, we introduce a new model that separates the influence of the glazing and the influence of the concentrator. As was discussed in previous chapters, the optical efficiency of translationally symmetric two dimensional concentrators is determined by the rays in the meridian plane. The angle of incidence in this plane is θ_T and the optical efficiency of a reflector trough will be modelled as a function of this angle. Figure 8.3 shows the measured optical efficiency as a function of the transverse projected angle of incidence for the system shown in Figure 8.2. The optical efficiency was calculated by dividing the measured short-circuit current of the concentrator module by the short-circuit current of a vertical reference module.

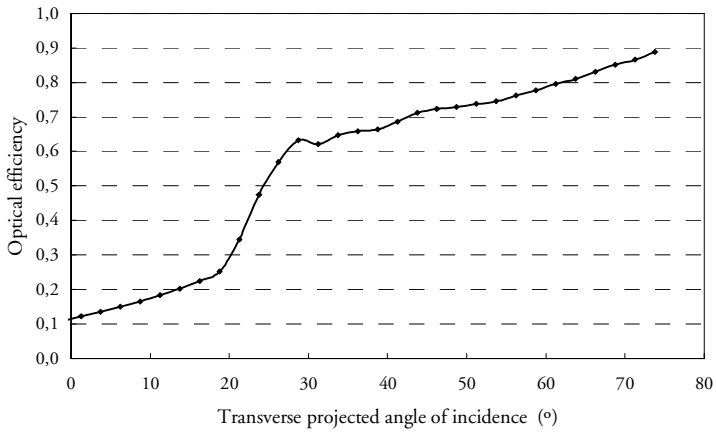

Figure 8.3 *The optical efficiency measured as a function of the transverse projected angle of incidence.*

At equinox, the transverse projected angle of incidence is constant all day for a system facing south. A concentrator for wall integration, shown in Figure 3.12, was placed facing south. The results of measurements during two days around equinox are presented in Figure 8.4. The figure shows that the optical efficiency is independent on the longitudinal angle.

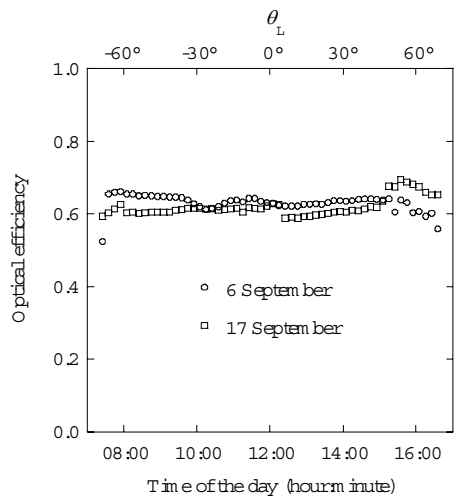

Figure 8.4 *Optical efficiency during two days around equinox. The optical efficiency is constant at changing longitudinal angles.*

The transmittance of a glazing depends on the true angle of incidence on the glazed surface. Equation 8.3 defines the proposed model, where R_T models the concentrator and f_L models the glazing.

$$\eta_{opt} = R_T(\theta_T) f_L(\theta_i) \qquad \text{Equation 8.3}$$

As the transmittance for glass as a function of the angle of incidence is known in most cases, measurements on the concentrator as a function of the transverse angle at zero longitudinal angle is what is required to fully model the system. The model assumes that the glazing can be removed from the system before the measurements are performed. If for some reason this is not possible, R_T can be obtained according to Equation 8.4.

$$R_T = \frac{K(0,\theta_T)}{f_L(\theta_T)} \qquad \text{Equation 8.4}$$

$K(0,\theta_T)$ in Equation 8.4 describes a measurement of the optical efficiency in the meridian plane of the concentrator when glazing is used. This method can for example be useful when using outdoor measurement data where the glazing had to be kept on for climate protection.

The angular dependence of the absorption of the PV cell in the concentrator is not accounted for in the proposed model. Figure 8.5 shows the absorption as a function of the incidence angle for a CIGS thin film cell and for a monocrystalline silicon cell (Brogren, Nostell, Karlsson 2000).

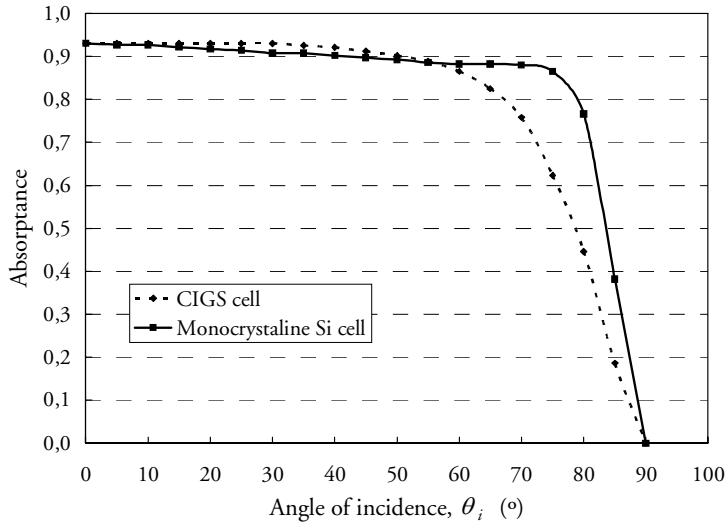

Figure 8.5 *Absorption of a CIGS thin film cell and a monocrystalline silicon cell*

The absorption of both PV cell types is almost constant up to 70°, the absorption is only influenced at large longitudinal angles. Unless the system is mounted facing east or west with a maximum irradiation incident at large longitudinal angles, it will not influence the optical efficiency of the system.

Measurements of the short circuit current of a concentrating module for wall integration and a reference module mounted on a vertical surface beside the concentrator were performed for two summer months in Älvkarleby, Sweden (60.5°N, 17.4°E). The model defined by Equation 8.3 was used to estimate the short circuit current of the concentrating module using the current of the reference module. Figure 8.6 shows a comparison between the estimated current and the measured current.

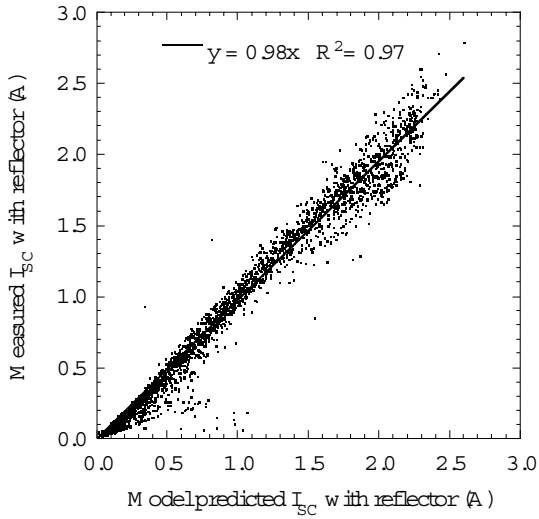

Figure 8.6 *Model prediction versus measured current for a parabolic concentrator for wall integration.*

As can be seen from the figure, the model predicts the short circuit current of the module in the concentrator well for the two summer months.

8.3 Annual direct irradiation

The extraterrestrial irradiation in the north-south vertical plane is symmetric over the year with one peak at the summer solstice and one peak at the winter solstice. These peaks occur at different angles depending on the latitude, the winter peak at 90°-latitude-23.45°, and the summer peak at 90°-latitude+23.45°. At high latitudes such as Sweden, the winter peak is close to the horizon, 6° in Älvkarleby and 11° in Lund. Since the light has to pass trough more atmosphere close to the horizon, the irradiation that arrives in the winter is limited and the peak is suppressed. It is suppressed even further by the large cloud cover during the winter months, which makes the peak almost disappear. Figure 8.7 shows a diagram of the irradiation incident on a surface tracking the sun in the north-south vertical plane in Lund, Sweden (55.72°N, 13.22°E). It is divided into angular intervals of 2°.

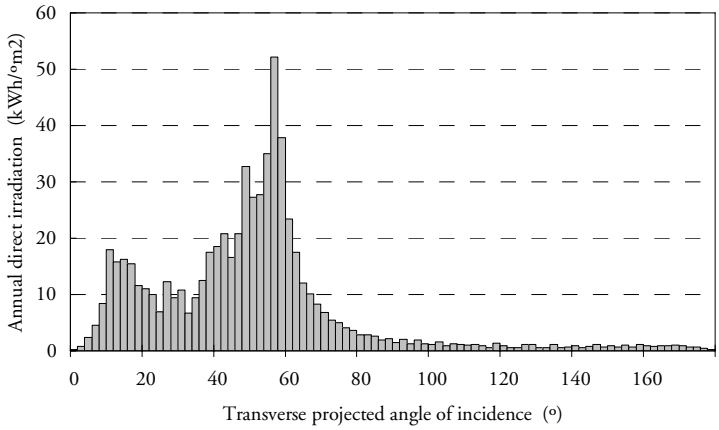

Figure 8.7 *Annual direct irradiation on a solar tracking surface. The transverse projected angle is 0 at the horizon in Lund (55.72°N, 13.22°E).*

The highly asymmetrical irradiation during the year makes stationary asymmetrical concentrators an interesting option since most of the irradiation is concentrated into a small angular interval. If for example a system collects all irradiation between 40° and 65° it will collect 55% of the annual direct irradiation incident on the surface. If the yearly irradiation has two peaks, as is the case for more southern latitudes, it is not possible to use stationary collectors with a reasonable concentration ratio.

9 Structured reflectors

One of the problems facing concentrator systems for photovoltaic applications is that the performance is lower than expected. In an ideal system, a concentration ratio of 3 should treble the electric energy from the modules. However, the performance increase for the current prototype systems is typically 50%-75% of the geometrical concentration ratio. One obvious way to increase the electrical output per cell area is to increase the concentration ratio. If the concentration ratio were increased from 3 to 6, we could at least expect a doubling of the electrical output. However, this would be at the expense of a changed acceptance interval, since the maximum concentration ratio of a stationary, asymmetric concentrator is $2/(\sin\theta_1 - \sin\theta_2)$ where θ_1 and θ_2 are the acceptance angles of the concentrator. If the system is to be used in a stationary mode it is not easy to change the acceptance interval since the angular distribution of the irradiation is determined by the latitude and the climate of the site. This sets a limit for the concentration ratio. Figure 9.1 shows a translationally symmetric concentrator, MaReCo, that was used to evaluate structured reflectors. The figure also shows the local coordinate system that will be used throughout this chapter.

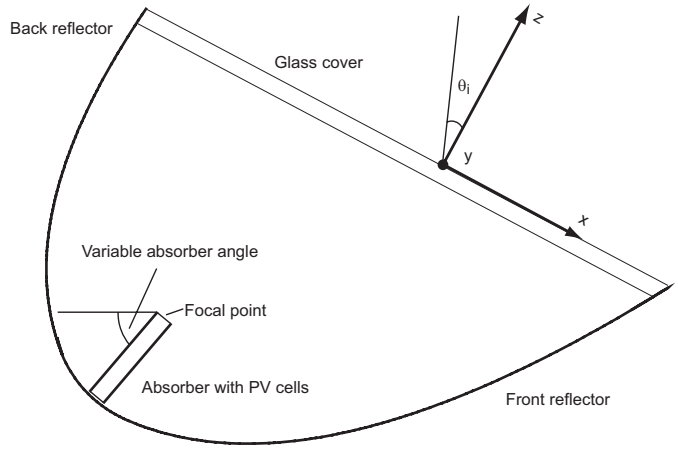

Figure 9.1 *Sketch of a translationally symmetric concentrator, MaReCo. The local coordinate system is shown in the figure.*

A symmetric three dimensional concentrator has a theoretical maximum concentration ratio of $1/\sin^2(\theta_{max})$ as it was derived in Section 2.1.The difference between the two- and the three dimensional systems is due to the conservation of the skewness of the two dimensional concentrator (Bortz, Shatz, and Ries 1997). The skewness, which is further discussed in Section 2.2 is the directional component, k_y, of the incident light that is parallel to the axis of symmetry, the y-axis of Figure 9.1.

The light at the exit aperture of an ideal three-dimensional concentrator fills up the phase-space completely. To break the translational symmetry of a two dimensional concentrator such as the MaReCo could be a way to increase the concentration ratio as this would change the skewness of the rays and possibly increase the phase-space volume at the exit aperture. This can be seen from Equation 2.4 and Equation 2.5 where the increased concentration ratio is due to the non-zero dk_y component, i.e. concentration of the component of the incident light perpendicular to the meridian plane.

The skewness of the rays can in the case of trough concentrators be changed by introducing a structured reflector where the structures are oriented perpendicular to the y-axis of Figure 9.1.

Apart from increasing the concentration ratio, a structured reflector might solve the problem that creates the largest electrical losses in the system, the highly non uniform irradiation of the cells. The high local intensity in parts of the cell creates high local currents and temperatures and this creates high resistive losses. Standard cells have a relatively high

series resistance, and if standard cells are used in concentrator systems, the high local currents will cause large resistive losses that can be observed as a reduced fill factor. The characteristics of the cells are discussed in more detail in Section 4.3. The structure widens the narrow strip of light on the cells and this might prove to be an important improvement to the trough design.

9.1 Proposed structures

Figure 9.2 shows three structures that were investigated for increasing the performance of the MaReCo. The structures are small in comparison with the dimensions of the trough, typically in the range of centimetres for a trough of 5m.

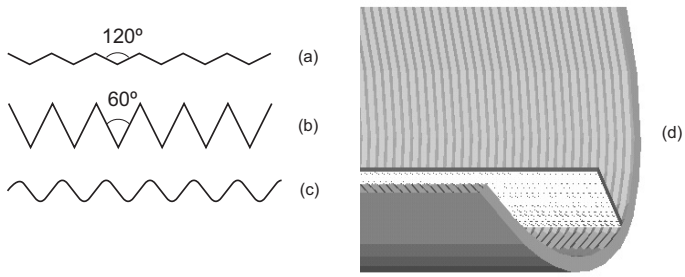

Figure 9.2 *Evaluated structures. Structure (a) is V-shaped with an opening angle of 120°, structure (b) is V-shaped with an opening angle of 60°, and structure (c) is sinusoidal shaped. (d) shows a sketch of a trough fitted with V-shaped reflectors.*

The sun is a light source with almost parallel light, the angular spread is roughly 0.28°. Using the local coordinate system of Figure 9.1, the incident light can be divided into three directional componets, k_x, k_y, and k_z. A translationally symmetric concentrator does not affect the skewness, k_y in the reflections. This means that the angular spread at the absorber is limited to the x-direction. But maximum concentration ratio is achieved when the exit rays fill up the phase space at the exit aperture completely, i.e. the rays exit in a hemisphere, where all directions are equally probable, instead of in a plane. This would be achieved if the k_y components of the light could be mixed in the reflections as is the case for the k_x-components.

Structures (a) and (b) of Figure 9.2 will selectively mix the direction cosines in a controlled pattern due to the planar facets of the microstructure (Leutz and Ries 2003). The sinusoidal structure (c) will mix the direction cosines more randomly.

Structure (a) and structure (b) are described in Figure 9.3. Figure 9.3a shows the directional components, k_x and k_y, of the incident light projected onto a half circle.

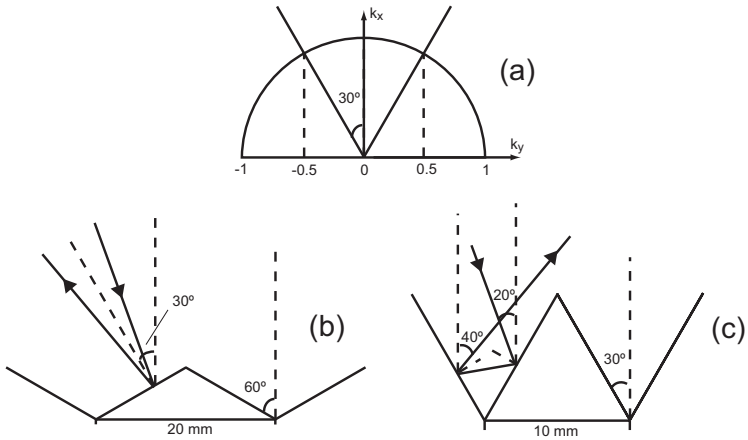

Figure 9.3 *Selective mixing of reflected rays in the two-dimensional phase space. The étendue limited by the angular interval -30<θ<=30 is equal to the étendue comprising the rest of the possible angles. The V-shaped structures reflect all rays of one angular interval into the other, and vice versa, thereby mixing the direction cosines.*

The étendue limited by the angular interval -30<θ<30 is equal to the étendue comprising the rest of the possible angles. The V-shaped structures reflect all rays of one angular interval into the other, and vice versa, thereby mixing the direction cosines. Figures 9.3b and 9.3c show how the V-shaped microstructures mix the k_x and k_y components. Both structures mix the incident parallel light, but the structure in Figure 9.3c will reflect the rays twice while the structure of Figure 9.3b only reflects the incident rays once. This will lead to increased reflection losses for the structure of 9.3c. It is always desirable to increase k_y in the reflections, but it is only when the light source is in the meridian that decreasing k_y is beneficial.

The optical properties of the structured concentrators were evaluated using Monte Carlo ray tracing performed in ZEMAX, a commercial ray tracing package (ZEMAX 2005).

9.2 Changed illumination of the absorber

The main explanation for the relatively low gains from using asymmetric parabolic concentrators for photovoltaic applications is the highly non uniform irradiation distribution on the cells and this was one of the reasons for evaluating the structured reflectors. Figure 9.4 and Figure 9.5 show the resulting irradiation distribution of the cells facing the front and back reflector for the three structures and for a smooth reference trough. The simulation was performed for an azimuth angle of 15° and a solar altitude of 40°.

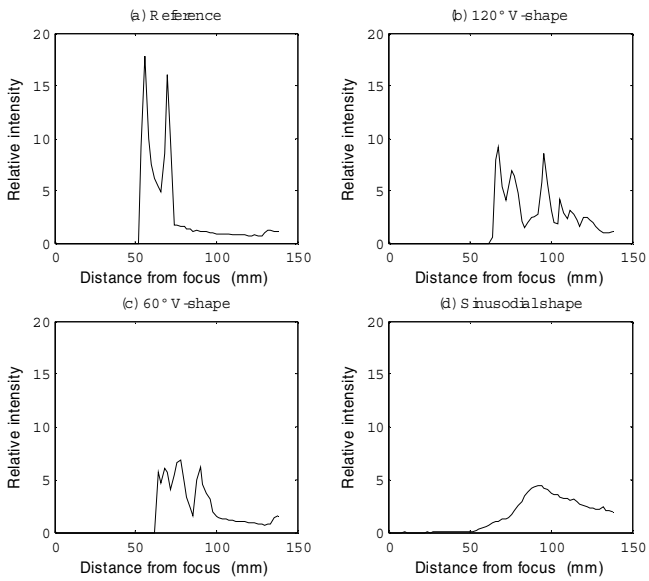

Figure 9.4 *Irradiation distribution on the cells facing the back reflector. The y-axis shows the intensity relative to the sun beam for an azimuth angle of 15° and a solar altitude of 40°.*

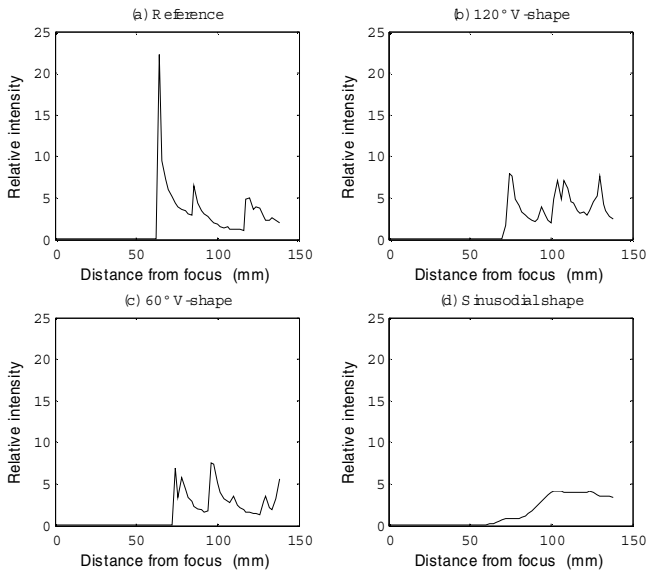

Figure 9.5 *Irradiation distribution on the cells facing the front reflector. The y-axis shows the intensity relative to the sun beam for an azimuth angle of 15° and a solar altitude of 40°.*

As can be seen from the figures, all structures considerably reduce the peak intensity on the cells and this will result in a higher fill factor, i.e. the resistive losses in the cells will be reduced. The effects of non-uniform illumination of the cells are described in more detail in Section 4.3. The sine structure clearly creates the greatest reduction in peak intensity, it never exceeds the beam intensity by more than a factor of five, and almost half the cell is illuminated. This makes the structure very interesting in combination with standard silicon cells, since they are sensitive to high irradiation spots due to their relatively high series resistance.

For the V-shaped structures, the reduction in intensity is slightly larger for the 60° structure, but this is due to the higher optical losses due to a higher number of multiple reflections.

Previous measurements on a slightly diffusing reflector described in Chapter 7 showed that a slight reduction in peak intensity can improve the output of the cells considerably. However, the problem with that reflector is that the total reflectance of the reflector is low.

If microstructured reflectors are used, the wider strip of light can be achieved without large reflection losses since a reflector with very high reflectance can be used.

9.3 Optical efficiency and annual output

The structured reflectors will introduce a higher average number of reflections at a given angle of incidence. Simulations were performed for a large interval of angles in the azimuth and solar altitude directions to study the optical efficiency of the three proposed troughs. A simulation of a smooth reference was performed as a reference for comparison with the current design of the stand-alone MaReCo.

Figure 9.6 shows the optical efficiency as a function of the solar altitude when the source was in the meridian plane, the xz plane of Figure 9.1.

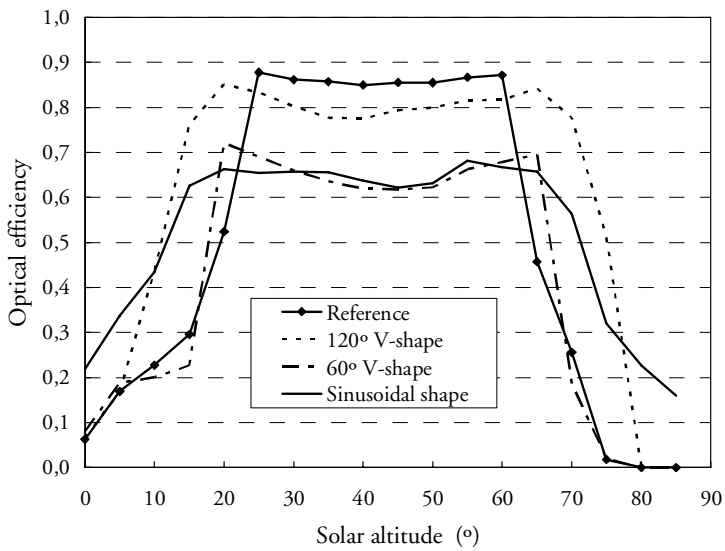

Figure 9.6 *Optical efficiency in the meridian plane. The sun is normal to the trough aperture at 60° solar altitude. The reflectance at normal incidence was 0.92 in the simulations.*

In the interval 25° to 60°, the reference has a higher optical efficiency than any of the structured reflector troughs. This is due to the higher number of reflections for the structured reflectors. However, the difference between the 120° structure and the reference is small within the interval

of acceptance. Outside the interval of acceptance (20° to 65°) all structured reflectors perform better than the reference. This means that the interval of acceptance increases when structured reflectors are used as it is possible for light outside the interval of 20° to 65° to reach the absorber. The sinusoidal structure has the lowest optical efficiency inside the interval, but also the smallest decrease outside the interval.

Simulations for other angles of incidence show that the optical efficiency of the sinusoidal structured reflector and the 60° V-shaped structure has a local minimum in the meridian plane, the efficiency increases as the azimuth angle increases. This is shown in Figure 9.7 where the azimuth angle was varied while the solar altitude was constant at 40°.

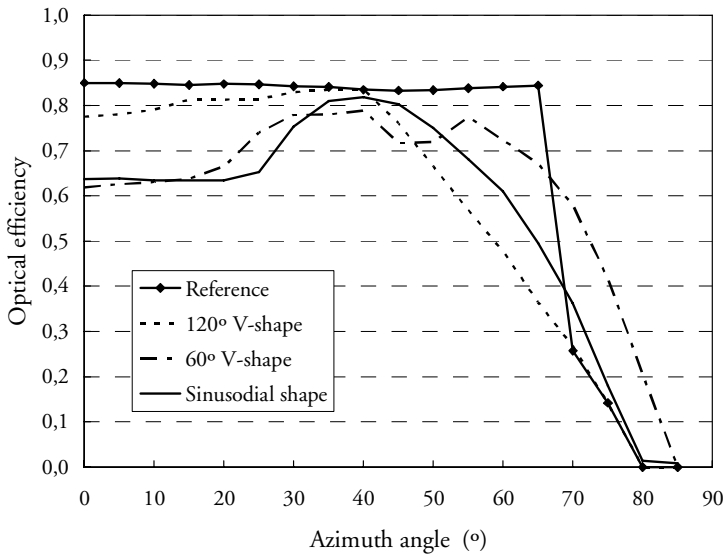

Figure 9.7 *Optical efficiency as a function of the azimuth angle at a constant solar altitude of 40°*

Using climate data for Lund, Sweden (55.75°N -13.22°E), the optical efficiency at different angles of incidence was weighted by the incident irradiation in each angular interval to get an evaluation of the different reflectors during a year of operation. Both direct and diffuse irradiation was included in the calculations.

This does not give any absolute figures of the annual output, and more importantly is does not take into account the higher efficiency of the cells due to the more uniform illumination, but it makes it possible to compare the different structures over the year.

Table 9.1 shows the annual irradiation of the cells for the different cases compared with the reference.

Table 9.1 Relative annual irradiation incident on the cells

	Reference	120° V-shaped structure	60° V-shaped structure	Sinusoidal structure
Relative annual irradiation	1.0	0.93	0.89	0.92

As expected considering that the MaReCo was optimized for this climate, the smooth reflector receives the highest annual irradiation. The 120° V-shaped structure and the sinusoidal structure show a mere 7-8% decrease. This indicates that small improvements in other areas such as uniformity of the light will improve the trough system using structured reflectors.

9.4 Increased concentration ratio

The increased concentration ratio given by the structured reflector can be exploited in two ways, either by reducing the cell area of the given system to get a lower system price, or by changing the shape of the trough to make use of the wider interval of acceptance which was seen in Figure 9.6. The interval of acceptance is directly connected to the size of the aperture. If the interval is smaller, the aperture is larger and vice versa. An interesting development would be to increase the trough aperture, creating a smaller angular acceptance interval for a smooth reflector system, but to use a structured reflector. As could be seen from Figure 9.6, the interval widens when a structured reflector is used. This will make it possible to accept almost all the light in the interval 20°-65° while increasing the concentration ratio. The use of the sinusoidal structure would create the same possibilities, but as the rays are more randomly reflected it would need a more thorough study of the geometry to use it optimally.

It is evident from Fig. 9.6 that the interval of acceptance in the current simulations was approximately 10° larger for the 120° V-shaped structure. In principle, it should be possible to decrease the present angular interval from 20°-65° to 25°-60° using the structured reflector. This would increase the concentration ratio by 27%.

9.5 Choice of structure

Of the three proposed structures, the 60° V-shaped structure receives the lowest annual irradiation. The 120° V-shaped structure has the highest optical efficiency when the sun is in the meridian plane, but the annual irradiation on the cells is roughly the same as for the sinusoidal structure. This is due to two characteristics of the sinusoidal structure, the higher optical efficiency at large azimuth angles, and the larger interval of acceptance. All three structures create a more uniform irradiation distribution on the cells which could be seen in Figure 9.4 and Figure 9.5. The sinusoidal structure has the largest homogenizing effect, while the two V-shaped structures show a more moderate reduction in peak intensity.

If the electricity production during a few hours of the day has the highest priority, the choice would be the 120° V-shaped reflector structure as this has approximately the same optical efficiency as the reference in the meridian plane, while still reducing the peak intensity on the cells. However, if the annual electricity production is important, the sinusoidal structure should be chosen. The yearly irradiation on the cells is approximately the same as for the V-shaped structure, and the irradiation is considerably more uniform over the cells.

The best choice for a system that is to produce electricity all the year is to use sinusoidal structured reflectors, and to change the size of the aperture to increase the concentration ratio. For a smooth reflector this would reduce the interval of acceptance, but as Figure 9.6 shows, the interval of acceptance widens when the sine structure is used, and this would compensate for the increased aperture size.

10 Contributions to co-authored articles

Article IV

Optical properties, durability, and system aspects of a new aluminium-polymer-laminated steel reflector for solar concentrators

Measurements on concentrators with different reflector materials were performed by the author.

Article V

Design, Building Integration and Performance of a Hybrid Solar Wall Element

The photovoltaic section of the article was written by the author. This consisted of measurements of the optical efficiency, simulation of the annual electricity output, and an analysis of the system in a photovoltaic perspective.

Article VI

PV performance of a multifunctional PV/T hybrid solar window

The photovoltaic section of the article was written by the author. This consisted of measurements of the optical efficiency, simulation of the annual electricity output, and a general analysis of the system.

Article VII

A new model and method for determination of the incidence angle dependence of the optical efficiency of solar concentrators

A ray tracing study of the optical efficiency of the three concentrators was performed by the author. The author took part in co-authoring large parts of the article which focus mainly on the optical characteristics and the biaxial model of the systems.

Article VIII

A new model and method for determination of the incidence angle dependent g-value of windows and sunshades

The author simulated the sunshades in a ray tracing study. The analysis of the model and its application on sunshades was largely performed in cooperation with the author.

Building Integration of Solar Energy (Fieber 2005)

A TRNSYS model of the solar window was developed by the author. This model calculates the annual output of hot water, electricity and passive gains in the building. The model made it possible to simulate different user strategies and their implications on the annual performance of the solar window. A ray tracing study of the optical performance of the solar window at different angles of incidence was also performed by the author.

Summary

There is clearly a need for renewable electricity, and the main obstacle for photovoltaic solar energy production is the high price of the generated electricity. This problem is addressed in the thesis by looking at low concentrating hybrids for generation of heat and electricity.

The first part of the thesis explained the basic principles of non-imaging optics and light concentrators. The most common concentrators were described and discussed.

Measurements were performed on two stand-alone MaReCo concentrators. MaReCo is an asymmetrically truncated wedge CPC intended for building integration on flat roofs. The aluminium absorber in the concentrator has monocrystaline silicon cells laminated on the surface. Two different reflector materials were used, one concentrator had reflectors of anodized aluminium and one had aluminium-polymer-laminated steel reflectors. The steel based reflector has a lower total reflectance and is slightly diffusing. The current-voltage characteristics and the irradiation distribution on the cells at different angles of incidence were measured. It was found that the short-circuit current was slightly higher for the concentrator with aluminium reflectors due to the higher total reflectance. However, the fill factor was higher for the steel based system. Measurements of the irradiation distribution on the cells in the two concentrators were performed for two angles of incidence. The conclusion was that the concentrated strip of light was wider and the peak intensity was lower for the steel based concentrator. This explains the increased fill factor.

Using an estimated optical efficiency for the systems at different angles of incidence, yearly simulations of the output of electricity and heat were performed. No difference in annual output between the systems was found and it was concluded that the steel based reflector is preferred due to its rigidness and its slightly diffusing properties. A study was made to determine the optimum absorber angle, and it was found that the absorber angle does not influence the total annual output unless it can be changed during the year. One of the concentrators had cells on both sides of the absorber and it was found that the side facing the front reflec-

tor generated more electricity and heat. If mounting space in unlimited, and the lowest possible cost per kWh is the most important parameter, the economically optimized system has cells facing the front reflector only. However, this will limit the production mainly to the summer, since the front reflector has a near horizontal aperture. If the total annual energy production is more important, or if mounting space is limited, it is recommended to have cells on both sides of the absorber. The system will then yield energy during the whole year, something that is of importance if it is integrated into residential buildings.

A new biaxial model of the optical efficiency of concentrators was developed to enable more accurate estimates of the performance of future prototype systems. The commonly used biaxial model is based on measurements of the optical efficiency in the longitudinal and transverse direction, keeping the other angle at 0° during the measurement. This is difficult to carry out for concentrators where normal incidence is outside the acceptance interval. Another problem with the model is that is tends to overestimate the influence of the cover glazing as it is accounted for twice. The presented model solves these problems by modelling the reflector as a function of the transverse angle of incidence, and the glazing as a function of the true angle of incidence. As the transmittance of the glazing as a function of the angle of incidence is easily calculated, all that is required for the new model is measurements in the transverse plane of the concentrator. The new model was evaluated during two summer months when the current from a module in a concentrator and the current from a reference in the plane of the concentrator aperture were measured. It was found that the model was successful in modelling the current from the concentrator module using the measured reference current.

The measurements of the current-voltage characteristics of the MaReCo showed that the largest decrease in efficiency was due to the high local intensities on small parts of the cells. The short-circuit current was high when the system was collecting optimally, but it resulted in a low fill factor. The diffusing steel reflector obtained higher fill factor values due to the slightly wider strip of light on the cells. Structured reflectors were evaluated as a possible solution to this problem. The structured reflectors offer two benefits, a more uniform illumination on the cells, and an increased concentration ratio. Two V-shaped structures and one sinusoidal structure were evaluated in a stand-alone MaReCo using Monte Carlo ray tracing. The results of the simulations were compared with simulation on a smooth reference. Within the interval of acceptance, 20° to 65°, it was found that the smooth reflector system had the highest optical efficiency in the transverse plane. The efficiency was higher for the structured reflectors outside the interval of acceptance which shows that the

structures widen the interval of acceptance for a given geometry. A study of the irradiation distribution on the absorber was performed to evaluate the homogenizing effects of the structured reflectors. All three structured reflectors were found to decrease the peak intensity and widen the strip of light on the cells. The highest peak reduction and widening was found for the sinusoidal reflector where the irradiation never exceeded 5 times the solar beam in the simulations. It was found that the optimum use of structured reflectors is when the geometry of the concentrator is designed with the structure in mind. This means that the interval of acceptance of a smooth concentrator should be decreased when if is fitted with structured reflectors to make use of the wider interval of acceptance given by the structure. A decreased interval of acceptance translates to a greater concentration ratio, and the system will thus collect more light onto the cells. The homogenizing effect of the structured reflectors will lead to a higher utilization of the collected light as the fill factor of the cells will increase when the peak intensity is decreased. These results show that structured reflectors constitutes an interesting topic of further research as their application will increase the efficiency of current two dimensional concentrators by yielding a higher concentration ratio and by increasing the fill factor of the cells.

References

Adsten, M., Helgesson, A., & Karlsson, B. (2005). Evaluation of CPC-collector designs for stand-alone for- or wall installation. Accepted for publication in *Solar Energy 2005*.

Bortz, J., Shatz, N., & Ries, H. (1997). *C*onsequences of étendue and skewness conservation of nonimaging devices with inhomogeneous sources and targets. *Proceedings of SPIE Vol. 3139*, pp 59-75.

Brogren, M., Wennerberg, J., Kapper, R., & Karlsson, B. (2003). Design of concentrating elements with CIS thin film solar cells for wall integration. *Solar Energy Materials & Solar Cells Vol. 75*, pp 567-575.

Brogren, M., Nostell, P., & Karlsson, B. (2000). Optical efficiency of a pv-thermal hybrid CPC for high latitudes. *Solar Energy Vol. 69* (Suppl.), pp 173-185.

Brogren, M., Helgesson, A., Karlsson, B., Nilsson, J., & Roos, A. (2004). Optical properties, durability and system aspects of a new aluminium-polymer-laminated steel reflector for solar concentrators. *Solar Energy Materials and Solar Cells Vol. 82*, pp 387-412 .

Chant, V.G., & Håkansson, R. (1985). The *MINSUN simulation and optimisation program*. Application and users guide. IEA SH & C Task VII, Ottawa.

Coventry J.S. (2005) Performance of a concentrating photovoltaic/thermal solar collector. *Solar Energy Vol. 78* (2), pp 211-222.

Duffie, J.A., & Beckman, W.A. (1980). *Solar Engineering of Thermal Processes*. Wiley Interscience, New York.

Feuermann, D., & Gordon, J.M. (2001). High-concentration photovoltaic designs based on miniature parabolic dishes. *Solar Energy Vol. 70* (5), pp 423-430.

Fieber, A. (2005). *Building Integration of Solar Energy – A Multifunctional Approach.* (Report EBD-T--05/3). Lund, Sweden: Div. Energy and Building Design, Dept. Construction and Architecture, Lund University.

Fraidenraich, N. (1998). Design procedure of V-trough cavities for photovoltaic systems. *Progress in Photovoltaics: Research and Applications Vol. 6* (1), pp 43-54.

Green, M.A. (1998). *Solar Cells – Operating principles, Technology and System Applications*. University of New South Wales.

Helgesson, A., Krohn, P. & Karlsson, B. (2004). Development of a MaReCo-Hybrid for Hammarby Sjöstad, Stockholm. *Proceedings of Eurosun 2004*, Freiburg, Germany.

IEA-PVPS Task 7 (2005). *Designing with Solar Powe*r. Edited by Prasad D. and Snow M. IEA-PVPS Report.

Karlsson, B., & Wilson, G. (1999). MaReCo – A large asymmetric CPC for high latitudes. *Proceedings of ISES Solar World Congress*, Jerusalem, Israel.

Leutz, R., Suzuki, A., Akisawa, A., & Kashiwagi, T. (1999). Design of a nonimaging Fresnel lens for solar concentrators. *Solar Energy Vol. 65* (6), pp 379-387.

Leutz, R., & Ries, H. (2003). Squaring the Circle – The Use of Microstructures for Converting and Homogenizing Beam Cross-sections. *Proceedings of SPIE Vol. 5186* .

Mallick, T.K., Eames, P.C., Hyde, T.J., & Norton, B. (2004). The design and experimental characterisation of an asymmetric compound parabolic photovoltaic concentrator for building facade integration in the UK. *Solar Energy Vol. 77* (3), pp 319-327.

McIntire, W. R. (1982). Factored approximations for biaxial incident angle modifiers. *Solar Energy Vol. 29* (4), pp 315-322.

McMahon, T.J., & von Roedern, B. (1997). Effects of light intensity on current collection in thin-film solar cells. *Proceedings of 26th PVSC conference*, Anaheim, USA.

Mills, D.R., & Giutronich, J.E. (1978). Asymmetrical non-imaging cylindrical solar concentrators, *Solar Energy Vol. 20*, pp 45-55.

Miñano, J.C., González, J.C., & Benítez, P. (1995). A high-gain, compact, nonimaging concentrator: RXI. *Applied Optics Vol. 34* (34), pp 7850-7856.

Perers, B., & Karlsson, B. (1993). External reflectors for large solar collector arrays, simulation model and experimental results. *Solar Energy Vol. 51* (5), pp 327-337.

Piszczor, M.F. Jr., O'Neill, M.J., & Fraas, L.M. (1993). A novel space photovoltaic module using a linear Fresnel lens and a line-focus tandem cell receiver. *Proceedings of the 23rd Photovoltaic Specialists Conference*, Louisville, KY, USA.

Rabl, A. (1976). Optical and thermal properties of compound parabolic concentrators. *Solar Energy Vol. 18*, pp 497-511.

Rönnelid, M., & Karlsson, B. (1997). Irradiation distribution diagrams and their use for estimating the collectable energy. *Solar Energy Vol. 61*, pp 191-201.

Rönnelid, M., & Karlsson, B. (2003). Optimised truncation of a wide acceptance angle CPC. *Proceedings of ISES Solar World Congress 2003* in Gothenburg, Sweden.

Sala, G., Arboiro, J.C., Luque, A., Zamorano, J.C., Minano, J.C., Dramsch, C., Bruton, T., & Cunningham, D. (1996). The EUCLIDES prototype: An efficient parabolic trough for PV concentration. *Proceedings of the 25th Photovoltaic Specialists Conference*, Washington D.C. USA.

Schramek, P., & Mills, D.R. (2003). Multi-tower solar array. S*olar Energy Vol. 75* (3), pp 249-260

Souka, A.F., & Safwat, H.H. (1966). Optimum orientations for the double exposure flat-plate collector and its reflectors. *Solar Energy Vol. 10*, pp 170-174.

Vant-Hull, L.L., & Hildebrandt, A.F. (1976). Solar thermal power system based on optical transmission. *Solar Energy Vol. 18* (1), pp 31-39

Wenham, S.R., Green, M.A., & Watt, M.E., *Applied Photovoltaics*, Centre for Photovoltaic Devices and Systems, University of New South Wales, Australia .

Williamson, D.E. (1952). Cone channel condenser optics. *Journal of the Optical Society of America Vol. 42*, pp 712-715.

Winston, R., & Hinterberger, H. (1975). Principles of cylindrical concentrators for solar energy. *Solar Energy Vol. 17*, pp 225-258.

Winston, R., Miñano, J.C., Benítez, P., Shatz, N., & Bortz, J.C. (2005). *Nonimaging optics,* Elsevier Academic Press, London, UK.

ZEMAX version February 3, 2005, ZEMAX Development Corporation, San Diego, California, USA.

Appendix A

Basic function of the electronic load

The electronic load is schematically shown in Figure A.1. A more detailed description is shown in Figure A.2.

An Operational amplifier compares the actual voltage over the electronic load connected to the solar cell with a control voltage from the logger. If the voltage over the electronic load is higher than desired, the output voltage from the op-amplifier is increased, and this increases the current through the power transistor (T1). This causes the voltage over the load to be reduced as the current from the cells increases and the measuring point on the IV-curve is moved towards lower voltage.

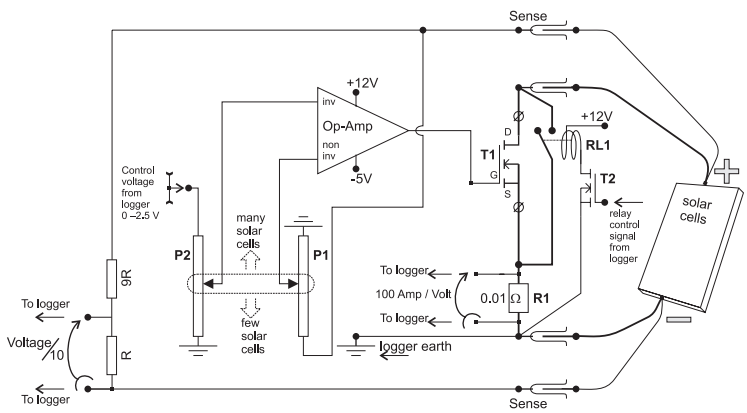

Figure A.1 *Principle drawing of the electronic load for measuring IV-characteristics.*

Voltage ranges

The logger produces excitation voltages up to 2.5 V. To make it possible for the electronic load to measure at higher voltage ranges, a potentiometer acting like a voltage divider is connected to the solar cells. This is the potentiometer P1 shown in the figure.

To be able to measure on solar cell arrays with less than 2.5 V maximum voltage, another potentiometer is added in the control circuit (P2). The two potentiometers are mechanically connected in opposition as the figures show. When the left potentiometer is moved up in the figure to compensate for a higher open circuit voltage, the right potentiometer will use a larger part of the 2.5V control signal to further compensate for the higher voltage.

Measurement of current

A four terminal shunt resistance, R1, of 0.01 Ω is used for the current measurements. With a 4 wire arrangement, the voltage drop of the connection of two wires conducting the current is not affecting the voltage measured by the other two wires. The tolerance of the resistor is ±1%. The maximum power is 2 W according to the specifications, which allows for 14 A continuous current through R1.

Low resistance

To reduce the resistance for the short circuit measuring, a relay, RL1, is used for this point. When the relay closes the circuit, most of the current goes through the switch. To furthermore minimise the internal resistance, attention has been paid to reducing the wire length between the connections, relay, and shunt resistance. The (Ø 4 mm) connectors on the front panel are also doubled if two wires in parallel are used to reduce the resistance.

Sense input

In order to exclude resistance of the connecting wires that carries the current in the I-V-measurements, the voltage is measured with separate wires connected to the sense input on the front panel of the electronic load. In case voltage sensing wires are not used, two 3 Ω resistances connect the sense input to the voltage of the connectors on the front panel. If the voltage sensing wires are connected to an active panel before connecting

the wire for current measurements, a large current will pass through the 3 Ω resistance causing overheating. By choosing resistors with a high positive temperature coefficient this potential overheating is prevented.

1:10 voltage reduction

The resistors in the voltage divider are constructed from an integrated (thick film) resistor network with fifteen resistors of the same value. Nine resistors are connected in parallel together with one single resistor in series. In this way a 1:10 voltage divider is realized. The advantages of doing the voltage divider in this way is that it is simple to make and that all resistors are expected to have the same temperature coefficient. It has also proved to be accurate. Finally the voltage divider can be tested with a voltage source and a voltage meter. If the precision demands are not met, the resistor network can be easily discarded and replaced.

Preventing oscillations

An electronic load should be able to produce a very low and stable resistance. This is especially important for solar panels with few cells and high irradiation. This requires a large amplification of the control voltage to current and if a high amplification is used there could be a tendency of oscillation. The power transistor is prevented from amplifying and radiating high frequencies by using a ferrite bead connected close to the drain terminal and also by a capacitor between drain and gate for negative feedback.

A 10 nF/3 kΩ network is connected to the output of the operational amplifier to help compensating for the phase shift caused by the internal capacitance of the power transistor.

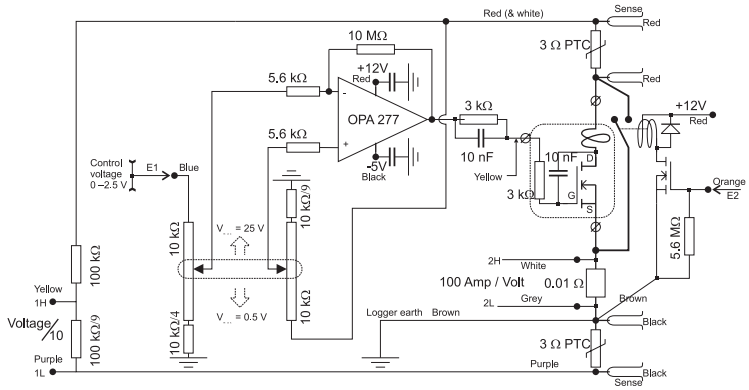

Figure A.2 Detailed drawing of the electronic load.

Article I

ELECTRICAL AND THERMAL CHARACTERIZATION OF A PV-CPC

Johan Nilsson, Håkan Håkansson, Björn Karlsson
Division of Energy and Building Design, Department of Architecture and Built Environment,
Lund University, P.O. Box 118, Lund, SE-22100, Sweden,
Phone: +46-46-2227606, Fax: +46-46-2224719, E-mail: johan.nilsson@ebd.lth.se

Abstract – Long term evaluation of an asymmetric CPC PV-thermal hybrid built for high latitudes, MaReCo (MaximumReflectorCollector), is performed in Lund, lat 55.7º, and this paper discusses output estimates and characteristics of the system. The output estimates are calculated using the MINSUN simulation program. To get the input for MINSUN, measurements were performed on two MaReCo prototypes. These measurements show that the front reflector collects most of the irradiation in the summer, and the back reflector in the spring and fall. Two different reflector materials were used, anodized aluminium and aluminium laminated steel. The steel based reflector was selected for its rigidness. The output estimates show no difference in yearly output between the two reflector materials, both back reflectors deliver 168 kWh/(m^2 cell area) of electricity compared to 136 kWh/m^2 cell area for cells without reflectors. The cells facing the front reflector deliver 205 kWh/(m^2 cell area) of electricity. The estimated output of thermal energy was 145 kWh/(m^2 glazed area) at 50°C. The estimates show that the optimal placement of the photovoltaic cells is facing the front reflector, but having cells on both sides is in most cases the best option.

1. INTRODUCTION

In view of the high costs of photovoltaic modules, it is necessary to find ways to reduce the cost of a PV system considerably to generate more extensive use. One approach is to use concentrating reflectors to increase the irradiation on the photovoltaic cells. This approach is promising due to the low cost of the reflectors, which is significantly lower than the cost of the cells and this has been shown to reduce the energy cost (Perers and Karlsson 1993). The electricity generation is impeded by high temperatures, and cooling the cells actively with water is one efficient way to increase the yield (Rönnelid et. al. 1999). Another benefit from cooling the cells with water is the possibility to use the hot water for heating provided that the produced heat fulfils a demand and replaces heat from other sources. By rising the temperature of the cooling water it can be utilized for heating, however at the expense of lower electrical yield.

In Sweden, and other high latitude countries, the solar radiation over the year is asymmetric because of the high cloud coverage during the winter months and thus concentrated to a small angular interval of high irradiation. This makes the use of stationary reflectors or concentrators attractive.

An asymmetric compound parabolic reflector system with two truncated parabolic reflectors, MaReCo (MaximunReflectorCollector) has been built considering the conditions of high latitude (Adsten, Helgesson, Karlsson 2005), and the aim of our current project is to evaluate this system for a PV/T hybrid. The system is described in Figure 1.

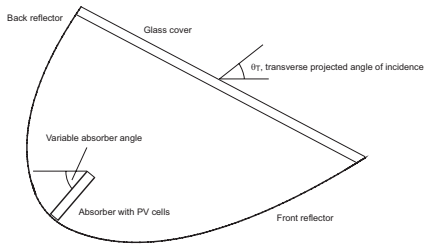

Figure 1 The MaReCo PV-thermal hybrid. Both parabolic reflectors have the same focal point, at the top of the absorber. The photovoltaic cells are laminated on the absorber. The glass cover tilted in 30º is for weather protection. The absorber angle is the angle between the absorber and the horizontal. Also shown is the transverse projected angle of incidence.

The glazed aperture is tilted in 30º from the horizontal. The photovoltaic cells used are standard monocrystaline silicon cells for non concentration applications for keeping the cost of the system low. The aperture of the front reflector is tilted 2º from the horizontal and has a geometrical concentration ratio (aperture area/cell area) of 3.5. The aperture of the back reflector is tilted 8º from the vertical and the geometrical concentration ratio is 2.5.

2. SOLAR CLIMATE

For a two dimensional system such as a concentrator with an east-west axis, the direction of the direct irradiance vector on a surface can be represented by two orthogonal components. If the surface is facing south, it can be divided into one component parallel with the east-west axis, and one that is normal to it. The parallel component will not contribute to the irradiation of the surface and can be ignored. The other component will fall on the surface in an angle determined by the transverse projected angle of incidence, i.e. the angle of the component in the meridian plane. The transverse projected angle of incidence is shown in Figure 1. By making a diagram of the amount of irradiance falling in each angle interval of the transverse projected angle, it is possible to design reflectors with an adjusted acceptance interval.

The system was evaluated in Lund, Sweden. Figure 2 shows the angular distribution of irradiation during a year in Lund for a plane tilted in 30º.

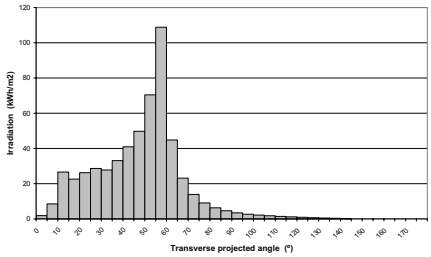

Figure 2 Yearly irradiation per angle interval in Lund at latitude 55.7°. The irradiation was measured at a surface tilted 30° from the horizontal, which is the tilt of the glass cover.

As can be seen in the figure, most of the irradiance is in the interval between 20° and 65° and the design of the MaReCo, which has an angle of acceptance in this interval, is well suited for these conditions. The angle of acceptance is defined as the angle interval where the system collects all of the irradiation. Outside this interval, a fraction of the incident light is collected if the concentrator is truncated.

3. THE EVALUATED SYSTEM

Two different MaReCo prototypes were characterized, MaReCo1 and MaReCo2. Table 1 shows data for the systems. The third prototype, MaReCo3 was used for long term outdoor measurements.

	MaReCo1	MaReCo2	MaReCo3
Cells facing back reflector	2	12	0
Cells facing front reflector	3	0	20
Absorber angle	45	20	65
Trough material	Anodized aluminium	Steel with aluminium coating	Anodized aluminium
Length (m)	1	2	3.5

Table 1 Evaluated prototypes. The absorber angle and the placement of the reflectors are defined in Figure 1.

The cells were laminated onto an aluminium profile that was eloxidized to a dark colour to improve its heat absorbing properties. One of the variants had cells on one side of the absorber only, and the other side was just absorbing heat.

MaReCo1 and MaReCo2 were not of full length, the full size MaReCos have a length of 3-5 meter. One effect that will be more pronounced in the small scale evaluations compared to the full size systems is the shading of the outermost cells by the trough gables. In the mornings and evenings, the part of the absorber closest to the gables will be shaded. In the full size system, the photovoltaic cells will be placed a longer distance from the gables to prevent shading of the cells. This is not possible in the short prototype systems. The effects of the shading have therefore to be corrected for when the performance of long collectors is simulated.

4. REFLECTOR MATERIALS

Two of the troughs had reflectors made of anodized aluminium, and one had reflectors of aluminium laminated steel (Brogren et. al. 2004). The advantage of the steel based reflector is its mechanical properties, i.e. its rigidness. A stainless steel parabolic reflector can be made with less mechanical support than an aluminium reflector. The disadvantage with the laminated steel reflector is its relatively low specular reflectance. Figure 3 shows a comparison between the reflectance of anodized aluminium and aluminium laminated steel.

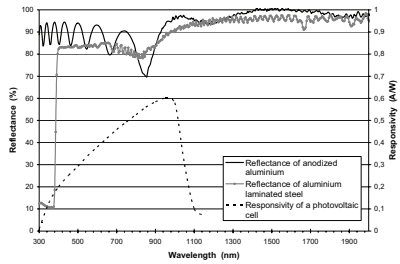

Figure 3 Reflectance as a function of wavelength for the two reflector materials. The responsitivity curve shows an example of the wavelength interval where the silicon cell is working.

The steel based reflector has very low reflectance below 400 nm since its plastic coating absorbs light below 400 nm. The reflectance of the steel based reflector is slightly lower in the wavelength interval where the solar cells operate.

By visual inspection, there was a considerably larger number of imperfections in the aluminium reflector troughs, which shows the difference in rigidness between the steel reflector and the aluminium reflector.

An interesting aspect of the steel based reflector is its slightly higher scattering of the light. It has been shown previously that more evenly distributed light over the cells increases the efficiency of the cell (Benítez and Mohedano 1999).

5. MEASUREMENTS

5.1 General measurements

The electrical performance and the irradiance distribution on the cells was measured for

different transverse projected angles of incidence.

To measure the characteristics at different transverse projected angles, the trough was manually rotated along its axis of symmetry and a potentiometer placed at the axis recorded the tilt of the trough. The potentiometer was calibrated in the beginning of the measurement by manually observing the angle of incidence with a graduated arc mounted on the side of the trough. A vary fast I-V tracker for monitoring the current and voltage from the cells at different loads was constructed to facilitate the measurements. Monitoring at a specific transverse projected angle of incidence was done in less than one second with this device. This made it possible to get the I-V characteristics and the fill factor as a function of the transverse angle of incidence in a short period of time. Only a fraction of the measured data is presented here.

The irradiance distribution on the cells was measured using a photodiode. The diode was placed on a rotating lever which was moved from the top to the bottom of the cell. The lever was rotated in a plane very close to the cell surface, and the angle of rotation was measured by a potentiometer. The photodiode aperture area was reduced by a plate with a 1 mm diameter hole to increase the spatial resolution. The irradiance distribution measurements were performed for transverse projected angles of 33º and 57º with the sun in the meridian plane.

The total incident irradiation was measured using a pyranometer that was mounted normal to the solar beam.

5.2 Short circuit current

Figure 4 and Figure 5 show the short circuit current (I_{SC}) and the fill factor as a function of transverse projected angle for the cells facing the back and front reflector.

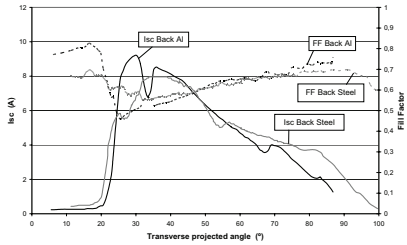

Figure 4 Short circuit current and fill factor for back reflectors of MaReCo1 and MaReCo2.

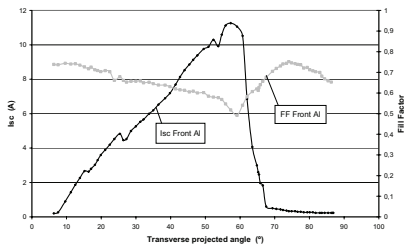

Figure 5 Short circuit current and fill factor for the front reflector of MaReCo1.

The short circuit current of the cell is approximately proportional to the irradiance and the fill factor is a measure of the resistive losses in the cells, a low fill factor corresponding to high losses (Green 1982).

At low transverse projected angles, the back reflector is providing most of the light on the cells. The back aluminium reflector has its best electrical performance in the interval between 25° and 55° transverse angle as seen in Figure 4. At higher transverse projected angles, in the summer, the front reflector contributes to the majority of the irradiation onto the cells. The optimal angle for this reflector is according to Figure 5 between 40° and 65°. This system will thus collect irradiation between a transverse projected angle of incidence of 25° and 65° efficiently. The two local minima of the curves, at 27° and 55° in Figure 5, occurs when the strip of concentrated light, which is only approximately 2 cm wide in practice, falls on

one of the two conducting fingers on the surface of the cell. This finger shades a part of the cell, and less photons reaches the p-n junction.

The front reflector and the back reflector are two examples of asymmetrical cylindrical concentrators (Mills and Giutronich 1979) with apertures between the focal point and the edge of the reflector. The aperture of the back concentrator is close to vertical and the aperture of the front reflector is horizontal. As can be seen in Figure 4 and Figure 5, both have a maximum flux concentration ratio at the limiting angles (20º and 65º) where all of the light is concentrated to the focal point. Due to the fact that the cells are slightly smaller than the absorber and thus not covering the whole absorber area, the peaks are shifted slightly in the figures.

The short circuit current of the two back reflectors differ slightly. The maximum short circuit current of the aluminium reflector is higher than that of the steel based reflector, and the steel based reflector is more efficient at higher angles where the short circuit current is approximately 1.5 A higher. The lower peak current of the steel based reflector is due to its lower specular reflectance.

The absorbers of the characterized MaReCos were placed at different tilt angles, as defined in Figure 1. The absorber angle of the aluminium trough was 45º and the absorber angle was 20º for the steel trough. The higher efficiency at high transverse angles of the steel based reflector system is due to its lower absorber angle, which decreases the number of reflections and thus the reflection losses. For a discussion on the effects of absorber angle, refer to section 5.6.

Both figures show that the fill factor is low when the short circuit current is high, i.e. when the light is concentrated more, it is utilized less. This is visible in Figure 4 which shows that the fill factor is higher for the steel based reflector cells. The internal losses in the cell are proportional to the square of the current, RI^2, and the output power of the cell is proportional to the current, UI, where U's dependence on the irradiance can be neglected. As the current increases when the irradiation on the cell increases, the relative losses increase more than the delivered power, and the fill factor decreases. Another aspect of this, visible in Figure 4, is that when the light is concentrated onto the finger of the cell (at 33° and 57° transverse projected angle of incidence), the short circuit current is significantly lower, and the fill factor is higher. This is explained by the fact that the electrical losses are reduced when light is concentrated close to the fingers and the current has less resistance to the conductor. This indicates that it is desirable to have the intensity maximum close to, but not on, the fingers (Benítez and Mohedano 1999).

5.3 I-V characteristics

The most important measure of the power delivered from the cells is the IV-plots, the relationship between the output current and the output voltage. Figure 6 and Figure 7 show these relationships at two different transverse projected angles, 35°, and 57°, close to the flux concentration maximum of the back and front reflectors respectively.

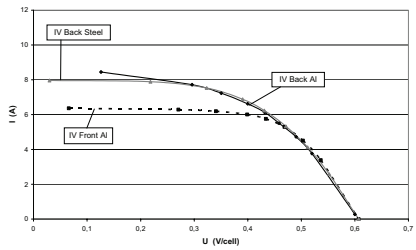

Figure 6 I-V characteristics at 35º transverse projected angle of incidence. The voltage of one cell is shown to make a comparison possible. The voltage at open circuit condition is the same for all geometries.

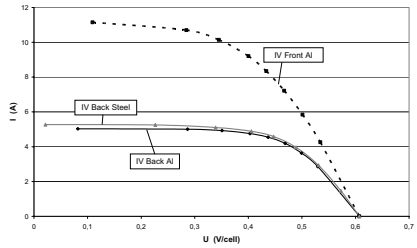

Figure 7 I-V characteristics at 57º transverse projected angle of incidence.

Figure 6 indicates that the aluminium reflector has slightly better performance than the steel based. The difference in fill factor between the steel and aluminium reflectors is small and the short circuit current is higher for the aluminium reflector.

The maximum power point for each curve was calculated by a parabolic fit to three discrete measured I-V points. In Figure 6, the maximum power was 2.7 W/cell for the back aluminium reflector, and 2.6 W/cell for the steel based reflector. The front reflector had a maximum power output of 2.4 W/cell at this angle of incidence.

Figure 7 shows the same characteristics at 57° transverse projected angle of incidence. The front reflector cells produce considerably more power in this case, 3.8 W/cell, compared to 2.0 W/cell for the back aluminium reflector cells and 1.9 W/cell for the steel based reflector cells.

5.4 Irradiance distribution

The irradiance distribution over the cells varies with the angle of incidence. The distribution was measured for the two prototypes at the two transverse projected angles of 33º and 57º as can be seen in Figure 8 and Figure 9. The transverse angles were selected as 33° and 57° to be able to study the back and front reflector at angles were they have high efficiencies.

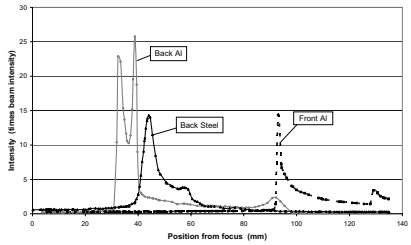

Figure 8 Irradiation distribution at 33º transverse projected angle of incidence. The intensity is measured in times the beam intensity of the sun, and 0 at the position axis means on the end of the absorber, at the focal point.

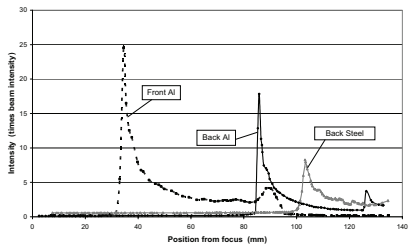

Figure 9 Irradiation distribution at 57º transverse projected angle of incidence. The intensity is measured in times the beam intensity of the sun, and 0 at the position axis means on the end of the absorber, at the focal point.

Figure 8 shows the irradiance distribution at 33° transverse angle. The front reflector gives a low intensity at the cells in this case, but both back reflectors seem to be working in their optimum range, all of the light is concentrated onto the cells. The peak intensity of the aluminium reflector is higher than the peak of the steel based reflector, 25 times the beam intensity of the sun compared to 14 times in the case of the steel based reflector. This is due to the higher specular reflectance of the aluminium. The steel based reflector is more diffusing, and this makes the strip of concentrated light slightly wider and less intense. The slightly lower peak in this case is not of great importance, as seen in Figure 4 the short circuit current is lower, but

the fill factor is higher. The coupling of these two factors makes the difference in intensity less significant, which will be shown in section 6. The peak intensity of the steel based reflector is shifted to the right of the aluminium one, and this is due to the different absorber angles of the two systems. The angle between absorber and the horizontal plane in the case of the steel based reflector is considerably smaller than the angle in the aluminium absorber case, and this shifts the peak towards the reflector. Section 5.5 discusses the influence of the absorber angle on the output.

Figure 9 shows the distribution at a higher solar height, 57°. At this height, the front reflector is more optimal, refer to Figure 5. The peak intensity is here 25 times the beam intensity of the sun, and all of the reflected light hits the cells. The back reflectors are less optimal in these conditions, and especially the steel based MaReCo with its cells in 20° with the horizontal plane has more multiple reflections before absorbing the light.

5.5 Optical efficiency and electrical output

Using the measured data as input, a simulation of the yearly output of heat and electricity has been performed using MINSUN (Chant and Håkansson 1985). This program was originally created for simulating solar heating systems, but it can be used to calculate the output of heat-electricity hybrids.

MINSUN uses hourly climate data, including direct and diffuse irradiation, from a large database to calculate the total annual irradiation on a specified surface. The irradiation data is used together with the incidence angle modifiers of the system to calculate the annual output. It is possible to use one of two different models of incidence angle modifier. The normal case for planar solar collectors and planar photovoltaic modules is to use $K_{\tau\alpha}$, which is defined in Eq. (1).

$$K_{\tau\alpha} = 1 - b_0\left(\frac{1}{\cos(\theta)} - 1\right) \qquad (1)$$

b_0 is the incidence angle modifier which is supplied as input data to the simulation, and θ is the angle of incidence. The alternative is to have MINSUN calculate the product between the incidence angle modifier as a function of the transverse projected angle (in the meridian plane), $\eta(\theta_T)$, and the modifier in the east-west horizontal direction, $g(\theta_L)$ by supplying values of the two functions in intervals of 10°. The total incidence angle modifier, the optical efficiency (Nilsson et. al. 2005), is then calculated according to Eq. (2).

$$f(\theta) = g(\theta_L) \cdot \eta(\theta_T) \qquad (2)$$

To calculate $g(\theta_L)$, we used Eq. (1) as $g(\theta_L)$, with a b_0 of 0.23. This value has been obtained in previous measurements in our laboratory. $\eta(\theta_T)$ was calculated according to Eq. (3) for a surface with a 30° tilt, as the glazing is tilted 30º.

$$\eta(\theta_T) = \frac{I_{sc} \cdot 1000}{I_{1000} \cdot C_g \cdot G \cdot \cos(\theta_T - 60)} \qquad (3)$$

I_{1000} is the short circuit current at an irradiance of 1000 W/m^2 on the module, which in this case was 4.55 A. C_g is the geometrical concentration of the concentrator system defined as the glazed aperture area divided by the cell area. θ_T is the transverse projected angle of incidence in degrees, and G is the total intensity normal to the sun. To get the efficiency relative to the incoming irradiation, the expression was divided by C_g. $G(\cos(\theta_T-60))$ is the irradiance at the glazing. The measurements were performed on very clear days with a low fraction of diffuse irradiation, and the total irradiation was treated as a beam irradiation incident in the incidence angle of the beam.

The short circuit current plots in Figure 4 and Figure 5 were used to calculate the angular dependence of the short circuit current I_{SC}. Applying Eq. (3) to the measured data gives incidence angle modifiers according to Figure 10.

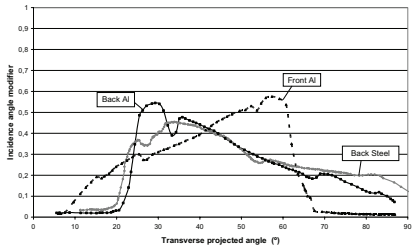

Figure 10 Incidence angle modifiers in the meridian plane. The incidence angle modifier, $\eta(\theta_T)$, was calculated using Eq. (3).

The MINSUN simulations were performed using a climate data file for Stockholm, Sweden (latitude 59.3N), as the small difference in the climate compared to Lund can be neglected in view of other assumptions made in the simulation.

A reference simulation with photovoltaic cells mounted with 30° tilt was done for comparison.

Prototype	Yearly electrical output per m^2 cell area	Improvement
MaReCo1, back reflector	168 kWh	22.6%
MaReCo2, back reflector	168 kWh	22.6%
MaReCo1, front reflector	205 kWh	49.1%
Cells without concentrator	136 kWh	0.0%

Table 2 Electrical output from different prototypes. The cells without concentrators were placed in a 30° tilt for the simulation to be able to compare it with the irradiation in the MaReCo.

As Table 2 shows, the result for the back aluminium laminated steel based reflector, MaReCo2, and the back anodized aluminium reflector, MaReCo1, are identical. The output increase from the reference simulation is 22.6%. Looking in detail at $\eta(\theta_T)$ in Figure 10 reveals that the peak modifier for the aluminium reflector is higher than for the steel based reflector, but the incidence angle modifier is higher at high solar angles for the steel based reflector. These two effects cancels out in the simulation. The front reflector seem to be more suitable for photovoltaic cells, the output increase from the reference simulation is here 49.1%.

These simulations show that if the target is to maximize the ratio (cell area)/kWh, the optimal placement of the cells is facing the front reflector.

5.6 Influence of absorber angle

The angle of the absorber, which was defined in Figure 1, influences the irradiance distribution over the absorber. As discussed in the previous section, the irradiance distribution on the cells affects the electrical output. Using Equation 3, the incidence angle modifier in the transverse direction was measured and calculated for three different absorber angles, 20°, 45°, and 70° and the results can be seen in Figure 11.

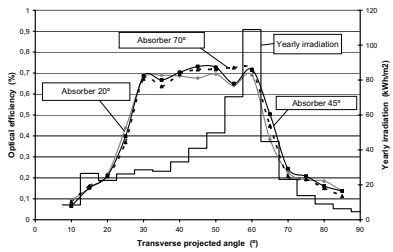

Figure 11 Optical efficiency for the MaReCo when the absorber is mounted in three different angles. The yearly irradiation shows the angular interval where the concentrator has to be optimized.

The measurements were performed when the sun was in the meridian plane of the trough and this makes the incidence angle modifier equal to the total optical efficiency as the incidence angle modifier in the east-west direction is 1 for this case. MaReCo2 was used in the measurements, having cells facing both back and front reflector. What is shown in the figure is the total optical efficiency of the system where the electricity from both sides of the absorber has been combined. The absorber

angle was changed, and the measurements were performed as described in section 5.2. The climatic data from Figure 2 is drawn in the figure to show at what angles the system has to be optimized. As seen from the figure, all three cases have favourable angular intervals, but the total output on a yearly basis is approximately the same. The irradiation incident on the MaReCo between 20º and 65º is collected onto the absorber in all three cases, the difference originates from the different distribution of light over the absorber, see Figure 8 and Figure 9. These differences in distribution accounts for the small differences at each angle, but as can be seen from Figure 11, there is no single angle which has better performance at all transverse projected angles. The distribution profile is shifted to the left or right when the absorber angle changes, but the profile stays the same. Since it is the intensity at a certain point that creates the output and the losses, the output change due to the angular shift is a small in comparison to other effects.

Yearly simulations show that the difference in output is approximately 3%, which is within the margin of error of the measurements.

6. OUTDOOR MEASUREMENTS

A MaReCo hybrid with aluminium reflectors and 20 cells facing the front reflector was placed outside for long term measuring. It is shown in Table 1 as MaReCo3. The absorber was tilted in 65º and had no cells facing the back reflector. The side facing the back reflector was untreated and had a relatively low absorptance. The thermal performance of this hybrid was evaluated by MLR and the electrical performance by measuring the short circuit current.

6.1 Thermal evaluation

MINSUN was used to evaluate the annual thermal performance of the hybrid. In order to perform heat calculations, MINSUN uses Eq. (4) to calculate the heat gained.

$$P = \eta_{0b}(\theta)\cdot G_b + \eta_{0d}(\theta)\cdot G_d - k_1\cdot\Delta T - (mC)_e\cdot\frac{dT}{d\tau}$$

η_0 is the optical efficiency for beam (b) and diffuse (d) irradiation.
k_1 [W/m^{2}K] is the loss coefficient per collector area
ΔT [K] is the difference between the ambient temperature and the temperature of the collector
$(mC)_e$ [J/m^2] is the heat capacity of the collector
$dT_f/d\tau$ [K/s] is the time derivative of the temperature of the cooling media
θ is the angle in incidence

The parameters were calculated for MaReCo3 doing an MLR analysis on measurement data for three summer months. The resulting values were η_{0b}=0.474, η_{0d}=0.334, k_1=3.85 W/m^{2}K, and $(mC)_e$=10691 J/m^2. Different fluid temperatures, ΔT, gives different delivered energy, and to be able to use the water for tap water or heating, it must be at least 50° C. When this temperature of the fluid was selected, the annual energy yield of the system was 145 kWh/m^2 glazed area. To demonstrate the difference, if a fluid temperature of 25° C was accepted, the yield would have been 264 kWh/m^2 glazed area.

A thermal MaReCo with a standard absorber has η_{0b}=0.6, η_{0d}=0.40, and k_1=2. The high k_1 for the hybrid is due to the high emittance of the photovoltaic cell as it is without the selective coating of a standard heat absorber. The low η_{0b} can be explained by two factors. The first factor is that absorber is untreated on the side facing the back reflector, it gives a shiny impression. This decreases the absorption of the back side. The second factor is due to problems in the manufacturing of the prototypes. The absorber is designed to make it possible to do the assembly in place when the system is erected, but the manufacturing precision is too low. The cupper pipe containing the heat collecting fluid has a bad thermal contact with the absorber profile, and the losses due to this is considerable as there will be a gap of air reducing the heat flow. In future prototypes, this has to be solved, or a less flexible absorber has to be used to increase the thermal output and reduce the overheating of the photovoltaic cells.

6.2 Electrical evaluation

To validate the experimental electrical measurements, the short circuit current was measured for MaReCo3 during three summer months. As comparison, the same type of absorber with the same type of cells was placed horizontally beside the MaReCo. The reason for having a horizontal reference is that as the trough only has cells facing the front reflector, the aperture is almost horizontal.

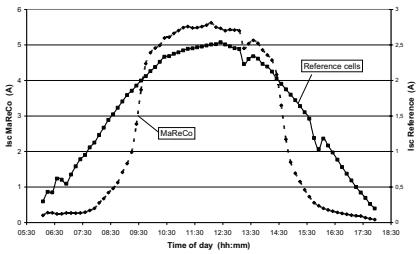

Figure 12 Short circuit current for horizontally mounted cells and the MaReCo with identical cells. The measurements were taken outdoors on a clear day with a very high percentage of direct irradiation.

The measurements in Figure 12 show that the short circuit current at high transverse angles (around noon) is similar for the reference and the concentrating system apart from the concentration factor, i.e. the concentrating system has the same angular dependence. This is an important observation, at the conditions where the irradiation has its maximum, the performance of the MaReCo is optimal. The cut-offs on the MaReCo graph is due to the small size of the concentrator trough. The gables are shading the cells as the sun is east or west of the trough glass surface as discussed in section 3.

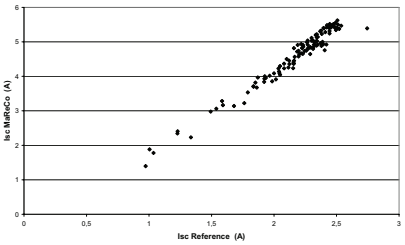

Figure 13 Short circuit current of MaReCo versus reference cells on clear days between 10.00 and 14.00 when no shading from the gables takes place.

Figure 13 shows measurements on clear days between 10.00 and 14.00. This figure clearly indicates a linear dependence between reference output and MaReCo output. The time interval of the measurements is to avoid the shading effects discussed earlier, effects that could be seen in Figure 12.

These measurements were performed on a clear day with a high percentage of direct insolation, but these ideal condition are not always present. Most days at the Swedish latitude have a high percentage of diffuse, isotropic irradiation. Figure 14 shows the performance of the MaReCo compared to the reference on a day with low direct irradiation, an almost isotropic sky.

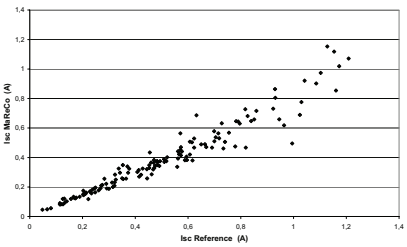

Figure 14 The short circuit current of the MaReCo versus the reference cells. Measurements taken on a cloudy day with high percentage of diffuse isotropic irradiation.

The output of the MaReCo is in this case the same as the output of the reference cells all day apart from the reduction due to the reflectance of aluminium in the reflectors, and the reflections on the cover glass. The optical efficiency can be derived from the figure to approximately 0.8.

The relationship between the reference output and the MaReCo output under a longer period with changing weather conditions is shown in Figure 15.

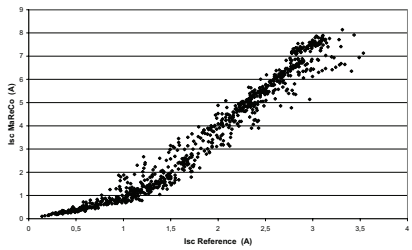

Figure 15 Short circuit current of MaReCo versus reference cells in all weather conditions. Measurements were taken under a period of one and a half months between 10.00 and 14.00.

The output of the reference can be seen as a measure of the amount of diffuse irradiation. Low output of the reference means low amounts of direct irradiation. The linear dependencies at high amounts of direct irradiation, and high amounts of diffuse isotropic irradiation can clearly be seen in this figure.

7. SIMPLE ELECTRICAL MODEL

The measured data for one of the summer months was used to create a simple electrical model of the MaReCo short circuit current as a function of the reference cell output. As was discussed in the previous section, the short circuit current measured for the MaReCo has an almost linear dependence on the current measured for the horizontal reference. This is due to the fact that the reference is parallel to the aperture of the front reflector where the cells are placed. The linear dependence is true both for days with a high amount of direct radiation and for days with a high amount of diffuse radiation. This leads to a model that treats the diffuse, isotropic, radiation and the direct radiation separately. When the sky is isotropic, the relation between the short circuit current of the MaReCo and the reference cells is modelled according to Eq.(5):

$$I_{SC,MaReCo} = R \cdot I_{SC,Ref} \cdot f_{diffuse} \quad (5)$$

R is the percentage of the incident irradiation that reaches the cells
f is the share of diffuse irradiation

R was taken from the measurements of optical efficiency, an average value of 0.7 was chosen. The reference is a measure of the incident irradiation. *f* was calculated through measurements of the global and diffuse irradiation against the horizontal reference.

When the sky is clear, and the direct irradiation dominates, the output from the MaReCo can be modelled according to Eq.(6):

$$I_{SC,MaReCo} = R \cdot I_{SC,Ref} \cdot C_{gf} \cdot f_{direct} \quad (6)$$

R is the percentage if the incident irradiation that reaches the cells
f is the share of direct irradiation
C_{gf} is the geometrical concentration of the front reflector, equal to 3.5

Adding these two models gives us a model for both direct and diffuse irradiation, which is defined by Eq.(7):

$$I_{SC,MaReCo} = R \cdot I_{SC,Ref} \left(f_{diffuse} + C_{gf} \cdot f_{direct} \right) \quad (7)$$

Figure 16 shows the relation between the modelled and the measured values. An ideal model would give a line $y=x$, and this line is clearly visible.

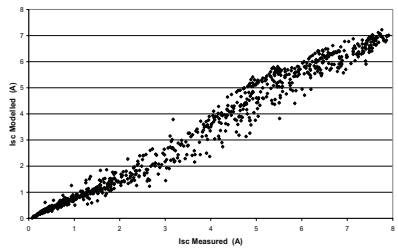

Figure 16 Modelled data versus measured data for a period of one month. All measurements were taken between 10.00 and 14.00 to avoid shading effects from the gables.

The correlation between the two data sets was 0.99, and the standard deviation of the difference between the modelled values and the measured values was 0.39 A. This, together with Figure 7 indicates that the model is a good tool to roughly estimate the output of the MaReCo at angles where there is no shading from the gables.

8. CONCLUSIONS

The objective was to estimate the annual electrical and thermal energy output from the MaReCo hybrid. This system is optimized for high latitudes such as Lund, Sweden, where the long term monitoring is to be performed. The IV-characteristics and the irradiance distribution on the cells of the hybrids were measured, both the back and front reflectors. Changing the back reflector from anodized aluminium to aluminium laminated steel did not change the energy output. This makes the steel based reflector an interesting option. The annual thermal output estimate for the MaReCo system was 145 kWh/m^2 of hot water at 50°C. If the absorber is improved, this can be significantly increased. The estimated output of electricity was compared with cells mounted in 30° tilt without reflector, and the MINSUN simulation show a 49% output increase for the front reflector and a 23% increase for the back reflector of MaReCo1, and 23% increase of the back reflector in MaReCo2. This shows that the optimal placement of the photovoltaic cells is facing the front reflector. This could also be seen from the measurement of the short circuit current, where the front reflector had considerably better performance.

The MaReCo is designed to collect most of the irradiation incident on the system during a year. The back reflector collects the light at low transverse angles, and the front reflector collects light at higher transverse angles. If the absorber has photovoltaic cells on one side only, the electricity production will be more unevenly distributed over the year. As the system is intended to be integrated into residential buildings, having an even electricity production is an important factor. Having cells on both sides will also increase the total electricity production considerably, another important factor in integration into residential buildings where roof space normally is limited. If space is unlimited, and the most important parameter is to produce electricity at the lowest price, the best choice is to have cells on the absorber facing the front reflector. In all other cases, photovoltaic cells should be placed on both sides of the absorber, the price of adding cells to the other side of the absorber is relatively low once a trough with cells on one side of the absorber is constructed.

The outdoor measurements show that a 2 fold increase in output can be expected at noon on a clear day, but the losses at higher azimuth angles and losses due to less direct irradiation makes the estimates given by the MINSUN simulations more probable.

Nevertheless, these results presented here clearly show the possibility to lower the cost of PV-electricity and hot water using the MaReCo hybrid.

REFERENCES

Adsten M., Helgesson A., Karlsson B., Evaluation of CPC-collector designs for stand-alone for- or wall installation, Accepted for publication in Solar Energy 2005

Benítez P. and Mohedano R., 1999. Optimum irradiation of concentrated sunlight for

photovoltaic energy conversion. Applied Physics Letters. 74 (17), 2543-2545

Brogren M., Helgesson A., Karlsson B., Nilsson J., and Roos A., 2004, Optical properties, durability and system aspects of a new aluminium-polymer-laminated steel reflector for solar concentrators, Solar Energy Materials and Solar Cells, 82, 387-412

Chant V.G. and Håkansson R., 1985, The MINSUN simulation and optimisation program. Application and users guide. IEA SH & C Task VII, Ottawa

Green M.,1982, Solar cells, Prentice-Hall Inc, USA

Mills D.R., Giutroich J.E., 1979, Symmetrical and asymmetrical ideal cylindrical radiation transformers and concentrators, J. Opt. Soc. Am. Vol. 69 (2), 325-328

Nilsson J., Brogren M., Helgesson A., Roos A., Karlsson B., Biaxial model for the incidence angle dependence of the optical efficiency of photovoltaic systems with asymmetric reflectors , Sent to Solar Energy 2005

Perers B. and Karlsson B., 1993, External reflectors for large solar collector arrays, simulation model and experimental results, Solar Energy. 51 (5), 327-337

Rönnelid, M., Perers, B., Karlsson B. and Krohn, P., 2000, Cooling of PV modules equipped with low-concentrating CPC reflectors, Proceedings ISES 1999 Solar World Congress 1999, Jerusalem, Israel, Vol. 3, pp 400-404. Elsevier Science

NOMENCLATURE

b_0	incidence angle modifier coefficient
C_g	geometrical concentration ratio of the system
C_{gf}	geometrical concentration ratio of the front reflector
$f(\theta)$	optical efficiency
$f_{diffuse}$	fraction of diffuse irradiation
f_{direct}	fraction of direct irradiation
$g(\theta_L)$	incidence angle modifier in the azimuth direction
G	incident irradiation (º)
I_{1000}	reference short circuit current at 1000 W/m^2 (A)
I_{SC}	short circuit current (A)
k_1	loss coefficient per collector area (W/m^{2}K)
$K_{\tau\alpha}$	planar incidence angle modifier
$(mC)_e$	heat capacity of the collector (J/m^2)
$\eta(\theta_T)$	incidence angle modifier in the solar altitude direction
η_{0b}	optical efficiency for beam irradiation used in heat calculations
η_{0d}	optical efficiency for diffuse irradiation used in heat calculations
R	Average optical efficiency
ΔT	difference between the ambient temperature and the temperature of the collector (K)
θ	angle of incidence (º)
θ_L	longitudinal projected angle of incidence (º)
θ_T	transverse projected angle of incidence (º)
$dT_f/d\tau$	time derivative of the temperature of the cooling media (K/s)

Article II

ARTICLE IN PRESS

Available online at www.sciencedirect.com
SCIENCE DIRECT®

ELSEVIER

Solar Energy xxx (2005) xxx–xxx

SOLAR ENERGY

www.elsevier.com/locate/solener

Biaxial model for the incidence angle dependence of the optical efficiency of photovoltaic systems with asymmetric reflectors

Johan Nilsson [a,*], Maria Brogren [b], Anna Helgesson [c], Arne Roos [b], Björn Karlsson [a,c]

[a] *Division of Energy and Building Design, Department of Construction and Architecture, Lund University, P.O. Box 118, 221 00 Lund, Sweden*
[b] *Division of Solid State Physics, Department of Engineering Sciences, Uppsala University, Box 534, 751 21 Uppsala, Sweden*
[c] *Vattenfall Utveckling AB, 814 26 Älvkarleby, Sweden*

Received 18 February 2004; received in revised form 31 August 2005; accepted 2 September 2005

Communicated by: Associate Editor Brian Norton

Abstract

The optical efficiency of concentrating solar thermal and photovoltaic systems with cylindrical geometries is asymmetrical about the optical axis. Biaxial models, based on projected incidence angles, are often used to estimate the annual performance of asymmetric concentrators. However, the use of projected angles tends to underestimate optical losses in the cover glass. In this work, a biaxial model for the incidence angle dependence of the optical efficiency, which uses the transverse projected incidence angle for determining the influence of the reflector and the real incidence angle to determine the influence of the glazing is proposed. The model gives an absolute value of the optical efficiency and it is valid for concentrating systems with translational symmetry, as well as for flat plate collectors and planar photovoltaic modules. The model is validated for a system with an east–west aligned parabolic reflector without a cover glass and it is shown that the dependence on the optical efficiency of the reflector on the longitudinal angle of incidence is negligible. The model is compared with the commonly used biaxial model and it is found that the difference is a couple of percentage points when the difference between the longitudinal projected incidence angle and the real incidence angle is large and the angle of incidence on the glass is high.

Keywords: Solar concentrators; Optical efficiency; Incidence angle dependence; Biaxial incidence angle modifier

1. Introduction

1.1. Background

The use of solar concentrators for increasing the output from solar collectors and photovoltaic modules is often cost-effective. However, before

* Corresponding author. Tel.: +46 46 2227606; fax: +46 46 2224719.
E-mail address: johan.nilsson@ebd.lth.se (J. Nilsson).

0038-092X/$ - see front matter © 2005 Elsevier Ltd. All rights reserved.
doi:10.1016/j.solener.2005.09.008

Nomenclature

a	absorber width (m)	K_L	longitudinal incidence angle modifier according to McIntire
β	inclination of the module (°)	K_T	transverse incidence angle modifier according to McIntire
b_0	incidence angle modifier coefficient	$\langle n \rangle$	average number of reflections
C_g	geometrical concentration ratio	η_n	optical efficiency at normal incidence for a planar isotropic system
f_L	optical efficiency of the glazing	η_{opt}	optical efficiency of the system
f'_L	optical efficiency of the system with glazing measured at constant transverse projected angle	v	inclination of the optical axis (°)
f'_T	optical efficiency of the system with glazing measured at constant longitudinal angle	ξ	angle between module and optical axis (°)
h	aperture height (m)	R_T	optical efficiency of the reflector
I_{SC}^{conc}	short circuit current of the concentrator system (A)	ρ	reflectance of the reflector
$I_{SC}^{reference}$	short current of the reference system (A)	S_L	shading function of the gables
k	normalization constant for the simple numerical model of optical efficiency of the reflector	θ_i	angle of incidence (°)
$K(\theta_L, \theta_T)$	biaxial incidence angle modifier according to McIntire	θ_L	longitudinal projected angle of incidence (°)
		θ_T	transverse projected angle of incidence (°)
		φ	angle between module and aperture (°)

investment in a concentrating solar energy system is made, it is appropriate to calculate the annual thermal or electrical energy output. Predicting the annual output at a specific location requires knowledge of the incidence angle dependence of the optical efficiency of the system. Measurements of the angular dependent performance of concentrators are time-consuming. Therefore, using a model for the incidence angle dependence of the optical efficiency is helpful. Furthermore, if the system is not yet constructed, measurements cannot be performed and a model for predicting the angular dependence is necessary.

For planar isotropic solar energy systems, an incidence angle modifier is often used to describe the incidence angle dependence of the optical efficiency. At a given angle of incidence, θ_i, the optical efficiency, η_{opt}, is given by the product of the optical efficiency at normal incidence, η_n, and the incidence angle modifier according to

$$\eta_{opt}(\theta_i) = \eta_n\left(1 - b_0\left(\frac{1}{\cos\theta_i} - 1\right)\right), \quad (1)$$

where b_0 is the incidence angle modifier coefficient (Souka and Safwat, 1966; Duffie and Beckman, 1980). The incidence angle modifier coefficient is found by a fit to measurement data or it can be estimated. A commonly used value for glazings and flat plate solar thermal collectors is 0.2.

1.2. Measurements of the optical efficiency of photovoltaic systems

The short-circuit current of a CIGS cell is independent on the illumination distribution on the cell as long as the strip of light is larger than half a millimetre, which is the case for the studied system (McMahon and von Roedern, 1997). This was also shown by Wennerberg et al. (2000). As for the temperature dependence of the short-circuit current, previous studies have shown that for the temperature increases that we can expect in our measurements, this dependence can be neglected (Brogren et al., 2003).

Since the short-circuit current of a photovoltaic module, at a constant temperature, in a concentrating system depends only on the irradiance on the module, which is determined solely by the optical efficiency of the concentrator, measurements of the short-circuit current as a function of real or projected incidence angles can be used to determine the optical efficiency if the current that is generated in the concentrating system is compared with the current from an identical module without concen-

trator and the result is divided by the geometrical concentration ratio, C_g. Hence, the optical efficiency is given by

$$\eta_{opt} = \frac{1}{C_g} \frac{I_{SC}^{conc}}{I_{SC}^{reference}}, \quad (2)$$

where I_{SC}^{conc} is the current from the module in the concentrator and $I_{SC}^{reference}$ is the current from the planar module mounted on the system aperture.

For methods for determining the optical efficiency of solar thermal and photovoltaic-thermal systems from measurements of the thermal output, the reader is referred to earlier work by the authors (Brogren et al., 2000; Helgesson and Karlsson, 2001).

The main source of error in the measurements is the system alignment. It is difficult to align the system and the reference to have their aperture normals facing exactly south. The error in alignment is estimated to approximately 3°. The current was measured as a voltage over a shunt resistance with a very high accuracy. The reference module and the module in the concentrator were calibrated before the measurements to give equal current, but there might be dynamic effects affecting the two modules differently. The dominant error is due to alignment errors and we estimate the total worst-case error of the short-circuit current due to misalignment to be approximately 0.1 A. This would occur at noon if the sun has an altitude between 20° and 30°.

1.3. Biaxial models for the incidence angle dependence of the optical efficiency

The optical efficiency of asymmetric concentrating systems has different incidence angle dependence in different directions. For asymmetric systems with translational symmetry, it is often convenient to define the projected transverse and longitudinal angles of incidence. These angles are defined in Fig. 1.

McIntire presents a biaxial incidence angle modifier, K, for the optical efficiency of asymmetric concentrating systems:

$$K(\theta_L, \theta_T) \approx K_L(\theta_L, 0) K_T(0, \theta_T), \quad (3)$$

which is obtained from measurements in the perpendicular transverse and longitudinal directions (McIntire, 1982). A disadvantage of this model is that it, like the uniaxial incidence angle modifier in Eq. (1), has to be normalized, i.e. that the optical efficiency is the product of the optical efficiency at

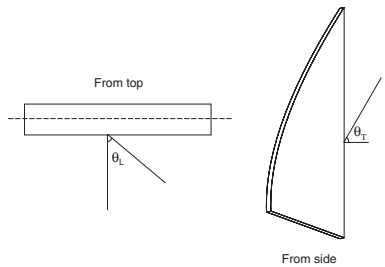

Fig. 1. Definition of the transverse and longitudinal incidence angles for the concentrating system. The left drawing is seen from the top of the system and the right is seen from the side.

normal angle of incidence and the biaxial incidence angle modifier, according to

$$\eta_{opt}(\theta_i) = \eta_n K(\theta_L, \theta_T). \quad (4)$$

Furthermore, it is not always possible to determine the factor K_L at $\theta_T = 0$, depending on how the projected angles of incidence are defined. However, the aspect of this model that may have the largest practical implications is that it underestimates the optical losses in the glazing, due to its utilisation of the projected longitudinal incidence angle to determine the transmittance of the cover glass, which leads to large errors at high angles of incidence (Rönnelid et al., 1997). On the other hand, the angular dependence of the glass is accounted for twice, both in the K_T and K_L, which reduces this effect.

The relationship between the real, the longitudinal, and the transverse angles of incidence is given by

$$\tan^2\theta_i = \tan^2\theta_T + \tan^2\theta_L \quad (5)$$

and is shown in Fig. 2. The lines are iso-incidence angles. However, all these combinations of the real and the projected incidence angles are not found for a concentrating system. The combinations of angles are determined by the celestial movement and the system geometry. As an example of the combinations that can be found, Fig. 3 shows the incidence angle of the direct solar radiation against a south wall in Älvkarleby (60.5° N, 17.4° E), Sweden, as well as the transverse and longitudinal projected incidence angles on the same wall, as functions of the time of the day on the 15th July and 23rd September. At noon, the transverse and the real incidence angles coincide with the solar altitude.

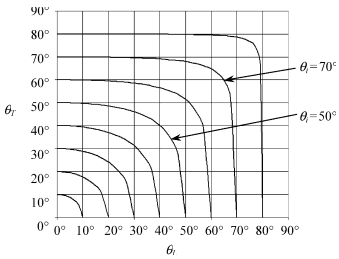

Fig. 2. Angular relationships between the projected angles θ_T and θ_L and the real incidence angle θ_i. The curves represent constant real incidence angle contours.

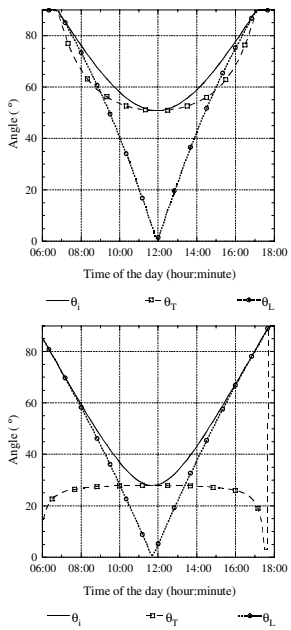

Fig. 3. The incidence angle of the direct solar radiation on a south-facing vertical wall, as well as the transverse and longitudinal projected incidence angles on the same wall, as functions of the time of the day on the 15th July (upper) and 23rd September (lower), in Älvkarleby (60.5° N, 17.4° E), Sweden.

1.4. Transverse projected angle and the orientation of translational symmetric reflector systems

The optical performance of a translational symmetric reflector system, such as the studied system, is determined solely by the transverse projected angle of incidence. As can be seen in Fig. 3 (lower), the transverse projected angle of incidence is constant during the day at equinox. A translational symmetric reflector system with the axis of symmetry aligned in the east–west direction will around the equinox have constant optical efficiency all day. This makes it possible to evaluate the angle dependencies of the cover glass and the absorber during equinox. Another option is to rotate through 90° counterclockwise and tilt it to the latitude angle. When the system is in this setup, the sun will move in the plane perpendicular to the system axis of symmetry all day, and it is possible to measure the optical performance as a function of the transverse projected angle of incidence.

When not stated otherwise in this article, the system is always aligned with the axis of symmetry parallel to the east–west axis, facing south. The transverse projected angle of incidence is then the angle of incidence on the glazing projected into the meridian plane.

1.5. Objectives

The objective of this work is to present and validate a biaxial model for the optical efficiency of asymmetric concentrating solar energy systems. The model is based on separate measurements of the effects on the optical efficiency of the reflector and the glazing.

1.6. The studied system

Fig. 4 shows a photograph of the prototype system that was used to conduct the investigation of the incidence angle dependence of the optical efficiency. The system includes an off-the-shelf thin film ST-50 CIGS module from Siemens and a parabolic over edge reflector of anodised aluminium with a solar reflectance of approximately 80% at near normal angle of incidence. The module consist of series connected cells that are extended perpendicular to the reflector. This ensures that all individual cells receives the same illumination in the translational symmetric reflector system. The characteristics of CIGS cells in concentrating systems have been dis-

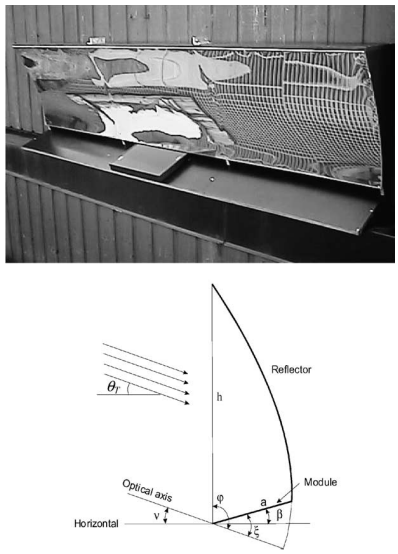

Fig. 4. Photograph of a 3X concentrating façade-mounted concentrating system with parabolic over edge reflector and thin film photovoltaic module (upper) and a schematic showing the cross-section of the concentrator (lower). The transverse incidence angle, θ_T, is defined in the schematic. φ is the internal angle between the glazing and the optical axis, and is in this case 115°.

cussed in earlier work by Brogren et al. (2003) and Wennerberg et al. (2000). A cross-section of the system is shown in the lower figure. The optical axis of the system is inclined at $v = 25°$, which means that all irradiance incident on the parabolic reflector at angles less than 25° will be reflected back out of the system without reaching the cells. The module plane has an inclination of, $\beta = 20°$, and the angle between the module plane and the optical axis is given by $\xi = \beta + v = 20° + 25° = 45°$. This results in a geometrical concentration ratio, C_g of

$$C_g = \frac{h}{a} = \frac{\cos^2\left(\frac{\xi}{2}\right)}{\cos^2\left(\frac{v+90°}{2}\right)} = 2.95, \quad (6)$$

where h is the height of the vertical aperture and a is the width of the module plane, as indicated in Fig. 4. In its original design, the system does not include a glazing. The height of the vertical aperture, h, is 974 mm and the width of the module, a, is 330 mm. This 3X concentrating photovoltaic system is further described elsewhere (Brogren et al., 2001a,b, 2003). For discussions about other low concentrating systems refer to Zacharopoulos et al. (2000) and Tripanagnostopoulos et al. (2002).

2. New biaxial model

The biaxial model that is proposed in this paper is based on separate measurements of the influence of the reflector and glazing. This requires that the glazing can be removed from the system or that the measurements are performed before the glazing is applied. It is possible, however, to determine the contribution of the reflector from measurements with the glazing present, using a compensation for the glazing in the expression for the effect of the reflector. This procedure is described in Section 4.3. The proposed biaxial model can be written

$$\eta_{opt} = R_T(\theta_T) f_L(\theta_i), \quad (7)$$

where $R_T(\theta_T)$ describes the dependence on the optical efficiency of the system on the reflector as a function of the transverse incidence angle, and $f_L(\theta_i)$ describes the dependence on the optical efficiency of the system on the glazing as a function of the real incidence angle. Note that, unlike in Eq. (3), it is the real incidence angle that is used to describe the longitudinal dependence in Eq. (7).

2.1. Incidence angle dependence of the optical efficiency of the reflector

We will show that the optical efficiency of the reflector is independent of the longitudinal angle of incidence by measuring $f_L(\theta_L)$ without a glazing. For our system, measuring the optical efficiency at $\theta_T = 0$ makes no sense, since the lower acceptance angle is 25°, all light falling on the reflector below this angle of incidence is reflected out of the system. However, measurements of the optical efficiency as a function of the longitudinal angle of incidence at constant θ_T can be used to show that the reflector function, R_T, is independent of θ_L. Measurements of the current generated in the concentrating system on the 6th and 17th September 2003, close to the autumn equinox, were compared with the current generated in a vertical module mounted on the aperture using Eq. (2) and the resulting optical efficiency as a function of the time of the day is shown in Fig. 5. Around the equinoxes, the transverse

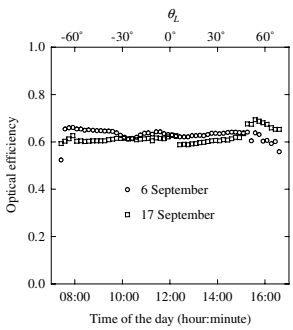

Fig. 5. Optical efficiency of the parabolic over edge reflector as a function of the time of the day on two days close to the autumn equinox, when θ_T is constant. The global irradiance was around 800 W/m^2 at noon and the diffuse fraction was about 10% during the whole day on both dates.

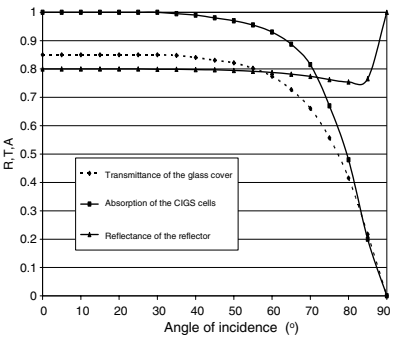

Fig. 6. Calculated optical properties of aluminium and glass, and the normalised conversion efficiency of a CIGS module, as a function of incidence angle.

incidence angle, θ_T, is constant at about 30° (90°-latitude) during the entire day, which is shown in the lower graph in Fig. 3. The longitudinal angle, however, changes from −90°, at 06:00 in the morning to 90° at 18:00 in the evening, and the change is +15° per hour.

Fig. 5 shows that the optical efficiency of the reflector is independent of θ_L as it is constant when the longitudinal angle changes during the day.

Assuming that the reflectance of the reflector material is independent of the angle of incidence, the influence of the reflector on the optical efficiency of the system is largely determined by the average number of reflections, $\langle n \rangle$, in the reflector, and the optical efficiency of the reflector, η^R_{opt}, can be described by

$$\eta^R_{opt} = \rho^{\langle n \rangle}, \quad (8)$$

where ρ is the reflectance of the reflector. For a reflector of aluminium, the assumption that the total solar reflectance is independent of the angle of incidence is valid within a few percent for incidence angles below 80°. This is shown in Fig. 6, which also displays the angular dependent transmittance of a 3 mm glass, as well as the measured normalised incidence angle dependent conversion efficiency of the thin film CIGS module, which is used in the 3X concentrating system. The incidence angle dependent conversion efficiency of the module was obtained from outdoor measurements and the angular dependent reflectance and transmittance values were obtained from Fresnel calculations, using tabulated complex indices of refraction.

The number of reflections, $\langle n \rangle$, is determined solely by the projected transverse incidence angle and the system geometry. Thus, the influence of the reflector on the optical efficiency of a translational symmetric concentrating system with a specific geometry can be formulated by an equation with the transverse incidence angle θ_T as the only parameter. This function can be a theoretical function that is derived from the geometry and the measured solar reflectance, or it can be obtained from measurements or ray tracing.

The optical efficiency of the 3X concentrating over edge parabolic reflector was obtained from measurements of the short-circuit currents as a function of the transverse incidence angle. The measurements were performed close to the autumn equinox, when the longitudinal angle changes by +15° per hour and the transverse incidence angle is constant. As discussed in Section 1.4, if the system is placed appropriately (rotated 90° clockwise and tilted to the latitude angle), the sun moves in the transverse plane of the system. It is thus possible to monitor the optical efficiency as a function of the transverse angle of incidence θ_T as the sun moves across the sky. The effect on the optical efficiency of the reflector, R_T, was determined using the expression:

$$R_T(\theta_T) = \frac{1}{C_g} \frac{I_{SC}^{conc}(\theta_T)}{I_{SC}^{reference}(\theta_T)}. \quad (9)$$

The result is shown in Fig. 7. With the system mounted as described above, high positive transverse incidence angles corresponds to the morning hours, 90° represents 6:00 a.m., and the transverse incidence angle is negative after 12:00 p.m.

If it is not possible to mount the system as described above, a comparison between the current that is generated in the concentrating system and the current that is generated in a module without a concentrator can still be performed by calculating θ_T at each point. However, in this kind of measurement, the longitudinal incidence angle is not zero, but changes with the time of day. Thus, in order for the comparison to give the influence of the reflector as a function of the transverse angle alone, the longitudinal incidence angle dependence of the reflector has to be the same as for the reference module. This is the case for the concentrating system without a glazing, which was shown in Fig. 5.

Fig. 8 shows the measured short-circuit currents as functions of the time of day for the vertical module and for the module with a reflector mounted as the system is described in Fig. 4, as well as the resulting optical efficiency.

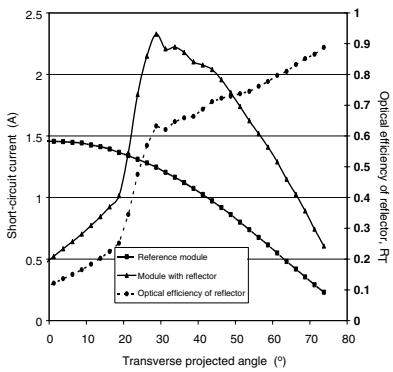

Fig. 7. Short-circuit currents for the module in the concentrating system and a reference module of the same size without a reflector, as functions of the transverse projected angle on 24th September 2003.

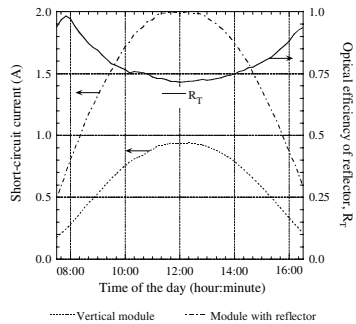

Fig. 8. Measured short-circuit currents for the module in the concentrating system and a vertical module of the same size without a reflector, and the optical efficiency of the reflector, as functions of the time of the day on 15th July 2003.

2.2. Formulation of a simple numerical model for R_T and a comparison with ray-tracing

An analysis of the geometry of the concentrating system shown in Fig. 4 gives that at transverse incidence angles below 25°, no radiation that is reflected in the reflector will reach the module. However, at $\theta_T < 25°$, direct radiation reaches the module at an angle of incidence of $70° - \theta_T$. The θ_T dependence of the optical efficiency of the system, compared to the optical efficiency of a vertical module, is thus given by

$$R_T(\theta_T) = \frac{a \cdot \cos(70° - \theta_T)}{h \cdot \cos(\theta_T)} \quad (10)$$

for θ_T below the lower acceptance angle. For θ_T higher than 25°, part of the beam radiation reaches the module directly and part is reflected in the reflector before reaching the module and the expression for the θ_T dependence of the optical efficiency can be formulated as

$$R_T(\theta_T) = \frac{k \cdot [h \cdot \cos(\theta_T) - a \cdot \cos(70° - \theta_T)] + a \cdot \cos(70° - \theta_T)}{h \cdot \cos(\theta_T)}$$
$$= k + (1-k)\frac{a \cdot \cos(70° - \theta_T)}{h \cdot \cos(\theta_T)}, \quad (11)$$

where k is dependent on the reflectance of the reflector. Using numerical values of a and h, and a curve fit to the measured θ_T dependence of the optical efficiency in Figs. 7 and 8, a parametric expression for $R_T(\theta_T)$ was formulated:

$$R_T(\theta_T) = \begin{cases} 0.33784\frac{\cos(70^\circ-\theta_T)}{\cos\theta_T} \\ \quad \text{for } \theta_T < 25^\circ, \\ 0.45 + 0.1864\frac{\cos(70^\circ-\theta_T)}{\cos\theta_T} \\ \quad \text{for } \theta_T \geqslant 25^\circ. \end{cases} \quad (12)$$

The normalisation constant, k, that is used to get a good fit to measurement data was 0.45. In an ideal system without resistive losses in the photovoltaic cell, no angular dependence of the absorption of the cells, and with a perfect geometry, this constant would be equal to the reflectance of the reflector as the average number of reflections is close to unity. The reflector of the measured system contains dents and other imperfections due to the manufacturing process. These imperfections will cause undesired reflections, some of the light incident within the interval of acceptance will be reflected out of the system, and some of the light will be reflected in a slightly different direction generating multiple reflections etc. The electrical losses that has significance for the normalization constant are discussed in Section 6.2.

The model for R_T is shown in Fig. 9, together with the measured R_T. The model was also compared with results from ray-tracing, using a three-dimensional CAD model of the system and the commercial ray-racing program ZEMAX (ZEMAX, 2004). No cover glass was used in the simulations and the source of the rays was placed at the vertical aperture. The angle of incidence was chosen as the transverse projected incidence angle, and it was varied from 0° to 90° in steps of 5°. The source generated 10,000 rays for each angle of incidence. The error in each simulated angular optical efficiency was less than 3% for all angles of incidence. The results from ray-tracing, using reflectance values of 0.8 are included in Fig. 9. As the measured values are divided by the current of the reference module that is mounted on the aperture, the ray-tracing values in the figure are divided by the absorption of the cells at the angle of incidence from Fig. 6 to enable a comparison. The absorber is mounted in 20° from the horizontal in the studied system, i.e. when the transverse angle of incidence is 70° and the sun is in the meridian plane all of the light incident on the system aperture is absorbed at normal incidence at the absorber resulting in maximum absorption. The angle of incidence on the reference cells will in this case be 70°, an angle where the absorption has dropped almost 20% as can be seen in Fig. 6. This explains why R_T reaches 1 before 70° and can have a value >1.

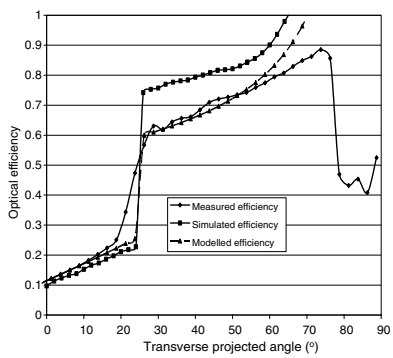

Fig. 9. Comparison between the measured R_T, the simple parametric model, and normalized ray-tracing.

At low θ_T, only light that reaches the module directly contributes to the optical efficiency. At θ_T above 25°, the optical efficiency increases rapidly with increasing θ_T due to the fact that all light that is reflected in the parabolic mirror reaches the module. At even higher θ_T, a larger fraction of the light reaches the module directly, due to a reduced effective reflector area and an increased effective module area at high θ_T. At $\theta_T > 70$, no direct radiation is reflected in the parabolic mirror, as all of it reaches the module directly. The dips in the optical efficiency that can be seen in the curves from ray-tracing are due to multiple reflections in the parabolic mirror at high θ_T. At $\theta_T = 60°$, the average number of reflections is 1.5. The lower optical efficiency due to the multiple reflections is only noticeable at a small angular interval. In this interval, the influence is small, and this indicates that multiple reflections can be neglected in the model.

3. Validation of the model for R_T

3.1. Comparison between model and measurements for single days

Fig. 10a shows the measured optical efficiency of the reflector on a summer day (15th July 2003) and Fig. 10b an autumn day (6th September 2003, close to equinox) together with the model predictions for

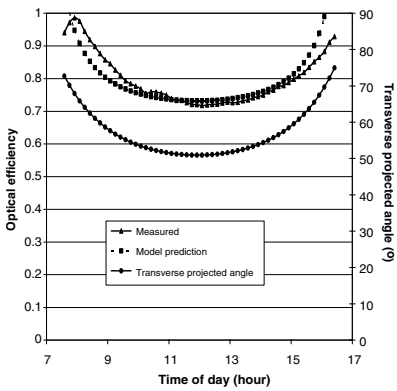

Fig. 10a. Comparison between our model prediction and the measured optical efficiency on the 15th July 2003.

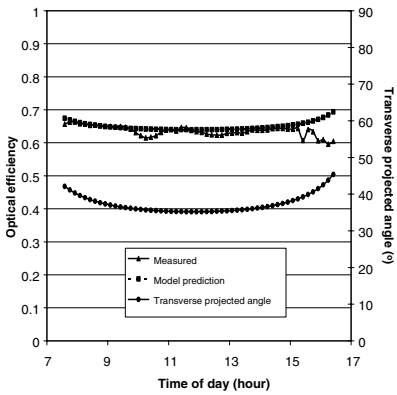

Fig. 10b. Comparison between our model prediction and the measured optical efficiency on the 6th September 2003.

the optical efficiency (Eq. (12)), using $k = 0.45$. The figures show that there is a good agreement between the model and the measured optical efficiency, both for high and moderate projected transverse incidence angles. The flat optical efficiency on 6th September, is due to a constant $\theta_T = 36°$ during this day.

3.2. Comparison between model and measurements for long periods of time

Fig. 11 shows a comparison between the measured short-circuit currents for the vertical module and the module with a parabolic over edge concentrator for the period 10th July to 12th September 2003. Data for every 10th minute for 7:30–16:30 is included in the graph. It can be seen that the concentrating module produces approximately twice the current of the vertical module of the same size. Furthermore, there is a knee in the function at low and moderate currents. The knee, which is indicated in Fig. 11, can be explained by the fact that low and moderate currents are mostly generated in the mornings and in the afternoons, when direct radiation reaches the module in the concentrating system at a more favourable angle of incidence than for the vertical module, since the module in the concentrating system is tilted 20° from the horizontal. This results in a high optical efficiency at the high transverse incidence angles in the mornings and in the afternoons, which was shown in Fig. 10a.

In order to study how well the model describes long-term system efficiency, the measured short-circuit currents for the vertical module during the period 10th July to 12th September 2003 were used in the parametric model (Eq. (12)), together with the geometrical concentration ratio and the calculated θ_T, to predict the generated short-circuit current

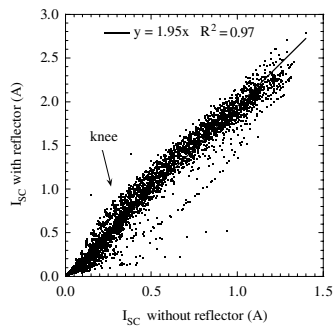

Fig. 11. Comparison between measured short-circuit currents from the module with 3X reflector and the module without reflector, during the period 10th July to 12th September 2003.

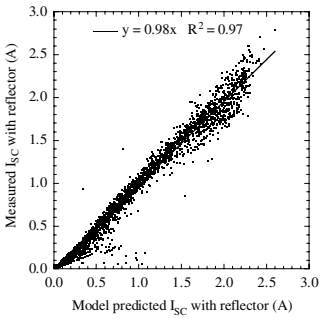

Fig. 12. Comparison between model predictions of the short-circuit current from the module in the concentrator, based on the R_T function and the measured short-circuit current from the vertical module, and the measured short-circuit current from the module with reflector, during the period 10th July to 12th September 2003. One data point for every tenth minute, 7:00–17:00, is included in the graph.

from the module with the 3X reflector during this period. The predicted and the measured short-circuit currents are shown in Fig. 12. The comparison indicates that the model describes the optical efficiency well. There is a tendency that the measured values are lower than the model predictions and the difference is largest at high currents. This is discussed in Section 6.2.

4. Formulation of the complete model

4.1. The effect of a cover glass

The influence of the reflector was measured without a glazing. However, the unsatisfying long-term durability outdoors of most inexpensive reflector materials often necessitate that a cover glass is used, although this reduces the optical efficiency of the system significantly. To a first approximation, the addition of a cover glass will not, per definition, influence the function R_T. Neither does the reflector have any effect on the longitudinal incidence angle behaviour, which was shown above. Thus the angular dependence of the optical efficiency due to the glazing can be assessed separately. In this work, we have chosen to use the incidence angle dependent transmittance of a 3 mm glass, obtained from Fresnel calculations, for the f_L function. The calculated angular transmittance of the glass as a function of incidence angle was shown in Fig. 6. However, for any given cover glass, the angular dependent transmittance can be measured using for instance spectrophotometry. It is also possible to use an incidence angle modifier (Eq. (1)), for example with $\eta_n = 0.9$ and $b_0 = 0.2$, to model the angular dependent transmittance of the glass.

4.2. The effect of the angular dependence of the cell absorption

The absorption of the pv cells as a function of the angle of incidence is described in Fig. 6. As can be seen from the figure, the absorptance is almost constant up to 70°, where it starts reducing rapidly. As the cells are used for measuring the incidence angle dependence of the reflector, this effect will to a small extent introduce an error in the measurements as the transverse projected angle of incidence differs from the angle at which the light is incident on the cells. A ray tracing simulation was performed to study this effect and to be able to estimate the size of error introduced. Fig. 13 shows the result of this simulation, performed for the same date as Fig. 8, July 15. The reflectance was set to 1 in order to remove the effects of the aluminium mirror. As can be seen from the figure, the error is 2–3% during the part of the day when the irradiation is high, and we conclude that the effects can be neglected in the model as they are less than other errors in the measuring

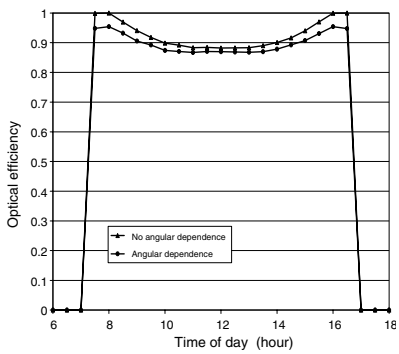

Fig. 13. The influence of the angular dependence of the absorber on the ray tracing results. The reflectance of the reflector was set to 1.

process. The errors will be further discussed in Section 6.2.

4.3. Measurement of the R_T function with a cover glass present

The expressions for R_T and f_L were obtained by performing separate measurements and calculations on the reflector and the glazing, respectively. If the cover glass cannot be removed from the system, this procedure cannot be followed and the R_T function has to be obtained in some other way. R_T can be found by measuring the incidence angle dependence of the optical efficiency of the entire system (including glass and reflector) in the longitudinal and transverse directions, while keeping the other projection of the incidence angle as close to zero as possible in at least one of the measurements. (For the 3X system with a parabolic over edge reflector with a lower acceptance angle of 25°, it makes little sense to measure at $\theta_T < 25°$.) This gives the functions f'_L and f'_T, for the longitudinal and transverse incidence angle dependence of the optical efficiency. The R_T function is then obtained as the ratio between these functions for $\theta_L = 0$, according to

$$R_T(\theta_T) = \frac{f'_T(\theta_T)}{f'_L(\theta_T)}. \quad (13)$$

4.4. Graphical representation of the model

When R_T and f_L have been obtained from measurements, modelling, or ray tracing, the biaxial model for the incidence angle dependence of the optical efficiency can be formulated. Fig. 14 shows the factors f_L and R_T that determine the optical efficiency of the studied 3X concentrating system. Since the functions f_L and R_T depend on different angles of incidence (θ_i and θ_T, respectively) and these angles have a relationship that changes with the time of day and the time of the year, it is not relevant to present their product, η_{opt}, graphically. The optical efficiency at any given moment in time is obtained by taking the product of $f_L(\theta_i)$ and $R_T(\theta_T)$, using the real angle of incidence and the transverse projection angle at that time.

4.5. Application of the model on flat plate collectors and planar pv modules

A flat plate collector or planar module is symmetrical in the transversal and longitudinal directions by measuring the incidence angle dependence in both directions it can be shown that f'_T and f'_L are identical functions. The R_T function will in this case according to Eq. (13) be equal to 1 for all angles of incidence. The model, formulated by Eq. (7), will in this case be reduced to Eq. (14):

$$\eta_{opt} = R_T(\theta_T) f_L(\theta_i) = [1] \cdot f_L(\theta_i) = f_L(\theta_i). \quad (14)$$

This shows that the same methodology and model can be used for concentrator systems as well as for more simple systems such as the flat plate collector or the planar module.

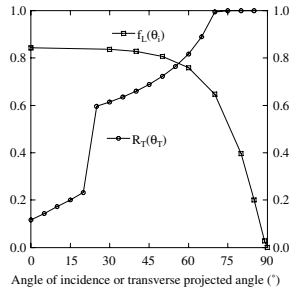

Fig. 14. The factors f_L and R_T that determine the optical efficiency of the 3X concentrating system with a parabolic over edge reflector and a vertical glazing.

5. Comparison between the proposed model and the previous biaxial model

Fig. 15 shows a comparison between the model predictions obtained by the proposed and McIntire's biaxial models for a summer day and a day close to the autumn equinox. Since it is not possible to measure the longitudinal dependence of our system at $\theta_T = 0$, and our system does not include a glass in its original design, we have used a simulated glass, which is the same as the glass for which the transmittance is shown in Fig. 6, in the calculations. Our model is thus the model presented in Fig. 14 above. Our interpretation of McIntire's model is equal to our model for the reflector function, but it uses the projected longitudinal incidence angle for determining the influence of the cover glass. The comparison shows, that there is little difference between the models at the autumn equinox (lower figure), when the difference between the real and

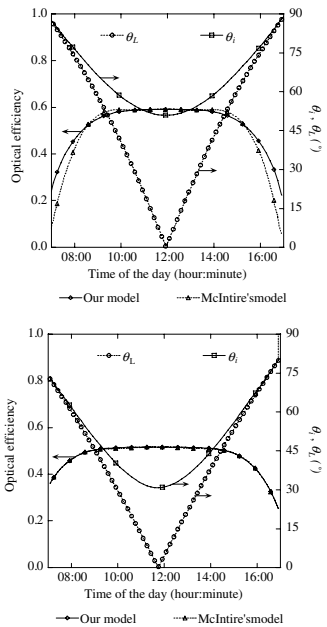

Fig. 15. Optical efficiency as a function of the real (our model) and the projected longitudinal (McIntire) angle of incidence on the 15th July (upper) and the 19th September (lower). The real and the projected longitudinal incidence angles are included in the graphs.

the longitudinal incidence angles never exceeds 30°. However, in summer, when the real incidence angle is high during the entire day and there is a significant difference between the real and the projected angles in the mornings and in the afternoons, a difference between the two models is noticeable, and this difference increases with increasing incidence angle. This is explained by the fact that, at angles of incidence above 50°, the transmittance of the glass drops fast with increasing angle of incidence. The difference between the two models is visible, for example at 14:30 in the upper diagram below. At 14:30 on 15th July, the real angle of incidence is 62.5°, while the projected longitudinal angle is 51.0°, and McIntire's model gives an optical efficiency that is too high, underestimating the transmission losses in the glass.

6. Discussion

6.1. Effects of diffuse radiation

Fig. 16 shows the optical efficiency of the 3X over edge parabolic reflector on a day with little direct radiation. The optical efficiency is obtained using Eq. (2), i.e. it is measured in comparison to a planar module that is mounted vertically beside the concentrating system. The observed optical efficiency for diffuse radiation is 65%, which is almost as high as for direct radiation. The fact that the system seems to concentrate diffuse radiation can be explained by the anisotropy of the diffuse radiation at the test site, the low concentration ratio, which allows the module to see a wide angular interval of the sky, and the low lower acceptance angle (25°) of the studied system. Where the systems are mounted, on a wall that faces south and approximately 1.2 m above the ground, the diffuse radiation that is incident at angles below 25° is negligible.

If the reflector would be ideal ($R = 1.0$) then the isotropic diffuse irradiance on the concentrator module should be equal to the diffuse irradiance on a module tilted 20° from the horizontal and almost twice as high as the irradiance on a vertical module. This effect is further increased by shadow

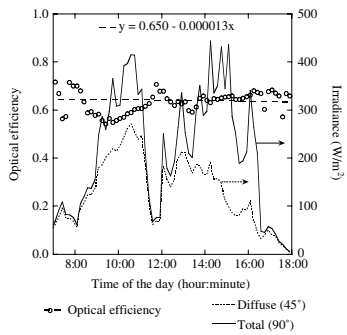

Fig. 16. The optical efficiency of the 3X concentrating over edge parabolic reflector, the total irradiance on the south vertical, and the diffuse irradiance on a surface inclined at 45° towards south, on 15th September 2003, as a function of the time of the day.

effects on the irradiance from angulars below $\theta_T = 25°$.

Fig. 12 which compare model values and measurements also indicate that the efficiency of the concentrator is similar for diffuse and beam irradiance.

6.2. Effects of concentration on cells designed for one sun's illumination

A comparison between the measured optical efficiency, the results from ray-tracing simulations, and the parametric model shows that the measured, the simulated, and the modelled curve are identical below $\theta_T = 25°$. However, when θ_T exceeds 25°, radiation is focussed at the front edge of the module. The module that is used in the test system is designed for one sun's illumination. Furthermore, the contacts are placed on the edge of the module closest to the reflector, and the series resistance of the cell increases with the distance from the contacts to the point where the electron is generated. As the light image from the reflector moves from the reflector edge to the focal point as the sun moves from a transverse angle of 90–25°, the series resistance increases. The voltage drop given by the series resistance will slightly increase the shunt current, and thus decrease the short circuit current, when the series resistance increases with the decreasing transverse projected angle.

These effects are introduced in the model through the normalisation constant, k, and explain the low measured optical efficiency for θ_T above 25°, which was shown in Fig. 9.

6.3. Effects of gables

It has been assumed that the east–west aligned reflector is long in comparison to the photovoltaic module and that there are no edge effects. In the case of a concentrating system with gables that shadows the cells or thermal absorber in early mornings and late evenings, a function $S_L(\theta_L)$, which is essentially a step-function that is 1 without shading and 0 when the module or absorber is shaded, can be introduced in the expression for the optical efficiency.

6.4. Measurement errors

The reference is mounted in the plane of the concentrator aperture. If the plane of the reference is not completely parallel with the plane of the concentrator aperture, it will introduce an error. The analysis is sensitive to this error, an error of 3° will e.g. mean a shift of 10 min in the measured data. This could mean that instead of using the measured reference current for 11:00, the current for 11:10 should be used in order to get correct model predictions. Fig. 10a shows exactly this kind of error, the graphs have the same shape, but there is a clear shift between them. Another error is introduced if the system normal is not pointing perfectly south. As with the previous example, a 3° angle between the south axis and the aperture normal equals 10 min. Looking at Fig. 9, a 3° shift would clearly create a large error compared to the simulated case around the angle of acceptance.

7. Conclusions

A new biaxial model for the incidence angle dependence of the optical efficiency for solar energy systems, $\eta_{opt} = R_T(\theta_T) f_L(\theta_i)$, was proposed. The model uses as parameters the transverse projected incidence angle for determining the effect of the reflector and the real incidence angle to determine the effect of the glazing. The model is valid for all translational symmetric concentrating systems, as well as for flat plate solar collectors and planar photovoltaic modules. Furthermore, the model gives an absolute value of the optical efficiency, i.e. it does not have to be normalised. The model was applied on a system with an east–west aligned asymmetric parabolic reflector without a cover glass and it was shown that the dependence of the optical efficiency of the reflector on the projected longitudinal angle of incidence was negligible. The new model was compared with the commonly used biaxial model, $\eta_{opt} = \eta_n K_T(\theta_T) K_L(\theta_L)$, and it was found that the difference between the models can be a couple of percentage points.

Acknowledgments

This work was supported by Elforsk AB and carried out under the auspices of the Swedish national Energy Systems Programme, which is financed by the Swedish Energy Agency, the Swedish Foundation for Strategic Research, and Swedish industry. The Swedish Energy Agency's Solar heating programme (FUD) is acknowledged for financial support.

References

Brogren, M., Nostell, P., Karlsson, B., 2000. Optical efficiency of a PV-thermal hybrid CPC module for high latitudes. Solar Energy 69 (1–6), 173–185.

Brogren, M., Karlsson, B., Håkansson, H., 2001a. Design and modelling of low-concentrating photovoltaic solar energy systems and investigation of irradiation distribution on modules in such systems. In: Proceedings of 17th EUPVSEC, Munich, Germany.

Brogren, M., Wennerberg, J., Kapper, R., Karlsson, B., 2001b. Design of concentrating elements with thin film solar cells for wall integration. In: Proceedings of 12th PVSEC, Cheju, Korea.

Brogren, M., Wennerberg, J., Kapper, R., Karlsson, B., 2003. Design of concentrating elements with CIS thin film solar cells for wall integration. Solar Energy Materials and Solar Cells 75, 567–575.

Duffie, J.A., Beckman, W.A., 1980. Solar Engineering of Thermal Processes. Wiley Interscience, New York.

Helgesson, A., Karlsson, B. 2001. Study of incidence angle dependence on optical efficiency based on outdoor measurements, modelling of incidence angle dependence of non-symmetrical collectors. In: Proceedings of NorthSun, Holland.

McIntire, W.R., 1982. Factored approximations for biaxial incident angle modifiers. Solar Energy 29 (4), 315–322.

McMahon, T.J., von Roedern, B., 1997. Effects of light intensity on current collection in thin-film solar cells. In: Proceedings of 26th PVSC Conference, Anaheim, USA.

Rönnelid, M., Perers, B., Karlsson, B., 1997. The factorisation of incidence angle modifiers for CPC collectors. Solar Energy 59 (4–6), 281–286.

Souka, A.F., Safwat, H.H., 1966. Optimum orientations for the double exposure flat-plate collector and its reflectors. Solar Energy 10, 170–174.

Tripanagnostopoulos, Y., Nousia, T.H., Souliotis, M., Yianoulis, P., 2002. Hybrid photovoltaic/thermal solar systems. Solar Energy 72 (3), 217–234.

Wennerberg, J., Kessler, J., Hedström, J., Stolt, L., Karlsson, B., Rönnelid, M., 2000. Thin film pv modules for low-concentrating systems. Solar Energy 69 (Suppl.), 243–255.

Zacharopoulos, A., Eames, P.C., McLarnon, D., Norton, B., 2000. Linear dielectric non-imaging concentrating covers for pv integrated building facades. Solar Energy 6 (5), 439–452.

ZEMAX version November 1, 2004. ZEMAX Development Corporation, San Diego, California, USA.

Article III

MICRO-STRUCTURED REFLECTOR SURFACES FOR A STATIONARY ASYMMETRIC PARABOLIC SOLAR CONCENTRATOR

Johan Nilsson and Björn Karlsson
Division of Energy and Building Design, Department of Architecture and Built Environment,
Lund University, P.O. Box 118, Lund, SE-22100, Sweden
Phone +46 46 2227606, fax +46 46 2224719, johan.nilsson@ebd.lth.se

Ralf Leutz
Physics Department, Philipps-University, Renthof 5, 35037 Marburg, Germany
Phone +49 6421 2824148, fax +49 6421 2826535, ralf.leutz@physik.uni-marburg.de

Abstract – One of the main problems in using parabolic concentrators with standard PV cells is the highly non-uniform illumination of the cells. This effect causes high resistive losses in the cells, and the resulting efficiency of the systems is lowered considerably. To solve this problem, we introduce three different structured reflectors that will create a more uniform illumination, and also possibly increase the concentration ratio. The maximum concentration ratio of translational symmetric compound parabolic reflectors (CPCs) is limited by the independent conservation of the étendue of the reflected rays in the symmetry planes. By adding a surface micro-structure to the reflectors, it is possible to selectively mix the angular distribution in the reflections, and increase the concentration ratio. Three different structures were evaluated in an existing trough system by Monte Carlo ray tracing, and it was found that structures improve the system performance by increasing the concentration ratio and by homogenizing the light on the cells. The yearly irradiation collected in the evaluation system is slightly lower than for a reference with smooth reflectors, but the more uniform illumination of the cells will generate a net increase of the total system performance compared to a system that was optimized with smooth reflectors. The benefit of the increased concentration ratio is increased flexibility in designing new systems with concentration ratios surpassing the theoretical limit of trough concentrators.

1. INTRODUCTION

In view of the high costs of photovoltaic modules, it is necessary to find ways to reduce the cost of a PV system considerably to facilitate more extensive use. By using concentrating reflectors to increase the irradiance on the cells, expensive PV cell area can be exchanged by considerably less expensive reflector area. This has been shown to reduce the cost of the electricity produced (Perers and Karlsson 1993). Many reflector systems are based on compound parabolic concentrator reflectors, or CPCs (Welford and Winston 1989).

Parabolic reflectors are ideal concentrators for distant sources, all light incident parallel to the optical axis of the reflector is reflected into the focal point.

The sun is an extended source with a half-angle θ_S=0.28°. Sunlight produces a focal line in a parabolic trough concentrator. The geometrical concentration ratio C of the parabolic trough of unit width and a rim angle ψ defines the half-width of the focal line r_t

$$r_t = \frac{1}{C} = \frac{\theta_s}{\cos(\psi)\sin(\psi)} \qquad (1)$$

For $\theta_{max}=\pi/4$, i.e. a rim angle of 45°, the average geometrical concentration ratio of the parabolic trough reaches its maximum of 104, with a peak at $C_{max}=\sin\theta_{max}/\sin\theta_S=144$. A parabolic shape will concentrate sunlight into a hot spot of high

geometrical concentration, independent of the acceptance half-angle θ_i (Welford and Winston 1989) of the system.

The high local intensities on the PV cells in parabolic troughs make the use of concentrator cells necessary to reduce the losses due to the high local currents (Luque, Sala, and Arboiro 1998). These cells are expensive and are produced in small series, but if the light could be more uniformly distributed over the cells, it would be possible to use standard silicon cells in the systems, and this would reduce the system price significantly. To address this problem, we will evaluate three different structured reflectors that will create a more uniform light distribution.

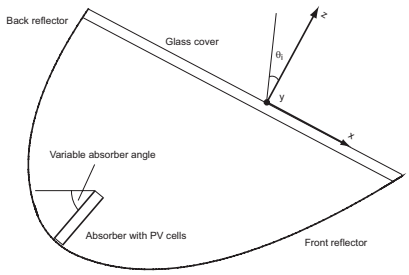

Figure 1 System layout of the asymmetric parabolic trough concentrator. Shown is the local coordinate system

Stationary asymmetric CPC systems such as the MaReCo, MaximumReflectorCollector, which is shown in Fig. 1 (Nilsson, Håkansson and Karlsson 2003) are suitable for northern latitudes such as Sweden due to the relatively low solar altitude and the high cloud coverage during the winter. It consists of two parabolic aluminium mirrors tilted in 20º and 65º, the absorber is an aluminium profile with copper pipes in the middle to collect heat, and standard monocrystaline silicon cells are laminated on the profile. The system is designed to accept all irradiation between 20º and 65º in the meridian plane.

The system has an average concentration ratio of 3.5 for the lower reflector and 2.4 for the upper reflector. This system was chosen as the evaluation platform for the proposed reflectors.

Even though the concentration ratio is low for the system, local intensities of 30 times the solar beam have been measured on the cells due to the parabolic shape of the mirrors (Nilsson, Håkansson and Karlsson 2003). The high local intensity at the focal point creates high local currents in the illuminated part of the cells, and the relatively high resistance of standard cells that are used in this system causes large losses. The large difference between 3.5, the concentration ratio, and 30, the real intensity at the centre of the strip of light, indicates that rational changes to the geometry of the reflectors have a large potential for performance improvement.

1.1 Maximum concentration ratio

The principle of étendue conservation states that a translational symmetric two-dimensional compound parabolic reflector (CPC) system has a maximum concentration ratio of $1/\sin(\theta_i)$, where θ_i is the half-angle of acceptance in the symmetry plane for y=0 (see Fig. 1). For a three-dimensional concentrator such as the CPC of rotational symmetry, the maximum concentration ratio is $1/\sin^2(\theta_i)$ accordingly. Independently conserved quantities in the translational symmetric system are the two-dimensional étendues in the symmetry planes (Leutz and Ries 2005).

$$\begin{aligned} \Delta x \Delta k_x &= const \\ \Delta y \Delta k_y &= const \end{aligned} \qquad (2)$$

This limits the part of the phase space that is filled with light at the exit aperture of the system (Bortz, Shatz and Winston 2001). The phase space is completely filled at the exit aperture when the rays are exiting at all angles in three dimensions into a hemisphere. If the angular space is not evenly filled at the exit aperture, it limits the concentration ratio by a factor $\sin(\theta_{exit})$. For translational symmetric systems, k_y is not affected by reflections and this dictates that both k_y and Δy are constant independently.

The angles opened by the directional vector components k_x, k_y are small for sources with small angular spread and concentrators with smooth reflectors. Breaking the symmetry of the reflector surface will selectively mix the directions of the reflected rays. While for smooth reflectors the étendues in the symmetry planes (Eqn. 2) are independently conserved, selective mixing leads to the conservation of total étendue

$$\Delta x \Delta k_x \Delta y \Delta k_y = const \qquad (3)$$

By breaking the symmetry of the trough's smooth reflectors, i.e. affecting the directional components of the reflected rays, it is possible to achieve concentration ratios greater than the limit of two-dimensional concentrators $1/\sin(\theta_i)$, approaching the three-dimensional limit $1/\sin^2(\theta_i)$ (Rönnelid, Perers and Karlsson 1994; Rönnelid and Karlsson 1998). Breaking the symmetry leads to the increase of the light throughput (étendue) of the concentrator. The ideal concentrator is characterized by rays of all possible directions at the exit aperture. This tells us that complete mixing of the different angles is desirable. Three different micro-structures were proposed as possible solutions for breaking the symmetry, all shown in Fig. 2 (showing the *xy*-plane). All structures are oriented perpendicular to the translational symmetry axis.

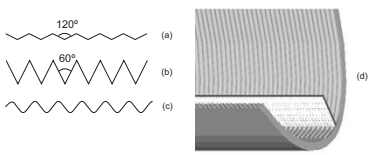

Figure 2 Different micro-structures. The structure (a) has an opening angle of 120º, the structure (b) has an angle of 60º, and the structure (c) is sinusoidal shaped to obtain complete randomization. The MaReCo with structured reflectors is shown in an artist's view (d).

Selective mixing can be obtained by creating a V-shaped structure on the reflector with an angle of 120º(a) or 60º(b) according to Fig. 2 (Leutz and Ries 2003). Structure (c) in the figure is a sinusoidal wave. The sinusoidal shaped structure has all possible surface normals from -45º to 45º depending on the position on the reflector. This creates randomization of the angles of the rays after reflection.

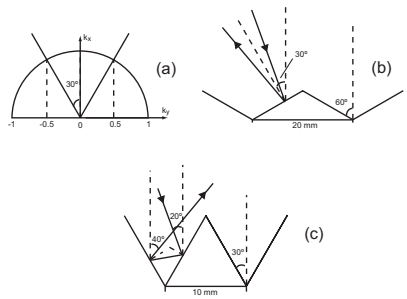

Figure 3 Selective mixing of reflected rays in the two-dimensional phase-space. The étendue limited by the angular interval -30<θ<=30 is equal to the étendue comprising the rest of the possible angles. The V-shaped structures reflect all rays of one angular interval into the other, and vice versa, thereby mixing the étendue.

Figure 3(a) shows the two-dimensional étendue of incidence projected onto a half-circle. The étendue limited by the angular interval $-30° < \theta <= 30°$ is equal to the étendue comprising the rest of the possible angles. The V-shaped structures reflect all rays of one angular interval into the other, and vice versa, thereby mixing the étendue.

The two V-shaped structures mix the étendue in different ways. The structure (a) with an angle of 120º will create this in one reflection, and the 60º structure (b) will produce the same result by reflecting every ray twice. As can be seen in Fig. 3, the exit angle with the trough cross section will be the same, but the rays might travel in different directions along the axis of symmetry after being reflected. The

obvious drawback of the 60º structure is the lower optical efficiency due to the double reflection. All reflected rays will have a lower intensity in this case compared to the 120º structure. The behaviour of the sine-shaped structure will be evaluated using a statistical method, Monte Carlo ray tracing.

2. METHOD

The proposed changes to the structure of the MaReCo reflectors were evaluated by Monte Carlo ray tracing. Four sets of simulations were performed, one for each structured reflector, and one reference simulation with smooth reflectors. 3D models of the four systems were constructed and simulated in ZEMAX, a commercial ray tracing package (ZEMAX 2004).

The cover glass of the system was omitted in all cases, and the source of the rays was placed vertically in front of the system aperture. The source generated 25 000 rays at a specific angle at random locations, and the rays were detected at the trough aperture as a measure of the incident flux, as well as on the front and back side of the absorber. The angle of incidence was varied in both azimuth direction and solar altitude from 0º to 85º in steps of 5º and one simulation was done for each angle resulting in 324 simulations for each reflector type. Figure 4 defines these angles of incidence, where α is the solar altitude and γ is the azimuth angle.

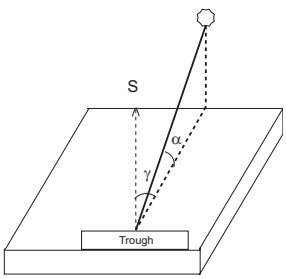

Figure 4 Definition of the angles used in the simulations, α is the solar altitude and γ is the azimuth angle.

The normalized absorptance of the PV cells was modelled according to Fig. 5 (Brogren, Nostell and Karlsson 2000).

The detectors on the aperture and on the absorber consisted of one bin each to detect the incident flux. The optical efficiency of the system was calculated according to

$$\eta_{opt}(\alpha,\gamma) = \frac{\Theta_{FrontAbs} + \Theta_{BackAbs}}{\Theta_{Aperture}} \qquad (4)$$

where Θ_i is the detected flux at a detector i.

The reflector material was aluminium with a specular reflectance of 92% at normal incidence. Its reflectance as a function of the angle of incidence can be seen in Fig. 5. The maximum error in flux detected by the detectors for each angle is estimated to 2%.

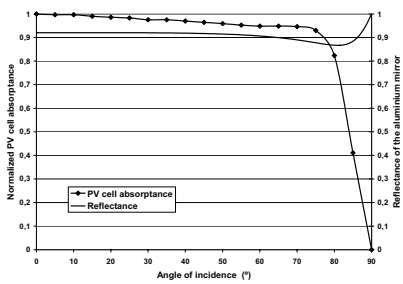

Figure 5 Normalized absorptance of the PV cell (a) and reflectance of the aluminium mirror (b) used to model the incidence angle dependency of the system

The detectors were fitted with 70 bins in the y direction of the absorber, i.e. each bin was 2 mm wide, in order to be able to analyse the uniformity of the irradiance distribution on the cells. This second round of simulations was performed for certain angles of incidence, now using 500 000 rays for higher spatial resolution.

3. RESULTS

3.1 Changes in the light distribution

One of the main challenges in improving low concentration CPC systems such as the MaReCo is the highly non-uniform irradiance distribution on the PV cells. Solving this problem is the main objective when introducing the structured reflectors.

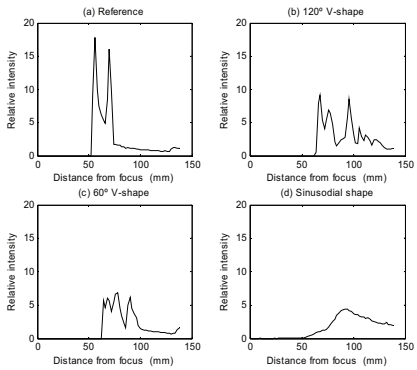

Figure 6 Irradiance distribution on the cells of the upper absorber for α=40°, γ =15°. Four different reflector structures a-d.

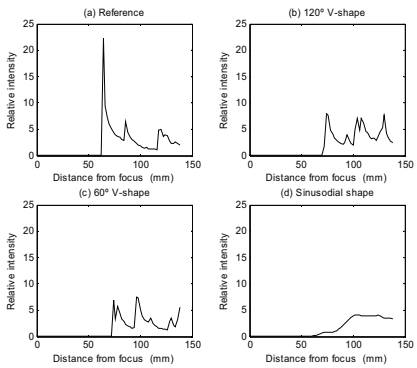

Figure 7 Irradiance distribution on the cells of the lower absorber for α =40°, γ =15°. Four different reflector structures a-d

Some of the results from the simulations are shown in Fig. 6 and Fig. 7 where the former illustrates the irradiation distribution on the cells facing the upper reflector for an azimuth angle of 15º and a solar altitude of 40º. The latter shows the irradiation distribution on the cells facing the lower reflector at the same angle of incidence.

As can be seen from the figures, all three structural changes reduce the peak intensity of the light incident on the absorber. This will result in a higher fill factor of the cells, i.e. the resistive losses in the cells will be lower. The highest peak reduction is obtained by using the sinusoidal micro-structure. Fig. 6 and Fig. 7 show a maximum intensity of 5 times the sun for this reflector. This intensity should be low enough for the standard cells in the MaReCo system. For the V-shaped structures, the 60º structure seems to reduce the peaks slightly more than the 120º structure, but on the other hand, the overall irradiation on the cell (the integrated intensity profile) is larger for the 120º structure which could explain the greater reduction of the peaks. The peaks for the V-shaped structures can reach levels of almost 10 times the sun. At these intensities, the high resistance of the standard cell becomes a problem, even though it will cause considerably less losses than for the case of the reference reflector where the intensity can be as much as 25 times the beam of the sun. An important point to make about the Figs. 6 and 7 is that the absorber connects to the reflector at x=140 mm. If the light distribution is non-zero at the parabola's focus, x=0 in the figures, it can be an indication that some of the light is reflected outside the absorber and lost.

3.2 Comparison of the optical efficiency of the systems

The optical efficiency of the system is defined as the ratio between the incident and the absorbed flux, as described by Eqn. 4. The micro-structured reflectors change the path of the rays, and will in some cases cause the rays to miss the absorber. On the other hand, the increased concentration ratio of the structured

reflectors will make the system absorb irradiation outside the acceptance interval of the reference system, i.e. outside the angular interval of 20º and 65º in the meridian plane. Figure 8 shows the optical efficiency of the four reflector systems when the solar altitude is changed at a constant azimuth angle of 0º, i.e. in the cross-sectional plane of the trough facing south (the *xz*-plane).

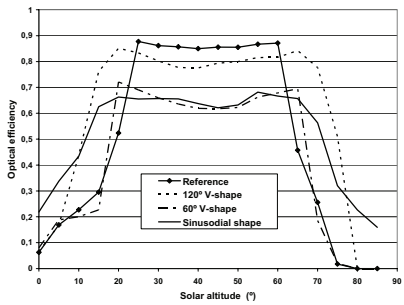

Figure 8 Optical efficiency as a function of solar altitude in the *xz*-plane. Normal incidence is equal to a solar altitude of 60º

The optical efficiency of the reference system is high between 20º and 65º, but drops rapidly outside this interval. The efficiency does not drop exactly at 20º and 65º in the figure, but this is due to the choice of interval in the simulations. If the interval was smaller, this effect would be more clear. The well defined interval of acceptance is a characteristic of parabolic troughs. The shape of the trough was designed to accept all light in this interval as a compromise considering the yearly irradiation incident on a south facing surface tilted in 30º, as the trough aperture. The 120º structured reflector has a slightly lower peak efficiency, around 7% lower, but the acceptance angle interval is larger, around 10º at both ends. The wider interval is due to the increased concentration ratio, and the slightly lower peak efficiency is due to the fact that the randomization of the reflected rays in some cases will cause multiple reflections. The sinusoidal shaped reflector and the 60° structure show considerably lower peak efficiencies, most of the rays are reflected more than once. For the 60° structure this effect can be explained with Fig. 3c, where most rays incident on the reflector are reflected twice. The higher number of multiple reflections for the sinusoidal structured reflector is due to the large randomization of the reflected rays, which is evident in the figures of light distribution on the cells where the light is more evenly distributed in spite of the fact that the mirror's global shape is parabolic.

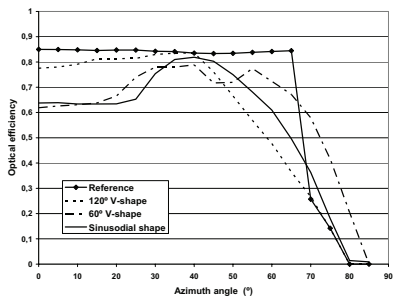

Figure 9 Optical efficiency as a function of the azimuth angle at a constant solar altitude of 40º

Figure 9 shows the optical efficiencies of the four reflector systems at changing azimuth angle. The solar altitude in the simulation was kept constant at 40º, within the interval of acceptance for the smooth reference trough.

As expected, the reference reflector shows an almost constant optical efficiency at all angles up to 70º, where the acceptance limit of a transverse angle of 65º is exceeded. The transverse angle is the angle of the solar vector projected into the *xz*-plane. As the solar altitude was constant at 40º throughout the simulation, the transverse angle became 65º at an azimuth angle of approximately 67º. As can be seen from Fig. 8, the optical efficiency of the reference drops considerably once this angle is reached. Another aspect that can be seen from Fig. 8, is that the efficiency is almost constant

in this interval which explains the constant efficiency of Fig. 9. The 120° structured reflector has an efficiency close to the reference up to azimuth angles of 45º, where it starts to drop. At large azimuth angles, more and more of the rays are reflected outside the absorber. The efficiency of this reflector never exceeds the reference in the simulated case. The 60° structure and the sine-shaped structure have a 25% lower efficiency at low azimuth angles, but as the angle increases, the efficiency follows suit. At angles of around 70º, both structures have a higher efficiency than the reference, the 60° structure having the highest efficiency.

3.3 Evaluation of the MaReCo using different reflectors in Lund, Sweden

Insolation is not equal for all angles of incidence, it is highest in the middle of the day, around 0º azimuth angle. The yearly direct insolation in Lund, Sweden, 55.73 N, 13.22 E was divided into angular intervals of 5º in the solar altitude and azimuth directions. The optical efficiencies at different angles were multiplied by the irradiation values to get a local evaluation of the concentrator performance. This is not equal to the annual output, but it allows for a comparison of the four reflectors at this specific site.

The diffuse part of the yearly insolation was treated separately. The diffuse sky was treated as isotropic all year, i.e. the different parts of the sky were assumed to radiate equally strong, or lambertian. The efficiencies of the troughs for diffuse radiation were calculated according to Eqn. 5, where α is the solar altitude, γ is the azimuth angle, and θ is the angle of incidence on the aperture of the trough. The limits of α were set to 0° and 150º instead of 0° and 180º since the 30º tilted aperture will not receive any irradiation from the interval 150º to 180º.

$$\eta_{diffuse}(\alpha,\gamma)=\frac{\sum_{\alpha=0}^{\alpha=150}\sum_{\gamma=-90}^{\gamma=90}\eta_{direct}(\alpha,\gamma)\cdot\cos(\theta)}{\sum_{\alpha=0}^{\alpha=150}\sum_{\gamma=-90}^{\gamma=90}\cos(\theta)} \quad (5)$$

Table 1 shows the result of these calculations.

	Reference	120º V-shape	60º V-shape	Sinusoidal shape
$\eta_{diffuse}$	0.32	0.36	0.30	0.35

Table 1 Optical efficiencies of the micro-structured reflectors for diffuse radiation

The optical efficiency for diffuse radiation exceeds the reference efficiency in case of the 120° V-shaped micro-structured reflector and for the sinusoidal shaped reflector, even though these reflectors create more multiple reflections. The reason for this can be seen in Fig. 6, as the interval of acceptance is smaller for the reference case. As smaller interval of acceptance practically means that the cells see a smaller part of the sky.

The optical efficiency for diffuse radiation was multiplied by the total diffuse radiation on a surface tilted 30º, modelling the aperture. The diffuse irradiation was then added to the direct irradiation from the previous calculations. Table 2 shows the result of the irradiation calculations.

	Reference	120º V-shape	60º V-shape	Sinusoidal shape
$\eta_{diffuse}$	1	0.93	0.89	0.92

Table 2 Annual irradiation on the PV cells of the system relative to the reference

Considering the fact that the MaReCo was optimized for climate of Lund, it is not surprising that the smooth reflector receives the highest yearly irradiation. The 120º structure and the sinusoidal shaped structure show a mere 7-8% decrease in accepted irradiation over the year.

4. DISCUSSION

4.1 The 120° V-shaped reflector structure

The 120º structure has the highest overall optical efficiency of the three evaluated structures. The simulations show that 7% less irradiation reaches the cells over a year, when compared to a reference concentrator with smooth reflectors. The main advantage of this reflector compared to the other two structured reflectors is that it has roughly the same average number of reflections as the smooth reference. This can be seen in Fig. 8 where the optical efficiency is close to the reference inside the interval of acceptance as long as the azimuth angle is small. When the azimuth angle increases, more rays are reflected out of the concentrator, and the efficiency drops as Fig. 9 shows. At small azimuth angles, this structure would be preferred to the reference as the interval of acceptance is wider for the structured reflector and this gives a higher degree of freedom in designing the system. However, it is less efficient as the azimuth angle increases.

Considering the irradiance distribution, this reflector shows the lowest peak reduction of the three structures, although uniformity is still considerably better than for the reference case.

This reflector would be the best choice when the irradiation is concentrated within small azimuth angles, or for east-west tracking. The small 7% reduction in total yearly irradiation shows that it could improve stationary concentrators as well due to the more homogenous irradiation distribution. If the generated electricity is more valuable in the middle of day, this would be another reason for choosing this reflector.

4.2 Sinusoidal reflector structure

The sine structured reflector has almost the same overall optical efficiency as the 120º structured reflector, only 8% less irradiation reaches the absorber in this case compared to the reference. At small azimuth angles, the efficiency is considerably lower compared to the reference. As the interval of acceptance is less pronounced, the efficiency decreases slowly outside the 20-65° interval rather that showing the step characteristic of the reference. As the azimuth angle increases, Fig. 9 shows an increasing optical efficiency, and at larger azimuth angles, the sinusoidal structure shows a higher efficiency than the reference.

Of the three proposed micro-structures, this one shows the most uniform irradiation profile on the absorber, most of the peaks are removed, and the intensity in Fig. 6 and Fig. 7 is never higher than 4.5 times the intensity of the sun.

This reflector shows an overall efficiency similar to the 120º V-shaped reflector in the evaluation with the local climate, but the more uniform irradiation distribution generated by the sinusoidal micro-structure makes it a promising candidate for use in the stationary MaReCo system, especially if the irradiation is evenly distributed over the azimuth angles.

Important for this reflector is the ratio between the length of the period of the structure and the amplitude. As it was chosen in the studied case, the slope of the reflector at y=0 is somewhere between the slope of the 120º structure and the 60º structure. Had the amplitude been larger, more multiple reflections would have resulted in a decreasing optical efficiency. This would also decrease the angular interval of the surface normal from the evaluated $-45° < \theta < 45°$. This would result in less randomization of the reflected rays. A more detailed study of the optical effects of different ratios between period and amplitude of sinusoidal micro-structures is beyond the scope of this article.

4.3 The 60° V-shaped reflector structure

The 60º structured reflector decreases the reflected intensity compared to the reference mainly due to the fact that most rays are reflected twice upon impinging at the reflector. These reflection losses are the main reason for the 11% reduction in yearly irradiation on the cells. This is evident from Fig. 8 as the optical efficiency is 25% lower than the reference inside the interval of acceptance at zero azimuth angle. As the azimuth angle increases, the efficiency of this reflector system increases. At large azimuth angles, the efficiency is higher than the efficiency of the reference. The interval

of acceptance in the meridian plane, shown in Fig. 8, is the same as for the reference, clearly showing that this reflector system has a lower efficiency at small azimuth angles.

The intensity peak reduction on the absorber generated by this micro-structure is similar, or slightly larger than at the 120º structured reflector but as less light is collected at the absorber, this is to be expected.

This reflector shows some of the features of the 120º structured reflector, and some of the sinusoidal structured reflector, but of the three, it has the least benefits.

5. CONCLUSIONS

5.1 Illumination of the cells

The two goals of introducing structured reflectors were to increase the concentration ratio and to get a more uniform illumination distribution on the PV cells. By breaking the symmetry, the system became an actual 3D concentrator system, and a new illumination distribution was created. As was seen in Fig. 6 and Fig. 7, all three structures reduced the peak irradiation, creating a more uniform distribution. However, reducing the peak illumination by accepting less irradiation on the cells is not the solution to the problem, but it was shown that during a year in Lund, the reflector system with a 120º angle received 7% less irradiation on the cells, 11% less for the 60º structured reflector, and 8% less for the sine structured reflector.

In a previous measurement study on the MaReCo reflector system (Nilsson, Håkansson and Karlsson 2003), three reflector materials were tested. One of these materials, aluminium laminated steel, was slightly diffusing, reducing the peaks of high irradiation. When this material was used in the system, the fill factor of the cells was increased by as much as 12% even though the peak reduction was smaller than for any of the reflectors tested here. This tells us that the introduction of structured reflectors has a large potential for increasing the fill factor, and thus the power output of the system in parabolic trough systems such as this, since the reduction of yearly illumination is only 7% or 8% in the best cases.

We conclude that the small decrease in total irradiation is acceptable considering the larger gains in fill factor.

5.2 Increased concentration ratio

The increase of concentration ratio achieved by the phase space mixing due to the structured reflector can be exploited in two ways: either by reducing the cell area of the given system to get a lower system price, or by changing the shape of the trough to make use of the wider interval of acceptance seen in Fig. 8. The MaReCo trough is designed to accept as much irradiation as possible in an interval of 20º to 65º in the meridian plane of incidence, thereby discarding almost all of the irradiation outside this interval. This interval is connected directly to the size of the aperture, if the interval is smaller, the aperture can be larger and vice versa. In future studies on the structured reflectors, the trough aperture will be increased, creating a smaller angular interval for a smooth reflector system. As could be seen from Fig. 8, the interval of acceptance widens when a structured reflector is used. This will make it possible to accept almost all light in the interval of 20º to 65º while increasing the concentration ratio. The use of the sinusoidal structure would create similar possibilities as the V-shaped structures, but due to the randomness of the reflections, a more thorough study on the geometry would have to be performed to make the best use of it.

5.3 Robustness of the system

The MaReCo trough was created for PV/thermal hybrids that have PV cells laminated on a thermal absorber using a copper pipe inside the absorber for collecting the heat. The fluid keeps the cells at a lower temperature, and this increases the electricity output as well as produces hot water. A known problem with this type of hybrids is destruction of the cells if the circulation pump stops working when the trough is collecting at peak irradiation. Hot spots occur on the cell surface due to the high intensity peaks, and without the cooling of the

cells the heat can not be dissipated at an adequate rate. The results are delamination of the cells or cracking of the cells due to the thermal expansion of the different materials in the module. Reducing the intensity peaks with structured reflectors, this problem will almost certainly be solved as the cell will have a much more uniform temperature distribution. This will make the performance less restricted by heat conductivity and cooling.

REFERENCES

Perers B. and Karlsson B. (1993), External reflectors for large solar collector arrays, simulation model and experimental results, Solar Energy, 51 (5), pp. 327-337.

Bortz J., Shatz N., and Winston R. (2001), Performance limitations of translationally symmetric nonimaging devices, Nonimaging Optics: Maximum Efficiency Light Transfer VI, Roland Winston, Editor, Proceedings of SPIE Vol. 4446.

Rönnelid M, Perers B. and Karlsson B (1994), Optical properties of nonimaging concentrators with corrugated reflectors, in Optical Materials Technology for Energy Efficiency and Solar Energy Conversion XIII, Volker Wittwer, Claes G. Granquist, Carl M Lampert, ed. pp 595-602, Proc. SPIE 2255.

Leutz R. Ries H. (2003), Squaring the Circle – The Use of Microstructures for Converting and Homogenizing Beam Cross-sections, In Proceedings of SPIE International Symposium on Optical Science and Technology; Design of Efficient Illumination Systems, volume 5186, San Diego, California, August 2003

ZEMAX version November 1, 2004, ZEMAX Development Corporation, San Diego, California, USA

Nilsson J. Håkansson H. and Karlsson B. (2003), Monitoring of electrical and thermal performance of PVCPC hybrids, Proceedings of ISES 2003 Solar World Congress, Göteborg, Sweden, June 2003

Welford W.T., Winston R. (1989), High Collection Nonimaging Optics, Academic Press Inc, New York

Leutz, R., Ries, H. (2005), Micro-Structured Light Guides Overcoming the Two-Dimensional Concentration Limit, Applied Optics, in print

Brogren M., Nostell P., Karlsson B. (2000), Optical efficiency of a PV-thermal hybrid CPC module for high latitudes, Solar Energy, 69 (Suppl), pp173-185

Luque A., Sala G., Arboiro J.C. (1998) Electric and thermal model for non-uniformly illuminated concentration cells. Solar Energy Materials and Solar Cells, 51, pp 269-290

Rönnelid M., Karlsson B. 1998, Optical acceptance function of modified compound parabolic concentrators with linear corrugated reflectors. Applied Optics, Vol 37 No 22 pp 5222-5226

Article IV

Available online at www.sciencedirect.com
SCIENCE DIRECT®
Solar Energy Materials & Solar Cells
ELSEVIER
Solar Energy Materials & Solar Cells 82 (2004) 387–412
www.elsevier.com/locate/solmat

Optical properties, durability, and system aspects of a new aluminium-polymer-laminated steel reflector for solar concentrators

Maria Brogren[a,*], Anna Helgesson[b], Björn Karlsson[b,c], Johan Nilsson[c], Arne Roos[a]

[a] *Division of Solid State Physics, Department of Engineering Sciences, Uppsala University, Box 534, Uppsala 751 21, Sweden*
[b] *Vattenfall Utveckling AB, Älvkarleby 814 26, Sweden*
[c] *Division of Energy and Building Design, Department of Construction and Architecture, Lund University, P.O. Box 118, Lund 221 00, Sweden*

Received 27 December 2003; accepted 13 January 2004

Abstract

A newly developed aluminium-polymer-laminated steel reflector for use in solar concentrators was evaluated with respect to its optical properties, durability, and reflector performance in solar thermal and photovoltaic systems. The optical properties of the reflector material were investigated using spectrophotometer and scatterometry. The durability of the reflector was tested in a climatic test chamber as well as outdoors in Älvkarleby (60.5°N, 17.4°E), Sweden. Before ageing, the solar weighted total and specular reflectance values were 82% and 77%, respectively, and the reflector scattered light isotropically. After 1 year's outdoor exposure, the total and specular solar reflectance had decreased by less than 1%. However, after 2000 h in damp heat and 1000 W/m^2 simulated solar radiation, the optical properties had changed significantly: The light scattering was anisotropic and the total and specular solar reflectance values had decreased to 75% and 42%, respectively. The decrease was found to be due to degradation of the protective polyethylene terephthalate (PET) layer, caused by UV radiation and high temperature. The conclusions are that the degradation is climate dependent and that PET is not suitable as a protective coating under extreme conditions, such as those in the climatic test chamber. However, the results from

*Corresponding author. Angstrom Laboratory, Department of Engineering Sciences, Uppsala University, P.O. Box 534, Uppsala S-75121, Sweden. Tel.: +46-18-471-31-31; fax: +46-18-500-131.
E-mail address: maria.brogren@angstrom.uu.se (M. Brogren).

0927-0248/$ - see front matter
doi:10.1016/j.solmat.2004.01.029

388 M. Brogren et al. / Solar Energy Materials & Solar Cells 82 (2004) 387–412

outdoor testing indicate that the material withstands exposure in a normal Swedish climate.

Keywords: Solar concentrators; Reflector materials; Optical properties; Accelerated ageing; Durability

1. Introduction

1.1. Concentrating solar energy systems

Due to the relatively high material and production costs of solar cells and solar thermal absorbers, it is desirable to find alternative ways of reducing the cost of photovoltaic electricity and solar heat. One approach is to use concentrators that increase the irradiance on the modules or absorbers and thus the electricity or heat production per unit receiver area, which in turn reduces the area needed for a given output. Concentrating systems use lenses or reflectors to focus sunlight onto the solar cells or solar thermal absorbers. High concentration of solar radiation requires tracking of the sun around one axis or two axes, depending on the geometry of the system. The higher the concentration, the more concentrator material per unit area of solar cell or thermal absorber area is generally needed. It is therefore more appropriate to use lenses than reflectors in highly concentrating systems, because of their lower weight and material costs. Lenses, typically point-focus or linear-focus Fresnel lenses with concentration ratios of 10–500×, are most often manufactured out of inexpensive plastic material with refracting features that direct light onto a small or narrow area of photovoltaic cells or on a linear thermal absorber. The cells are usually silicon cells. Single- or mono-crystalline silicon approaches accounted for 93% of the annual cell production in 2002 [1]. Cells of GaAs and other compound materials have higher conversion efficiencies than silicon, and can operate at higher temperatures, but they are often substantially more expensive [2]. Concentrator module efficiencies range from 17% and upwards and concentrator cells have been designed with conversion efficiencies in excess of 30% [3,4]. Concentrator systems that utilize lenses are unable to focus scattered light, limiting their use to areas with mostly clear weather.

In areas with a lot of diffuse irradiation, as well as for moderate (5–20×) and low (<5×) concentration ratios, reflectors are often more cost-effective than lenses and therefore the most common type of concentrator. Below 5× concentration, it is possible to construct cost-effective static concentrators, both for photovoltaic and solar thermal systems [5,6]. These are mostly two-dimensional parabolic troughs or plane booster reflectors. Plane mirrors in front of the collector area increase the collected energy with 20–50% and reduce some of the diurnal variation [7].

1.2. Solar reflector materials

Reflectors for solar energy applications should fulfil a number of requirements

- They should reflect as much as possible of the useful incident solar radiation onto the solar thermal absorbers or the photovoltaic cells.

- The reflector material and its support structure should be inexpensive compared to the solar cells or thermal absorbers onto which the reflector concentrates radiation.
- The high reflectance should be maintained during the entire lifetime of the solar collector or photovoltaic module, which is often longer than 20 years.
- If cleaning is necessary, the surface should be easily cleaned without damaging its optical properties and the maintenance should not be expensive.
- The construction must be mechanically strong to resist hard winds, snow loads, vibrations, etc.
- The reflector should preferably be lightweight and easy to mount.
- The reflector material should be environmentally benign and should not contain any hazardous compounds.
- The visual appearance of the reflector should be aesthetical, since solar concentrators often are large and must be placed fully visible on open spaces so that the concentrator aperture is not shaded by objects in the surroundings.

The optical requirement that must be fulfilled for reflector materials in solar thermal applications is a high reflectance in the entire wavelength range of the solar spectrum (300–2500 nm). In photovoltaic applications, photons with lower energy than the band gap of the solar cell, which corresponds to wavelengths longer than about 1100 nm for a silicon cell, do not contribute to the photoelectric conversion but only to overheating. High cell temperatures reduce the output voltage and a high reflectance in the infrared is therefore counterproductive in photovoltaic applications. Hence, metals that are free electron-like and obey the Drude model [8] are suitable as reflectors for solar thermal applications, but not optimal for photovoltaics. There are no known metals that combine a low reflectance in the near-infrared with a high reflectance in the ultraviolet and in the visible. However, such a selective reflectance can be obtained by an application of thin films on top of the reflecting metal, which are absorbing in the near-infrared, for example doped tin oxide [9].

Among the Drude metals, silver and aluminium are the best solar reflectors [10], with a solar hemispherical reflectance of approximately 97% and 92%, respectively. Due to its lower cost, the material which is most often used for solar reflectors today is anodised aluminium. However, if the anodised aluminium is not protected, for example by a glazing, a plastic foil, or a lacquer, its optical performance degrades severely in only a couple of months [11]. The degradation of silver is essentially as rapid as that of aluminium [12]. Due to the limited corrosion resistance of the free electron-like metals, they are often used in back surface mirrors, evaporated on the back of a glass or polymer substrate that protects the metal from oxidation. Among the state-of-the art in solar reflector materials are back-surface-silvered low-iron glass or polymethylmethacrylate (PMMA) [13]. However, glass mirrors tend to be brittle and heavy. Front surface mirrors, on the other hand, are often bendable and of light weight, but more susceptible to chemical attack [14].

A solar reflector is not subject to the same high temperatures and thermal cycling as a solar absorber. Nevertheless, environmental conditions impose stringent

demands on the material, whose surface will deteriorate more or less upon exposure to the environment. Loss of solar reflectivity can result from erosion or oxidation of the surface, dirt accumulation on the reflector, and action of cleaning agents [15]. While degradation caused by accumulation of dust on the reflecting surface is essentially reversible, surface oxidation is not [16].

The optical performance of solar reflectors thus depends on the mechanical and chemical properties of the surface and the protective coating, if such is present. For flexible reflective foils, a support of sheet metal may be necessary, while only a simple frame construction is needed if the reflector is self-supporting, which is the case for corrugated sheets. When installing booster reflectors, the cost of the reflector material, the frame and support construction, as well as mounting and installation of the reflector must be taken into account. Maintenance should also be included in life-cycle cost.

1.3. Swedish experiences with booster reflectors

Since the beginning of the 1980s, several large ground-based solar thermal collector systems have been installed in Sweden. These collectors show the lowest costs of solar energy systems in Sweden. During the 1990s, a number of solar energy systems in Sweden and Denmark have been equipped with external, trapezoidal corrugated booster reflectors of aluminium. One example is the installation in1994 of a collector field at Östhammar (60.2°N, 18.2°E) in Sweden. In the Östhammar system, the reflectors are made of a corrugated lacquered aluminium sheet with an initial solar reflectance of about 63%. The use of reflectors increases the annual heat production from 380 to 490 kWh/m^2, an increase of almost 30% [17]. The solar reflectance of the booster reflectors in the Östhammar system is low, partly due to the thick layer of poly(vinylidene fluoride)-based lacquer (PVF2). If the booster reflectors in the Östhammar solar collector field had been made of highly reflective anodised aluminium with a solar reflectance of 85%, the annual output could have been as high as 530 kWh thermal energy per m^2 collector area, or 40% higher than without reflectors. However, the durability of the lacquered reflector has shown to be good, while the optical properties of anodised aluminium reflectors often have degraded severely after 10 years outdoor exposure.

1.4. Reflector laminates

Aluminium is often used as a reflector material, for internal as well as external reflectors, in solar energy systems. In order to be self-supporting in the latter case, the aluminium sheet must often be thicker than 4 mm. Stainless steel, on the other hand, is rigid and does not have to be as thick as an aluminium sheet. Austenitic steel has a long-term stable but rather low solar reflectance (67%) [14].

One way for cost-minimization of concentrators, which is proposed in this article, is to laminate a thin aluminium foil on a steel substrate, thus obtaining the good mechanical properties of steel, the high solar reflectance of aluminium, and the

degradation protection of the plastic laminate. In this way, the reflector performance can be improved without significantly increasing the material cost.

The technique of combining different materials by lamination is not new. For example, thin, flexible metal-polymer laminates can be purchased on rolls. Traditionally, these laminates are used within the packaging industry, but there are other applications as well. The combination of materials with different properties makes it possible to tailor the properties of the product for different applications. As stated above, a solar reflector material should have high reflectance, long durability, mechanical strength, and low cost. Since high reflectance is a property that is determined by the surface of the material, it can be created using thin films (for example of aluminium). The substrate is then chosen to fulfil specific requirements on mechanical properties and a protective coating is used to prevent degradation of the reflective layer. The lamination process will differ with the choice of materials in the laminate. If the substrate is a rigid steel sheet, it may be impossible too to use a roll process, and if the protective coating is a lacquer, spray painting may be utilized instead of lamination of the top layer.

1.5. Objective of this work

The overall objective of an ongoing Swedish project is to increase the performance of low-concentrating solar energy systems with reflectors, without increasing system cost [18]. The approach is to design and manufacture new reflector materials that combine the mechanical properties of steel sheet with the high solar reflectance of aluminium. Consequently, a reflector laminate consisting of a polymer coated highly reflective aluminium foil on a rigid steel sheet has been produced and reflectors have been manufactured of this material. The reflectors are primarily intended for large ground-based collector fields in which its use is expected to increase the annual thermal output by 40% compared to the yield without reflectors.

In the work that is presented in this article, the optical properties and degradation of the new reflector material have been evaluated.

2. The new reflector material

2.1. Design and manufacturing of a laminated Al-on-steel reflector

Because of its rigidity, a steel sheet with a thickness of 0.50 mm was chosen as substrate for the new reflector laminate. A 4 μm layer of polyurethane glue was applied on the steel sheet and it was hot pressed together with a reflective laminate which is a sandwich of 25 μm polyethylene terephthalate (PET)/20 nm evaporated aluminium/9 μm rolled aluminium foil/20 μm PET. The thicker PET is the top layer. The final product thus consists of the following layers:

- Protective layer of 25 μm clear, UV stabilised PET, which has a high-solar transmittance (see Section 5), high melting point (255°C) and good stability in

ultraviolet radiation. However, according to the product specifications, PET is not long-term stable at higher temperatures than 110°C.

- Reflective layer of aluminium, evaporated directly on the back of the protective film. Evaporated aluminium gives a high solar reflectance with a low diffuse component. However, the surface must be protected from exposure to humidity, high temperature, and air pollutants in order to keep its optical properties long-term stable.
- Substrate, which is a laminate of 9 μm aluminium (which protects the evaporated aluminium from moisture and provides a fairly good "back up reflectance" if the evaporated aluminium would be damaged) and 20 μm PET that, in turn, is heat laminated on a 0.50 mm steel sheet. Mechanical testing, performed by the manufacturer, showed that the steel sheet is mechanically strong and has a stiffness constant, $k > 10\,000$ N/m, which makes the reflector self-supporting.

Fig. 1 shows a schematic of the manufacturing process for the Al-on-steel reflector sandwich. To date, 200 m^2 of the Al-on-steel reflector have been manufactured using this process.

2.2. Construction of a booster reflector of trapezoidal corrugated Al-on-steel for a solar collector

Part of the produced reflector sheet has been trapezoidal corrugated and a large booster reflector has been constructed from the corrugated sheet and installed in front of a conventional flat plate solar collector in Älvkarleby (60.5°N, 17.4°E), Sweden, see Fig. 2. The heat production from the collector with a booster reflector of Al-on-steel is continuously monitored and compared to the output of similar collectors without reflectors in order to evaluate the performance of the new reflector material in a solar energy system.

Corrugation makes the metal sheet more rigid and prevents deformation. A trapezoidal corrugation can be obtained by bending or rolling. However, rolling often requires a minimum production volume in order not to result in a too

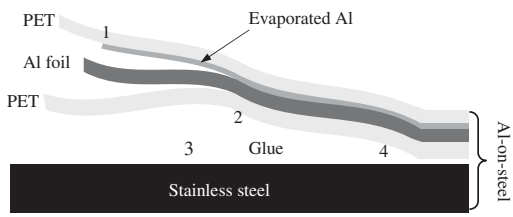

Fig. 1. The manufacturing of the Al-on-steel reflector. A 20 nm layer of aluminium is evaporated on a 25 μm PET foil (1), the PET foil with evaporated aluminium, a 9 μm rolled aluminium foil, and a 20 μm PET foil are laminated together (2), a 4 μm layer of glue is applied on a 0.5 mm thick sheet of stainless steel (3), the PET/Al/Al/PET sandwich and the steel sheet is hot pressed together to form the reflector laminate (4).

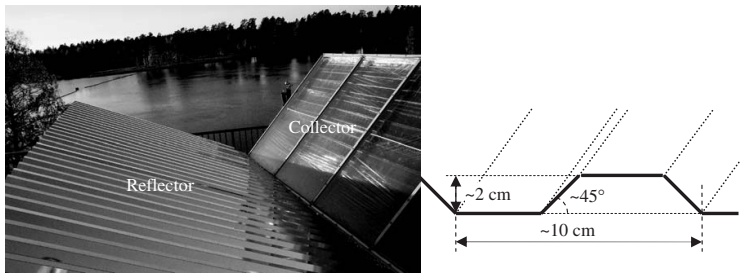

Fig. 2. A 18 m^2 trapezoidal corrugated Al-on-steel booster reflector, mounted in front of a 13 m^2 planar solar collector in Älvkarleby (60.5°N, 17.4°E), Sweden (left) and a schematic picture of the trapezoidal corrugation (right).

expensive product. Thus, for economical reasons, the corrugation of the single reflector was shaped by bending instead of rolling.

The solar collector, which faces south, has an absorber area of 13 m^2 and an inclination of 45°. Both reflector and collector are 6 m wide. The inclination of the 18 m^2 reflector is 25°. There is a 0.2 m gap between the bottom of the collector and the reflector in order to prevent a build-up of snow or leaves in front of the collector.

In the mornings and in the afternoon, when solar radiation hits the reflector at a non-zero azimuth angle, some of the reflected radiation has been found to miss the collector. To avoid these effects, a wider reflector should be used.

2.3. Construction of photovoltaic-thermal MaReCo systems with Al-on-steel reflectors

In addition to the large trapezoidal corrugated reflector in Älvkarleby, the Al-on-steel reflector material will be used in so called MaReCo concentrators [19–22] for a several $kW_{electric}$ photovoltaic-thermal co-generation system in Hammarby sjöstad, a new residential area in Stockholm (59.2°N, 18.3°E), Sweden. In principle, the photovoltaic-thermal MaReCo consists of an asymmetrically truncated compound parabolic concentrator trough using a hybrid absorber, with solar cells laminated on one side of a standard thermal absorber [23], which is placed along the focal line of the concentrator trough. This system also includes a cover glass that prevents convective and radiative thermal losses as well as protects the hybrid absorber and the reflector.

The Hammarby sjöstad system is designed, ordered, and manufactured, and will be delivered and installed during spring 2004.

3. Experimental methods

The Al-on-steel material was exposed to a number of tests, which are summarised in Fig. 3. The methods that were used are described in the following sections and the

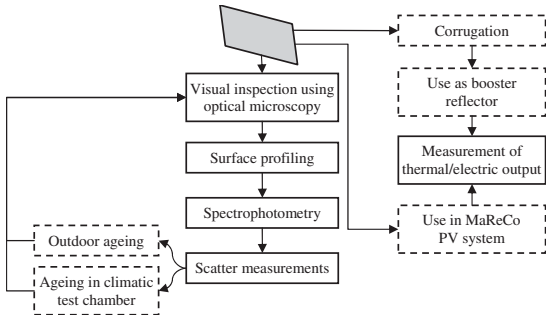

Fig. 3. The methods used for analysis of the Al-on-steel reflector laminate.

results that were obtained are presented in Section 4. The material is also tested according to the agreed upon conditions in the International Energy Agency's Solar Heating and Cooling Programme's Task 27 testing group [24]. These tests are ongoing and the results not yet available.

3.1. Optical microscopy and surface profilometry

The surface of the Al-on-steel reflector was analysed using an Olympus BX 60 optical microscope equipped with a Ikegami ICD-700PAC CCD color camera, which was connected to a computer for image analysis. Photographs of the surface were taken before and after ageing.

The surface profile of the Al-on-steel reflector was measured before and after ageing, using a Veeco Dektak V 200-Si profilometer. The scan length was 5 mm in all scans. The surface roughness (RMS) was calculated from measurement data. The calculation was performed by first fitting a second-order polynomial curve to measurement data, then subtracting this curve from the data in order to account for a bent sample, and finally calculating the standard deviation of the resulting curve.

3.2. Spectrophotometry

The wavelength-dependent diffuse and total reflectance, $R_{\mathrm{diff}}(\lambda)$ and $R_{\mathrm{tot}}(\lambda)$, at near normal angle of incidence were measured using a Lambda-900 spectrophotometer from Perkin-Elmer, equipped with an integrating sphere. The measurements were performed at every fifth nanometre for wavelengths, λ, between 200 and 2550 nm. It was considered sufficient to measure the reflectance in this wavelength interval as it covers more than 98.5% of the total terrestrial solar power [25].

The diffuse reflectance was measured by letting the specularly reflected beam escape through a 3.4×3.4 cm^2 square port in the integrating sphere, while the total reflectance was measured with the port closed. The diameter of the integrating sphere was 15 cm. The large dimensions of the exit port in combination with the relatively

small sphere radius results in an angular interval of $\pm 6.5^\circ$ within which the scattered radiation that exits the sphere in the corners of the port is defined as "specular". Hence, a significant part of the low-angle scattered radiation may not be included in the radiation that is measured as diffuse. On the other hand, the image of the light source on the sample is oblong, which results in an oval specularly reflected beam, of which the top and bottom parts almost hit the sphere wall instead of escaping through the exit aperture Thus, light that is reflected with an angle of only a fraction of a degree (which we would like to be measured as specularly reflected) may miss the exit aperture and be mistaken for diffuse reflectance. The square shape of the exit aperture in combination with the oblong image of the light source on the sample, thus results in an averaging over the angular interval $-6.5 < \theta < 6.5^\circ$, in which part of the reflected radiation will be measured as diffuse and part will be measured as specular. Hence, the geometry of the instrument makes the measured absolute values of the specular and diffuse reflectance uncertain within a few percent. However, it is possible to make a comparison between the values before and after ageing, provided that the scattering is isotropic. If the scattering is anisotropic, the uncertainty in the measured diffuse reflectance increases [26], and it may be necessary to measure the same sample several times, rotated around its surface normal, and to calculate the mean value of the measured diffuse reflectance values. In this work, the image of the light source on the exit port was inspected before the diffuse reflectance was measured and the sample was rotated around its surface normal as to let a virtual mean value of the "specular" image of the light source escape through the port.

Keeping the complication discussed above in mind, the specular reflectance $R_{\mathrm{spec}}(\lambda)$ was calculated as the difference between the measured $R_{\mathrm{tot}}(\lambda)$ and $R_{\mathrm{diff}}(\lambda)$. The integrated total solar reflectance, $R_{\mathrm{tot}}^{\mathrm{solar}}$, was calculated from measurement data using

$$R_{\mathrm{tot}}^{\mathrm{solar}} = \frac{\int_{305\ \mathrm{nm}}^{2537\ \mathrm{nm}} R_{\mathrm{tot}}(\lambda) G_{\mathrm{tot}}(\lambda)\, \mathrm{d}\lambda}{\int_{305\ \mathrm{nm}}^{2537\ \mathrm{nm}} G_{\mathrm{tot}}(\lambda)\, \mathrm{d}\lambda}. \quad (1)$$

In Eq. (1), $G_{\mathrm{tot}}(\lambda)$ denotes the wavelength dependent global solar radiation on a horizontal surface. The international reference solar spectrum for air mass 1.5 [25,27] was used in the calculations. Wherever the wavelength intervals of the measured reflectance spectra did not match the available irradiance data, the measured spectra were interpolated. The diffuse and specular solar weighted reflectance values, $R_{\mathrm{spec}}^{\mathrm{solar}}$ and $R_{\mathrm{diff}}^{\mathrm{solar}}$, were calculated correspondingly.

3.3. Accelerated ageing in a climatic test chamber

A $20 \times 30\ \mathrm{cm}^2$ sample of the laminated Al-on-steel reflector was aged for totally 2000 h in a VCL 4033/MH climatic test chamber from Heraeus-Vötsch. The sample did not have any edge tape or other edge sealing. A five-hour test cycle, see Fig. 4, was repeated 400 times. During half of each cycle a 2 kW metal–halogen lamp was lit that radiated in the wavelength range 280–3000 nm. The spectral distribution of the radiation from the metal-halogen has not been characterised and there is a possibility

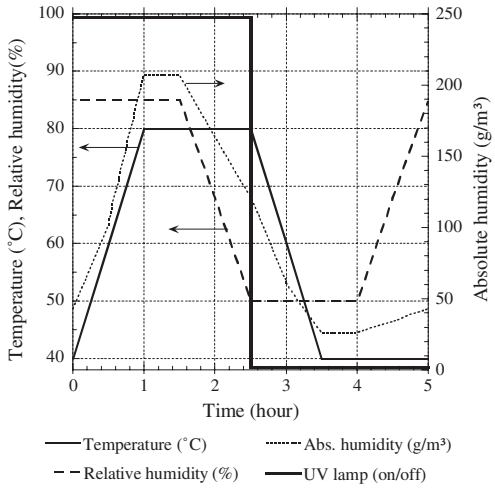

Fig. 4. Test cycle for accelerated ageing, which was repeated 400 times.

that there is disproportionally high ultraviolet irradiance in the test chamber compared to in real sunlight. If this is the case, it may cause unrealistic degradation due to irradiance at wavelengths below the terrestrial cut-off at about 300 nm [28]. The lamp was located in the middle of the ceiling of the chamber, 60 cm from the grid where the sample was placed, and the resulting irradiance on the sample was approximately 1000 W/m^2. In addition to radiation, the programmed test cycle included two different levels of high temperature and two levels of humidity. The relative humidity was set to vary between 50% and 85% and the temperature was set to vary between 40°C and 80°C, resulting in an absolute humidity varying between 25 and 210 g/m^3. The temperatures in the test were significantly lower than the temperatures that are used for temperature testing of solar thermal absorbers [29], since the operating temperatures of a reflector are lower than those of a thermal absorber and the aim was not to impose conditions that are essentially different from real operating conditions on the reflector material, but only to accelerate the degradation process. No air pollutants were injected in the climatic test chamber during the accelerated testing.

3.4. Outdoor exposure

In addition to accelerated ageing, the reflector material was exposed outdoors in Älvkarleby (60.5°N, 17.4°E), Sweden. A booster reflector of trapezoidal corrugated Al-on-steel was mounted facing north, at an inclination of 25° from the horizontal (see Fig. 2), on the 30th of September 2002. After 12.5 months (380 days), a 10 ×

10 cm^2 sample was cut out from the reflector and its optical properties were measured again.

3.5. Light scattering measurements

Spectrophotometers only assess the *total* hemispherical, the *total* specular ($-6.5 < \theta < 6.5°$, as discussed above), or the *total* diffuse reflectance, and thus give no information about changes in surface isotropy induced by ageing. In order to investigate the spatial distribution of the light scattering from the Al-on-steel reflector material before and after ageing, an in-house angle-resolved scatterometer was used [30]. The scatterometer utilized light from a HeNe laser ($\lambda = 632.8$ nm), which was incident on the sample while a silicon detector was moved in the hemisphere above the sample at a distance of 40 cm. The angular resolution of the instrument was one degree in the azimuth, χ, and zenith, ψ, directions, see Fig. 5.

4. Analysis of optical properties and degradation

4.1. Visual appearance of the reflector material before ageing

The visual appearance of the surface of the Al-on-steel reflector is almost specular, but with small dints across the surface, see Fig. 6. It is believed that they texture originates from the glue that is used in the lamination. The surface is rather easily scratched, but the scratches do not penetrate through the protective PET layer. Fig. 7 shows a photograph of the surface of the Al-on-steel reflector, taken with an optical microscope equipped with a CCD color camera, which was connected to a computer for image analysis. The sample area shown in the photograph is 320×240 μm^2. Several small defects are visible in the evaporated aluminium foil. The defects on this fresh sample of the Al-on-steel reflector may be starting points for corrosion.

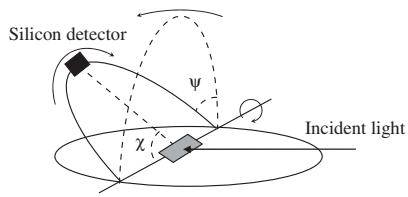

Fig. 5. Schematic picture of the experimental setup for measurement of light scattering from reflector surfaces. The detector sweeps the χ and ψ angles with a resolution of 1°. The incident HeNe laser beam is parallel to the table.

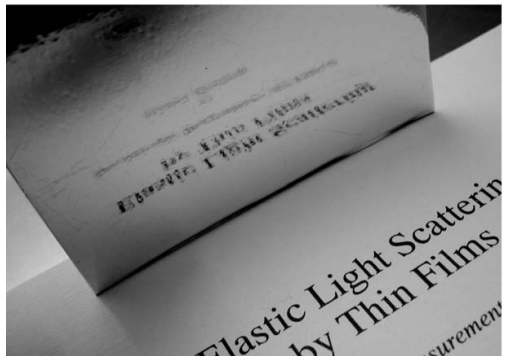

Fig. 6. Visual appearance of the Al-on-steel reflector: a photograph of a thesis on light scattering, reflected in the solar reflector laminate.

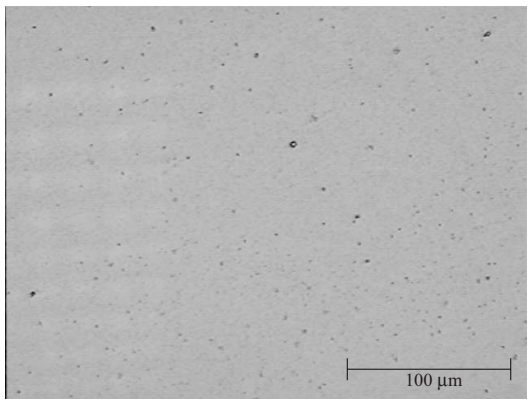

Fig. 7. Photograph of a 320 × 240 μm^2 area of the surface of the Al-on-steel reflector, taken with a optical microscope.

4.2. Reflectance of the reflector material before and after ageing

Fig. 8 shows the wavelength dependent specular and total reflectance of the Al-on-steel reflector material, measured at near normal angle of incidence. The ISO AM 1.5 solar spectrum [27] and the measured total reflectance of standard anodised aluminium are included in the figure for comparison. The integrated total, specular, and diffuse solar reflectance values of the Al-on-steel sample were 82%, 77%, and 5%, respectively. For the standard anodised aluminium, the corresponding values

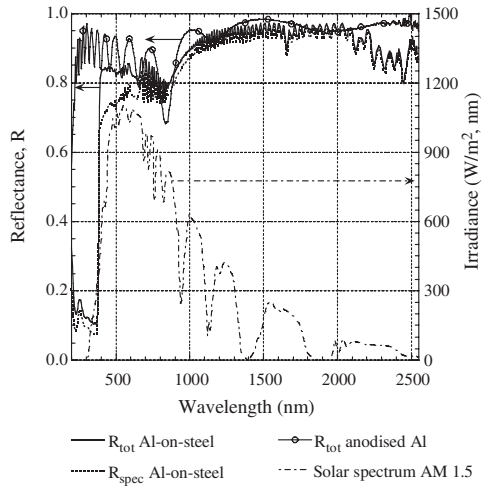

Fig. 8. Wavelength dependent total and specular reflectance of the Al-on-steel reflector material, measured at near normal angle of incidence. The total reflectance of bare anodised aluminium and the solar spectrum are included in the graph.

are 88%, 87%, and 1%. The difference in the total reflectance values of the laminate and the anodised aluminium can be explained by absorption in the PET layer, mainly in the ultraviolet, where there is a sharp cut-off in the reflectance spectrum at 400 nm. This cut-off causes a loss of 3% of the energy available in the solar spectrum.

The reflectance of aluminized plastic films depends on the thickness of the deposited aluminium layer and on the vacuum level during deposition [31]. The evaporation process that was used for deposition of the 20 nm aluminium film on PET has not been investigated further in this work. However, the defects that are visible on the fresh sample of the Al-on-steel reflector (Fig. 7) may stem from insufficient vacuum during deposition or be an indication that the deposited aluminium layer is too thin.

The measured total and diffuse reflectance spectra of the Al-on-steel reflector after 12.5 months of outdoor exposure are shown in Fig. 9. The calculated total solar reflectance was 82% and the specular solar reflectance was 76%. For comparison, the total and specular reflectance spectra of fresh and outdoor aged (9 months) anodised aluminium were measured. While the initial total and specular solar reflectance values for anodised aluminium were 88% and 87%, respectively, the values after 9 months of outdoor exposure were 83% and 79%. Thus the degradation of anodised aluminium is faster than the degradation of the new laminate under outdoor conditions.

Fig. 10 shows the measured total and specular hemispherical reflectance of the Al-on-steel reflector after 1000 and 2000 h of accelerated ageing. The initial total

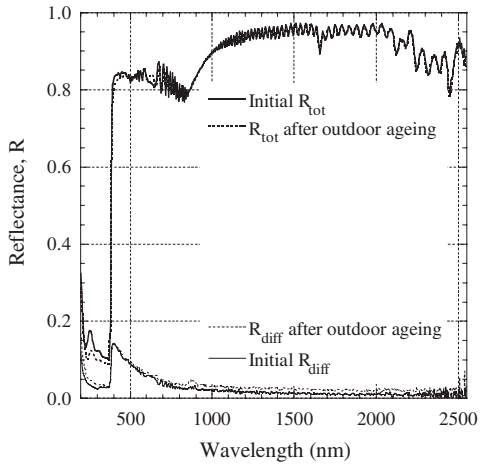

Fig. 9. Measured total and diffuse reflectance of the Al-on-steel reflector, initially and after 12.5 months of outdoor exposure.

hemispherical reflectance are shown for comparison. Note that, while the reduction in the total reflectance is small, the loss of specularity is significant. After 2000 h of accelerated ageing, the total solar reflectance was 75% and the specular solar reflectance was as low as 42%. The low specular reflectance after accelerated ageing is discussed in Section 4.5.

The results of the reflectance measurements on fresh and aged reflector samples are summarised in Table 1. Note the good durability of the reflector under real outdoor conditions, compared to the poor performance in the accelerated ageing test cycle. Worth noting is that no delamination of the reflector material was seen, neither after accelerated ageing nor after outdoor exposure.

4.3. Light scattering

Measurements of light scattering were performed on a fresh sample of Al-on-steel and on an Al-on-steel sample that had been exposed to damp heat for 2000 h in the climate chamber. The scatter distribution from standard anodised aluminium was also measured for comparison. The results for detector sweeps in the χ direction, while keeping $\psi = 0^\circ$, and in the χ direction, keeping $\chi = 0^\circ$, are shown in Figs. 11 and 12. It is evident from Fig. 11 that the distribution of the light scattering from the Al-on-steel reflector in the χ direction changes during the climatic test.

The appearing anisotropy was also seen when the scattering of a laser beam from the aged and the fresh reflector was studied. For the fresh sample, the scatter pattern consisted of a narrow ($\sim 5^\circ$) cone and an isotropic, very faint, background scatter. For the aged sample, the cone was wider ($\sim 8^\circ$), the diffuse background somewhat

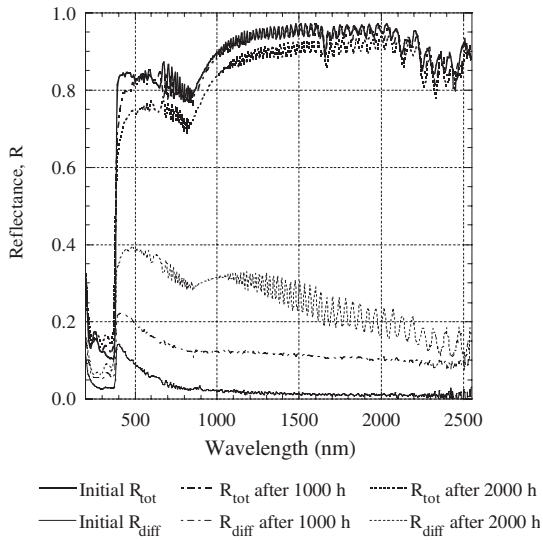

Fig. 10. Total and diffuse reflectance of the Al-on-steel reflector, initially and after 1000 and 2000 h of accelerated ageing.

Table 1
Measured total and specular solar reflectance of the Al-on-steel reflector material, initially, after 1000 and 2000 h of accelerated ageing, as well as after 12.5 months of outdoor exposure

Measured reflectance	R_{tot}^{solar} (%)	R_{spec}^{solar} (%)
Initially	82	77
After 1000 h of accelerated ageing	80	65
After 2000 h of accelerated ageing	75	42
After 12.5 months of outdoor exposure	82	76

stronger, and a band of diffuse scatter that was stronger than the isotropic background appeared in the scatter pattern.

4.4. Surface profiles of fresh and aged samples

Fig. 13 shows the surface profile of the Al-on-steel reflector, before and after accelerated ageing. Note the different scales on the X- and Y-axis. From measurement data, an initial surface roughness of 0.8 μm was calculated. After accelerated ageing, the roughness had increased to 2.1 μm. Several 5000 μm long scans in other directions and across other parts of the samples resulted in approximately the same surface roughness values.

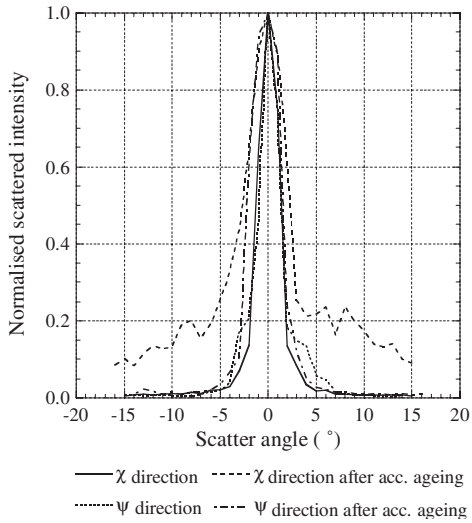

Fig. 11. Scattered intensity measured in the χ and ψ directions from a fresh sample of Al-on-steel and from a sample of Al-on-steel that had been aged for 2000 h in the climatic test chamber. The light source was a HeNe laser beam.

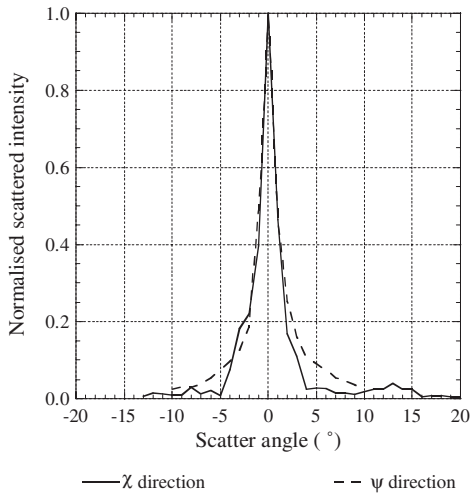

Fig. 12. Scattered intensity in the χ and ψ directions from a fresh sample of standard anodised aluminium. The light source was a HeNe laser beam.

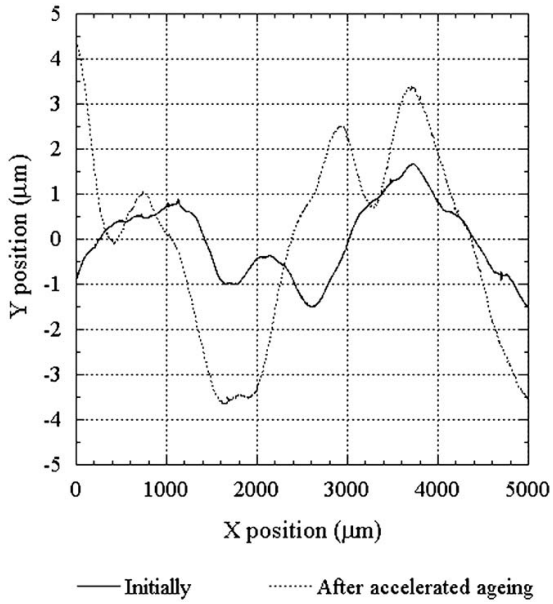

Fig. 13. Profilometer surface scans over 5000 μm of the Al-on-steel reflector material, before and after accelerated ageing. Note the different scales on the X-and Y-axis.

The measured low frequency surface profiles correspond well to the visual appearance of the surface. The initial roughness is believed to be caused by the last lamination step, in which the steel/glue/reflective laminate sandwich is pressed between rolls with a woven fabric. The indents on the surface probably stems from the movement of the glue beneath the reflective laminate in the pressing to places where there is room between the threads in the woven material. The surface roughness of the aged Al-on-steel reflector and the surface roughness was more than twice the roughness before ageing. The increase in surface roughness after accelerated ageing was visible without using the microscope: The dints from the manufacturing process were more visible after ageing. The increase of the surface roughness is believed to be the cause of the broadening of the peak of the forward scattered cone, see Section 4.3. However, it does not account for the anisotropy that was found in the light scattering measurements.

4.5. Analysis of the degradation of the protective coating

In order to find the cause of the increase in the diffusivity and in the anisotropy of the Al-on-steel reflector material after accelerated ageing, we wanted to study the transmittance of the isolated top PET layer of fresh and aged reflectors. This was done by firstly removing the PET/Al/Al/PET laminate from the steel sheet. Then the thin (20 μm) PET layer on the back of the two aluminium layers (the rolled foil and

the evaporated film) was gently scratched to puncture the protection of the back surface of the aluminium. After this, the PET/Al/Al/PET sandwich was submerged in a mixture of three parts 14.4 M nitric acid and one part 12.3 M hydrochloric acid, and the aluminium was etched away. The punctured 20 μm PET foil was removed and the 50 μm foil was rinsed, first in ethanol then in trichloroethylene and then in ethanol again, to remove any glue residues from the back of the foil.

The total and diffuse wavelength dependent transmittance, $T_{tot}(\lambda)$ and $T_{diff}(\lambda)$, of the isolated PET foils from the fresh reflector sample, the sample that had been aged for 2000 h in the climate chamber, and the outdoor exposed sample were measured. The results are shown in Fig. 14.

A comparison of the initial total transmittance of the protective PET layer with the transmittance after outdoor ageing show that the PET withstand outdoor exposure well. Actually, the solar transmittance increases slightly, due to a shift in the absorption edge to lower wavelengths. However, the PET that had been exposed to 2000 h of damp heat and radiation in the climate chamber was whitish and had a significantly higher diffuse component of the transmittance than the other samples, although the total transmittance was not drastically reduced. The "noise" that is seen in Fig. 14, at wavelengths longer than 1000 nm is actually interference in the 25 μm thick top PET layer. The distance between the interference fringes perfectly matches the thickness of the PET layer and the distance does not change during

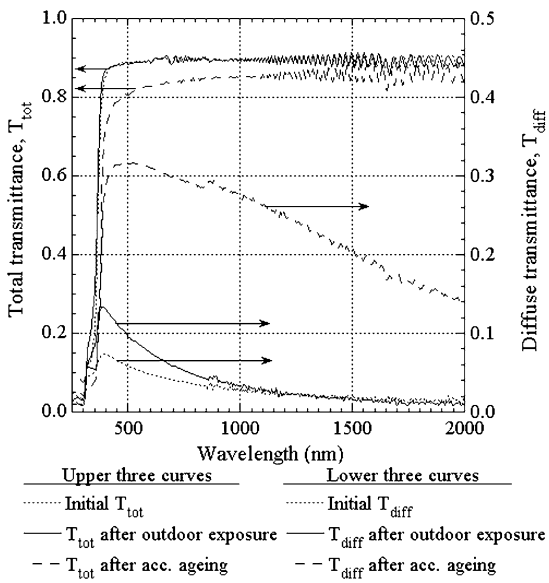

Fig. 14. Measured total and diffuse transmittance of the plastic foil, initially and after 12.5 months of outdoor exposure, as well as after 2000 h of accelerated ageing in the climate chamber.

ageing, which implies that ageing does not have any effect on the thickness or the real part of the refractive index of the PET layer.

The total and diffuse reflectance of the isolated PET foils from the fresh reflector sample, from the sample that had been aged for 2000 h in the climate chamber, and from the outdoor exposed sample were also measured to investigate if the foils were absorbing. In Fig. 15, the results for the fresh sample and the sample that had been aged in the climate chamber are shown. The total and diffuse reflectance of the outdoor aged sample are not included in the graph for clarity, since these two curves largely coincides with the total and diffuse reflectance of the fresh sample. The interference-like, wavelength-dependent variation in the diffuse spectra indicates surface roughness-induced scattering from the polymer interfaces. This effect is pronounced after accelerated ageing, which indicates that changes have taken place in the interface between polymer and aluminium [32].

The wavelength-dependent absorptance, $A(\lambda)$, of the PET foils was calculated using

$$A(\lambda) = 1 - R(\lambda) - T(\lambda). \quad (2)$$

It was found that the integrated solar absorption in the PET layer was 3% for the fresh and outdoor aged sample, while it was 6% for the accelerated aged sample. The decrease in transmittance of the PET layer after accelerated ageing is thus due to an increase in both absorption and reflectance. The measurements of the optical properties of the protective PET foil show that the degradation of the top PET layer fully accounts for the decrease in total reflectance of the Al-on-steel laminate after

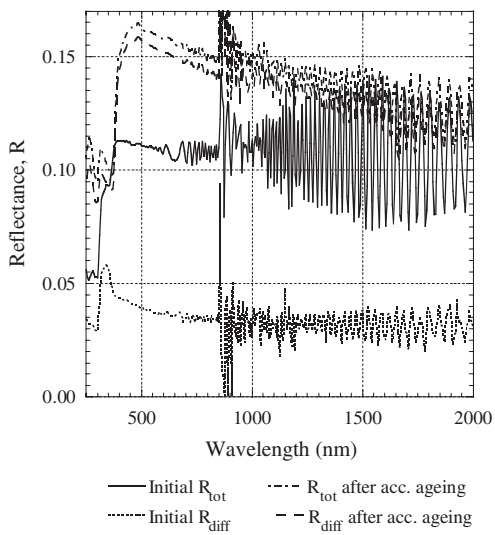

Fig. 15. Measured total and diffuse reflectance of the plastic foil, initially and after 2000 h of accelerated ageing in the climate chamber.

accelerated ageing. The solar weighted transmittance, reflectance, and absorptance of the three examined PET foils are shown in Table 2.

The anisotropic scattering could be understood from analysis of photographs of the aged reflector taken using the optical microscope, see Figs. 16 and 17. Fig. 16 displays the surface of the PET layer. There were clear signs of degradation in the form of cracks in the surface. The pattern was anisotropic, with longer distance between cracks in one of the two orthogonal directions. Hence, the different scattering in the χ and ψ directions. The degradation probably stems from the combination of ultraviolet radiation and cycling at high temperatures. In Fig. 17, the focus of the microscope was on the evaporated aluminium layer beneath the PET layer. The small dark spots (which were interpreted as defects in the aluminium layer) that were visible before ageing (see Fig. 7) had now grown. This shows that the thin evaporated aluminium film degrades fast when the protective coating is damaged. A thicker layer of evaporated aluminium would improve the durability of the specular reflectance, but the longer deposition time associated with a thicker film would result in a more expensive reflector material.

Table 2
Measured transmittance and reflectance of the protective 25 μm protective PET layer, before and after 2000 h of accelerated ageing, as well as after 12.5 months of outdoor exposure

Measured properties of the 25 μm PET foil	T_{tot}^{solar} (%)	T_{spec}^{solar} (%)	R_{tot}^{solar} (%)	A_{tot}^{solar} (%)
Initially	87	83	10	3
After 2000 h of accelerated ageing	80	53	14	6
After 12.5 months of outdoor exposure	87	81	10	3

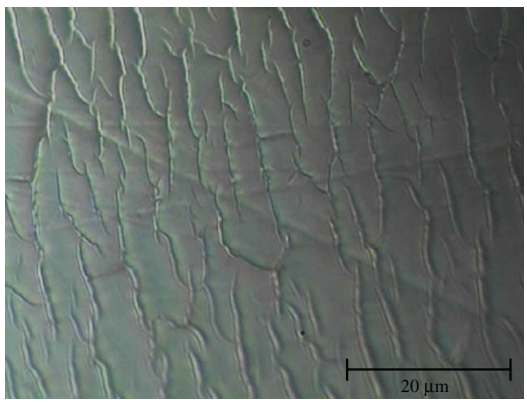

Fig. 16. Photograph of a 64×48 μm^2 area of the protective plastic coating on the Al-on-steel reflector after 2000 h of accelerated ageing, taken with an optical microscope.

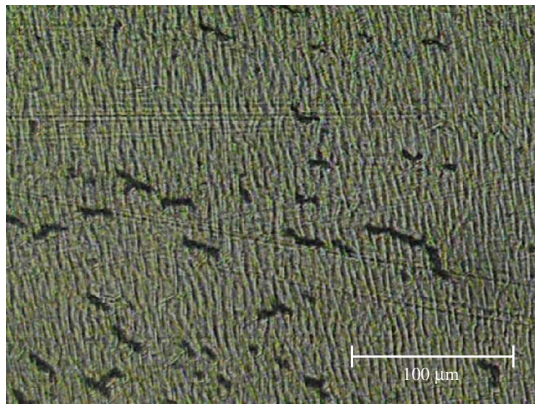

Fig. 17. Photograph of a $320 \times 240\ \mu m^2$ area of the Al-on-steel reflector after 2000 h of accelerated ageing. The photograph was taken with an optical microscope with focus on the evaporated aluminium surface beneath the plastic coating.

5. Performance of the reflector material in concentrating systems

5.1. Optical efficiency of a trapezoidal corrugated booster reflector

The thermal output of the south-facing large area solar collector with a booster reflector of trapezoidal corrugated Al-on-steel, which is installed in Älvkarleby, was measured on a sunny day in June 2003. The measurements were performed both with the reflector functioning and with the reflector covered by a tarpaulin. The result is shown in Fig. 18. The irradiance in the collector plane was also measured, as well as the thermal output of a similar collector with the same inclination (45°) but without reflector. These data are also included in the figure.

Analysis of the thermal energy output from the solar collector with and without functioning reflector shows that the output increases by almost 30% when the tarpaulin is removed from the reflector. At noon, the solar radiation is incident almost parallel to the collector normal and the incidence angle on the reflector is relatively high. Hence, the effective reflector area is relatively small, which results in the relatively low increase in total output at noon. The low increase in thermal output in the late afternoon is due to a low effective concentration ratio of the booster reflector in this configuration, which, in turn is due to the trapezoidal corrugation and to edge effects caused by the small reflector width. If the reflector had been wider, the effective concentration of the test system would have been higher in the afternoon. For some angles of incidence, the corrugation will function as a light trap and radiation will, in unfavourable cases, be reflected several times before reaching the collector plane. If it is not necessary for reasons of mechanical stability, corrugation of booster reflectors is therefore not recommendable.

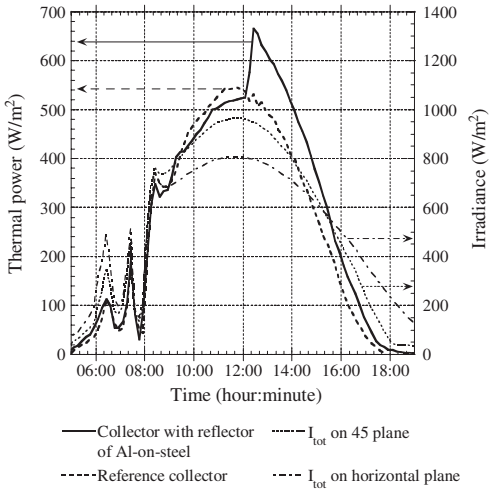

Fig. 18. Measured thermal power from a collector with a trapezoidal corrugated Al-on-steel reflector and a reference system without booster reflector on 26 June 2003. The collectors were mounted side by side in Älvkarleby (60.5°N, 17.4°E), Sweden and facing south with an inclination of 45°. A dark tarpaulin that covered the entire reflector surface was removed at 12:05 pm.

5.2. Power from solar cells with different reflectors

The generated current and electrical power as functions of voltage were measured outdoors for solar cells in two geometrically identical concentrating MaReCo [20–22] systems with different reflector materials. The investigated reflector materials were a standard anodized aluminium sheet and the Al-on-steel reflector. Fig. 19 shows the measured current–voltage characteristics and power as a function of voltage. At an ambient temperature of 15°C and a global irradiance of approximately 1000 W/m^2, the Al-on-steel reflector gives a 8% lower output than the anodised aluminium reflector, which is consistent with the difference in reflectance of the two reflector materials (7%) when considering the system geometry and that some radiation hits the module directly, without being reflected.

6. Discussion

6.1. Differences between outdoor testing and accelerated ageing

It is a common assumption that solar mirrors are less complex than solar cells and solar thermal absorbers [14], and therefore assessments of the durability of components of solar energy systems have mainly focussed on the active components.

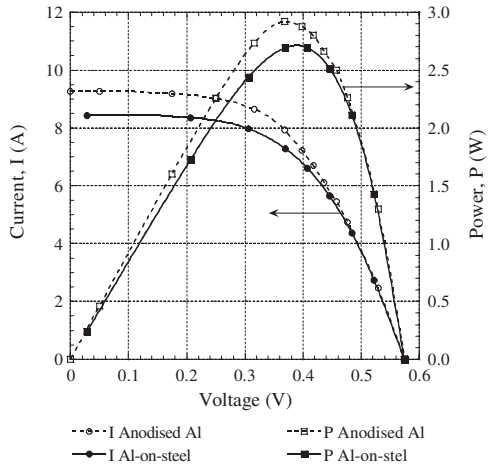

Fig. 19. Measured current-voltage characteristics and calculated power as function of voltage for modules in geometrically identical concentrating systems (MaReCo concentrators) with reflectors of different materials (Al-on-steel and anodised aluminium).

However, as reflector laminates are becoming more frequently used in solar energy applications, their degradation ought to be equally well assessed. Essentially different processes govern the degradation of reflective metallic layers, stiff or flexible substrates, and plastic laminates. Therefore, an understanding of the degradation mechanisms for the different components of a laminate is necessary to be able to predict its lifetime. Likewise, a thorough understanding of the corrosion mechanisms of the Al-on-steel material is necessary in order to interpret our results from accelerated ageing correctly and translate them into technical lifetime under real outdoor conditions. In this work, there was a significant difference between the results from outdoor ageing and accelerated ageing. The Al-on-steel reflector degraded much more when exposed to damp heat for 2000 h than during more than a year of outdoor exposure and the decrease in specular reflectance was disproportionably large after the accelerated tests. The accelerated test has been found to degrade organic laminates disproportionately faster than other types of reflector materials [33]. This indicates that testing at more intense ultraviolet radiation than that of real sunlight, in combination with temperatures as high as 80°C, is too tough for this kind of reflector. Therefore, we will not draw any conclusions from the accelerated ageing test about long-term performance of the Al-on-steel reflector material. During outdoor exposure, however, the laminate protected the reflective aluminium surface from air pollutants, thus prolonging the lifetime of this type of reflector compared to bare metal reflectors, such as anodised aluminium.

At the site of the outdoor ageing tests in Älvkarleby, Sweden, the air pollution levels and the salinity in the air are fairly low, since the site is located 10 km from the nearest industry and 10 km from the Baltic Sea, which has brackish water. Therefore, we do not know whether the material withstands exposure to higher concentrations of pollutants. Environmental tests, with controlled concentrations of air pollutants, in a test chamber would therefore be of interest to investigate if the reflector material withstands outdoor exposure in industrial areas. Alternatively, samples of the reflector could be mounted in areas with different types of heavy industries, which has been done elsewhere [16].

In general, degradation of materials does not depend linearly on variables such as concentration of air pollutants, temperature, time, humidity, or radiation levels. There may be threshold value of these variables, below which essentially no degradation takes place. For laminated reflectors, the degradation of the optical properties often depends more on the specific climatic conditions than on exposure time [33].

6.2. Cost of the Al-on-steel reflector

A self-supporting trapezoidal corrugated aluminium sheet costs about € 16 per m^2. The price of a flat mass produced Al-on-steel reflector is estimated by the manufacturer to €8 per m^2. The additional cost for corrugation, if this is desired, is estimated to € 3.30 per m^2.

Since the large scale cost of the new Al-on-steel laminate is expected to be 50% lower than the cost of an anodised aluminium reflector, and the reflectance of the new material is almost equally high as the reflectance of anodised aluminium, the Al-on-steel laminate would be the most cost-effective alternative.

6.3. Utilisation of the Al-on-steel reflector under a protective glazing

When the Al-on-steel reflector is used in the MaReCo collectors in Hammarby sjöstad, it will be protected by a cover glass. The cover glass is primarily intended to protect the hybrid absorber and to reduce convective and radiative heat losses, but it will also protect the Al-on-steel reflector from the rain, snow, dust and air pollutants, which may increase the durability of the reflector. However, the glass will prevent natural ventilation of the collector, and although the reflector trough is not thermally insulated, the reflector temperature may reach levels close to those in the climatic test chamber. Therefore, precaution should be taken to allow for sufficient ventilation around the reflector troughs.

7. Summary and conclusions

A newly developed laminated aluminium-on-steel reflector with a protective layer of PET was evaluated. The advantage of this material is that it combines the relatively high specular reflectance of aluminium with the stiffness of steel, which

makes it self-supporting and easy to shape into any concentrator geometry. The optical properties and degradation of the reflector were investigated and its system performance was tested in two solar energy applications: as a booster reflector for a solar thermal collector and as a concentrator in a photovoltaic system with MaReCo geometry.

Reflectance measurements on fresh Al-on-steel samples showed that the reflector had good optical properties for solar concentrator applications prior to ageing. It had an initial solar reflectance of 82% out of which 77% was specular. Results from reflectance measurements after more than a year of outdoor exposure indicate that the aluminium-laminated steel reflector has good durability in an outdoor environment, probably because of the plastic coating that protects the evaporated aluminium foil from moisture and air pollutants. However, the total reflectance decreased significantly and the light scattering became anisotropical when the material was exposed to damp heat and ultraviolet radiation in a climatic test chamber. It was found that the PET coating did not withstand the accelerated testing and that cracks in the PET layer caused the scattering. Therefore, the material may not be suitable as an internal reflector or in other applications where it may be exposed to high temperatures. However, the optical properties of the Al-on-steel reflector remained unchanged during one year of outdoor exposure in Sweden. Thus, given that the large-scale production cost of the laminate will be as low as the manufacturer expects, the material shows a potential as a cost-effective reflector in low-concentrating solar thermal and photovoltaic applications.

Acknowledgements

This work was carried out under the auspices of the national Energy Systems Programme, which is financed by the Swedish Foundation for Strategic Research, the Swedish Energy Agency, and Swedish industry. M. Brogren gratefully acknowledges the assistance of Farhad Zamany, Jonas Malmström, and Jacob Jonsson, Uppsala University. A. Roos and B. Karlsson would like to acknowledge the Swedish Energy Agency's solar heating programme for financing.

References

[1] M. Schmela, A bullish PV Year: Market Survey on Worlds Cell Production in 2002, Photon Int. (March, 2003) 42–48.

[2] R.M. Swanson, The Promise of Concentrators, Prog. Photovoltaics: Res. Appl. 8 (Millennium Special Issue) (2000) 93–111.

[3] M. Yamaguchi, A. Luque, High efficiency and high concentration in photovoltaics, IEEE Trans. Electron Dev. 46 (10) (1999) 2139–2144.

[4] L.J.A. Fraas, V. Sundaram, V. Dinh, T. Davenport, J. Yerkes. Over 35% efficient GaAs/GaSb stacked concentrator cell assemblies for terrestrial applications, in: 21st IEEE Photovoltaics Specialists Conference, Orlando, FL, 1990.

[5] G.R. Whitfield, R.W. Bentley, J.D. Burton, Increasing the cost-effectiveness of small solar photovoltaic pumping systems, Renew. Energy 6 (5–6) (1995) 469–475.
[6] B. Hellström, M. Adsten, P. Nostell, B. Karlsson, E. Wäckelgård, The impact of optical and thermal properties on the performance of flat plate solar collectors, Renew. Energy 28 (2003) 331–344.
[7] D.K. McDaniels, D.H. Lowndes, H. Mathew, J. Reynolds, R. Gray, Sol. Energy 17 (1975) 277.
[8] P. Drude, Lehrbuch der Optik, Verlag von S. Hirzel, Leipzig, 1900.
[9] M.E.W. Mwamburi, A. Roos, Preparation of solar selective SnOx: F coated aluminium reflector surfaces, Thin Solid Films 374 (2000) 1–9.
[10] C.G. Granqvist, Solar Energy Materials, Adv. Mater. 15 (21) (2003) 1789–1803.
[11] F.L. Bouquet, R.G. Helms, C.R. Maag, Recent advances in long-lived mirrors for terrestrial and space applications, Sol. Energy Mater. 16 (1987) 423–433.
[12] A.W. Czanderna, Stability of interfaces in solar energy materials, Sol. Energy Mater. 5 (1981) 349–377.
[13] P. Schissel, G. Jorgensen, C. Kennedy, R. Goggin, Silvered-PMMA reflectors, Sol. Energy Mater. Sol. Cells 33 (1994) 183–197.
[14] A. Roos, C.G. Ribbing, B. Karlsson, Stainless steel solar mirrors—A material feasibility study, Sol. Energy Mater. 18 (1989) 233–240.
[15] J.A. Duffie, New materials in solar energy utilization, Sol. Energy 6 (3) (1962) 114–118.
[16] V.L. Morris, Cleaning agents and techniques for concentrating solar collectors, Sol. Energy Mater. 3 (1980) 35–55.
[17] B. Karlsson, B. Perers, U. Henfridsson, Östhammar Hospital—Hot Water Production from a minor Solar Collector Field with Reflectors, in: ISES 1995 in search of the sun, Harare, Zimbabve, 1995.
[18] S. Larsson, The Swedish national solar heating R&D programme, in: ISES 2003, Göteborg, Sweden, 2003.
[19] J. Nilsson, H. Håkansson, Monitoring of electrical and thermal performance of PV–CPC hybrids, in: ISES Solar World Congress, Göteborg, Sweden, 2003.
[20] B. Karlsson, G. Wilson, MaReCo—A Large Assymetric CPC for High Latitudes, in: ISES 1999 Solar World Congress, Jerusalem, 1999.
[21] B. Karlsson, G. Wilson, MaReCo design for horizontal, vertical or tilted installation, in: EuroSun 2000, Copenhagen, Denmark, 2000.
[22] B. Karlsson, S. Larsson, G. Wilson, A. Andersson, MaReCo for large systems, in: Eurosun 2000, Copenhagen, Denmark, 2000.
[23] B. Karlsson, S. Larsson, L. Svensson, B. Hellström, Y. Safir, A Large Bifacial PV—Thermal Low Concentrating Module, in: 17th EUPVSEC, Munich, Germany, 2001.
[24] M. Köhl, IEA-SHC Task 27: Performance, Durability and Sustainability of Advanced Windows and Solar Components for Building Envelopes, in: Task 27 Workshop, Ottawa, Canada, 2002.
[25] ASTM, E 892, Standard Tables for Terrestrial Direct Normal Solar Spectral Irradiance for Air Mass 1.5: Table 1. 1992.
[26] A. Roos, Use of an integrating sphere in solar energy research, Sol. Energy Mater. Sol. Cells 30 (1) (1993) 77–94.
[27] ISO, ISO 9845-1 Solar energy—Reference solar spectral irradiance at the ground at different receiving conditions, Part 1: Direct normal and hemispherical solar irradiance for air mass 1.5, 1992.
[28] T. Fend, G. Jorgensen, H. Kuster, Applicability of highly reflective aluminium coil for solar concentrators, Sol. Energy 68 (4) (2000) 361–370.
[29] M. Koehl, Durability of solar energy materials, Renew. Energy 24 (2001) 597–607.
[30] M. Rönnelid, M. Adsten, T. Lindström, P. Nostell, E. Wäckelgård, Optical scattering from rough-rolled aluminum surfaces, Appl. Opt. 40 (2001) 2148–2158.
[31] R.N. Griffin, Thin film solar reflectors, Sol. Energy Mater. 3 (1980) 277–283.
[32] A. Roos, D. Rönnow, Diffuse Reflectance and Transmittance Spectra of an Interference Layer: 1. Model Formulation and Properties, Appl. Opt. 33 (1994) 7908–7917.
[33] M. Brogren, B. Karlsson, A. Roos, A. Werner, Analysis of the effects of outdoor and accelerated ageing on the optical properties of reflector materials for solar energy applications, Sol. Energy Mater. Sol. Cells (2003), submitted.

Article V

Design, Building Integration and Performance of a Hybrid Solar Wall Element

Andreas Fieber, Division of Energy and Building Design,
Department of Construction and Architecture, Lund University
P.O. Box 118, 221 00 Lund, Sweden andreas.fieber@ebd.lth.se
Phone +46-46-2227347 fax +46-46-2224719
Helena Gajbert, Division of Energy and Building Design, Lund University
Håkan Håkansson, Division of Energy and Building Design, Lund University
Johan Nilsson, Division of Energy and Building Design, Lund University
Tobias Rosencrantz, Division of Energy and Building Design, Lund University
Björn Karlsson, Division of Energy and Building Design, Lund University

The building industry and the solar energy industry calls for innovative and attractive building integrated active solar thermal and PV systems, in order to widen the acceptance and use of solar energy. As an answer to a widened understanding of building integration, a multifunctional wall element has been developed.

A PV/T component on the inside of an antireflective insulation window with concentrating mobile reflector screens makes the system fully integrated into the building, even its interior. The Solar Window provides PV electricity and warm water, besides passive space heating and day lighting. Simultaneously, the reflector screens act as sunshades and added internal insulation for the window. The reflectors have an optical concentration factor of 2.45, which decreases the required, cost-intensive PV cell and heat absorber area. The hybrid technology has synergetic effects such as cooling the PV cells for increased performance, and making use of heat generated in the cell. The climate protected system is a visible element in the exterior and particularly in the interior, and its performance is directly connected to the user behaviour, due to the operation of the reflectors, which can be switched between a closed, concentrating mode or an open, transparent mode.

Performance of a 1 m^2 prototype of the system, regarding its sun shading and U-value properties and its photovoltaic and active thermal output, has been measured. For a two-pane anti-reflective window, the U value is reduced from 2.8 to 1.2 W/ m^2K with the reflectors closed. The annual transmittance through the window is estimated to 609 kWh/ m^2, of which approximately 10% is expected to be delivered by the PV modules. About 20 % will be delivered as active solar heat and 30% as net passive space heating. The distribution is highly dependent on the daily operation of the reflectors, which to some extent could be automated.

1 The design of the Solar Window

As an answer to the search for truly building integrated solar energy systems, an experimental design was proposed, which combines all useable forms of solar energy into one system; active and passive heating, PV electricity and daylight. The concept also aims at visually exposing the system in a novel and attractive way. The key for this challenge was simply to use a window as the glazing for a solar collector. By using hybrid absorbers and pivoted reflectors behind the window, a multifunctional and responding building skin is achieved. The basic concept of building integration is

hence changed from the notion of the solar energy system being part of the building envelope, to the idea of the building envelope being part of the solar energy system.

The system consists of three main components: the window, the hybrid absorber and the reflector, see figure 1. The combination is intended to give synergy effects by ascribing the components multiple functions

The hybrid absorber is fixed in an angle of 20° to the horizontal plane. A 2 mm thick aluminium absorber has PV cells laminated on the upper side. The thickness

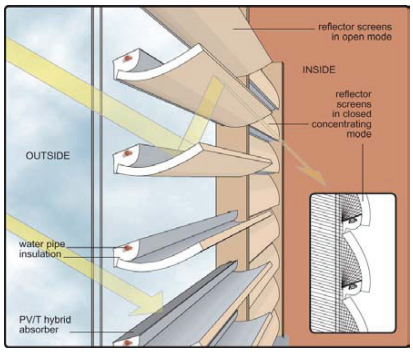

Figure 1: Description of the Solar Window in open and closed mode

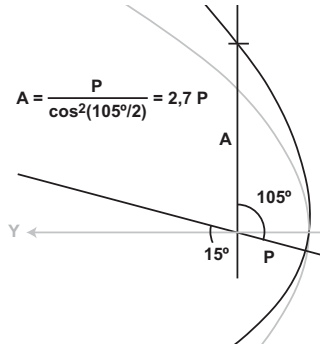

Figure 2: Concentrating geometry

reduces movements due to temperature differences, which otherwise puts the PV cells at risk of cracking. Water pipes are attached to the bottom for distributing active solar gains and for cooling the PV cells and the cavity between the window surface and the reflectors. Building integrated, they also serve as supporting structure for the absorbers and the reflectors, and as the pivot for the reflectors. EPS insulation around the pipes also makes endings for the rotation of the reflectors, and connects the insulation of the reflectors into a continuous convection shield.

The reflector screens are primarily intended for concentrating the solar radiation onto the hybrid absorber. Thus, the need for expensive absorber and PV cell area is reduced, as it is largely replaced by substantially cheaper reflecting material. The resulting distance between the fixed absorbers thus makes it possible to achieve transparency between them when the reflectors are of little use. Hence, daylight may filter through the structure, which also gives passive thermal gains. For passive solar house designs with use of large south facing window areas, risks of overheating and thermal losses are common. The reflectors are intended to reduce these problems, by serving as internal sunshades during daytime and as internal insulation during night time. The reflecting geometry is a two-dimensional parabolic curve, with the optical axis tilted by 15° from the horizontal plane, see figure 2. It has a geometrical concentration factor, i.e. the ratio between the glazed opening and the absorber area, of 2.45. The curve is extruded horizontally as a trough, and the reflector is constructed as a sandwich composition with a 35 mm EPS core between the reflective film on the concave side and a birch veneer on the convex side.

The window serves as the climate shield and as the solar radiation transmitter for the system. After the solar radiation is transmitted through the window, it is distributed as daylight, passive or active heating, or as PV electricity, in proportions

depending on the handling between the closed or open modes. For maximal input for the PV/T absorber through a vertical surface, the transmittance through the window needs to be maximized. Therefore, a highly transparent glass with anti-reflective coating is used. Due to the over-heating precautions by the solar shading and the cooling effect of the absorber, a higher transmittance of the glazing can be tolerated.

2 Building integration

The presence of the hybrid PV/T system inside a window makes it highly visible from the exterior as well as the interior. One of the basic ideas behind the design was to express the building integrated solar energy system architecturally in an attractive, maximally exposed way. Conceptually, the window is the traditional solar collector, hence an interesting starting point for integrating other solar technologies.

Other aesthetical considerations are mainly due to the reflectors. The curved concentrating geometry is decorative and expresses the capturing nature of a solar energy system. The backside facing the interior could be covered with any surface material suitable for the interior context. The modular nature of the reflectors, with no connection to the energy distribution, makes it possible to exchange them for alternative surface, thickness or reflecting geometry. The concave front facing the window will be highly visible from the exterior, and the mirror like surface might be the most critical aesthetical property for a wider acceptance. However, the curved mirror can generate interesting optical expressions in the façade. The extruded picture of the PV/T absorber is visible when the spectator is within the optical acceptance angle range, which means that the impression of the individual modules will differ much in height on a short distance. The overall impression of the façade will hence change when approaching it. The mobility of the reflectors also contributes to a dynamic façade expression.

Figure 3: Illustration of the initial design of the Solar Window building integrated

The system is initially intended for experimental integration into a low energy, single family house, designed simultaneously with the concept for the solar window, see figure 2. This house has an 18 m^2 south facing window structure prepared for the integration of the Solar Window system. The house is constructed with an EPS module system with integrated load-bearing wooden beams, with no thermal bridges. A central brick wall and a ceramic clad concrete floor absorb passive gains. The solar heating system is complemented by a pellet burner, and the PV system is grid-connected while also carrying a local DC circuit for reducing magnetic fields and eliminating losses in battery eliminators, used for DC powered devices.

3 Window properties

The Solar Window is evaluated for its properties as a building component. From this perspective, it can be regarded as a normal window with added features, such as solar shading and internal insulation by the reflector screens. The window consists of

a double-pane insulating glass unit (IGU). The panes are proposed to have anti-reflective coatings in order to increase the active thermal and PV performance for a vertically oriented element. The insulating and sun-shading properties of the reflectors and the anti-reflective coatings are objects for evaluation.

A 1 m^2 prototype of the solar window has been constructed for evaluation of the thermal properties. Five hybrid absorbers with reflectors were mounted in a wooden frame with a double pane IGU attached in the front. The U value of the window together with the closed reflectors has been calculated from measurements in a guarded hot-box, according to ISO 8990 (Johansson 2004, ISO8990 1994). The Solar Window was placed in a square shaped hole between a cold and a hot space of 21.6 m^3 each. The hot space contained a guarded measuring box, covering the hole and the heating device. The U value was calculated according to Eq. (1):

$$U = \frac{Q}{A \cdot \Delta T_n} \qquad \text{[Eq. (1)]}$$

U is the U-value of the construction (W/m^2K), Q is the power input for heating the guarded measuring box, A is the area of the window, and ΔT_n is the environmental temperature difference between the hot and cold space.

Tests were made for the window separately and with the solar window components attached with the reflectors in six different positions, with four intermediate opening angles between the fixed open or closed modes. The window separately represents a U value of 2.80 W/m^2K. The U value of the whole Solar Window differs between 2.42 in the fully open mode, to 1.33 for the fully closed mode, see figure 4.

The effect on the U value with the reflectors opened derives from the reduced convection due to interruption of cold downdraught. Hence, the effect of the open reflectors could be regarded as an added internal surface resistance, which varies by opening angle.

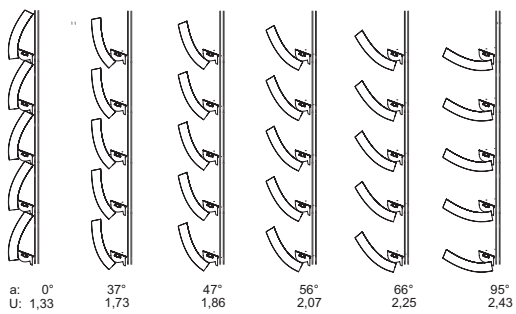

Figure 4: U values for different opening angles, a

The prototype construction was not made sufficiently airtight, why some compensation was made for this by sealing the gaps in its closed position. One measurement was made with the reflectors closed and sealed towards the absorber insulation, and another one also with added sealing between absorber insulation and window, in order to reduce the channel of cold downdraught to one individual module. These two steps made the U value drop from 1.33 to 1.22 and 1.17 W/m^2K respectively. Air tightness is hence an important criterion for further design studies.

The visual shading effect of the reflectors as sunshades in a closed position is total, which means that effective solar shading, visible shading and effective insulation is obtained simultaneously. However, the shading effect of the reflectors in an open position needs to be evaluated. Especially the risk of glare due to the concentration

of daylight from the reflectors needs to be observed and reduced to a minimum. A two-dimensional ray-tracing analysis, made by hand in a CAD program (see figure 5), shows that most of the radiation reflected will be distributed upwards to the next element above and then spread again. For solar angles at 20° and lower, there is a small risk of glare from the concentrated daylight. This problem is likely solved by reducing the rotation angle from 95° (which was set for minimizing the horizontal obstruction of view) to 90°.

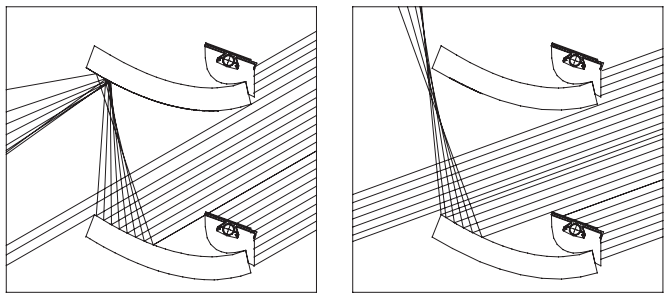

Figure 5: Ray-tracing illustrating the distribution of direct radiation with the reflectors opened at a solar height of 30° (left) and 20° (right).

4 User strategies

The final distribution between the different forms of solar gains, and the thermal losses through the structure, are dependent on how the system is regulated between the two reflector modes. The complexity also increases due to more subjective response from the users due to thermal comfort and wish for daylight and view.

The system was initially designed for integration into a single family house, where most bright hours during weekdays are characterised by the absence of the inhabitants. A rough operating schedule is outlined: during morning hours, with low solar flux and high user activity, the reflectors can be opened to allow for daylight, view and direct passive heat gain. During solar peak hours, with family members being at work or at school, the reflectors can stand closed for maximal active performance. Late afternoons and evenings have similar characteristics like the mornings, thus the reflectors are likely to be opened. For avoiding view inside (i.e. allow for privacy) and thermal losses during dark hours, the reflectors should be mainly closed until the next morning. When integrated into larger areas, zoning of the system allows for combinations of closed and open modules during this cycle.

Another operating strategy could be automating the movement for the reflectors on response to the radiation intensity and the outdoor temperature. It could be programmed for closure at radiation levels too high for thermal or visual comfort, or at levels too low for any practical use, e.g. at night time. In combination with other “intelligent house” technologies, such as sensors indicating occupant absence, obvious opportunities for keeping the reflectors totally closed can be maximally used. For calculations on passive gains in Stockholm, Sweden (lat 59.31), the reflectors were considered closed at transmitted irradiance levels below 50 W/m^2 and above 300 W/m^2, and opened at intermediate levels, from March to October. Concerns have been taken to the solar shading effect of the reflectors by using the computer tool

Parasol. For November to February, the system was operated as a window with no thermal and power production and the reflectors were considered closed or opened, depending on the most beneficial thermal energy balance, for every hour. The energy balance was calculated for every hour of the year, according to Eq. (2):

$$W = I - U \cdot \Delta T \qquad \text{[Eq (2)]}$$

W is the net energy gain through the window, I is the transmitted irradiation, U is the heat transfer coefficient of the and ΔT is the temperature difference between indoors and outdoors.

The calculations indicate an annual positive net energy balance of 10 kWh/m^2 for the winter season. For the warmer season, there is a loss of 14 kWh/m^2 for the dark period with irradiance levels below 50 W/m^2, and a passive gain of 214 kWh/m^2 for the opened mode, at levels between 50 W/m^2 and 300 W/m^2. At levels above 300 W/m^2, 245 kWh/m^2 are available for the PV/T absorber.

5 Photovoltaic properties

For monitoring the photovoltaic performance of the system, a separate prototype with a hybrid absorber with polycrystalline silicon cells and a reflector was constructed.

The optical efficiency *η(α)* is defined as the ratio between the performance of the concentrating module and a vertical module of the same area as the concentrating aperture. It was determined through outdoor measurements. The short circuit current I_{sc} of the concentrator module was monitored as a function of the angle of incidence β in the meridian plane. The optical efficiency (figure 6), was then derived according to

$$\eta(\alpha) = \frac{I_{sc} \cdot 1000}{I_{1000} \cdot C_g \cdot G \cdot \cos(\beta)} \qquad \text{[Eq. (3)]}$$

where I_{1000} is the short circuit current of the bare module at an irradiance of 1000 W/m^2 at normal incidence, C_g is the geometrical concentration of the concentrator system, β is the angle of incidence of beam irradiance, and G is the global intensity perpendicular to the sun.

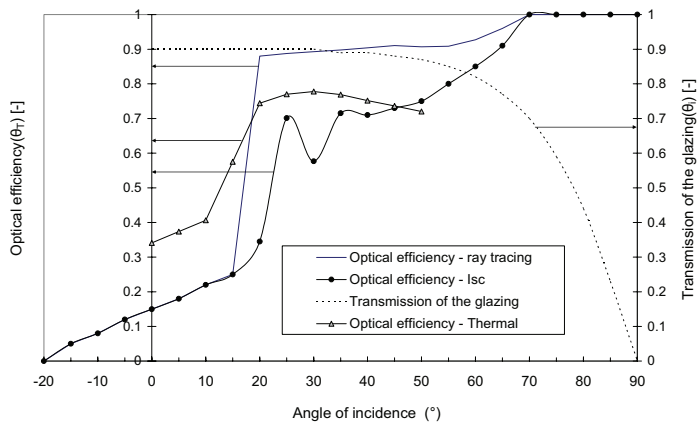

Figure 6: Optical efficiency $R_T(\theta_T)$ of the Solar Window and the transmittance of the glazing $f(\theta_i)$.

The measurements were performed during high irradiance and with a diffuse fraction of around 10%. The concentrator accepts all irradiance for solar altitudes exceeding 15° in the meridian plane, which means that the diffuse optical performance of the concentrator will be similar to that of a module tilted 20° with a correction for reflectance losses. This further means that the optical acceptance of diffuse irradiance will be around 70% of the beam efficiency. For this reason, the global intensity can be used in Eq (3) without significantly increasing the error of the model.

The optical efficiencies are functions of the projected angle of incidence in the transversal plane (i.e. the north south vertical plane) and the transmission of the glazing is given as a function of the conventional angle of incidence. Ray tracing represents the theoretical optical efficiency of the system at 85% reflectance. The graph labeled *Optical efficiency - Isc* in figure 6 contains contributions from measurements with corrections from ray tracing. The difference between measured values and ray tracing at $15°<\theta_T<60°$ is due to resistive losses in the cells when the reflector is effective. The cells on the prototype absorber did not cover the whole width of the absorber, which meant that for angles above 40° the reflected beam partly missed the cell. The angulars above 40° are instead generated by ray tracing. The transmission of the glazing has also been included in the graph as it was used in the calculations of the annual output.

A simulation software, MINSUN (Chant and Håkansson 1985), estimated the annual output of electricity using the optical efficiencies at different angles of incidence. The model used to describe the incidence angle dependence of the system in MINSUN is defined by Eq. (4)

$$\eta_{opt} = R_T(\theta_T) f_L(\theta_i) \qquad \text{[Eq. (4)]}$$

R_T describes the behaviour of the reflector as dependent of θ_T and f_L the transmission of the window glass as dependent of θ_i . θ_T is the projected angle of incidence in the transversal plane and θ_i is the conventional angle of incidence relative to the glass normal.

This model has previously been shown to describe the optical performance of an asymmetric compound parabolic reflector system such as this one well (Brogren et al, 2004).

The simulations show a 93% increase in electrical output for the concentrator module relative to the vertical reference module, which means that one square meter of this window annually would deliver 79 kWh of electric energy. The annual performance is 43% higher than that of an identical module tilted 20°.

The active area of the tested measured prototype covers only 87% of the total glazed area, which this has to be taken into consideration when an economical comparison is made with other systems. It is however possible to increase the active area of the window in a future full scale installation.

6 Solar thermal properties

The active thermal absorbers for water carried heat serves three purposes; delivering heat for domestic hot water and possibly also for space heating, reducing the heat load in the interior during summer and cooling the photovoltaic cells in order to increase the electrical efficiency. The full scale window prototype was used in indoor and outdoor measurements for determination of the incidence angle dependency and

the U value of the thermal collectors. Based on these results the annual energy yield has been derived.
To estimate a U value for the prototype of the solar wall operating as a solar collector, measurements of the heat loss from the collector have been performed in a dark surrounding at different temperatures of the inlet water. The values of U_0 and U_1 were estimated to 4.0 W/m^2·K and 0.046 W/m^2·K^2 and the resulting collector U value as a function of ΔT is shown in figure 7.

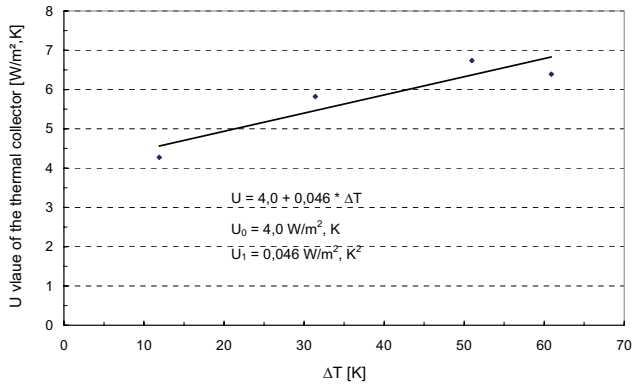

Figure 7. The U value of the thermal collector as a function of ΔT.

At ΔT = 30 K, the U value is 5.4 W/m^2·K per glazed wall area. During the measurements, the prototype was surrounded on both sides with the same temperature. In a building, however, the back side of the window will usually be surrounded with air of room temperature, which will suppress the heat losses. Approximately 10 % of the total heat losses, are estimated as border losses.

The indoor measurements have been performed by using a large solar simulator providing nearly parallel light and adjustable for solar altitude angles (Håkansson H. (2003 a and b). As described in Håkansson (2003 c) and Gajbert et al. (2004), the simulator provides relatively good parallel quality of light, though this has been achieved somewhat at the expense of the light distribution over the area. As different solar altitudes are simulated, there is a tendency of varying irradiation over the test area as the uneven light pattern moves. To continuously measure the variation of the total irradiation on the test area, a number of parallel connected photodiodes were evenly spread out over the front glass of the prototype, giving a current corresponding to the received total irradiation (Gajbert et al, 2004).

By indoor measurements of the thermal efficiency, the incidence angle dependence was derived. The prototype of the solar wall was placed perpendicular to the solar simulator and the simulator was raised in order to simulate every tenth degree of solar altitude angle, i.e. the incidence angle on the glazing projected in the transversal plane, θ_T. The optical efficiency, i.e. the zero-loss efficiency, of the prototype was calculated for different solar altitude angles, giving the incidence angle dependence for transversal angles, $\eta_T(\theta_T)$. The result was normalized by an outdoor measurement where the absolute value of the optical efficiency, at 30° incidence angle was registered.

The measured zero-loss efficiency has been divided by $f(\theta_l)$, the transmission of the glazing, as described in equation [3], resulting in a graph angular dependence of the reflector only, $R(\theta_T)$. These functions, $R(\theta_T)$ and $f(\theta_l)$, shown in figure 6, were used in MINSUN to simulate the annual thermal energy yield. The measured values of optical efficiency at high incidence angles are less reliable, due to the non-uniform light distribution on the small projected area. Therefore, for angles higher than 50°, the same theoretical values as were used for the electricity calculations, shown in figure 6, have been used. The difference between the theoretical graph of optical efficiency, calculated by ray tracing, and the calculated values is due to the reflections on the absorber, the collector efficiency, the multiple reflexes on the reflector at higher incidence angles, and on the unevenness of the reflector. Since the photovoltaic cell situated in front of the thermal absorber has an efficiency of 15%, only 85% of the in MINSUN simulated irradiation falling onto the absorber is taken into count for thermal energy yield.

The result of the simulations shows that the annual thermal energy provided by the Solar Window is 103 kWh/m^2 glazed surface, calculated at an operating temperature of 50°C. For operating temperatures of 40°C and 25°C the yield would be 155 and 250 kWh/a,m^2 respectively. However, as previously discussed, the real heat losses would probably be lower, because of the higher indoor temperature, thus implying higher yields.

7 Discussion and conclusion

A proper model for the regulating strategy of the system is needed to predict the distribution of gains and losses via the Solar Window. The complexity and interrelations between the different functions is a challenge for the modelling, which needs to integrate the spatial surrounding. A detailed model could be of much use for a regulation of an automated system for best performance and comfort.

The level of automation for the system is object for further studies. A range of products with different standard, from fully manual to fully automatic, is a likely development. It is however of importance that the control-function can be overridden manually at all times due to direct response from the user.

Performance of the system has been analysed separately for passive gains, active thermal gains and PV electricity yield. According to the proposed regulating schedule, passive gains are estimated to 210 kWh/m^2 annually. However, it is not examined how much of this is usable. The performance of the fully concentrated PV/T absorber is estimated to 79 kWh/m^2 of electricity, and at least 155 kWh/m^2 of heat for domestic hot water. Following the proposed regulating schedule, these figures might be reduced. For a more accurate and integrated analysis, long-term outside measurements will be made for the full window prototype with PV/T absorbers.

Cost estimations are dependent on where the system border is drawn, since the system also is the building envelope. For comparison with conventional solar energy systems, it might be fair to withdraw the window and sunshade cost if the same is done for the building material the conventional collector replaces. Production cost for the Solar Window excluding the glazing is estimated to approximately €250/m^2, but more thorough calculations need to be made.

Acknowledgements

This work was supported by the Swedish Energy Agency and Formas, the Swedish Research Council for Environment, Agricultural Sciences and Spatial Planning.

References

Adsten M., 2002. *Solar Thermal Collectors at High Latitudes – Design and Performance of Non-Tracking Concentrators*, Acta universitatis Upsaliensis, Uppsala, Sweden.

Brogren M. et al, 2004. *Biaxial model for the incidence angle dependence of the optical efficiency of photovoltaic and solar thermal systems with asymmetric reflectors*. Submitted to Solar Energy Journal.

Chant V.G. and Håkansson R., 1985. *The MINSUN simulation and optimisation program. Application and users guide*. IEA SH&C Task VII, Ottawa.

Fieber A. and Karlsson B. *Design, construction and performance of a multifunctional hybrid solar wall element,* In the proceedings of ISES Solar World Congress 2003, Gothenburg, Sweden

Gajbert H., Håkansson H., Karlsson B., (2004) *Measurement of concentrating solar collectors using a solar simulator with parallel light*, Submitted to Eurosun2004, Freiburg, Germany 20-23 June 2004.

Håkansson H., (2003) *A parallel beam solar simulator for testing of solar components*, In the proceedings of ISES Solar World Congress 2003, Gothenburg, Sweden 14–19 June 2003.

Håkansson H. (2003) *Solar laboratory,* In Solar Protection in Buildings, Wall M., Bülow-Hübe H. (eds), pp. 49-66. Dept. of Construction and Architecture, Lund University.

Håkansson H. (2003) *Solar laboratory*, In Solar Protection in Buildings: Part 2, Wall M., Bülow-Hübe H. (eds), pp. 29-67. Dept. of Construction and Architecture, Lund University.

ISO 8990 (1994) *Thermal insulation – Determination of steady-state thermal transmission properties – Calibrated and guarded hot box*, ISO 8990:1994 (E)

Johansson T. (2004) *Utvärdering av Solfönster, en integration av solhybrid och solskydd*, Dept. of Construction and Architecture, Lund University

www.parasol.se

Article VI

PV PERFORMANCE OF A MULTIFUNCTIONAL PV/T HYBRID SOLAR WINDOW

Andreas Fieber, Johan Nilsson and Björn Karlsson
Div. of Energy and Building Design, Dept. of Construction and Architecture, Lund University
P.O. Box 118, S-221 00, Sweden

ABSTRACT: A multifunctional wall element has been developed, with a PV/T absorber with concentrating reflector screens behind an insulation window. The system provides PV electricity besides hot water and daylight, and the reflector screens provide sunshade for the window. The reflectors have a geometrical concentration factor of 2.45, which decreases the required PV cell area. The hybrid strategy has synergetic effects such as cooling the PV cells for increased performance, and to simultaneously make use of the heat generated in the cell. The climate protected system is a visible element in the exterior and particularly in the interior, and its performance is directly connected to the operation of the reflectors, which can be switched between a closed, concentrating mode or an open, transparent mode.
This paper deals with the monitoring of a prototype of the system, concerning its photovoltaic performance. Out of an estimated annual energy gain via the window of 609 kWh/m^2, approximately 69 kWh is expected to be power from the PV modules.
The results will be used as a guideline for further investigation on the potential of implementing the system, with possible modifications of concentrating geometry or operating strategy, in glazed office façades.
Keywords: Building Integration, Concentrators, Hybrid

1 INTRODUCTION

1.1 Background

Building integrated photovoltaics (BIPV) offer a way to reduce installation cost of PV power by ascribing the PV panels additional functions. However, there is a challenge in meeting energy demands with the supply from the photovoltaic cells. One building application is to integrate PV panels as solar shading devices into the façades of a growing number of glazed office buildings. Hence, the production of PV electricity can simultaneously contribute to reducing the energy demand for cooling the building.

1.2 Concentrating systems in buildings

Using low-concentrating technologies for increasing the cost-efficiency of solar energy systems is a promising strategy, especially if the reflectors can be used for multiple purposes. In this case, the reflectors can be used as flexible solar shading devices. By placing the system behind the exterior glazing of the building, the glazing serves as a climate shell, both for the interior space and for the PV/T system.

2 DESIGN CONCEPT

2.1 Windows in BIPV

By using the window's light transmitting property for integrating solar energy systems, an architectural quality is obtained, since the window has a more penetrable character than i.e. the roof. This has been used mainly in partially transparent PV modules, where the PV cells are mounted between glass panes, with a distance that permits light to enter between the cells. Our alternative design suggests a way to put the cells together with reflectors behind the window glass, in order to protect it from the outer climate.

2.2 Concentrating reflectors

By using a low-concentrating technology, the cell area can be reduced and more efficiently used, leading to lower investment costs. The reflectors can be designed as pivoted sunshades. This also makes it possible to separate the PV modules with intermediate reflector area, thus allowing daylight to enter the interior when the reflectors are not used. Hence, the integration into glazed facades is a promising option for a low-concentrating system.

2.3 Hybrid system

Concentrating irradiation onto the PV cell generates high local temperatures, which demands cooling. Therefore, a PV/T absorber is designed in order to cool the cell for better performance, and simultaneously produce hot water for hygienic demands. This active thermal part of the system also contributes to cooling the interior space behind the window.

2.4 Design of the Solar Window

An initial design from this concept has been developed for application in residential housing, where heating demand is the most important design factor for a temperate climate, from an energy perspective [1]. For this application, the reflectors are made in a sandwich construction with a core of polystyrene and serve as added internal insulation in the closed mode. For the office application, they only serve as reflectors, and therefore they can be made in a thinner and harder material. In consequence with its integration into a glazed façade, it was suggested to make the reflectors out of glass. Anodized aluminum or sheet steel with an aluminized surface are other alternatives. The reflector geometry is a parabolic curve with a geometric concentration factor of 2.45, determined by a tilt of the optical axis of 15°, and a tilt of the fixed PV/T absorber of 20°, see figure 1.

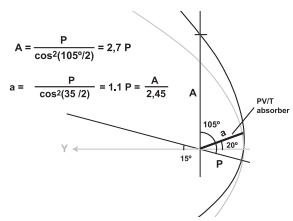

Figure 1: Geometry of the optical design.

The reflectors are pivoted along the upper edge of the absorber, and can hence be switched between a closed, active mode, and an open mode to let the sunlight directly into the building, according to figure 2.

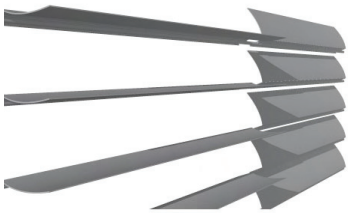

Figure 2: Illustration of the reflectors from the interior with one section in an opened mode (left) and one in a closed mode (right).

3 BUILDING INTEGRATION

3.1 Passive gains and daylight

For the residential house application, a main advantage was the option to gain passive heat from the sun at low irradiance levels. This is not desired in double skin office buildings, where the inner an outer glazing should have different properties. For the outer skin, mainly serving a wind-protection function, a high level of transmittance is required. For the inner layer, a low-E and sun shade coating is suggested to prevent from overheating and glare in the interior. However the transmittance can be relatively high due to the solar-shading effect of the reflectors at high irradiation levels.

Figure 3: Illustration of integration of the Solar Window into the glazed façade of a staircase of an ecological exhibition building in Malmö.

3.2 Aesthetics

The curved shape of the reflector expresses the collecting character of the hybrid solar window, why it deserves an exposure towards the exterior and the interior of the building. The shift between the two modes of operation, in combination with the changing appearance of the mirror-like concave side of the reflectors, offer a wide variety of façade expressions. The convex side of the reflectors facing the interior can be given any suitable surface.

3.3 Operating strategy

The option to operate the Solar Window as a Venetian blind makes it a complex task to predict the output of the active systems. To be able to make predictions, an operating strategy is described, that combines demands on energy performance and user comfort. The strategy must also be applicable for automation. For a residential house, it is suggested that the reflectors are opened during mornings, late afternoons and evenings to allow for daylight, view and passive heating while the house is actively occupied. During the middle of the day, the house is assumed to be mainly empty, why the reflectors can be closed and work optimally. During the nights they can also be closed, to prevent view inside and to insulate from thermal losses through the window. This corresponds fairly well to a suggested automation procedure where the reflectors are closed at irradiance levels below 50 W/m^2 and above 300 W/m^2. At intermediate levels, the reflectors are opened. For the application to an office façade, the control strategy will be determined in order to obtain an optimal combination between PV performance, daylight sufficiency and solar shading to prevent overheating.

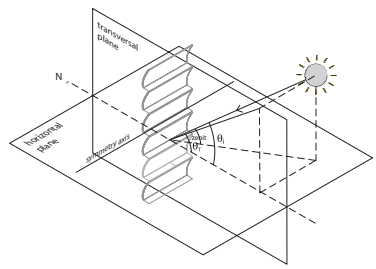

Figure 4: The geometry of the closed Solar Window with the angle of incidence in the transversal plane, θ_T, defined.

4 PHOTOVOLTAIC PROPERTIES

A prototype with an aluminum absorber laminated with polycrystalline silicon photovoltaic cells was built for measurements. The absorber contains water pipes for cooling the PV cells, and the reflector was made of anodized sheet aluminum with a reflectance of 0.87.

The optical efficiency of the reflector in the transversal plane (see figure 4), $R_T(\theta_T)$, is defined as the electricity generation of the system divided by the electricity generation from a system with identical cells mounted on a vertical surface of the same area as

the concentrator system aperture

For a 2-dimensional translational symmetric system such as this, the efficiency is determined solely by the irradiation projected in a plane normal to the symmetry axis, and it is enough to measure the performance at different solar heights when the sun is in this plane, see figure 4. By determining this efficiency at different angles of incidence, we obtain a complete description of the system's characteristics and it makes it possible to perform simulations to evaluate its true performance. The optical efficiency at different angles of incidence θ_T was monitored by measuring the short circuit current, I_{SC}, as a function of θ_T in the transversal plane The optical efficiency was calculated according to Eq. (1):

$$R_T(\theta_T) = \frac{I_{sc} \cdot 1000}{I_{1000} \cdot C_g \cdot G} \qquad \text{[Eq. (1)]}$$

I_{1000} is the short circuit current of the module at 1000W/m^2 at normal incidence, C_g is the geometrical concentration of the concentrator system, and G is the global intensity perpendicular to the glazing.

The geometrical concentration, C_g, was calculated as the aperture area divided by the PV cell area. Figure 5 shows the calculated values for the optical efficiency.

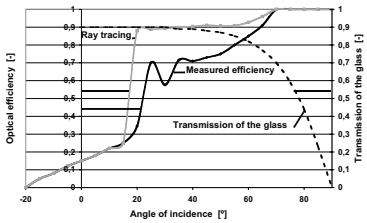

Figure 5: Optical efficiency $\eta(\theta_T)$ at different angles of incidence projected in the plane normal to the axis of symmetry

The measurements were performed during high irradiance and with a diffuse fraction of approximately 10%. The optical system accepts irradiance in all angles above 15º, with the correction for reflection losses. This can be seen from the curve labeled Ray Tracing in Figure 5. At 70º, all of the irradiance hits the cells without reflections, thus yielding an efficiency of 1. It was not possible to measure at incidence angles above 50º due to a construction limitation of the prototype, the efficiencies at these angles were derived from the ray tracing simulations. The large drop in efficiency around an incidence angle of 30º occurs when the strip of concentrated light falls on the conducting finger of the cell. This finger shades the cell considerably when the strip of concentrated light hits it. The measured efficiency evens out around 0.7 while the ray traced efficiency evens out around 0.9. The main reason for this is that the cells have losses due to their relatively large series resistance. The light is concentrated to a narrow strip of high irradiance, and this creates high local currents in the cell. The losses increase with increasing current, and thus results in a lower efficiency.

The optical efficiency was used to estimate the annual output of electricity for this system in Stockholm, Sweden, (lat 59.33). The simulations were performed in MINSUN [2]. Inputs to the simulations were the incidence angle modifier of the system concerning diffuse and beam irradiance. The model used to describe the incidence angle dependence of the optical efficiency as

$$\eta_{opt} = R_T(\theta_T) f_L(\theta_i) \qquad \text{[Eq. (2)]}$$

R_T describes the behaviour of the reflector only and f_L the transmission of the window glass. θ_T is the transversal component of the incident light and θ_i is the angle of incidence relative to the glass normal.

This model has previously been shown to describe the performance of similar systems well [3]. The glass component of the efficiency, $f_L(\theta_i)$, is shown in figure 5.

The calculation of the system efficiency for diffuse irradiance including the glass performance, the view factor of the sky, and the reflectance of the aluminum reflector was estimated to be 70% of the beam efficiency.

The results of the simulation were compared with a reference, which has identical cells of the same area as the prototype cells, and these cells are mounted on a vertical wall. The results show a 93% increase in electrical output compared to the reference. This means that one square meter of window would generate 69 kWh of electricity annually. A reference tilted in 20º from the horizontal would generate considerably more electricity, and comparing to this reference, the prototype produced 43% more electricity annually.

One factor that has to be taken into account if an economical comparison is to be performed is that only 90% of the window area is active. The rest is necessary to allow for the movement of the reflectors and the pipes for the thermal transport.

5 DISCUSSION

5.1 Variations of concentrating geometry

When varying the solar height, one interesting phenomena can be observed. When the sun is close to the acceptance angle of 15º, the strip of concentrated light is narrow and placed at the focal point at the outer end of the absorber. When the solar height is increasing, this strip is quickly moving over the absorber, and gets wider as it travels. This observation shows that the outer part of the absorber receives considerably less irradiation than the inner part. The resistive losses are also highest for current generated on the edges of the cell.

The PV cells are the most expensive part of the system, hence the system price per kWh of electricity produced would drop considerably if the electricity output per PV cell area could be increased. This can be obtained if the cell area can be reduced while accepting most of the irradiance. By using the observations in the previous paragraph, this can be obtained by making two modifications to the existing geometry, i.e. rotating the parabolic reflector and decreasing the size of the absorber. The parabolic reflector in the existing prototype is rotated 15º from the horizontal plane, which gives the system a minimum angle of

acceptance of 15º. By rotating the reflector 5º towards the horizontal, the light would hit the absorber closer to the reflector than what would be the case in the current geometry. At an angle of incidence at 25º the semi focus occurs in the center of the cell, as illustrated in figure 6. This means that the cell can be reduced by a factor of two and still accept all irradiation above 25º, corresponding to the time period between the equinoxes in the south of Sweden. This solution would generate a smaller annual output per glazed area but a higher output per cell area and a lower capital investment per delivered kWh. This geometry also has an advantage that the peaks of the highest intensity on the cell are avoided since the focus fall outside the cell. This however requires a modified technical design, since the reflector curvature will be wider than the cell, according tgo figure 6. Another alternative is to change the optical axis to 25º. This gives a similar concentration factor but also very local intensities on the edge of the cell. These alternatives will be further analyzed by detailed ray tracing.

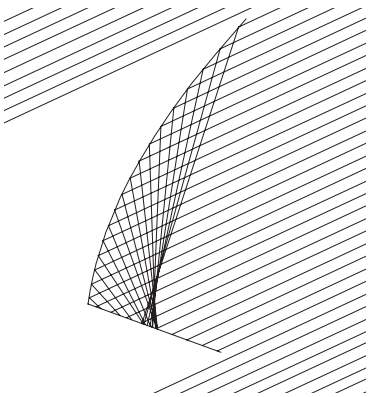

Figure 6: Ray tracing for the reflector with the optical axis at 15° and at a solar altitiude of 25°.

5.2 Operating strategy influence on PV performance

The photovoltaic performance of the Solar Window is dependent upon the chosen operating strategy. The calculated annual performance of 69 kWh applies for the reflectors in a continuously closed mode. The suggested operating strategy however implies that the reflectors should be opened for intensities below 300 W/m^2. Lower irradiation suggests the reflectors being opened. Since the PV/T absorber is in a fixed position, it is exposed to the non-concentrated irradiation even in the opened mode. It can then be regarded as a conventional PV cell mounted in a 20° tilt angle, with a 35 % aperture covering. For estimating the annual output due to the suggested operating strategy, the hours with an irradiation level below 300 W/m^2 towards the south-facing window were identified. The output was then calculated for every hour, as a concentrating system or as a conventional solar panel, depending on the mode. A more accurate annual performance is hence obtained.

In choosing the most suitable control strategy, it is suggested to compare PV performance with the amount of working hours with adequate daylight, and the thermal shading effect by the reflectors, which both should be maximized. Figure 7 below shows the relation between the PV output and the number of daily hours when the reflectors are opened, as functions of the maximum irradiance level for the reflectors being opened. The figure shows that regulating at 300 W/ m^2 annually gives 65 kWh/m^2 of electricity and 3700 hours of daylight, while regulating at 100 W/m^2 gives 75 kWh/m^2 of electricity and 2700 hours of daylight. As mentioned, a continuously closed reflector would deliver 69 kWh/m^2, and no daylight. In finding the optimal breaking point in order to determine a suitable maximal irradiance level, it is suggested to complete the parametric study with the shading effect of the reflectors in various operating. The shading effect when regulating at 300 W/m^2 is according to simulations around 240 kWh/m^2 annually.

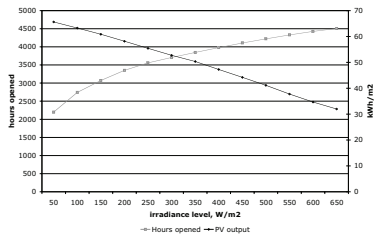

Figure 7: Annual number of hours with an opened reflector and annual output of the PV-module as a function of the irradiance level, where the reflector is closed. The dark hours are amitted.

CONCLUSION

Integrating low-concentrating PV/T systems into glazed façades might be a promising architectural feature, due to its many functions. However, there is a challenge in the complexity in finding an optimal control strategy, and future modifications of the concentrating geometry could be made in order to reduce investment cost.

REFERENCES

[1] Fieber A. et al, 2003, *Design, Construction and Performance of a Multifunctional Solar Wall*, in the proceedings of ISES 2003, Gothenburg

[2] Chant V.G. and Håkansson R., 1985. *The MINSUN simulation and optimisation program. Application and users guide*. IEA SH&C Task VII, Ottawa.

[3] Brogren M. et al. Biaxial model for the incidence angle dependence of the optical efficiency of photovoltaic and solar thermal systems with asymmetric reflectors. Submitted to Solar Energy Journal.

Article VII

A NEW MODEL AND METHOD FOR DETERMINATION OF THE INCIDENCE ANGLE DEPENDENCE OF THE OPTICAL EFFICIENCY OF SOLAR COLLECTORS

Anna Helgesson
Vattenfall Utveckling, 814 26 Älvkarleby, Sweden,
Phone number: +46 26 83 500,Fax Number: +46 26 83 670, E-mail address:
anna.helgesson@vattenfall.com
Johan Nilsson, Björn Karlsson
Division of Energy and Building Design, Department of Construction and Architecture,
Lund University, P.O. Box 118, 221 00 Lund, Sweden,
Phone Number: +46 46 222 76 06, Fax Number: +46 46 222 47 19, E-mail address:
johan.nilsson@ebd.lth.se

Abstract – A new biaxial method for modelling the incidence angle dependence of the optical efficiency of asymmetric collectors is developed. This method is based on measurements in both the longitudinal and the transverse planes of the collector. The model includes a function, $f_L(\Theta)$, that considers the influence of the glazing, and a function, $g_{TL}(\Theta_T)$, that considers the influence of the reflector. The analysis procedure is carried out in a number of steps. First the dependence of the glazing is derived from measurements in the longitudinal direction at times when Θ_T is constant. Then the influence of the reflector is determined from measurements in the transverse direction for constant Θ_L. The suggested method is evaluated by performing outdoor measurements on some different MaReCos. The results show that the suggested model is accurate for evaluation of asymmetric collectors. For a symmetric collector the model develops to a symmetric model. The impact of the angular dependence of the absorber and the impact on F´of uneven irradiance distribution on the absorber need to be further analysed. The paper also includes a discussion of the solar fraction of collector systems. A simple method for estimating the solar fraction is derived from Minsun simulation with the suggested biaxial model.

1. INTRODUCTION

In order to describe the collector output, a model, based on measurements of irradiance and temperatures is used (Perers, 1993):

$$\dot{q} = \left(\eta_{0b} K_{\tau\alpha}(\Theta) I_b + \eta_{0d} I_d - k_l \Delta T - (mC)_e \frac{dT_f}{dt} \right) \quad (1)$$

In this equation, η_0 is the optical efficiency for beam (b) and diffuse (d) radiation, k the heat loss factor, ΔT the temperature difference between the collector and the surroundings, and $(mC)_e$ the effective collector thermal capacitance. Θ is the incidence angle, i.e. the angle between the beam radiation onto the collector surface and the normal vector of the surface.

The optical efficiency for the beam irradiance (η_{0b}) is usually modelled with a standard b_0 expression (Duffie and Beckman, 1991):

$$\eta_{0b}(\Theta) = \eta_{0b} K_{\tau\alpha}(\Theta) = \eta_{0b} \left(1 - b_o \left(\frac{1}{\cos\Theta} - 1 \right) \right) \quad (2)$$

The factor $K_{\tau\alpha}$ is an incidence angle modifier that takes the effects of varying incidence angles (Θ) during the day into account. b_0 is a constant called the incidence angle modifier coefficient. This model works satisfactorily for flat-plate collectors. The model is, however, not valid for asymmetric collectors, like vacuum tubes, trough or CPC-collectors with different incidence angle dependence in different

directions. The asymmetric shape gives rise to differences in incidence angle dependence of the optical properties in longitudinal and transverse directions, figure 1.

In this paper, the development of a new method for modelling the incidence angle dependence of the optical efficiency of asymmetric collectors is described. This model is used in equation 1 as an alternative to the standard b_0 expression. The new method is then also tested on three CPC collectors with east-west reflectors and ray tracing.

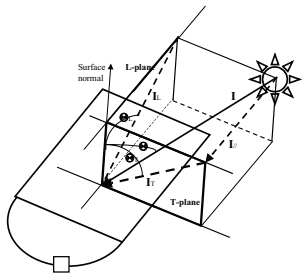

Figure 1 Transverse (T) and longitudinal (L) planes and incidence angles (Θ_T and Θ_L, respectively on a glazed trough collector. Θ is the incidence angle between the solar radiation (I) and the surface normal.

2. DEVELOPMENT OF A BIAXIAL INCIDENCE ANGLE MODIFIER METHOD

2.1 Background to the suggested biaxial incidence angle dependence model

For asymmetric collectors, an overall biaxial incidence angle modifier can be used in order to model the optical efficiency properly. One example of this is a product model, where the incident angle modifier is approximated by factoring it into two components (McIntire, 1982):

$$K(\Theta_L,\Theta_T)=K_L(\Theta_L,0)K_T(0,\Theta_T)=f_L(\Theta_l)f_T(\Theta_T) \quad (3)$$

In the equation above, the index T denotes the transverse and L the longitudinal planes (fig 1). The longitudinal plane is the plane including the surface normal and a line along the collector extension, and the transverse plane is the plane including the surface normal and that is perpendicular to the longitudinal plane. For a south facing collector trough, the transverse plane is then equal to the north-south plane. In equation 3, the angle dependence of the collector is determined from measurements made in two orthogonal planes, figure 2. This model strictly requires that the collector is characterized in the Θ_T = 0 and Θ_L=0 planes. For asymmetric collectors it is, however, not always possible to determine the factor KL(Θ_L,0) since Θ_T = 0 may be outside the acceptance angle interval of the collector. This means that the model described by equation 3 is strictly correct only when radiation is incident in either of the analysis planes. Furthermore, the model is not correct for a flat plate collector.

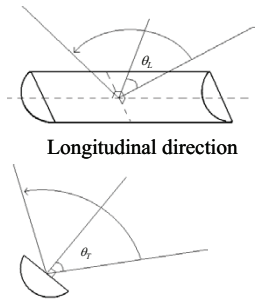

Figure 2 Definition of the longitudinal and the transverse directions for system with cylindrical geometry.

Figure 3 and equation 4 shows the relation between the total incidence angle (Θ_i) and the two projected angles (Θ_T and Θ_L). Note that all shown combinations of the angles are not found for concentrating systems, since the combination of angles is determined by the movement of the sun and by the system geometry. The largest errors when the angular dependence is

approximated by a biaxial product are expected for the angles when $\Theta_T = \Theta_L$.

$$\tan^2\theta_i = \tan^2\theta_T + \tan^2\theta_L \qquad (4)$$

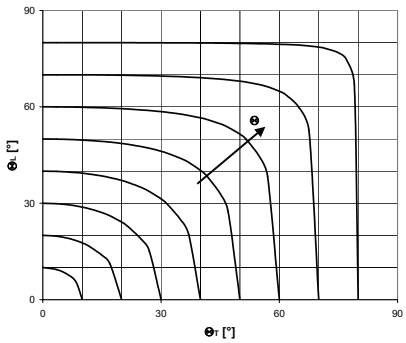

Figure 3: Relation between Θ, Θ_L and Θ_T. The curves represent constant Θ_i (increasing in steps of 10° from 10° to 80°).

In order to better characterise the incidence angle dependence of asymmetric collectors, a new method is suggested in this paper. In this model, the influence of the glazing and of the reflector of the optical efficiency is studied separately:

$$K_{\tau\alpha}(\Theta) = f_L(\Theta) g_{TL}(\Theta_T) \qquad (5)$$

In this equation, the factor $f_L(\Theta)$ gives basically the influence of the glazing and $g_{TL}(\Theta_T)$ gives the influence of the reflector. Equation 5 is, in principle, different from equation 3 since Θ_L is not used. Equation 5 is valid for asymmetric collectors, e.g. the MaReCo and vacuum tubes, as well as for flat-plate collectors having $g_{TL}(\Theta_T) = 1$ resulting in $K_{\tau\alpha}$ being a function only of Θ, just as expected. It can also be used for collectors with normal incidence outside the acceptance angular interval. This equation is also, in principle, similar to a ray tracing of the system.

Figure 4 shows the two projected incidence angles for a south-facing collector during the equinoxes. Then Θ_T has a constant value of (Φ-β), and for all days during the year, Θ_L has a minimum (0°) at noon. The minimum angle of incidence (and maximum direct irradiance) on a south-facing fixed surface at equinox is obtained if the surface is tilted with an angle (β) equal to the latitude (Φ). This means that Θ_T=0.

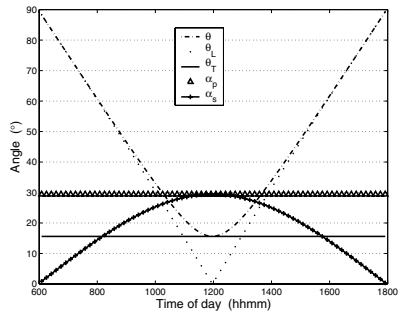

Figure 4 The incidence angle (Q), the transverse (QT) and longitudinal (QL) incidence angles, the solar altitude (as), and the effective solar height (ap) for a south-facing collector tilted 45° on March 22 (when δ≈0°). The figure shows that Θ_T(QT) and α_p (ap) are constant during that day. (The reason that Θ_L is not 0 exactly at noon is that the calculations were made for values from a database containing 10-minute mean values.)

This new model is based on an assumption where the glazing is considered to be isotropic. In the T plane, the incoming radiation is first transmitted through the glass and then reflected onto the absorber. Geometric effects and multiple reflections in the reflector affect the optical efficiency. In the L direction, only the properties of the glass and the absorber are important. This means that the incidence angle dependence in the L direction of an asymmetric collector should be similar to the dependence in the overall direction for a flat plate collector. This is shown in figure 5, where the optical efficiencies in the longitudinal plane for both a flat-plate reference and the Roof-MaReCo,

figure 11, are plotted versus the incidence angle. The incidence angle dependence in the T plane is, for an asymmetric collector, stronger than in the L plane.

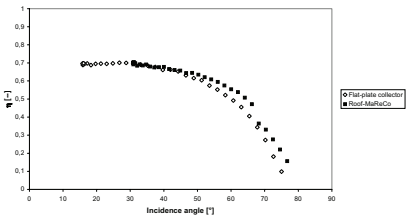

Figure 5 Comparison between the optical efficiency of a conventional flat plate collector and a Roof-MaReCo in the longitudinal plane monitored near equinox.

The discussion above leads to the conclusion that the incidence angle dependence in the L direction can be modelled with eq 2 using $b_0 = b_{0L}$ determined from measurements in the L direction in order to avoid any influence from the $g_{TL}(\Theta_T)$. Since the optical path length in the cover is determined by the real incidence angle (Θ), this angle, and not the longitudinal incidence angle Θ_L should be used in the expression for modelling the influence of the glazing. The factor $f_L(\Theta)$ is found from measurements in the L direction at times when Θ_T is constant, i.e. when the contribution from the reflector is constant. Since Θ_T has a constant value during the equinoxes (figure 6), these measurements are preferably done at either spring or autumn equinox. The effective solar height (α_p) is the angle between the south horizontal axis and the solar vector projected in a north-south plane.

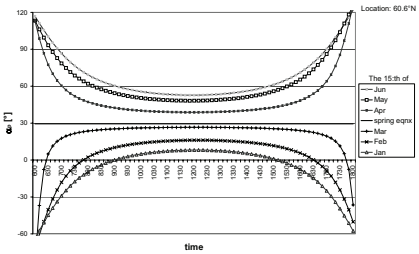

Figure 6 The effective solar height (α_p) for a south-facing surface for different dates during different months.

In order to study the influence of the reflector, measurements are made in the T direction at times when Θ_L=0 constant. Also these measurements can be made during the equinoxes, but with the collector turned 90° with a north-south extension instead of the usual east-west extension as shown in figure 7. If the collector is covered with a glass, the measurements result in a factor $F_T(\Theta_T)$ that includes the influence of both the reflector and the glazing, i.e.:

$$F_T(\Theta) = f_T(\Theta_T) g_{TL}(\Theta_T) \qquad (6)$$

where $f_T(\Theta_T)$ is the influence from the glazing in the T direction, and $g_{TL}(\Theta_T)$ is the wanted influence from the reflector. If the glazing is considered to be isotropic, the incidence angle dependence of the transmittance of the glass is the same in both evaluation planes, i.e. $f_T(\Theta_T) = f_L(\Theta_T)$, and the contribution from the reflector can then be derived as:

$$g_{TL}(\Theta_T) = \frac{F_T(\Theta_T)}{f_L(\Theta_T)} \qquad (7)$$

In practice Θ_L does not need to be constant when $f_L(\Theta)$ is known. The product of the influence from the glazing ($f_L(\Theta)$) and from the reflector ($g_{TL}(\Theta_T)$) then gives the wanted biaxial incidence angle dependence as:

$$K_{\tau\alpha}(\Theta) = f_L(\Theta)\frac{F_T(\Theta_T)}{f_L(\Theta_T)} = f_L(\Theta)g_{TL}(\Theta_T) \quad (8)$$

Equation 8 is valid for asymmetric collectors like the MaReCo, and is fundamentally more correct than equation 3. It is also valid for flat-plate collectors, where $g_{TL}(\Theta_T) = 1$, resulting in $K_{\tau\alpha}(\Theta)$ being a function that is only dependent on Θ, as expected.

Figure 7 A photo of a Spring/Fall-MaReCo turned 90°and tilted to latitude angle in order to study the dependence in the Θ_T direction during equinox.

If the old and the suggested models are compared, the old model can be expressed as:

$$K_{\tau\alpha}(\Theta)^{old} = f_L(\Theta_T)f_L(\Theta_L)g_{TL}(\Theta_T) \quad (9)$$

The old model assumes a biaxial behaviour of the glazing:

$$f_L(\Theta)^{old} = f_L(\Theta_T)f_L(\Theta_L) \quad (10)$$

The new model requires that the angular dependence in the longitudinal plane is independent of Θ_T and determined by Θ. This will further discussed in chapter 4.

Generally $f_L(\Theta_L)$ is normalized in the analysis while the optical efficiency η_{0b} is included in $g_{TL}(\Theta_T)$.

2.2 Ray tracing study of the proposed model

To study the proposed model defined by Eq. 5, a set of optical simulations of the geometry in figure 8 were performed. This geometry is similar to the MaReCo geometries, which are tested in this paper. The model functions were derived from the resulting simulations.

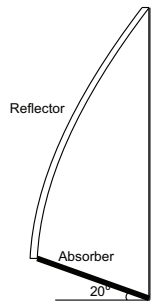

Figure 8 Geometry chosen for ray tracing simulation. The collector is extended into the paper. Optical axis of reflector parabola is directed towards 15°.

The simulations were conducted in the commercial ray tracing program ZEMAX (Zemax) for specular aluminium at a wavelength of λ=0.55 μm characterized by the complex optical constants n=0.96 and k=6.69 and a specular reflectance of 0.92 at normal incidence. $g_{TL}(\Theta_T)$ was obtained by simulating the reflector system without cover glazing at Θ_L =0. Θ_T was varied from 0º to 85º. $f_L(\Theta_L)$ was deducted from simulations of a 3 mm glass sheet where Θ_L was varied from 0º to 85º. To evaluate the model predictions, a system including glass cover was simulated, varying the angles of incidence both in longitudinal and transverse direction between 0º and 85º with all combinations of these angles. The old model described by Eq. 3 was also simulated for comparison. The simulations were performed on a system including the cover glazing, as would be the case in real measurements. $f_T(\Theta_T)$ was obtained by varying Θ_T at Θ_L=0. It was not possible to vary Θ_L at Θ_T=0 since this angle of incidence would be outside the acceptance interval of the reflector

system, Θ_T had to be set inside the interval. It was in the simulations set to 35º when Θ_L was varied.

Figure 9 shows a comparison between the proposed model (Eq. 5), the alternative model (Eq. 3), and ray tracing of the complete system with glass and reflector, but with constant angular dependence of the absorber. The simulations are performed for $\Theta_L = \Theta_T$.

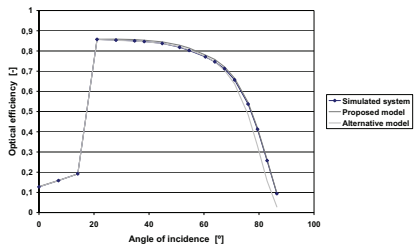

Figure 9 Comparison between models and simulation at angles of incidence where $\Theta_L = \Theta_T$.

As can be seen by the figure, both models give very good agreement at small angles of incidence. At larger angles, above 65º, the difference between the two models becomes visible, and this is due to the misrepresentation of the glazing in Eq. 3. The behaviour of the glazing is determined by the true angle of incidence. It is, however simulated by $f_L(\Theta_L)$ in Eq. 3. The error becomes larger since the function $f_L(\Theta_L)$ could not be derived for Θ_T=0.

3. PERFORMED MEASUREMENTS

3.1 Description of measurements carried out in order to characterize the biaxial optical performance

The new suggested method was analysed by testing it on three trough collectors with east-west symmetry during outdoor measurements. In order to find the different factors used in equation 5, a number of steps were made.

1. In a first step, the collector was tested according to a dynamic testing method (Perers, 1993). From these tests, the collector parameters were derived from an MLR analysis. Of special interest are the heat loss factor and the optical efficiency for diffuse irradiance. These parameters are then used in equation 11 in order to get the optical efficiency for beam irradiance η_{0b} of the collector (Helgesson et al., 2000). An example of this calculation is shown in figure 10, where both the monitored collector efficiency and the optical efficiency for beam radiation are shown for a Spring/Fall-MaReCo. The difference between the two curves is due to the heat losses and impact of diffuse irradiance. The loss free optical efficiency for beam irradiance is derived as:

$$\eta_{0b}(\Theta) = \left[\dot{q}_{um} - \left(\eta_{od} I_d - k_i \Delta T - (mC)_e \frac{dT}{d\tau} \right) \right] \Big/ I_b \quad (11)$$

The factor $f_L(\Theta_L)$ was obtained from measurements in the L direction at times when Θ_T was constant, i.e. preferably around the equinox. This can be seen in figure 6, showing the effective solar height (α_p) for different days during the year. (Θ_T is obtained as 90 – α_p)°. The measurements should be made for low collector temperature and very low fraction of high beam irradiance.

2. In the next step, the factor $F_T(\Theta_T)$ was decided from measurements in the T direction when Θ_L was nearly constant. Also these measurements were made around the equinox, but with the collector turned north-south instead of east-west (fig 7). These measurements should also be made for low collector temperature and very low fraction of high beam irradiance.

3. From the measurements in the T and the L directions, the factor $g_{TL}(\Theta_T)$ was then calculated according to equation 7.

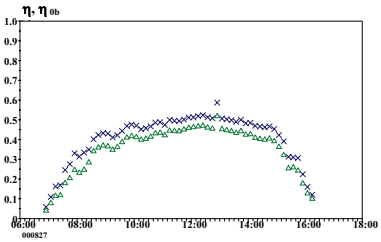

Figure 10 The collector monitored efficiency η and the derived optical (or "no-loss")beam efficiency η_{0b} from measurements on a Spring-Fall MaReCo.

3.2 The studied collectors

In order to improve the output/cost relation, a concentrating technology can be used. The idea is to replace some of the expensive absorber material with cheaper reflector material. This is the basic idea for the development of the MaReCo (Maximum Reflector Collector) (Karlsson and Wilson, 2000). This collector consists, in principle, of a parabolically shaped reflector trough with a single bifacial absorber that runs along the trough (fig 15). The reflector is specially designed for northern latitudes and consists of three parts; two parabolas and an intermediate circular section.

The measurements were made on collector prototypes placed at Vattenfall Utveckling's laboratory in Älvkarleby, Sweden. During the measurements, the flow of water through the collector was recorded together with the inlet and outlet temperatures of the water, the temperature of the ambient air, and the total and the diffuse solar irradiance in the collector plane. A multiple linear regression was then performed on the measured data in order to find the collector parameters in equation 1. In order to find the optical efficiency of the beam radiation, equation 11 was used. The measurements were carried out in both the longitudinal and the transverse directions.

By changing the tilt of the absorber and the optical axis, the performance of the MaReCo can be adapted to various conditions. One example of this is the Spring/Fall-MaReCo (fig 13), which is designed to have a lower optical efficiency during the summer than during the spring and fall. In this way, a larger collector area can be installed in order to increase the contribution from the collector during the heating season, without increasing the risk of overheating during the summer. In figure 11, the schematic of a Roof-MaReCo is shown. In order to fit into the roof, the Roof-MaReCo has a smaller collector depth than the stand-alone version. The Spring/Fall-MaReCo is very similar to the Roof-MaReCo, but with another tilt of the optical axis. For the Spring/Fall-MaReCo, radiation from angles over 45° relative to the horizon is reflected out of the collector. The performance of different kinds of MaReCos is further discussed in (Adsten et al., 2001).

Roof-MaReCo

The Roof-MaReCo is designed to be integrated into a roof. Figure 11 shows a photo and a schematic sketch of one evaluated Roof-MaReCo. This collector has a collector area of 6.3 m², and an optical axis that is normal to the collector glass. Figure 12 shows the projected energy incident on the aperture and the theoretical acceptance function for a standard Roof-MaReCo. It is visible in figure 12 that the collector is designed to keep a large fraction of the annual irradiation inside the acceptance interval, since the irradiation maximum is inside the acceptance interval.

a) 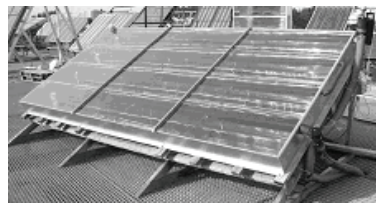

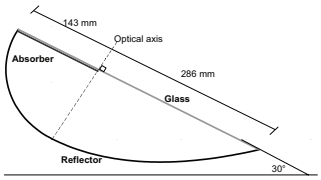

b)

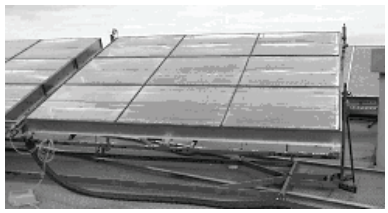

a)

Figure 11 a) Photo and b) schematic sketch of a Roof- MaReCo.

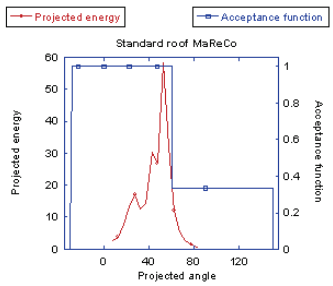

Figure 12 Projected annual energy incident on the aperture and theoretical acceptance function in the tranverse direction for the Roof-MaReCo

Spring/Fall-MaReCo

Figure 13 shows a photo and a schematic sketch of a tested Spring/Fall-MaReCo. Figure 14 shows the projected annual energy incident on the aperture and the theoretical acceptance function for the Spring/Fall-MaReCo. The collector is designed to keep a large fraction of the annual irradiation including the summer irradiation outside the acceptance interval, while the optical efficiency is designed to be high during the spring and the fall.

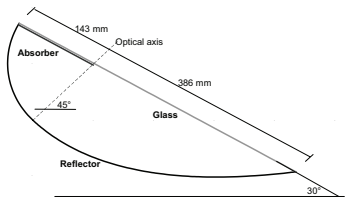

b)

Figure 13 a) Photo and b) schematic sketch of an evaluated prototype of a Spring/Fall-MaReCo. The Spring/Fall-MaReCo is designed for a roof tilt of 30° and the optical axis is tilted 45° from the horizon.

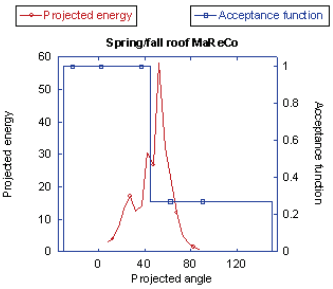

Figure 14 Projected annual energy incident on the aperture and theoretical acceptance function in the tranverse direction for the Spring/Fall-MaReCo.

Stand-Alone-MaReCo

Figure 15 shows a picture of a 500 m² large collector field with stand-alone MaReCos and a schematic sketch of a standard stand-alone

MaReCo. The standard MaReCo is designed with an acceptance angle interval of 20 – 65° relative to the horizon. Figure 16 shows the projected energy incident on the aperture and the theoretical acceptance function for the stand-alone MaReCo. The collector is designed to keep a large fraction of the annual irradiation inside the acceptance interval and to maximize the annual performance.

a)

b)

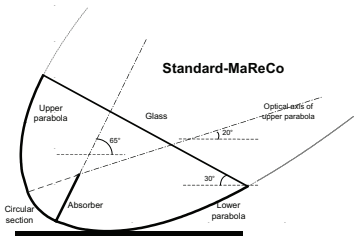

Figure 15 Photo of the field with 500 m² stand-alone MaReCo in front of the bio fuel burner in Torsåker, Sweden and b) a schematic sketch of a standard stand-alone MaReCo.

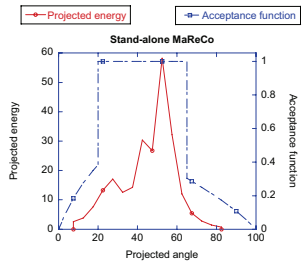

Figure 16 Projected annual energy incident on the aperture and theoretical acceptance function in the transverse direction for the Standalone-MaReCo.

3.3 Results from the measurements

Roof-MaReCo

The results of the measurements on the Roof-MaReCo are presented in figures 17-20. Figure 18 gives a b_0 value of 0.23. The linear correlation in the Θ_L-plane is very good. Figure 19 and figure 20 gives the results in Θ_T-plane. Figure 20 show the $f(\Theta_L)$-dependence from figure 17, the beam efficiency $F_T(\Theta_T)$ derived from figure 19 and the reflector function $g_{TL}(\Theta_T)$ as the ratio between these functions.

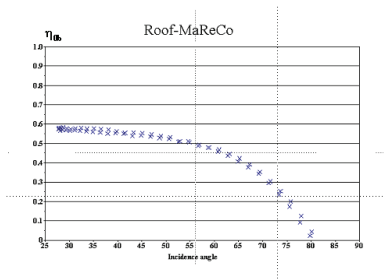

Figure 17 Angular dependence η_{0b} for getting $f_L(\Theta_L)$ in the longitudinal direction for a Roof-MaReCo monitored close to the equinox.

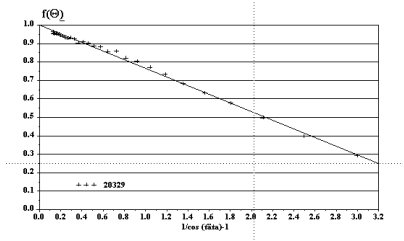

Figure 18 Dependence of the optical efficiency $f(\Theta_L)$ on the b_0 function in the longitudinal direction for a Roof-MaReCo , monitored close to the equinox. b_0 =0.23.

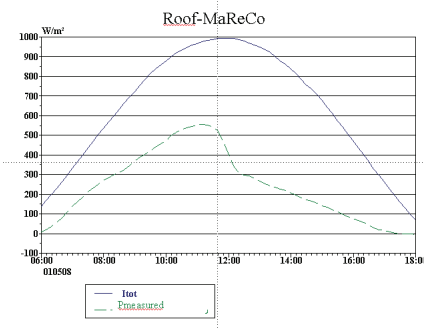

Figure 19 Monitored irradiance and power from a roof-MaReCo turned according to figure 7 and at latitude tilt for monitoring of Θ_T-dependence.

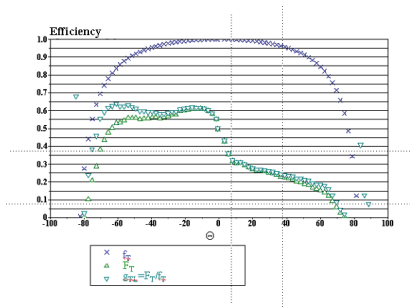

Figure 20 The $f_L(\Theta)$-dependence, the beam efficiency $F_T(\Theta_T)$ and the reflector function $g_{TL}(\Theta_T)$.

Spring/Fall-MaReCo

The results of the measurements on the spring/fall MaReCo are presented in figures 21-24. Figure 22 gives a b_0 value of 0.32. The linear correlation in the Θ_L-plane is good. Figure 23 and figure 24 gives the results in Θ_T-plane. Figure 24 shows the beam efficiency $F_T(\Theta_T)$ derived from figure 23 and the reflector function $g_{TL}(\Theta_T)$ as a ratio between $F_T(\Theta_T)$ and $f_L(\Theta_L)$ from figure 22. Figure 25 shows the variation of the optical efficiency for the Spring/Fall-MaReCo over the operating season.

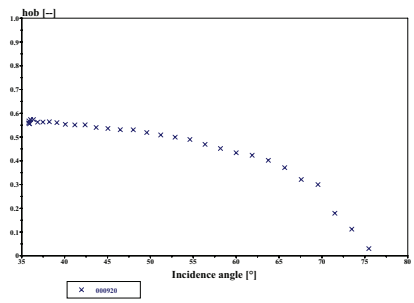

Figure 21 Angular dependence η_{0b} for getting $f_L(\Theta_L)$ in the longitudinal direction for spring-fall MaReCo monitored close to the equinox.

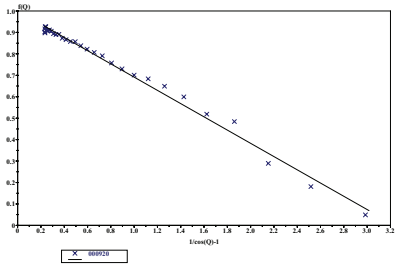

Figure 22 Dependence of the optical efficiency $f(\Theta_L)$ on the b_0 function in the longitudinal direction for a Spring-Fall-MaReCo , monitored close to the equinox. b_0 =0.32.

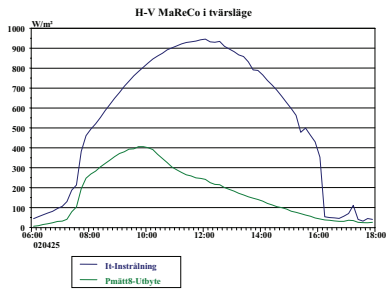

Figure 23 Monitored irradiance and power from a spring-fall-MaReCo turned according to figure 7 and at latitude tilt for monitoring of Θ_T-dependence.

The detailed method for deciding the incidence angle dependence in the transverse direction is further shown in figure 24. The total efficiency η is the efficiency monitored during one day close to the equinox at low operating temperatures. The optical efficiency is the no-loss optical efficiency for beam irradiance $F_T(\Theta_T)$ derived by eliminating the heat losses from the measured output. The optical efficiency for the reflector only $g_{TL}(\Theta_T)$ is derived by dividing the loss-free optical efficiency $F_T(\Theta_T)$ by the influence from the glazing $f_L(\Theta_T)$. This efficiency shows the contribution from the reflector only. The broken line gives the ideal optical efficiency. The optical axis of this collector is tilted 45°, meaning that the ideal reflector only operates for angles below 45°. This corresponds to an angle of incidence in the transverse plane of Θ_T=-15°. Above this angle, the reflector is not active and the absorber only works with radiation direct from the sun.

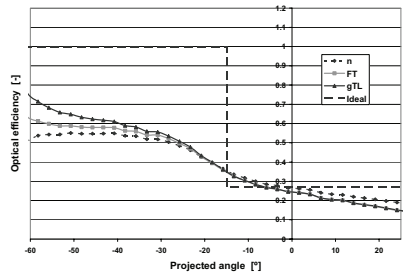

Figure 24 Diagram showing the monitored efficiency η, the beam efficiency $F_T(\Theta_T)$ and the reflector function $g_{TL}(\Theta_T)$ involved in the biaxial incidence angle dependence analysis of an asymmetric collector. (The angulars -60° and 0°corresponds to horizontal and 60° solar altitude.)

If e.g., for a certain occasion, $\Theta_T = \Theta_L = 45°$, then Θ = {eq 4} = 54.7°. Figure 24 gives that $\eta_{0b}*g_{TL}(\Theta_T=45°)$ = 0.62. The b_0=0.32 from figure 22 gives that $f_L(\Theta=54.7°)$ = 0.766. Equation 8 then gives $\eta_{0b}(\Theta=54.7°)$ = 0.766*0.62 = 0.475.

According to equations 8-10, the old model gives:

$\eta_{0b}(\Theta=54.7°)=f_L(\Theta_L=45°)*f_T(\Theta_T=45°)*\eta_{0b}*g_{TL}(\Theta_T=45°)$ = 0.867*0.867*0.62 = 0.466. The difference between the results from the two models is then 2 %.

Long term monitoring of the optical efficiency η0 of the collector during the period April-September is presented in figure 25. The figure shows that the efficiency varies between 0.32 and 0.57 corresponding to that Θ_T in figure 24 varies between -5 and -40° or projected solar altitudes of 20-55° in figure 6. This shows that it

is very convenient to scan over a wide angular interval during one day at equinox, with the collector tilted like in figure 7.

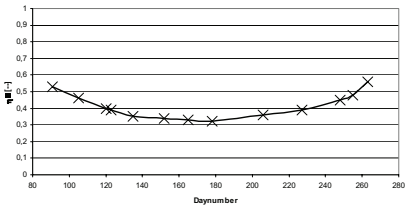

Figure 25 Variation of the optical efficiency η_0 during the evaluation period April – September near noon time for the Spring/Fall-MaReCo. η_0 includes effects of a low fraction of diffuse irradiance.

Stand-Alone-MaReCo

The results of the measurements on the stand-alone MaReCo are presented in figures 26-27. Figure 26 gives a b0 value of 0.27. Figure 27 gives the beam efficiency $F_T(\Theta_T)$ in the Θ_T-plane monitored indoors in a simulator . The figure shows that $F_T(\Theta_T)$ is nearly constant in the acceptance interval. This means that a standard b_0 function can be used in that interval as is used in [1].

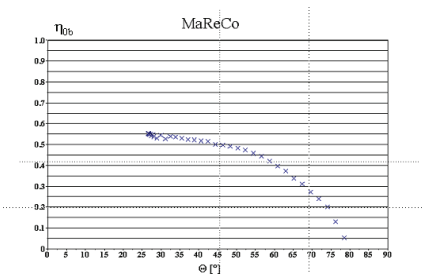

Figure 26 Angular dependence η_{0b} for getting $f_L(\Theta_L)$ in the longitudinal direction for a stand-alone MaReCo monitored close to the equinox.

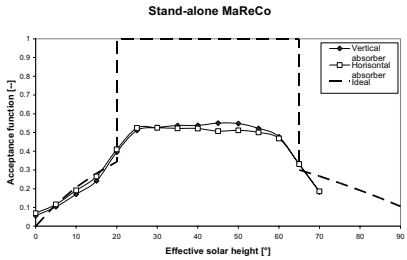

Figure 27 The monitored beam efficiency $F_T(\Theta_T)$ of a stand alone MaReCo monitored in the parallel beam solar simulator and the ideal acceptance angular dependence. The measurements where done with the absorber nearly vertical or horizontal as seen in figure 15. The wings of the ideal curve is an effect of truncation.(The angulars 0°, 60°and 90° corresponds to Θ_T -angulars of -60°, 0°and +30°.)

3.4 Simulations

Ray tracing simulations were performed on the Roof-MaReCo and the Spring/Fall-MaReCo to be able to compare the measured results with the theoretical optical efficiencies. Full size prototypes with cover glazing were modelled. The incidence angle dependence of the reflectance for the aluminium reflectors was modelled by the simulation software, as well as the incidence angle dependence of the absorber and glazing. The error in the simulations was estimated to less than 1%. These simulations should be close to the theoretical efficiency of the optical system and the results can be used to compare with performed measurements. As above the reflectance at normal incidence were supposed to be 0.92. The collector efficiency factor was set to F´=1.

Roof-MaReCo

What can be seen from the simulated efficiency in fig. 28 is that the theoretical efficiency resembles the ideal characteristics. The simulated as well as the monitored efficiency is slowly increasing with a decreased angle of incidence due a decreasing number of multiple

reflections. At 0º, the efficiency drops as the rays incident on the reflector are reflected out of the system, and the efficiency becomes determined by the fraction that impinges directly on the absorber. The ideal efficiency will be constant at a value of 0.33, which is the ratio between the absorber area and the total aperture area (143/(286+143)). The difference between simulated and measured curve is explained by a lower specular reflectance, imperfect geometry and effects of F' at non-uniform irradiance of the absorber. The overall agreement beteween measurements and simulations are acceptable. A reflectance of the reflector of 0.76, should give agreement.

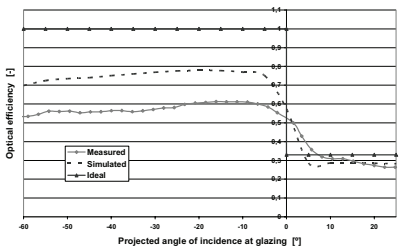

Figure 28 Ideal acceptance function, the measured beam efficiency $F_T(\Theta_T)$ and the same function simulated by ray tracing for a Roof-MaReCo.(The angulars -60°, 0° and 20° corresponds to horizontal, 60° and 80° solar altitude.)

Spring/Fall-MaReCo

The theoretical optical efficiency shown in fig. 29 describes the behaviour of the system at ideal conditions without manufacturing errors or heat losses. The large difference between the simulated and measured curve is as above explained by low reflectance, impact of F´and also of an imperfect geometry. The geometrical impact is larger with a higher concentration factor. It is seen in the interval between -60º and -20º, equivalent to a solar height of 0º to 40º, that the theoretical efficiency is increasing, while the measured reflectance is decreasing. This is to a large extent a F´-effect. It is shown that F´ is strongly dependent of the light distribution on the absorber. When all light impinges on the absorber edge the F´-value is around a factor of 0.80 of the value when the light is concentrated on the absorber tube in the middle of the absorber (Hellström, 2004). This effect occurs when the solar vector is parallel to the optical axis. The slope of the measured curve is also determined by the decreasing number of reflections. Above -15º, or 45º solar height, the rays incident on the parabolic part of the reflector are reflected back out of the trough, and the efficiency drops. At larger angles, the efficiency is determined by the light directly incident on the absorber, and at angles around normal incidence on the glazing, the efficiency is constant. The ideal efficiency will be constant at a value of 0.27 as this is the ratio between the absorber area and the total aperture area (143/(386+143)). The decreasing measured reflectance for positive angles is because of shadow effect from the collector edge. The difference between the ideal and the theoretical efficiency is due to reflection losses at the glazing and reflector, and absorption losses due to the incidence angle dependence of the absorber.

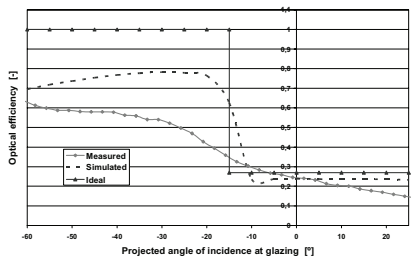

Figure 29 Ideal acceptance function, the measured beam efficiency $F_T(\Theta_T)$ and the same function simulated by ray tracing for a Spring/Fall MaReCo. (The angulars -60°, 0° and 20° corresponds to horizontal, 60° and 80° solar altitude.)

4. A CRITICAL ANALYSIS OF THE BIAXIAL MODEL

The suggested biaxial model in equation 8 implies that the optical efficiency in the longitudinal direction is independent of Θ_T . This is also indicated by measurements close to equinox presented in figure 30. Simulations on the geometry in figure 8 on a collector where the absorptance of the absorber is independent of the incidence angle showed a neglible impact of Θ_T on the dependence in Θ_L direction. The glass-reflector combination fulfilled the requirement for equation 8.

One effect not accounted for by the proposed model is the incidence angle dependence of the absorber. This effect will vary depending on the placement and tilt of the absorber. Fig. 30 shows assumed the absorptance of the absorber as a function of angle of incidence modelled according to literature (Duffie and Beckman, 1991). The figure also shows ray tracing simulations of the system in figure 8 when the longitudinal angle was changed from 0º to 90º at three different values of projected solar height ΘT . The glazing, reflector, and absorber were modelled in this simulation. The result shows a distinct dependence of Θ_T . Changes in Θ_T works as a shift in the angle of incidence towards the absorber. The effects can be explained by two factors. First, at a given angle of incidence at the glazing, the longitudinal angle has different values depending on the projected solar height. For an angle of incidence of 50º, the longitudinal angle would be 35º for the graph of 45º projected solar height, and the longitudinal angle would be 50º for the graph at 20º projected solar height. The longitudinal angle strongly affects the incidence angle upon the absorber in the simulated geometry, and as can be seen from Fig. 31, a difference of 15º in angle of incidence has an influence on the absorption. The second effect in the simulated case is that the angle of incidence of the light striking the absorber directly, without being reflected is increasing with decreasing Θ_T . Both effects contribute to increase the reflection losses from the absorber at low projected solar heights.

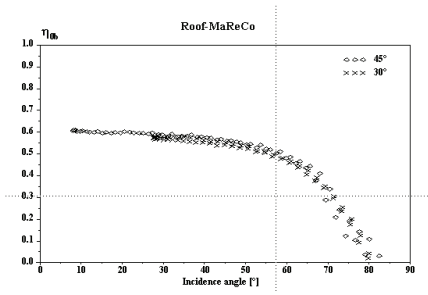

Figure 30 Comparison of angular dependence of beam efficiency η_{0b} in the longitudinal plane f(Θ_L) for the Roof-MaReCo for two days when the collector was tilted 30° and 45° respectively. The Θ_T-angles are 30° and 15° respectively.

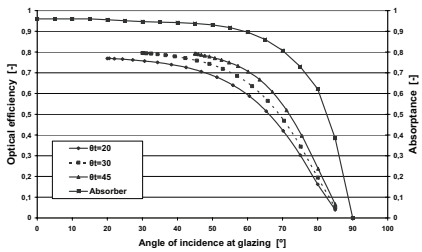

Figure 31 Comparison of angular dependence of beam efficiency η0b derived from ray tracing on the geometry in figure 8 in the longitudinal plane f(Θ_L). The Θ_T-angles are 20°, 30° and 45° respectively. In the figure is also the given angular dependence of the absorber only.

This effect of Θ_T on the angular dependence in Θ_L-direction can however not easily be seen in the collector measurement, figure 30, and should therefore be investigated in detail. Optical imperfections and a rough and non-flat absorber surface will suppress the effects. The effect is also supposed to be smaller in the MaReCo-geometries with the absorber parallel to the glazing.

5. COMPARISON OF THE SOLAR FRACTION OF THREE DIFFERENT COLLECTOR SYSTEMS WITH DIFFERENT TILTS

In order to study the solar fraction of three domestic hot water systems a method described below was used. The studied systems were a flat-plate system, a Roof-MaReCo system and a system with a Spring/Fall-MaReCo. Due to the reflector, the MaReCo and the flat-plate collectors have different performance for different tilt angles. This was investigated by combining Minsun simulations with a very simple system model. The optical efficiency was, for this case, modelled in the same way as described in connection with figures 20, 21 and 24 above, with the biaxial incidence angle dependence given as a table with intervals of 5°.

The first step in the analysis was to determine the area of the three systems to exactly cover the heat load (here hot water) during July. This was done by studying the simulated energy output (E) (at T_{OP} = 50°C) from 1 m² of the collectors and the heat load (L), including storage losses, in kWh during the month. In this case, the hot water load was supposed to be 4 800 kWh/year, equally distributed over the year with a monthly load of 400 kWh. The maximum collector area for avoiding overproduction in July is then estimated as:

$$A_{c,July} = \frac{L_{July}}{E_{July}} \quad [m^2] \qquad (12)$$

The total yearly production of the different collectors is then calculated by multiplying the collector area with the total energy output per m² during a year. The solar fraction (S_F) is then calculated by dividing the total production by the total load during the year:

$$SF = \frac{\text{total production}}{\text{total load}} = \frac{A_{c,July} * E_{yr}}{L_{yr}} = \left[\frac{L_{July}}{L_{yr}}\right]\left[\frac{E_{yr}}{E_{July}}\right] \qquad (13)$$

The first bracket includes a parameter only depending on the load, and the second a parameter only depending on the solar collector. This means that the solar fraction, in a simplified way, can be expressed as a product of a load factor and a collector factor. For a given system, the load factor is constant. In the case studied here, this factor is 1/12, since the hot water load is assumed to be constant during the year. The collector factor varies, however, with the tilt angle.

Figure 32 shows the solar fraction of the three tested systems as a function of the tilt angle. The results show that, for low tilt angles, the Spring/Fall-MaReCo gives the highest solar fraction of the three studied systems. For angles in the interval of 40° and 70°, the Roof-MaReCo gives the highest solar fraction. For near vertical collectors, the flat-plate collector gives the highest solar fraction.

The corresponding areas is visible in figure 33. It is seen that the maximum areas for the MaReCo collectors increases quickly when the optical axis is lower than the irradiance maximum at around 52° in figures 12 and 14. The collector area for maximum solar fraction for both the Roof-MaReCo and for the Spring/Fall-MaReCo systems is 14.8 m². The maximum solar fractions for these systems are 0.71 and 0.62 respectively. The flat-plate collector has a maximum solar fraction of 0.80 for a tilt of 90°. The area of this collector is then 15.4 m².

At a tilt of 45° the roof-MaReCo has a solar fraction of 0.70 for a required area of 13.3 m², while the flat plate collector has a solar fraction 0.54 for an area of 6.5 m². This means that generally the MaReCo collectors requires larger areas.

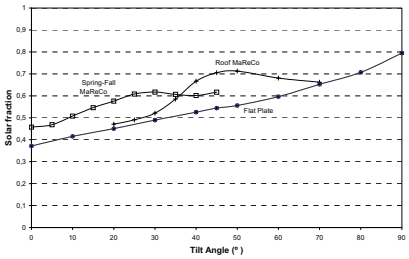

Figure 32 Solar fraction as a function of tilt angle for three different systems.

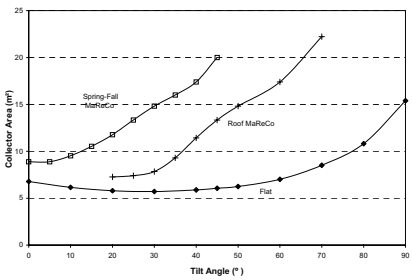

Figure 33 The areas corresponding to the collectors in figure 32.

6. DISCUSSION AND CONCLUSIONS

In the paper a new method for characterisation of the incidence angle dependence of the optical efficiency of asymmetric collectors is suggested and tested. The suggested method is an alternative when a more thorough analysis of the incidence angle dependence is needed.

One drawback with the method is that it requires relatively complicated measurements and evaluation.

The impact of the angular dependence of the absorber should be further investigated by measurements and ray tracing. The impact on F´ of uneven irradiance distribution on the absorber need to be further analysed in order to analyze the differences between measurements and ray tracing. The model should also be applied for use for describing the optical performance of vacuum tubes.

The biaxial function for a vacuum tube with a plane absorber is suggested as:

$$K_{\tau\alpha}(\Theta)^{vaccum} = \frac{F_T(\Theta) f_L(\Theta_L)}{F_T(\Theta_L)} \qquad (14)$$

$F_T(\Theta_T)$ is measured in the transversal plane across the tubes and gives the influence of the absorber only. $f_L(\Theta_L)$ is measured in the longitudinal plane along the tubes and gives influence of tubes and the absorber. This means that the ratio $f_L(\Theta_L)/F_T(\Theta_L)$ will give the longitudinal influence of the tubes.

The biaxial function for a vacuum tube with a tubular absorber is simply suggested as:

$$K_{\tau\alpha}(\Theta)^{vaccum1} = F_T(\Theta_T) f_L(\Theta_L)$$

$F_T(\Theta_L)$ is however supposed to be 1 for a single tube.

REFERENCES

Adsten, M., Helgesson, A. & Karlsson, B., 2001. Evaluation of asymmetric CPC-collector designs for stand-alone, roof- or wall integrated installation. Submitted to Solar Energy.

Duffie, J. & Beckman, D., 1991. Solar engineering of thermal processes; second edition. John Wiley & Sons, Inc., USA.

Helgesson, A. & Karlsson, B. (Vattenfall Utveckling AB) & Nostell, P. (Dep. of Material Science, The Ångström Laboratory, Uppsala University), 2000. Angular dependent optical properties from outdoor measurements of solar glazings. J. Solar Energy, vol 69, nos 1 – 6, pp 93 102.

Hellström, B., 2004. Derivation of efficiency factors for uneven irradiation on a fin absorber. J. Solar Enerby, vol 77, no 3, pp261 – 267.

Karlsson, B. & Wilson, G., 2000. MaReCo design for horizontal, vertical or tilted installation. Contribution to the EuroSun 2000 Conference in Copenhagen.

McIntire, W.R., 1982. Factored approximations for biaxial incident angle modifiers. Solar Energy, vol 29, no 4, pp 315 – 322.

Perers, B., 1993. Dynamic method for solar collector array testing and evaluation with standard database and simulation programs. In Solar energy, vol. 50, No. 6, pp 517 526.

ZEMAX version November 1, 2004, ZEMAX Development Corporation, San Diego, California, USA.

NOMENCLATURE

A	Collector area	m²
b_0	Incidence angle modifier coefficient	--
E	Energy output	kWh/m²
$F_T(\Theta_T)$	Total dependence (including glazing and reflector effects) in the T-direction	
$f_L(\Theta)$,		
$g_{TL}(\Theta_T)$	functions for the incidence angle of the glazing and the reflector respectively	
H_{eff}	Effective solar height	°
I	Total, beam (b) or diffuse (d) radiation	W/m²
$K_{\tau\alpha}(\Theta)$	Incidence angle modifier	--
k_l	Heat loss factor	W/m²,°C
L	Heat load	kWh
$(mC)_e$	effective collector thermal capacitance	J/m²,°C
$\dot{q}$	collector output	W/m²
S_F	Solar fraction	--
T_{OP}	Operating temperature	°C
ΔT	Temperature difference between collector and ambient	°C
dT_f/dt	time variation of fluid temperature	°C/s
η_0	optical efficiency for beam (b) or diffuse (d) radiation	--
Θ	Incidence angle (T = transversal and L = longitudinal)	°

Article VIII

A NEW MODEL AND METHOD FOR DETERMINATION OF THE INCIDENCE ANGLE DEPENDENT G-VALUE OF WINDOWS AND SUNSHADES

Tobias Rosencrantz, Johan Nilsson, Björn Karlsson
Energy and Building Design, Lund University, P.O. Box 118, Lund, SE-221 00, Sweden,
Phone Number +46 46 22 48 51, Fax +46 46 222 47 19, e-mail: tobias.rosencrantz@ebd.lth.se

Abstract – The development of a new method for modelling the incidence angle dependent g-value of asymmetric sunshades is described. The new model is tested by monitoring the g-value of four different sunshades and also by performing ray tracing. For asymmetric components, an overall biaxial incidence angle modifier can be used in order to model the optical efficiency properly. One example of this is a product model, where the incident angle modifier is approximated by factoring it into two components $g(\theta_L,\theta_T)=g_L(\theta_L, 0)g_T(0, \theta_T)$. In the equation above, the index T denotes the transverse and L the longitudinal planes. The longitudinal plane is the plane including the surface normal and a line along the window extension, and the transverse plane is the plane including the surface normal and perpendicular to the longitudinal plane. This means that the model described by equation 1 is strictly correct only when radiation is incident in either of the analysis planes. In order to better characterise the incidence angle dependence of asymmetric components, an alternative method is suggested in this paper. In this model, the influence of the glazing and of the sunshade on the system is studied separately: $g_{sys}(\theta_i,\theta_T) = g_w(\theta_i)g_{sh}(\theta_T)$. In this equation, the factor $g_w(\theta_i)$ basically gives the influence of the glazing and $g_{sh}(\theta_T)$ gives the influence of the sunshade. This equation is, in principle, different from the product above since θ_L is not used. $g_{sh}(\theta_T)$ is obtained as a ratio between $g_{sys}(0,\theta_T)$ and $g_w(0,\theta_T)$: $g_{sh}(\theta_T) = g_{sys}(\theta_L=0,\theta_T)/g_w(\theta_L=0,\theta_T)$. This equation is also valid for plane windows having $g_{sh}(\theta_T) = 1$ resulting in g being a function only of θ, just as expected. In the T plane, the incoming radiation is first transmitted through the sunshade and then transmitted through the glass. Geometric effects and multiple reflections in the sunshade affect the system g-value. In the L direction, the properties of the glass are important. This means that the incidence angle dependence in the L direction of a window with a sunshade device should be similar to the dependence in the overall direction for a plane window.

1. INTRODUCTION

1.1 Background

Solar shading devices are used in buildings to lower the energy consumption for cooling and to increase the indoor comfort by preventing overheating (Bülow-Hübe, 2001). Today there is no standard procedure for the characterisation of exterior sunshades which are not parallel to the glazing surface. The standard ISO 15099 only accounts for internal and interpane solar shadings situated parallel to the panes with intimate thermal-optical contact. We suggest a method for this characterization by applying a new biaxial incidence angle model for both a window and solar shading. This could also lead to improvement in understanding the optimized design and geometry of the solar shading. This could make it easier to choose the right solar shading device for a specific building.

1.2 Measurements of g-value

The g-value or the total solar energy transmittance is defined as the direct transmittance through the glazing system plus the energy absorbed in the system which is transmitted towards the room (ISO 15099). The g-value is thus a measure of the efficiency of the solar shading device.

The g-values of several shading devices on the market have been measured using both outdoor guarded twin-boxes and an indoor solar simulator in the Solar Shading project (Wall & Bülow-Hübe, 2001 & 2003). However, the g-value was for the most part not evaluated against the incidence angle of the solar radiation.

1.3 Objectives

The objectives of this paper are to apply an angle dependence model for external asymmetric solar shadings in combination with a window. Characterization of different external solar shadings and ray tracing simulations are performed in order to verify this new model.

1.4 Biaxial model for incidence angle dependence

For asymmetric components, an overall biaxial incidence angle modifier can be used in order to model the optical efficiency properly. McIntire presented a biaxial incidence angle modifier for the optical efficiency of asymmetric concentrating solar collectors. The incidence angle modifier was obtained from measurements in the perpendicular transverse and longitudinal directions (McIntire, 1982). Equation 1 defines this model.

$$G(\theta_L, \theta_T) = G_L(\theta_L,0)G_T(0, \theta_T) \quad (1)$$

In the equation above, θ_T and θ_L, denotes the angular of incidence projected in the transverse and the longitudinal planes. The longitudinal plane is the plane including the surface normal and a line along the window extension, and the transverse plane is the plane including the surface normal and perpendicular to the longitudinal plane, according to fig 1. In equation 1, the angular dependence of the window is determined from measurements made in two orthogonal planes, figure 1.

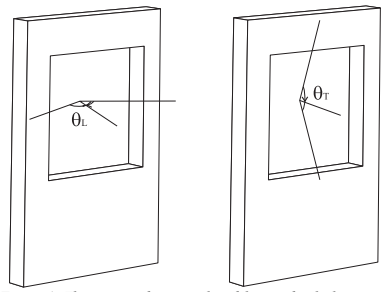

Figure 1. The projected traversal and longitudinal planes and the angles θ_T and θ_L projected in these planes.

$$\tan^2 \theta_i = \tan^2 \theta_L + \tan^2 \theta_T \quad (2)$$

Figure 1 and equation 2 shows the relation between the incidence angle (θ_i) and the two projected angles θ_T and θ_L. The model described by equation 1 is strictly correct only when radiation is incident in either of the analysis planes (Nilsson et al., 2005).

1.5 Sunshades studied

Four different solar shadings were studied; Venetian blind, Awning, Diffuse film, and Screen. The Venetian blind was characterized outdoors, while the others were measured indoor in the Solar Simulator of Energy and Building Design, Lund University. The awning and the Venetian blind are asymmetric shadings while the screen and the diffuse film are symmetric shadings.

2. THE NEW MODEL AND METHOD OF VALIDATION

2.1 New model

In order to systematically characterize the incidence angle dependence of asymmetric components, a new method and model is suggested in this paper. In this model, the influence of the glazing and of the solar shading on the system g-value is studied separately. If the sunshade has no edge effects and do not introduce any light scattering an optical model given by equation 3 is proposed.

$$g_{sys}(\theta_i,\theta_T)=g_w(\theta_i)g_{sh}(\theta_T) \quad (3a)$$

$$g_w(\theta_i)=g_w(\theta_L,\theta_T) \quad (3b)$$

$$g_{sh}(\theta_T)=g_{sys}(\theta_L=0,\theta_T)/g_w\,(\theta_T) \quad (3c)$$

g_{sys} is the measured g-value of the sunshade in combination with the window. g_w is the measured g-value of the bare window.

In this equation, the factor $g_w(\theta_i)$ basically gives the influence of the glazing and $g_{sh}(\theta_T)$ gives the influence of the solar shading. Equation 3 is, in principle, different from equation 1 since θ_L is not included. $g_{sh}(\theta_T)$ is obtained as a ratio between g_{sys} and $g_w(\theta_T)$. Equation 3 is also valid for plane windows having $g_{sh}(\theta_T) = 1$ resulting in g_{sys} being a function of only θ_i, just as expected. In the T plane, the incoming radiation is first transmitted through the solar shading and then transmitted through the glass. Geometric effects and multiple reflections in the sunshade affect the g-value. In the L direction, the properties of the glass are important. This means that the incidence angle dependence in the L direction of a window with a transparent solar shading device should be similar to the dependence in the overall direction for a plane window.

$$g_{sys}(\theta_L,\theta_T=C) \approx g_w(\theta_i) \quad (4)$$

Most sunshades introduce scattering. This means that the g-value functions will be affected and the function $g_{sh}(\theta_L,\theta_T=C)$ is expected to show a weaker angular dependence than $g_w(\theta_i)$. Many sunshades like awnings exhibit edge effects. This means that equation 3 has to be extended with an end effect function h (θ_L)

$$g_{sys}(\theta_i,\theta_T,\theta_L) = g_w(\theta_i)g_{sh}(\theta_T)h(\theta_L) \quad (5)$$

2.2 Outdoor measurements of external solar shadings

Four different types of external solar shading devices were characterized indoors and outdoors. The Venetian blind was measured outdoor in the hot box arrangement at Energy and Building Design, Lund University (M.Wall and H Bülow-Hübe, 2001). Two well insulated vertical boxes with constant temperatures measured the energy flow through windows and solar shading devices. Both boxes faced south direction. One box with a window only served as a reference box and the other box had both window and solar shading. The g-value of the solar shading was then defined as:

$$g_{sh} = g_{sys}/g_w \quad (6)$$

The windows were double glazing units with 4 mm clear glass and 12 mm space between the panes. The

measurement methodology and techniques are described in details elsewhere (Wall and Bülow-Hübe, 2001).

The Venetian blind was measured in both horizontal and vertical position. The angle of the lamellas of the Venetian blind was 0° for both the horizontal and vertical placement, seen in figure 2.

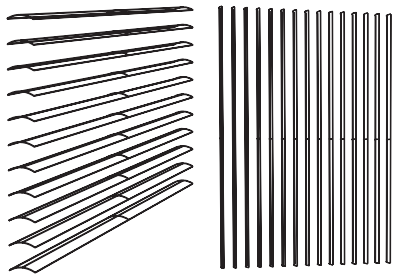

Figure 2. Drawing of the studied Venetian blind. a. Horizontal. b. Vertical.

The Venetian blind was measured near spring equinox when the transverse projected incidence angle (θ_T) is constant 34° at latitude 56°, see figure 3. When the blind was aligned vertical, fig 2b, the measurements gave the incidence angle dependence in the transverse plane at a constant longitudinal angle of 34°. By measuring both vertical and horizontal, it was possible to obtain the dependence in both longitudinal and transverse direction.

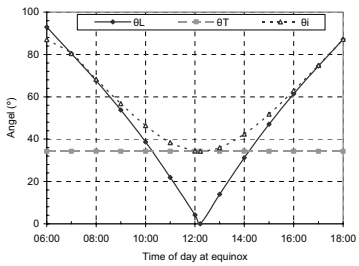

Figure 3. The projected transverse and longitudinal angles (θ_T) (θ_L) and the incidence angle (θ_i) at the equinox, when θ_T=(90-latitude)

2.3 Indoor measurements of external solar shadings

The measurements were performed with the solar simulator in the solar laboratory Energy and Building Design, Lund University see (Wall and Bülow-Hübe, 2003). The solar simulator makes indoor measuring possible for sunshades, windows and solar heating components in a standardized way. The irradiance incident on the window and calorimetric box was 950 W/m^2 at normal incidence. The measurements were performed for incidence angles corresponding to the equinox thereby making the comparison with the outdoor measurements convenient. The indoor measurements were performed for awning, diffuse film and screen, where the diffuse film and screen were mounted closely to the window.

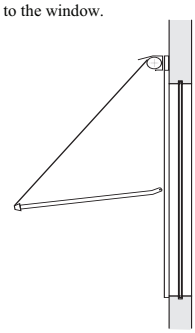

Figure 4. Principal drawing of the awning.

The calorimeter window was a double glazed unit (DGU) with 4 mm glass panes and 12 mm space between the panes, i.e. the same configuration as for the outdoor measurements.

2.4 Ray tracing simulations

The optical simulations were performed in a commercial ray tracing program, ZEMAX (ZEMAX, 2005).

The light incidents on the window system and the fraction of the light transmitted through the system were detected. The blind material was simulated by the optical properties of aluminium at a wavelength of 550 nm with a refractive indices of n=0.96093 and k=-6.6856. The reflectance at normal incidence was 85%. Five percent of the reflected light was reflected specularly and the remaining was supposed to be diffusely reflected with a Lambertian distribution. The simulated window consisted of two panes with 4 mm glass, with a total transmittance of 69% at normal incidence.

The source of 2 500 rays was placed vertically outside the external light detector and the angle of incidence was varied in each simulation. In one set of simulations, the longitudinal angle was kept at 34º and the transverse angle was varied from 0º to 88º in steps of 2º. This should be identical to the measurements performed at the spring equinox with the blind rotated 90º, fig 2b. The other set was performed at a constant transverse angle of 34º, equal to the transverse angle at the equinox in Lund, Sweden, fig 2a. The longitudinal angle was then varied

from 0º to 88º in steps of 2º. This gave a total of 88 simulations.

The estimated error in the derived transmittance of the system was 2% for each angle of incidence.

3. RESULTS, ANALYSIS AND MODELS

3.1 Results of outdoor measurements on a Venetian blind

The Venetian blind characterized outdoors is seen in figure 2. It was monitored in both horizontal and vertical position. In figure 5 results of measurements of the Venetian blind in the horizontal position is shown. The slat angle of the individual blinds is horizontal 0°. The g-values of the system, window and sunshade are plotted in the graph, where the g-value of the sunshade is calculated from equation 3c.

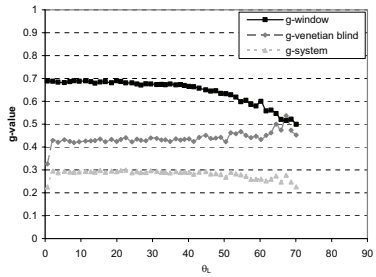

Figure 5. Outdoor measurements of g-values of system, window and Venetian blind as functions of longitudinal angle θ_L for a Venetian blind in horizontal position and 0° slat angle. θ_T=34°.

The measurement as function of the longitudinal angle (θ_L) ends at 75° since the measurement errors increases rapidly for high angles of incidence.

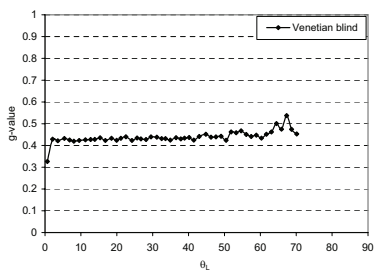

Figure 6 g_{sh}-value of Venetian blind as a function of longitudinal angle (θ_L). θ_T=34°.

In figure 6 the g_{sh}-value of the Venetian blind is shown separately as a function of longitudinal angles. As seen, the g_{sh}-values are nearly constant at angles up to 70°. This means that g_{sys} and g_w have a similar angular dependence in the longitudinal direction. Thus, equation 3 is valid for the blind. The g-value for a vertically placed Venetian blind, fig 2b, is shown in figure 7 as a function of the transverse incidence angle (θ_T).

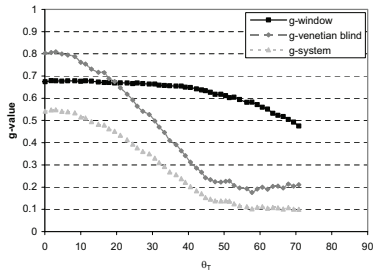

Figure 7. The g-value of the Venetian blind in vertical position as a function of transverse angle (θ_T). θ_T=34

In figure 7 there is as expected a considerably larger variation of the g-values compared to the measurements in the longitudinal direction position. Figure 8 shows only the g_{sh}-value of the Venetian blind as a function of the transverse angle. The g_{sh}-values decreases with increasing θ_T until complete shadowing occur and then it remains at a constant level, when the scattered light reaches the absorber.

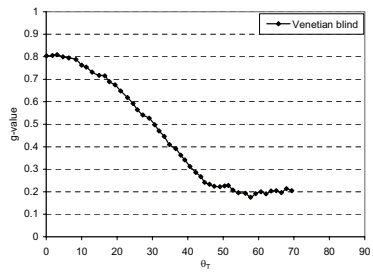

Figure 8 g_{sh}-value of the Venetian blind as function of transverse angle (θ_T). θ_T=34.

3.2 Comparison of measurements and ray tracing

Figure 9 shows the *g_{sh}-value* as a function of the transverse angle (θ_T) for a Venetian blind where the individual blinds is horizontal. The blinds are made of aluminum and the light reflected from the blinds is highly diffuse. Both the ray tracing and the measurements are included in the figure.

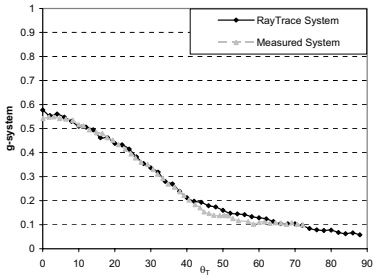

Figure 9. g_{sys}-value of both ray tracing and measurements for a Venetian blind with the window as function of the transverse incidence angle (θ_T).

The graphs differ at large transverse angles due to the reflecting surface of the blind. The simulation assumes a large diffuse component with a Lambertian distribution, but the graphs indicate that the near specular component of the reflected light is higher. The overall agreement between measurements and ray tracing is satisfying. When the light is incident from the horizon, all of the light is transmitted directly through the blind, and almost nothing is reflected. As the transverse angle increases, more and more light is reflected from the blind, and less is transmitted directly. This can be seen from the almost linear decrease in transmittance with increasing angle of incidence. At approximately 42º, no light is transmitted directly and all light is reflected from the blinds. Since the surface is assumed to be nearly Lambertian, the incidence angle has an influence only on the small specularly reflected component. This is also seen in the figure 9, where g_{sys} is almost constant above 42º.

Figure 10 shows the transmission as a function of the longitudinal angle of incidence at a constant transverse angle of 34º. For small and medium angles, the g_{sh} values are constant. At large longitudinal angles, the scattering of the reflected light decreases the reflectance of the window slightly and this results in an increasing transmittance of the system. The scattered light will suppress the angular dependence of the window.

At longitudinal angles below 60º, g_{sh} is constant and Equation 3a is valid. The ray tracing in figure 10 shows good agreement with the measurements in figure 6 for angles below 60°. For higher angles the ray tracing predict a higher g_{sh}. This is explained by larger scattering for high angles of incidence in the ray tracing simulation.

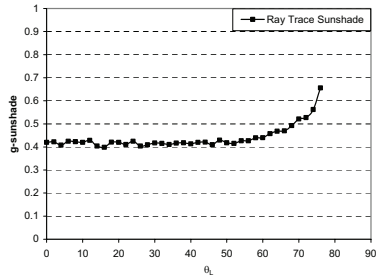

Figure 10. g_{sh}-value from ray tracing of Venetian blind as a function of the longitudinal angle (θ_L). θ_T=34°.

Figures 5-10 show that measurements of the transverse incidence angle dependence are enough to characterize the behavior of a Venetian blind for small and medium longitudinal angles. For very large longitudinal angles of incidence g_{sys} increases due to scattering. The irradiance for these high angles is however low. Figure 11 shows a comparison between the model defined by Equation 3a and ray tracing simulations of the system for angles where $\theta_T=\theta_L$. Equation 3c has been used to obtain $g_{sh}(\theta_T)$. The model approximates the g-value of the system well for small and large angles. For incidence angles in the range of 30º-60º the model tends to overestimate the g-value. This is due to the diffusing effect of the blinds, an effect that can not be described completely by incidence angle dependence in the transverse direction. The diffusivity tends to decrease the incidence angle at the glazing and this increases the transmittance of the glass for large angles of incidence.

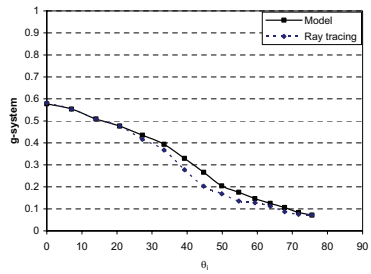

Figure 11. Comparison of g_{sys} from the model and ray tracing of the Venetian blind as a function of the angle of incidence in the plane where $\theta_T=\theta_L$.

3.3 Results of indoor measurements on an awning.

The measurements of the awning are described in this section. Figure 12 illustrates the results of the measurements of g_{sh} as a function of θ_T for a light and a dark short awning characterized in the solar simulator.

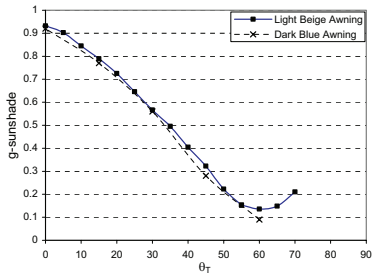

Figure 12. g_{sh}-values measured in the simulator of relatively short awnings as function of the transverse angle θ_T.

Figure 13 shows the measurements at constant transverse angle of 34°, corresponding to equinox for a fully extended awning with its arm turned 120° from the original upper position in figure 4. The measurements were performed for 0° to 80° in the longitudinal direction.

The awning has a more complex behavior than for example the Venetian blind since the awning exhibits edge effects at non zero angles in the longitudinal direction. As shown in figure 13 the g-value of the awning increases with increasing longitudinal angle, due to edge effects.

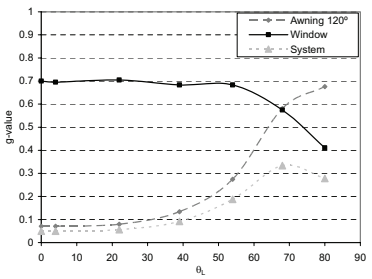

Figure 13 g-values of system, window and awning as functions of longitudinal angle θ_L. θ_T=34°.

For a very long awning compared to the window the shadow should have covered the window for all θ_L without any un-shaded edge effects. The g_{sys}-value would then have been 0.08 for all θ_L as indicated in figure 13. The g_{sh}-value of the awning is dependent on both the longitudinal and transverse angles. The model of the awning is given by the extended equation 5, where $h(\theta_L)$ gives the edge effect of the shading. The window dependency $g_w(\theta_i)$ is very small compared to the edge effect $h(\theta_L)$ and can be included in the $h(\theta_L)$-function. This means that the angular dependence of the awning can be written:

$$g_{sys}(\theta_i,\theta_T) = g_{Sh}(\theta_T)h(\theta_L) \quad (7)$$

3.4 Results of indoor measurements on a diffuse film and a screen.

The diffuse film and the screen are symmetric and have the same optical geometry in all directions. Figure 14 shows the g-values of the diffuse film, window and system as function of the longitudinal angle θ_L.

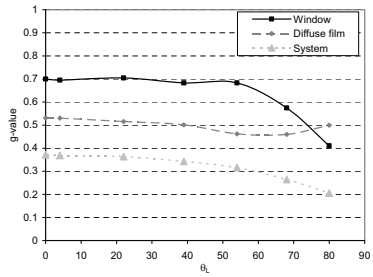

Figure 14. g-values of system, window and diffuse film as function of longitudinal angle θ_L. θ_T=34°.

The g_{sh} -values for the diffuse film is nearly constant. This means that g_{sys} for the diffuse film is similar to the window g_w for angles between 0° and 80°. The measurements of higher angles increase the measurement errors and the inaccuracy, therefore they are not shown here.

A screen fabric was measured in the same mode as the diffuse film with a constant transverse angle of θ_T=34°. The screen was very dense with only 3 % direct transmittance. Thus, most of the transmitted rays were diffusely scattered. In figure 15 the g-values of the system, window and screen are shown as a function of the longitudinal angle. The g-values of the screen g_{sh} are nearly constant and follow the angular dependence of the window g-value, g_w.

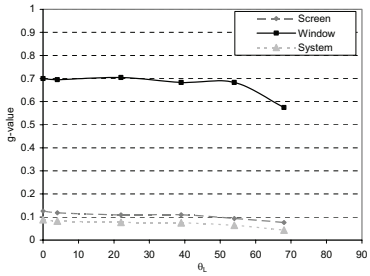

Figure 15. g-values of system, window and screen as a function of the longitudinal angle θ_L. θ_T=34°.

It can be concluded that the g-value of the diffuse film and the screen is almost independent of the longitudinal incidence angle. This means that angular dependence of the diffuse film and the screen can be written

$$g_{sys}(\theta_i,\theta_T) = g_w(\theta_i)g_{sh}(\theta_T) \quad (8)$$

and the shadow function $g_{sh}(\theta_T)$ is an angular independent constant.

In table 1 the models are summarized.

Table 1 Summary of equations presented in the paper.

Parameters / Shades	$g_w(\theta_i)$	$g_{sh}(\theta_T)$=	$h(\theta_L)$
1. Windows	$g_w(\theta_i)$	1	1
2. Shades without scattering	$g_w(\theta_i)$	$g_{sh}(\theta_T)$	1
3.Venetian blind	$g_w(\theta_i)$	$g_{sh}(\theta_T)$	1
4. Awning	1	$g_{sh}(\theta_T)$	$h(\theta_L)$
5. Screen / Diffuse film	$g_w(\theta_i)$	$g_{sh}(\theta_T)$=C	1

4 CONCLUSION

We have shown that the proposed model can be used for Venetian blinds, Awnings, Screens and Diffuse films. The model describes the incidence angle dependence of the Venetian blind well. In the case of the Awning, the model has to be extended to account for the effect of the edges at non zero longitudinal angles. For the symmetric Screen and Diffuse film, the shading devices can be modeled by a constant as the g_{sh} of the shading is independent of the angle of incidence.

Another effect that was observed was the increased g-value of the window at high angles of incidence when the solar shading devices tend to diffuse the irradiance. A window normally has low g-value at large angles of incidence, but since most of the shading devices diffuse the light as it is transmitted, some of the transmitted light is incident on the window at angles where the g-value of the window is higher. This means that the product model under estimate the g-value of the system, g_{sys} and the g-value of the shading device, g_{sh}, for high angles of incidence.

REFERENCES

Bülow-Hübe H. (2001) *Energy efficient window systems. Effects on energy use and daylight in buildings.* (Report TAB—01/1022), Lund, Sweden. Div. Energy and Building Design, Dept. Construction and architecture, Lund University.

McIntire, William R. *Factored approximations for biaxial incident angle modifiers, 1982 Solar* Energy, Vol 29 no 4 pp 315-322 1982

Nilsson J, Brogren M., Helgesson A, Karlsson B. and Roos A., (2005). B*iaxial model for the incidence angle dependence of the optical efficiency of photovoltaic systems with asymmetric reflectors,* Submitted to Solar Energy

ISO 15099:2003. Thermal performance of windows, doors and shading devices -- Detailed calculations.

Wall M. and Bülow-Hübe H. (2001) *Solar Protection in buildings.* (Report TAB—01/3060), Lund, Sweden. Div. Energy and Building Design, Dept. Construction and architecture, Lund University.

Wall M. and Bülow-Hübe H. (2003) *Solar Protection in buildings. Part 2 2000-2002.* (Report EBD-R--03/1), Lund, Sweden. Div. Energy and Building Design, Dept. Construction and architecture, Lund University.

ZEMAX version February 3, 2005, ZEMAX Development Corporation, San Diego, California, USA

LUND UNIVERSITY

ISSN 1671-8136
ISBN 91-85147-15-X